

Connecting String/ M Theory to the Electroweak Scale and to LHC Data

by
Piyush Kumar

A dissertation submitted in partial fulfillment
of the requirements for the degree of
Doctor of Philosophy
(Physics)
in The University of Michigan
2007

Doctoral Committee:

Professor Gordon L. Kane, Chairperson
Professor Dante E. Amidei
Professor Douglas O. Richstone
Associate Professor James D. Wells
Assistant Professor Leopoldo A. Pando Zayas

© $\frac{\text{Piyush Kumar}}{\text{All Rights Reserved}}$ 2018

TO MY PARENTS & MY WIFE

ACKNOWLEDGEMENTS

I would like to express my heartfelt gratitude to my advisor Prof. Gordon Kane. I am really grateful to him for accepting me as a student when I transferred to Michigan, for his continuous encouragement and for inspiring me by his infectious enthusiasm about physics. I would also like to thank other professors - most notably Bobby Acharya, Joseph Lykken and James Wells, for the various illuminating discussions and collaborations I had with them which helped me gain insight and perspective about various branches of theoretical high-energy physics.

I have also benefitted a great amount by interactions with fellow students and postdocs in the particle theory group. I would like to thank them, particularly Konstantin Bobkov, Jacob Bourjaily, Joshua Davis, David Morrissey, Jing Shao, Manuel Toharia, Diana Vaman and Ting Wang, for increasing my understanding of many topics as well as offering constructive criticism.

Finally, I would like to thank my family. My mother and father, for everything they did for me and for having so much confidence in their eldest son. My brother and sister, for always looking up to their elder brother. And my wife, Kriti, for her unconditional love, care and support as well as for being my best friend.

TABLE OF CONTENTS

DEDICATION	ii
ACKNOWLEDGEMENTS	iii
LIST OF FIGURES	vii
LIST OF TABLES	xv
LIST OF APPENDICES	xvii
CHAPTER	
I. Introduction	1
II. Why is it important to do String Phenomenology?	5
III. The Hierarchy Problem and Supersymmetry Breaking	8
3.1 Low Energy Supersymmetry	12
3.2 String/ M Theory and the Hierarchy Problem	16
IV. Top-Down String Phenomenology	19
4.1 Type IIA Intersecting D-brane Constructions	23
4.1.1 General construction of intersecting brane models.	25
4.1.2 A local MSSM-like model	27
4.1.3 Low energy effective action and soft terms	33
4.1.4 Some phenomenological implications	44
4.1.5 Summary of Results	49

4.2	<i>M</i> Theory compactifications on singular G_2 Holonomy Manifolds	50
4.2.1	The Moduli Potential	53
4.2.2	Supersymmetric Vacua	57
4.2.3	Examples of G_2 Manifolds	68
4.2.4	Vacua with spontaneously broken Supersymmetry	70
4.2.5	Vacua with charged matter in the Hidden Sector	87
4.2.6	Relevant Scales	103
4.2.7	Phenomenology	131
4.2.8	Summary of Results	156
V. Distinguishing String Constructions from Experimental Observables .		159
5.1	Examples	160
5.2	The “String” Benchmark Pattern Table - Results	166
5.3	Procedural Details	171
5.4	Distinguishability of Constructions	177
5.4.1	General Remarks	177
5.4.2	Why is it possible to distinguish different Constructions? . . .	180
5.4.3	Explanation of Signatures from the Spectrum	182
5.4.4	Explanation of Spectrum from the Soft Parameters	199
5.4.5	Explanation of Soft Parameters from the Underlying Theoretical Construction	206
5.5	Distinguishing Theories Qualitatively	208
5.6	Possible Limitations	211
5.7	Summary and Future Directions	217
VI. From Low Scale Data to High Scale Theory - Obstacles and Resolutions		221
6.1	Uncertainties Due to the S Term	225
6.1.1	Example: SPS-5 with an Unmeasured Higgs Soft Mass	228
6.1.2	Origins and Uses of the S Term	232
6.2	New Physics: Complete GUT Multiplets	234
6.2.1	Shifted Gauge Running	235
6.2.2	Yukawa Effects and Useful Combinations	239
6.2.3	Some Numerical Results	242
6.3	The (S)Neutrino Connection	249
6.3.1	Running Up	251
6.4	Putting it All Together: an Example	256
6.4.1	Step 1: Running Up in the MSSM	257
6.4.2	Step 2: Adding GUT Multiplets	260
6.4.3	Step 3: Adding a Heavy Neutrino Sector	263

6.4.4 Results	264
6.5 Summary	265
VII. Conclusions	271
APPENDICES	273
BIBLIOGRAPHY	285

LIST OF FIGURES

Figure

- 4.1 Cosmic ray positron excess due to LSP annihilations. Crossed points are HEAT experimental data. The dotted line is from the standard cosmological model without taking into account the LSP annihilation contributions. The solid line is for the \widetilde{W} LSP model, the dashed line is for the \widetilde{H} LSP model and the dashed-dotted line is for the mixed \widetilde{B} - \widetilde{H} LSP model. B_s is the boost factor. 49
- 4.2 Positive values of s_1 plotted as a function of α for a case with two condensates and three bulk moduli for the following choice of constants $b_1 = \frac{2\pi}{30}, b_2 = \frac{2\pi}{29}, N_i^1 = \{1, 2, 2\}, N_i^2 = \{2, 3, 5\}, a_i = \{1, 1/7, 25/21\}$. The qualitative feature of this plot remains the same for different choices of constants as well as for different i . The vertical line is the locus for $\alpha = \frac{b_2 N_i^2}{b_1 N_i^1}$, where the denominator of (4.63) vanishes. 60
- 4.3 Left - A_2/A_1 plotted as a function of α for a case with two condensates and three bulk moduli. The function diverges as it approaches the loci of singularities of (4.63), *viz.* $\alpha = \frac{b_2 N_i^2}{b_1 N_i^1}$.
 Right - Positive $s_i, i = 1, 2, 3$ for the same case plotted as functions of α . s_1 is represented by the solid curve, s_2 by the long dashed curve and s_3 by the short dashed curve. The vertical lines again represent the loci of singularities of (4.63) which the respective moduli s_i asymptote to. The horizontal solid (red) line shows the value unity for the moduli, below which the supergravity approximation is not valid.
 Both plots are for $b_1 = \frac{2\pi}{30}, b_2 = \frac{2\pi}{29}, N_i^1 = \{1, 2, 2\}, N_i^2 = \{2, 3, 5\}, a_i = \{1, 1/7, 25/21\}$ 61

4.4	<p>Plots of positive $s_i, i = 1, 2, 3$ as functions of A_2/A_1.</p> <p>Top Left: Same choice of constants as in Figure(4.3), i.e. $b_1 = \frac{2\pi}{30}, b_2 = \frac{2\pi}{29}, N_i^1 = \{1, 2, 2\}, N_i^2 = \{2, 3, 5\}, a_i = \{1, 1/7, 25/21\}$.</p> <p>Top Right: We increase the ranks of the gauge groups but keep them close (keeping everything else same) - $b_1 = \frac{2\pi}{40}, b_2 = \frac{2\pi}{38}$.</p> <p>Bottom Left: We introduce a large difference in the ranks of the gauge groups (with everything else same) - $b_1 = \frac{2\pi}{40}, b_2 = \frac{2\pi}{30}$.</p> <p>Bottom Right: We keep the ranks of the gauge groups as in Top Left but change the integer coefficients to $N_i^1 = \{1, 2, 2\}, N_i^2 = \{3, 3, 4\}$.</p>	62
4.5	<p>Plots of positive $s_i, i = 1, 2, 3$ as functions of A_2/A_1. The constants are $b_1 = \frac{2\pi}{30}, b_2 = \frac{2\pi}{29}, N_i^1 = \{1, 0, 1\}, N_i^2 = \{1, 1, 1\}, a_i = \{1/10, 1, 37/30\}$. s_1 is represented by the solid curve, s_2 by the long dashed curve and s_3 by the short dashed curve. The red curve represents the volume of the internal manifold as a function of A_2/A_1.</p> <p>Right - the same plot with the vertical plot range decreased.</p>	64
4.6	<p>Plot of ν as a function of A_2/A_1 for the choice $b_1 = \frac{2\pi}{5}, b_2 = \frac{2\pi}{4}$. The red solid curve represents the exact numerical solution whereas the black dashed curve is the leading order approximation given by (4.72).</p>	66
4.7	<p>Potential multiplied by 10^{32} plotted as a function of one modulus s. For our particular choice of constants in (4.97), the modulus is stabilized at the supersymmetric AdS minimum $s^{(1)} = 26.101$. The maximum is de Sitter, given by $s^{(2)} = 27.185$.</p>	76
4.8	<p>Potential multiplied by 10^{32} plotted as a function of two moduli s_1 and s_2 for the values in (4.110). The SUSY AdS extremum given by (4.111) is a saddle point, located between the non-supersymmetric AdS minima given by (4.113).</p>	79
4.9	<p>Plots of $L_{A,+}^{(c)}, L_{A,-}^{(c)}$ and $B_A^{(c)}$, where $c = \overline{1, 2}$, corresponding to the two real solutions of the system (4.115) as functions of parameter A in the range $0 \leq A < 1$. Both left and right graphs have $L_{A,+}^{(c)}$ - long dashed line, $L_{A,-}^{(c)}$ -short dashed line, $B_A^{(c)}$ - solid line.</p> <p>Left: Plots of $L_{A,+}^{(1)}, L_{A,-}^{(1)}$ and $B_A^{(1)}$ corresponding to the first real solution at each A. There is a critical value $A = 1/7$ where $L_{A,-}^{(1)} = 0$ and becomes positive for $A > 1/7$.</p> <p>Right: Plots of $L_{A,+}^{(2)}, L_{A,-}^{(2)}$ and $B_A^{(2)}$ corresponding to the second real solution at each A.</p>	83

4.10 Plots of $\tilde{L}_{A,+}^{(c)}$, $\tilde{L}_{A,-}^{(c)}$ and $\tilde{B}_A^{(c)}$, where $c = \overline{1,2}$, corresponding to the two real solutions of the system (4.191) as functions of parameter A . $\tilde{L}_{A,+}^{(c)}$ - long dashed curve, $\tilde{L}_{A,-}^{(c)}$ - short dashed curve, $\tilde{B}_A^{(c)}$ - solid curve. Black color: $\tilde{L}_{A,+}^{(1)}$, $\tilde{L}_{A,-}^{(1)}$ and $\tilde{B}_A^{(1)}$ corresponding to the first real solution. Red color: $\tilde{L}_{A,+}^{(2)}$, $\tilde{L}_{A,-}^{(2)}$ and $\tilde{B}_A^{(2)}$ corresponding to the second real solution. Left plot: when $\delta = 27/4$ the real solutions exist in the range $0.877781 < A < 1$. Right plot: when $\delta = 8$ the real solutions exist st in the range $0.915342 < A < 1$ 101

4.11 $\log_{10}(m_{3/2})$ as a function of P for case 1) - top plots and case 2) - bottom plots. The light grey area represents possible values of $\log_{10}(m_{3/2})$ in the range where $\rho_{crit} \leq \rho \leq 10$ consistent with the SUGRA approximation. The dark area indicates the region of interest where $-16 \leq \log_{10}(m_{3/2}) \leq -14$ such that $240 \text{ GeV} \leq m_{3/2} \leq 24 \text{ TeV}$. The dark solid curve corresponds to $\log_{10}(m_{3/2})$ when $\rho = \rho_{crit}$. The lower boundary of the light grey area represents the $\log_{10}(m_{3/2})$ curve when $\rho = 10$. The dashed curve corresponds to $\rho = 1.01$. Top left: Case 1) when $P - Q = 1$. Top right: Case 1) when $P - Q = 3$. Bottom left: Case 2) when $P - Q = 1$. Bottom right: Case 2) when $P - Q = 2$. 110

4.12 The gravitino mass distribution with the x-axis denoting the logarithm of the gravitino mass (to base 10). Left: Distribution corresponding to scan one in (4.240). Middle: Distribution corresponding to scan two in (4.241) for which manifolds with the number of moduli $N < 50$ were excluded from the scan. Right: Distribution corresponding to scan three in (4.242) for which manifolds with the number of moduli $N < 100$ were excluded from the scan. 118

4.13 The gravitino mass distribution with the x-axis denoting the logarithm of the gravitino mass (to base 10). Left: Distribution corresponding to scan four in (4.243). Middle: Distribution corresponding to scan five in (4.244) for which manifolds with the number of moduli $N < 50$ were excluded from the scan. Right: Distribution corresponding to scan six in (4.245) for which manifolds with the number of moduli $N < 100$ were excluded from the scan. 120

4.14 The gravitino mass distribution with the x-axis denoting the logarithm of the gravitino mass (to base 10). Scans for the smallest possible choice $(Q - P)_{min} = 3$. Left: Distribution corresponding to the scan with $P_{max} = 200$. Middle: Distribution corresponding to the scan with $P_{max} = 100$. Right: Distribution corresponding to the scan with $P_{max} = 30$ 120

4.15 Plot of $\log_{10}(m_{3/2})$ as a function of P for $Q - P = 3$. Short-dashed curve corresponds to $N = 50$. Long-dashed curve corresponds to $N = 500$ 123

4.16 Absolute values of $(M_{1/2})_A^{(1)}$ -left and $(M_{1/2})_A^{(2)}$ -right in units of gravitino mass as functions of q . As parameter A varies over $0 \leq A < 1/7$ - on the left and $0 \leq A \leq 1$ - on the right the whole light grey region is covered.
Left plot: $A = 0$ - long dashed line, $A = 1/9$ - solid line, $A = 5/36$ - short dashed line.
Right plot: $A = 0$ -long dashed line, $A = 0.5$ - solid line, $A = 0.95$ - short dashed line. 135

5.1 Cartoon to illustrate the method used to distinguish constructions. 170

5.2 Plot of number of events with opposite-sign dileptons and ≥ 2 jets and number of events with three leptons and ≥ 2 jets. The black dot represents the lower limit of observability of the two signatures, according to conditions in equation (5.1). Note that the HM-A and overlapping HM-B and HM-C construction can be distinguished easily from the PH-A, PH-B, II-A, IIB-K and IIB-L constructions, as they occupy very different regions. The plots are best seen in color. 185

5.3 Plot of number of events with clean dileptons and number of events with clean trileptons. “clean” means not accompanied by jets. The black dot represents the lower limit of observability of the two signatures, according to conditions in equation (5.1). The models below the observable limit have not been shown. Note that the HM-A and overlapping HM-B and HM-C constructions can be distinguished from the PH-A, PH-B, II-A and IIB-L constructions, since the latter are not observable with the given luminosity. The plots are best seen in color. 187

5.4 Plot of number of events with 0 leptons, 1 or 2 b jets and ≥ 6 jets and number of events with 2 leptons, 0 b jets and ≥ 2 jets. The black dot represents the lower limit of observability of the two signatures, according to conditions in equation (5.1). The models below the observable limit have also been shown to emphasize that the II-A construction has very different number of events for these signatures compared to other constructions even *without* imposing the observability constraint. Note that the PH-B and II-A constructions can be distinguished from the PH-A, IIB-K and IIB-L constructions because they have very different slopes. The plots are best seen in color. 189

5.5	Plot of number of events with 2 leptons, 0 b jets and ≥ 2 jets and number of events with 2 leptons, 1 or 2 b jets and ≥ 2 jets. The black dot represents the lower limit of observability of the two signatures, according to conditions in equation (5.1). The models below the observable limit have not been shown. Note that the PH-B and II-A constructions can be distinguished from each other since the former is not observable while the latter is observable. One can also partially distinguish the PH-A and IIB-L constructions. The plots are best seen in color.	190
5.6	Plot of the charge asymmetry in events with a single electron or muon & ≥ 2 jets & the ratio of number of events with same sign different flavor (SSDF) dileptons and ≥ 2 jets and number of events with 1 tau and ≥ 2 jets. The models which are below the observable limit as defined by (5.1) are not shown. Note that the IIB-K construction can be distinguished from the PH-A and IIB-L constructions, as the former occupies a mostly horizontal region while the latter occupy a mostly vertical region. The overlapping IIB-K and PH-A models can be distinguished from Figure 5.7. The plots are best seen in color.	197
5.7	Plot of the peak of the \cancel{E}_T distribution and the charge asymmetry in events with a single electron or muon & ≥ 2 jets. The models which are below the observable limit as defined by (5.1) are not shown. Note that this plot distinguishes the overlapping PH-A and IIB-K models in Figure 5.6. The plots are best seen in color.	198
5.8	Left : The ratio $r \equiv m/ M $ as a function of θ for four different values of $\alpha(T + \bar{T})$ represented by various curves. Right: The universal soft parameters as a function of θ for $\alpha(T + \bar{T}) = 1.5$. The solid curve stands for trilinears, dotted dashed curve for scalars and dashed curve for gauginos.	202
5.9	Left : Plots for gaugino mass parameters as a function of $\text{Re}(t)$: The solid curve stands for M_3 , dotted-dashed for M_2 and dashed for M_1 . Right : The ratio M_1/M_2 as a function of $\text{Re}(t)$. $\text{Re}(t)$ varies from 1 to 1.5. The plots are shown for a given value of δ_{GS} and $m_{3/2}$. δ_{GS} is -15 and $m_{3/2}$ is 20 TeV.	204
5.10	Plot of number of events with 1 lepton and ≥ 2 jets and number of events with opposite sign dileptons and ≥ 2 jets, each sampled with ~ 50 models, except PH-A (~ 100 models).	212
5.11	The same plot as in Figure 5.10, in which the IIB-K construction is sampled with ~ 100 models and the PH-A construction with ~ 400 models.	213

5.12	Plot with x axis showing number of events with 2 leptons, 0 b jets and ≥ 2 jets, and y axis showing the number of events with 2 leptons, 1 or 2 b jets and ≥ 2 jets each sampled with ~ 50 models, except PH-A (~ 100 models).	214
5.13	The same plot as in Figure 5.12, in which the IIB-K construction is sampled with ~ 100 models and the PH-A construction with ~ 400 models.	216
6.1	Deviations in the running of some of the SPS-5 soft masses due to setting $m_{H_d}^2 = (1000 \text{ GeV})^2$ at the low scale. The solid lines show the running of $m_{H_u}^2$, m_E^2 , and m_L^2 with this perturbation, while the dashed lines show the unperturbed running of these soft masses. The unperturbed low-scale value of the down-Higgs soft mass is $m_{H_d}^2 \simeq (235 \text{ GeV})^2$	229
6.2	Deviations in the running of some of the SPS-5 soft masses due to setting $m_{H_d}^2 = (1000 \text{ GeV})^2$ at the low scale. The solid lines show the running of $m_{U_{1,2}}^2$, $m_{D_{1,2}}^2$, $m_{U_3}^2$, and $m_{D_3}^2$ with this perturbation, while the dashed lines show the unperturbed running of these soft masses.	230
6.3	The shift in the running of the gauge couplings (left) and the gaugino masses (right) due to 7 sets of $\mathbf{5} \oplus \bar{\mathbf{5}}$'s with mass $\tilde{\mu} = 10^{11} \text{ GeV}$. The universal gaugino mass is taken to be 700 GeV.	237
6.4	Running of the first generation soft scalar masses with $N_{\mathbf{5} \oplus \bar{\mathbf{5}}} = 7$ and $\tilde{\mu} = 10^{11} \text{ GeV}$ for the mSUGRA input parameters $m_0 = 300 \text{ GeV}$, $m_{1/2} = 700 \text{ GeV}$, $\tan \beta = 10$, and $A_0 = 0$. The dashed lines show the actual running of these parameters, while the solid lines show the running from low to high using the RG equations of the MSSM, ignoring the additional heavy multiplets.	243
6.5	Running of the soft scalar masses of $Q_{1,3}$ and $U_{1,3}$ with $N_{\mathbf{5} \oplus \bar{\mathbf{5}}} = 7$ and $\tilde{\mu} = 10^{11} \text{ GeV}$ for the mSUGRA input parameters $m_0 = 300 \text{ GeV}$, $m_{1/2} = 700 \text{ GeV}$, $\tan \beta = 10$, and $A_0 = 0$. The dashed lines show the actual running of these parameters, while the solid lines show the running from low to high using the RG equations of the MSSM, ignoring the additional heavy multiplets.	244
6.6	Running of the soft scalar masses of $Q_{1,3}$ and $U_{1,3}$ with $N_{\mathbf{5} \oplus \bar{\mathbf{5}}} = 3$ and $\tilde{\mu} = 10^4 \text{ GeV}$ for the mSUGRA input parameters $m_0 = 300 \text{ GeV}$, $m_{1/2} = 700 \text{ GeV}$, $\tan \beta = 10$, and $A_0 = 0$. The dashed lines show the actual running of these parameters, while the solid lines show the running from low to high using the RG equations of the MSSM, ignoring the additional heavy multiplets.	245

6.7	Running of the soft scalar mass combinations m_{B_3} and m_{B_1} with $N_{\mathbf{5}\oplus\bar{\mathbf{5}}} = 3$ and $\tilde{\mu} = 10^4$ GeV for the mSUGRA input parameters $m_0 = 300$ GeV, $m_{1/2} = 700$ GeV, $\tan\beta = 10$, and $A_0 = 0$. The dashed lines show the actual running of these parameters, while the solid lines show the running from low to high using the RG equations of the MSSM, ignoring the additional heavy multiplets. The small deviations in these figures arise from higher loop effects.	246
6.8	Running of the soft scalar mass combinations m_{X_3} and m_{X_1} with $N_{\mathbf{5}\oplus\bar{\mathbf{5}}} = 3$ and $\tilde{\mu} = 10^4$ GeV for the mSUGRA input parameters $m_0 = 300$ GeV, $m_{1/2} = 700$ GeV, $\tan\beta = 10$, and $A_0 = 0$. The dashed lines show the actual running of these parameters, while the solid lines show the running from low to high using the RG equations of the MSSM, ignoring the additional heavy multiplets. The small deviations in these figures arise from higher loop effects.	247
6.9	Running of the soft scalar masses of H_u , L_3 , and U_3 for SPS-5 input parameters at M_{GUT} with three additional heavy RH neutrinos of mass $M_R = 10^{14}$ GeV. The solid lines show the full running, including the neutrino sector effects, while the dashed lines show the low-to-high running of the soft masses in the MSSM, with the neutrino sector effects omitted.	253
6.10	The high scale (M_{GUT}) values of the soft scalar masses extrapolated using the MSSM RG equations, without including neutrino sector effects. The low-scale (500 GeV) values of the soft masses used in the extrapolation were obtained from SPS-5 input parameters at M_{GUT} with three additional heavy RH neutrinos of mass M_R . The deviations from $m_i(M_{GUT}) = 150$ GeV represent the discrepancy between the MSSM extrapolated values and the correct value in the full theory with heavy RH neutrinos. These discrepancies are shown as a function of the heavy neutrino scale M_R	254
6.11	Scale dependence of the soft scalar masses for the input soft parameters given in Table 6.1. No new physics effects beyond the MSSM were included in the running.	259
6.12	High scale values for the soft scalar mass differences Δm_{ij}^2 defined in Eq. (6.38) as a function of the mass scale $\tilde{\mu}$ of the $N_{\mathbf{5}\oplus\bar{\mathbf{5}}}$ heavy GUT multiplets for $N_{\mathbf{5}\oplus\bar{\mathbf{5}}} = 3, 5, 7$	262
6.13	High scale values for third family and Higgs boson soft scalar mass differences Δm_{ij}^2 (as defined in Eq. (6.35)) as a function of the mass scale M_R of the heavy RH neutrinos. $N_{\mathbf{5}\oplus\bar{\mathbf{5}}} = 5$ GUT multiplets were included in the running above the scale $\tilde{\mu} = 10^{10}$ GeV.	265

6.14	High scale values for the soft trilinear A terms as a function of the mass scale of the heavy RH neutrinos. $N_{\mathbf{5} \oplus \mathbf{5}} = 5$ GUT multiplets were included in the running above the scale $\tilde{\mu} = 10^{10}$ GeV.	266
B.1	Left: F as a function of θ_n^α . Middle: G as a function of θ_n^α . Right: H as a function of θ_n^α (for $l=1$). From [49], $\theta_n \in [0, 1)$	281

LIST OF TABLES

Table

4.1	Brane content for an MSSM-like spectrum. The mirror branes a^*, b^*, c^*, d^* are not shown. ρ can take values 1, $1/3$. For concreteness, we take $\rho = 1$ for calculating the soft terms. However, the parameter space for the soft terms remains the same for both $\rho = 1$ and $\rho = 1/3$	28
4.2	The MSSM spectrum from intersecting branes. The hypercharge normalization is given by $Q_Y = \frac{1}{6}Q_a - \frac{1}{2}Q_c - \frac{1}{2}Q_d$	29
4.3	Angles between a brane P and the orientifold plane on the j th torus: θ_P^j	42
4.4	Parameter choices for three particular models. All masses are in GeV. We set $Re t^3 = Re t^2$. $ \Theta_3 $ will be fixed by the condition $\sum \Theta_i ^2 = 1$. $Re s$, $Re u^2$ and $Re u^3$ are determined by requiring gauge coupling unification.	46
4.5	Soft terms at the unification scale. The input parameters for calculating the soft terms are shown in Table 4.4. m_0 denotes the average of scalar masses. In both models, they are roughly the gravitino mass. The sign of the trilinears is according to the convention used by SUSPECT. It should be kept in mind that this is opposite to the convention used in supergravity formulas.	46
5.1	<p>The String Pattern Table Results</p> <p>A “Yes” for a given pair of constructions indicates that the two constructions are distinguishable in a robust way, while a “No” indicates that the two models are not distinguishable with available data ($5 fb^{-1}$ in this case). A ”Probably Yes (No)” means that the two models are (aren’t) distinguishable in large regions of their parameter spaces.</p>	166

5.2 **The String Pattern Table**

An “OC” for the i^{th} row and j^{th} column means that the signature is observable for many models of the i^{th} construction. The value of the j^{th} signature for the i^{th} construction is (almost) always consistent with the condition in the second row and j^{th} column of the Table. An “ONC” also means that the signature is observable for many models of i^{th} construction. However, the value of the signature (almost) always does *not* consistent with the condition as specified in the second row and j^{th} column of the Table. A “Both” means that some models of the i^{th} construction have values of the j^{th} signature which are consistent the condition in the second row and the j^{th} column while other models of the i^{th} construction have values of the j^{th} signature which are not consistent with the condition. An “N.O.” for the i^{th} row and j^{th} column implies that the j^{th} signature is *not* observable for the i^{th} construction, i.e. the values of the observable for all (most) models of the construction are always below the observable limit as defined by (5.1), for the given luminosity ($5 fb^{-1}$). So, the construction is not observable in the j^{th} signature channel with the given amount of “data” 168

5.3 **The String Pattern Table**

An “OC” for the i^{th} row and j^{th} column means that the signature is observable for many models of the i^{th} construction. The value of the j^{th} signature for the i^{th} construction is (almost) always consistent with the condition in the second row and j^{th} column of the Table. An “ONC” also means that the signature is observable for many models of i^{th} construction. However, the value of the signature (almost) always does *not* consistent with the condition as specified in the second row and j^{th} column of the Table. A “Both” means that some models of the i^{th} construction have values of the j^{th} signature which are consistent the condition in the second row and the j^{th} column while other models of the i^{th} construction have values of the j^{th} signature which are not consistent with the condition. An “N.O.” for the i^{th} row and j^{th} column implies that the j^{th} signature is *not* observable for the i^{th} construction, i.e. the values of the observable for all (most) models of the construction are always below the observable limit as defined by (5.1), for the given luminosity ($5 fb^{-1}$). So, the construction is not observable in the j^{th} signature channel with the given amount of “data” 178

6.1 The low-energy scale ($M_{low} = 500 GeV$) soft supersymmetry breaking spectrum used in our analysis. The soft scalar masses listed in the table correspond to the signed square roots of the actual masses squared. In this table we also the high scale values of these soft parameters obtained by running them up to $M_{GUT} \simeq 2.5 \times 10^{16} GeV$ using the RG evolution appropriate for the MSSM. 270

LIST OF APPENDICES

Appendix

A.	Some Soft Supersymmetry Breaking Parameters for Intersecting D-brane Models	274
B.	Kähler metric for visible chiral matter in M theory	276
	B.0.1 Particular Case	278
	B.0.2 General Case	280
C.	Useful Combinations of Scalar Masses	282
	C.0.3 S Term Effects	282

CHAPTER I

Introduction

We are about to enter a unique era in high energy physics. For the first time in history, the energy and technology required to probe the electroweak scale in a controlled manner is at hand. The Large Hadron Collider (LHC), which will supposedly turn on by the end of this year, will be able to achieve this. We have many reasons to believe that the mysteries of the electroweak scale (the Standard Model) will be revealed at the LHC.

Even though this thesis will focus on forthcoming data from the LHC, we are very fortunate that forthcoming data from many other closely related fields in particle physics and cosmology will complement and supplement data from the LHC. For example, major clues about extensions to the Standard Model can come from indirect information from rare decays, magnetic moments, proton decay and particularly WIMP¹ detection in Dark Matter detection experiments. In addition, any extension to the Standard Model of particle physics with an underlying microscopic origin will also affect astrophysical/cosmological observables. Recent data from WMAP, Supernovae and Galactic Clusters as well as forthcoming data from PLANCK, LIGO/VIRGO and LISA will further constrain various approaches aiming to explain the origin

¹Weakly Interacting Massive Particle

of the electroweak scale. Therefore, in my opinion, it is fair to say that we are on the threshold of a unique data-rich era.

Assuming one obtains data confirming the existence of new physics beyond the Standard Model, we, as theorists, would have to grapple with the following questions :

- What is the broad framework for new physics?
- What is the spectrum of particles and the effective theory at \sim TeV scale within this broad framework?
- What is the structure of the underlying deeper, short distance, theory?

These questions are collectively known as the “*Inverse Problem*”. The first two questions pertaining to the Inverse Problem above have been receiving more and more attention in the past few years. However, the third question - the *deeper* Inverse Problem, has not even been addressed in a systematic way. This is hardly surprising, as this is arguably the most challenging problem in fundamental physics. The goal of this thesis is to explore the third question and try to get insights about addressing the deeper Inverse Problem in a meaningful way. In this thesis, the nature of the underlying theory will be assumed to be string/ M theory. This is because of the following reasons. At present, string theory is the only known consistent theory of quantum gravity, at least at the perturbative level. But for the purposes of this thesis, more importantly, it is the only known ultra-violet complete theory which can naturally give rise to effective four dimensional theories of particle physics with the most important features of the Standard Model, namely, non-abelian gauge fields and chiral fermions. In addition, string theory can address *all* open questions in particle physics and cosmology within its framework

and hopefully, solve them. Therefore, it seems reasonable to assume the existence of such a theory providing an underlying microscopic theoretical structure to our universe.

Even if one assumes the existence of string theory as the fundamental microscopic theory, it is still a herculean task to solve the deeper Inverse Problem, to say the least. One has to first explore this question carefully and identify approaches in which the question can be addressed meaningfully. In my opinion, the first steps towards addressing the deeper Inverse Problem are:

- String/ M theory constructions should be developed enough to make contact with low energy physics.
- Various specific classes of constructions, with “reasonable assumptions”, should be systematically analyzed to the extent that predictions for real experimental observables, say, signatures at the LHC, can be made.
- Effort should be made to identify experimental observables which probe and are sensitive to the properties of the underlying microscopic construction, or equivalently, different microscopic constructions should be distinguished on the basis of experimental observables.
- The origin of distinguishability should be understood in terms of the structure of the theory.
- This program should be complemented with a bottom-up program - that of finding the effective theory which explains all data. A combination of top-down and bottom-up approaches will be much more powerful than either.

In this work, all steps mentioned above will be examined and studied. The thesis is organized as follows. In chapter II, the motivation for and importance of string phenomenology will be

described in detail. Chapter III will try to explain the hierarchy problem, which is one of the most important problems in particle physics, within the context of field theory as well as string theory. Then, in chapter IV, two particular examples of string/ M theory compactifications will be analyzed, with a particular emphasis on their predictions for low-energy physics (of the order of the electroweak scale). In chapter V, it will be shown that many string motivated constructions can be distinguished on the basis of patterns of signatures at the LHC and the origin of distinguishability can also be explained on the basis of the underlying theoretical structure of the constructions. Finally, a more bottom-up approach to the Inverse Problem, *viz.* to go from data to theory in a more model-independent way will be studied in chapter VI. This will be followed by conclusions in chapter VII.

CHAPTER II

Why is it important to do String Phenomenology?

Before moving on to discuss more technical aspects of the dissertation in subsequent chapters, it is worthwhile to review the current status of string phenomenology, its importance and its role in the future.

At first glance, making reliable predictions from string theory might seem a long shot. A background independent non-perturbative formulation of string theory is not at hand at present. One does not even have a microscopic non-perturbative definition of string theory in general backgrounds such as backgrounds with Ramond-Ramond (RR) fluxes or cosmological backgrounds. There are also no hints of a deep underlying “vacuum selection principle” which would uniquely predict the properties of the vacuum which we live in, in a natural way. In fact, recent developments point in the opposite direction – towards a vast multitude of possibilities for four dimensional string vacua. This vast multitude of possibilities has been given the name - “Landscape”. The extent of the landscape of four dimensional string vacua is not known. In addition to the well known examples of Calabi-Yau compactifications, many other kinds of compactifications have been studied in the literature, some of them recently – such as generalized Kähler compactifications, non-Kähler compactifications like G_2 compactifications,

etc. and compactifications with non-geometric fluxes. In such a situation, the goal of making reliable predictions for low energy physics from string theory appears to be quite challenging.

Therefore, in my opinion, the situation warrants a pragmatic approach if one is still interested in connecting string theory to real observable physics. In fact, developments in the last twenty years and particularly in the last five years or so, actually give us a clue as to what the pragmatic approach might be. Even though we may not have a good understanding of the *entire* M theory landscape in all its glory, we have gained a lot of understanding about different corners of M theory, such as weakly and strongly coupled heterotic string theory, Type IIA and IIB string theories and M theory on G_2 manifolds. Detailed studies of these corners have shown that string theory has the ability to address *all* issues in particle physics and cosmology. For example, the origin of forces and matter, in particular non-abelian gauge fields and chiral fermions, can be explained. The origin of more than one flavor and hierarchical yukawa couplings can also be explained in the various corners, albeit in different ways. Heterotic string constructions and M theory constructions can naturally give rise to gauge coupling unification at a high scale. In Type II constructions, gauge coupling unification is less natural, but it is possible to construct models in which the gauge couplings unify. Model building in heterotic and type II string theories is a healthy area of research with many semi-realistic examples, and new approaches to model building are emerging. Moreover, in recent years, there has been a lot of progress in understanding *dynamical* issues - such as the stabilization of moduli¹, supersymmetry breaking and generation of hierarchy between the Planck and electroweak scales. Regarding connection to cosmology, many approaches to achieving inflation in string theory have been proposed in the literature. Many of these issues will be analyzed in detail in subse-

¹moduli are effective four dimensional scalar fields which characterize the size and shape of the internal manifold in a string compactification; astrophysical observations require that these scalars be sufficiently massive.

quent chapters in the context of specific string/ M theory constructions.

A pragmatic approach, therefore, in my opinion as well as of many other people is to systematically study models in *all* corners of the entire M theory landscape (where it is possible to do so) in a way such as to connect to real physics observables like collider (LHC) observables, dark matter (DM) observables and inflationary observables to name a few, and then use data to gain insights about the nature of the underlying theory. Developments in the last few years have actually made it possible to address each of these issues in a reliable way. In a string/ M theory construction, all such observables come from the *same* underlying microscopic physics, implying that forthcoming data has a great potential to constrain and favor or rule out specific classes of constructions in string/ M theory.

In the absence of a breakthrough in discovering a deep dynamical principle which uniquely selects the vacuum we live in, science should proceed in small systematic steps, which makes the pragmatic approach described above a sensible one to pursue. Of course, a breakthrough in some of the conceptual issues mentioned in the previous paragraphs would sharpen the approach further and make it even more useful.

Hoping that the case for string phenomenology has been made, the subsequent chapters will deal with various aspects of string phenomenology. After a detailed explanation of the hierarchy problem and its importance, two particular string/ M theory constructions will be studied so as to connect them to observable physics. Then, a general approach which allows us to distinguish different string constructions on the basis of their predictions for pattern of experimental observables, such as LHC signatures, will be described. This will be followed by a discussion of some issues in going from low-scale data to a high scale theory in a more model independent way (although still within the framework of supersymmetry).

CHAPTER III

The Hierarchy Problem and Supersymmetry Breaking

In this chapter, we would like to explain the Hierarchy Problem in detail, which is the most important problem in particle physics at present. This chapter is organized as follows. The nature of the problem will be first elucidated in a simple manner. We will then describe the paradigm of low energy supersymmetry which is perhaps the most appealing solution to the problem. Finally, since our interest lies in connecting String/ M theory to the (observed) electroweak scale, we will discuss the various approaches to the problem in String/ M theory. It turns out that the issue of supersymmetry breaking is intimately connected to the Hierarchy Problem, which will also be explained.

To begin, let's first state the Hierarchy Problem. The Hierarchy problem is actually two separate problems:

- What is the origin of the electroweak scale and why is it so much smaller than the fundamental mass scale M_{plank} ?
- Since the higgs mass parameter in the Standard Model is not protected by any symmetry, why is the higgs mass of the order of the electroweak scale instead of some very high cutoff

scale even though it is disturbingly sensitive to almost any new physics in any imaginable extension of the Standard Model?

The first part of the Hierarchy Problem is known as the Gauge Hierarchy Problem while the second part is known as the Technical Hierarchy Problem. As seen from above, the Gauge Hierarchy Problem is extremely simple to state and understand conceptually, but incredibly challenging to answer in a compelling way from an underlying theory. This would be explained in more detail later in this chapter. Let us now try to understand the technical hierarchy problem. The electrically neutral part of the Standard Model Higgs field is a complex scalar H with a classical potential

$$V = m_H^2 |H|^2 + \lambda |H|^4. \quad (3.1)$$

The Standard Model requires a non-vanishing vacuum expectation value (VEV) for H at the minimum of the potential. This will occur if $\lambda > 0$ and $m_H^2 < 0$, resulting in $\langle H \rangle = \sqrt{-m_H^2/2\lambda}$. Since we know experimentally that $\langle H \rangle$ is approximately 174 GeV, from measurements of the properties of the weak interactions, it must be that m_H^2 is very roughly of order $-(100 \text{ GeV})^2$. The problem is that m_H^2 receives enormous quantum corrections from the virtual effects of every particle that couples, directly or indirectly, to the Higgs field. For example, we have a correction to m_H^2 from a loop containing a Dirac fermion f with mass m_f . If the Higgs field couples to f with a term in the Lagrangian - $\lambda_f H \bar{f} f$, then the corresponding Feynman diagram yields a correction

$$\Delta m_H^2 = -\frac{|\lambda_f|^2}{8\pi^2} \Lambda_{\text{UV}}^2 + \dots \quad (3.2)$$

Here Λ_{UV} is an ultraviolet momentum cutoff used to regulate the loop integral; it should be interpreted as at least the energy scale at which new physics enters to alter the high-energy

behavior of the theory. The ellipses represent terms proportional to m_f^2 , which grow at most logarithmically with Λ_{UV} (and actually differ for the real and imaginary parts of H). Each of the leptons and quarks of the Standard Model can play the role of f ; for quarks, eq. (3.2) should be multiplied by 3 to account for color. The largest correction comes when f is the top quark with $\lambda_f \approx 1$. The problem is that if Λ_{UV} is of order M_{Planck} , say, then this quantum correction to m_H^2 is some 30 orders of magnitude larger than the required value of $m_H^2 \sim -(100 \text{ GeV})^2$. This is only directly a problem for corrections to the Higgs scalar boson squared mass, because quantum corrections to fermion and gauge boson masses do not have the direct quadratic sensitivity to Λ_{UV} found in eq. (3.2). However, the quarks and leptons and the electroweak gauge bosons Z^0 , W^\pm of the Standard Model all obtain masses from $\langle H \rangle$, so that the entire mass spectrum of the Standard Model is directly or indirectly sensitive to the cutoff Λ_{UV} .

Furthermore, there are contributions similar to eq. (3.2) from the virtual effects of any arbitrarily heavy particles that might exist, and these involve the masses of the heavy particles, not just the cutoff.

For example, suppose there exists a heavy complex scalar particle S with mass m_S that couples to the Higgs with a Lagrangian term $-\lambda_S |H|^2 |S|^2$. This gives a correction

$$\Delta m_H^2 = \frac{\lambda_S}{16\pi^2} [\Lambda_{UV}^2 - 2m_S^2 \ln(\Lambda_{UV}/m_S) + \dots]. \quad (3.3)$$

This problem arises even if there is no direct coupling between the Standard Model Higgs boson and the unknown heavy particles. For example, suppose there exists a heavy fermion F that, unlike the quarks and leptons of the Standard Model, has vector-like quantum numbers and therefore gets a large mass m_F without coupling to the Higgs field. [In other words, an arbitrarily large mass term of the form $m_F \bar{F}F$ is not forbidden by any symmetry, including weak isospin $SU(2)_L$.] In that case, no one-loop diagram like (3.2) exists for F . Nevertheless

there will be a correction to m_H^2 as long as F shares some gauge interactions with the Standard Model Higgs field; these may be the familiar electroweak interactions, or some unknown gauge forces that are broken at a very high energy scale inaccessible to experiment. This would give rise to a contribution :

$$\Delta m_H^2 = C_H T_F \left(\frac{g^2}{16\pi^2} \right)^2 [a\Lambda_{UV}^2 + 24m_F^2 \ln(\Lambda_{UV}/m_F) + \dots], \quad (3.4)$$

where C_H and T_F are group theory factors¹ of order 1, and g is the appropriate gauge coupling.

Therefore, the important point is that these contributions to Δm_H^2 are sensitive both to the largest masses and to the ultraviolet cutoff in the theory, presumably of order M_{Planck} . Thus, the “natural” squared mass of a fundamental Higgs scalar, including quantum corrections, should be more like M_{Planck}^2 than the experimentally favored value. Even very indirect contributions from Feynman diagrams with three or more loops can give unacceptably large contributions to Δm_H^2 . The argument above applies not just for heavy particles, but for arbitrary high-scale physical phenomena such as condensates or additional compactified dimensions.

It could be that there is no fundamental Higgs boson, as in technicolor models, top-quark condensate models, and models in which the Higgs boson is composite. Or it could be that the ultimate ultraviolet cutoff scale is much lower than the Planck scale. These ideas are certainly worth exploring, although they often present difficulties in their simplest forms. But, if the Higgs boson is a fundamental particle, as we will assume in this work henceforth, and if there really is physics far above the electroweak scale which will also be assumed, then we have two remaining options: either we must make the rather bizarre assumption that there do not exist *any* high-mass particles or effects that couple (even indirectly or extremely weakly) to the Higgs

¹Specifically, C_H is the quadratic Casimir invariant of H , and T_F is the Dynkin index of F in a normalization such that $T_F = 1$ for a Dirac fermion (or two Weyl fermions) in a fundamental representation of $SU(n)$.

scalar field, or else some striking cancellation is needed between the various contributions to Δm_H^2 .

3.1 Low Energy Supersymmetry

Theories with “low energy supersymmetry” have emerged as the strongest candidates for physics beyond the SM. By “low energy supersymmetry”, one means that supersymmetry remains an unbroken symmetry at very low energies compared to the fundamental scale M_{Planck} ; it is somehow broken at a scale such that it gives rise to masses of extra particles which are required by supersymmetry, to be of the order of the TeV scale, so as to solve the (Technical) Hierarchy Problem (this will become clear soon). There are strong reasons to expect that low energy supersymmetry is the probable outcome of experimental and theoretical progress and that it will soon be directly confirmed by experiment. In the simplest supersymmetric world, each particle has a *superpartner* which differs in spin by 1/2 and is related to the original particle by a supersymmetry transformation. Since supersymmetry relates the scalar and fermionic sectors, the chiral symmetries which protect the masses of the fermions also protect the masses of the scalars from quadratic divergences, leading to an elegant resolution of the hierarchy problem. Comprehensive reviews of supersymmetry from a particle physics and phenomenological perspective can be found in [1].

Historically though, supersymmetry had been proposed entirely from a mathematical and formal perspective. It was found that the Coleman-Mandula Theorem [2] for interacting quantum field theories could be generalized if one postulates a fermionic symmetry which connects bosons to fermions and vice versa. This is known as the Haag-Lopuszanski theorem [3]. Thus, before its good phenomenological properties were realized, supersymmetry was studied purely

as a formal theory in the 1970s. Supersymmetry is also a critical ingredient in the microscopic formulation of String theory. It also turns out that many solutions of string theory give rise to low energy supersymmetry, as will be discussed in detail in chapter IV. It is therefore, remarkable that a symmetry which was proposed entirely from a formal point of view has the potential to solve many problems in particle physics as well.

Supersymmetry must be a broken symmetry, because exact supersymmetry dictates that every superpartner is degenerate in mass with its corresponding SM particle, a possibility which is decisively ruled out by experiment. Possible ways to achieve a spontaneous breaking of supersymmetry depend on the form of the high energy theory. In many ways, it is not surprising that supersymmetry breaking is not yet understood — the symmetry breaking was the last thing understood for the Standard Model too (assuming it is indeed understood).

An important clue as to the nature of supersymmetry breaking can be obtained by returning to the motivation provided by the hierarchy problem. Supersymmetry forced us to introduce two complex scalar fields for each Standard Model Dirac fermion, which is just what is needed to enable a cancellation of the quadratically divergent (Λ_{UV}^2) pieces of eqs. (3.2) and (3.3). This sort of cancellation also requires that the associated dimensionless couplings should be related (for example $\lambda_S = |\lambda_f|^2$). The necessary relationships between couplings indeed occur in unbroken supersymmetry. In fact, unbroken supersymmetry guarantees that the quadratic divergences in scalar squared masses must vanish to all orders in perturbation theory.² Now, if broken supersymmetry is still to provide a solution to the hierarchy problem even in the presence of supersymmetry breaking, then the relationships between dimensionless couplings

²A simple way to understand this is to recall that unbroken supersymmetry requires the degeneracy of scalar and fermion masses. Radiative corrections to fermion masses are known to diverge at most logarithmically in any renormalizable field theory, so the same must be true for scalar masses in unbroken supersymmetry.

that hold in an unbroken supersymmetric theory must be maintained. Otherwise, there would be quadratically divergent radiative corrections to the Higgs scalar masses of the form

$$\Delta m_H^2 = \frac{1}{8\pi^2}(\lambda_S - |\lambda_f|^2)\Lambda_{\text{UV}}^2 + \dots \quad (3.5)$$

We are therefore led to consider “soft” supersymmetry breaking. This means that the effective Lagrangian of the MSSM can be written in the form

$$\mathcal{L} = \mathcal{L}_{\text{SUSY}} + \mathcal{L}_{\text{soft}}, \quad (3.6)$$

where $\mathcal{L}_{\text{SUSY}}$ contains all of the gauge and Yukawa interactions and preserves supersymmetry invariance, and $\mathcal{L}_{\text{soft}}$ violates supersymmetry but contains only mass terms and coupling parameters with *positive* mass dimension. Without further justification, soft supersymmetry breaking might seem like a rather arbitrary requirement. Fortunately, theoretical models for supersymmetry breaking do indeed yield effective Lagrangians with just such terms for $\mathcal{L}_{\text{soft}}$. If supersymmetry is broken in this way, the superpartner masses can be lifted to a phenomenologically acceptable range. Furthermore, the scale of the mass splitting should be of order the Z mass to TeV range because it can be tied to the scale of electroweak symmetry breaking.

Thus, we see that low energy supersymmetry provides an elegant solution to the Technical Hierarchy Problem. As we will see shortly, it also mitigates the Gauge Hierarchy Problem by breaking the electroweak symmetry radiatively through logarithmic running, which explains the large number $\sim 10^{13}$. Apart from the Hierarchy problem, low energy supersymmetry has had many other “successes” as well:

- *Radiative electroweak symmetry breaking.* With plausible boundary conditions at a high scale (certain couplings such as the top quark Yukawa of $O(1)$ and no bare Higgs mass

parameter μ in the superpotential), low energy supersymmetry can provide the explanation of the origin of electroweak symmetry breaking [4, 5, 6]. To oversimplify a little, the SM effective Higgs potential has the form $V = m^2 h^2 + \lambda h^4$. First, supersymmetry requires that the quartic coupling λ is a function of the $U(1)_Y$ and $SU(2)$ gauge couplings $\lambda = (g'^2 + g^2)/2$. Second, the m^2 parameter runs to negative values at the electroweak scale, driven by the large top quark Yukawa coupling. Thus the “Mexican hat” potential with a minimum away from $h = 0$ is derived rather than assumed. As is typical for progress in physics, this explanation is not from first principles, but it is an explanation in terms of the next level of the effective theory which depends on the crucial assumption that the \mathcal{L}_{soft} mass parameters have values of order the electroweak scale. Once superpartners are discovered, the question of supersymmetry breaking must be answered in any event and it is a genuine success of the theory that whatever explains supersymmetry breaking is also capable of resolving the crucial issue of $SU(2) \times U(1)$ breaking.

- *Gauge coupling unification.* In contrast to the SM, the MSSM allows for the unification of the gauge couplings, as first pointed out in the context of GUT models by [7, 8, 9]. The extrapolation of the low energy values of the gauge couplings using renormalization group equations and the MSSM particle content shows that the gauge couplings unify at the scale $M_G \simeq 3 \times 10^{16}$ GeV [10, 11, 12, 13]. Gauge coupling unification and electroweak symmetry breaking depend on essentially the same physics since each needs the soft masses and μ to be of order the electroweak scale.
- *Cold dark matter.* In supersymmetric theories, the lightest superpartner (LSP) can be stable. This stable superpartner provides a nice cold dark matter candidate [14, 15].

Simple estimates of its relic density are of the right order of magnitude to provide the observed amount. LSPs were noticed as good candidates before the need for nonbaryonic cold dark matter was established.

3.2 String/ M Theory and the Hierarchy Problem

As mentioned in the previous subsection, low energy supersymmetry alone can only mitigate the Gauge Hierarchy Problem, but it cannot solve it. An explanation of the *origin* of the electroweak scale has to come from an underlying microscopic theory which incorporates both non-abelian gauge theories and gravitation, like String/ M theory. This subsection is devoted to the various approaches in String/ M Theory to the Hierarchy Problem.

The particle spectrum of string theory consists of a finite number of massless states and an infinite number of massive states characterized by the string scale. For a phenomenological description of the consequences of string theory for low-energy physics, it should not be necessary to describe the dynamics of massive states. Formulating an effective theory based entirely on fields corresponding to massless (light) degrees of freedom is the most natural thing to do in such a situation. Such a description is useful not only for a phenomenological analysis, but also for addressing certain theoretical issues, such as the occurrence of anomalies.

In principle, it must be possible to describe string theory by a classical action $S(\phi, \Phi)$, ϕ denoting the light degrees of freedom and Φ denoting the heavy degrees of freedom. One could then imagine integrating out the heavy fields Φ from the action and obtain a low-energy effective action for the light fields $S_{eff}(\phi)$. However, at present, the exact string theory action $S(\phi, \Phi)$ is not known (even at the classical level). Therefore, it is not possible to construct the low-energy effective action for the light fields. What is usually done is to study string S -matrix

elements and construct a classical action for the massless fields that reproduces them. Such an action is extremely useful since it can be written as a systematic expansion in number of derivatives, the higher derivatives being unimportant at low energies.

Since string theory and M theory live in ten and eleven dimensions respectively, in order to connect to four dimensional physics, one needs to compactify ten or eleven dimensions to four and construct solutions of the compactified equations of motion. Since supersymmetry makes small masses stable against radiative corrections (for example, it makes the Higgs mass natural) in an elegant way, one wants to compactify to four dimensions so as to preserve $\mathcal{N}=1$ supersymmetry in four dimensions. The requirement of $\mathcal{N}=1$ supersymmetry³ in four dimensions is also useful from a technical point of view, as it is much easier to find solutions to the equations of motion⁴. Restricting oneself to $\mathcal{N}=1$ compactifications does not guarantee low energy supersymmetry in the sense of giving rise to superpartners of $\mathcal{O}(\text{TeV})$, since supersymmetry can still be broken at around the compactification scale, which is near the string scale or the eleven dimensional Planck scale (typically much above the TeV scale).

Therefore, one has to find mechanisms within $\mathcal{N}=1$ compactifications to generate or at least accommodate a large hierarchy. If one wants a high string scale or eleven dimensional Planck scale ($\geq M_{unif}$), one mechanism to generate hierarchies is by strong gauge dynamics in the hidden sector. This works for many regions of the entire M theory moduli space – weakly [16] and strongly coupled [17] heterotic string theory, type IIA string theory [18] and M theory on G_2 manifolds [19]. Keeping the string scale high, a second mechanism is to utilize the discretuum of flux vacua obtained in flux compactifications of Type IIB string theory and obtain a small

³Compactifications preserving more supersymmetries in four dimensions are uninteresting phenomenologically as they do not give rise to chiral fermions.

⁴Compactifications satisfying supersymmetry conditions (which are first order equations) automatically obey the equations of motion and are also stable against quantum corrections.

scale by tuning the flux superpotential to be very small in Planck units [20, 21]. A third way of obtaining a small scale is to relax the requirement of a high string scale, making it sufficiently small⁵ [22]. Finally, it turns out that Type IIB flux compactifications cause *warping* of the extra dimensions which can also give rise to the observed hierarchy of scales [24]. In this work, we will analyze the consequences of many of the above mechanisms in detail in later sections.

⁵The precise value will depend on explicit constructions.

CHAPTER IV

Top-Down String Phenomenology

As mentioned in the previous subsection, in order to connect string/ M theory to four dimensional physics, we are interested in compactifications of string/ M theory to four dimensions with $\mathcal{N}=1$ supersymmetry.

In general, string compactifications fall into two general categories—one based on free or solvable world-sheet CFTs and the second based on compactification on a smooth compact manifold. Compactifications based on free conformal field theories (CFTs) are characterized by singular spaces called orbifolds. Compactifications based on smooth manifolds require the smooth manifold to satisfy certain conditions so as to have $\mathcal{N}=1$ supersymmetry in four dimensions. These are known as Calabi-Yau manifolds. On the other hand, phenomenologically interesting M theory compactifications with $\mathcal{N}=1$ supersymmetry in four dimensions are characterized by *singular* manifolds of G_2 holonomy. Specific kinds of singularities are required to obtain non-abelian gauge groups and chiral fermions. It is also important to realize that different regions of the M theory moduli space are connected to each other through a web of dualities [25].

There are two main approaches to string phenomenology within (ten-dimensional) string

theory. Historically, the first approach is concerned with the $E_8 \times E_8$ heterotic string constructions. The $E_8 \times E_8$ theory is interesting because it can produce $\mathcal{N}=1$ supersymmetry in four dimensions and it also has gauge fields which can generate chiral fermions in four dimensions. The most promising compactifications of the heterotic string giving rise to a semi-realistic spectrum and interactions are orbifold compactifications in the weakly coupled regime [26]. These have the advantage that CFT techniques can be used to compute the complete massless spectrum, as well as many of their interactions. Perturbative heterotic string compactifications on Calabi-Yau manifolds give a less detailed but global picture. Compactifications of the strongly coupled heterotic string have also been constructed [27, 28].

The other approach to string phenomenology is more recent. It was realized in the mid-1990s that type I, IIA and IIB string theories are actually different states in a single theory, which also includes states containing general configurations of D-branes (boundaries of open strings). This, together with the understanding of dualities, has led to a deeper understanding of type I/II, $\mathcal{N}=1$, four-dimensional vacua. The most promising models for phenomenological purposes in this approach are type II orientifold compactifications. Conformal field theory techniques in the open string sectors, which end on D-branes, allow for exact constructions of consistent $\mathcal{N}=1$, four-dimensional chiral models with non-Abelian gauge symmetry on type II orientifolds. Within this framework, chiral matter can appear on the worldvolume of D-branes at orbifold singularities and/or at the intersections of D-branes in the internal space (in type IIA picture). The intersecting D-brane configurations also have a T-dual description (in type IIB) in terms of D-branes with open string 2-form fluxes on them. As in the heterotic case, type II compactifications on Calabi-Yau manifolds are useful for a global picture.

Finally, one can study compactifications in eleven-dimensional M theory. It is believed that

the different ten-dimensional string theories are particular limits of a deeper eleven dimensional theory, known as M theory [25]. Even though a quantum description of M theory is not available at present, its low energy limit is described by eleven dimensional supergravity which is well understood. In the M theory approach, phenomenologically interesting compactifications on manifolds with G_2 holonomy (for $\mathcal{N}=1$ supersymmetry) require the presence of appropriate gauge and conical singularities. At present, it has not been possible to construct a physically interesting global compactification in this approach, because of its mathematical complexity. However, the existence of these compactifications is guaranteed by dualities with $E_8 \times E_8$ heterotic string theory and type IIA string theory [29, 30, 31]. Also, local constructions with phenomenologically interesting gauge groups and chiral spectrum have been constructed in the literature [32].

The first step towards obtaining a low energy description of String/ M theory compactifications is to derive the spectrum of massless particles. As mentioned above, heterotic and type II compactifications on orbifolds and orientifolds respectively have the advantage that CFT techniques can be employed to compute the complete massless spectrum. Therefore, a great amount of work on these compactifications has been done in the literature. However, since any given string compactification has to satisfy many stringy consistency conditions (such as the tadpole cancellation conditions), it is quite challenging to construct a global model with a massless spectrum which has three families, is MSSM-like, and does not have fractionally electrically charged states or charged chiral exotics.

Once the massless spectrum is determined, one has to construct the four dimensional low-energy effective action consistent with the symmetries of the theory. One first obtains the low-energy effective action in the *field theory approximation*. This means that the compactification

radius is assumed to be larger than the string length or the eleven dimensional Planck length, so that we can restrict attention to massless fields in the ten or eleven dimensional theory. One can then calculate higher order corrections to this approximation. We are interested in theories with $\mathcal{N}=1$ supersymmetry in four dimensions, which combined with gravity gives rise to $\mathcal{N}=1$ supergravity. The vacuum structure of $\mathcal{N}=1$ supergravity in four dimensions is specified completely by three functions—the (holomorphic) gauge kinetic function (f) which determines the gauge couplings, the (holomorphic) superpotential (W) which determines the Yukawa couplings and the Kähler potential (K) which is a general function of all the four dimensional chiral superfields and determines the Kähler metric for the matter fields among other things. The effects of higher order corrections to the field theory approximation can be incorporated within the $\mathcal{N}=1$ supergravity formalism by including them as corrections to the above three functions - K, W & f . These functions depend non-trivially on the closed string moduli which characterize the size and shape of the extra dimensions, and the matter fields. Deducing the dependence of the three functions K, W and f on the moduli is an important task. This can be done by the calculation of various string scattering amplitudes. Alternatively, part of the effective action can also be determined by a dimensional reduction of ten dimensional supergravity. In the four dimensional supergravity theory, these moduli are classically represented as *massless* chiral superfields. This is disastrous for two reasons: a) All four dimensional masses and couplings are functions of the moduli. So, unless the moduli are stabilized, the masses and couplings cannot be predicted. b) Massless scalars have been ruled out by cosmological and astrophysical observations. Therefore, one has to stabilize the moduli and make them massive. In addition, as emphasized in the previous chapter, one also has to break supersymmetry and generate the hierarchy between the Planck and electroweak scales.

Thus, starting from a string/ M theory compactification, it is an extremely daunting task to get a realistic matter spectrum, stabilize the moduli and break supersymmetry in a controlled manner in such a way as to generate the hierarchy.

In the following, we will focus on two corners of the M theory moduli space - that of type IIA string theory on toroidal orientifolds and M theory on G_2 manifolds. We will see that issues related to model-building such as constructing the massless chiral matter spectrum can be better understood in the type IIA picture while issues related to supersymmetry breaking and moduli stabilization can be better understood in the M theory picture. We will start with the type IIA constructions and then move on to M theory on G_2 manifolds.

4.1 Type IIA Intersecting D-brane Constructions

This section is devoted to the detailed study of a particular class of models based on type II string theory compactifications on toroidal orientifolds with Dp -branes wrapping intersecting cycles on the compact space. This approach to string model building is distinguished by its computability and simplicity, together with very appealing phenomenological possibilities. In these models, gauge interactions are confined to D-branes. Chiral fermions are open strings which are stretched between two intersecting branes. They are localized at the brane intersections. If certain conditions are satisfied, there will be massless scalars associated with the chiral fermions such that we have $\mathcal{N}=1$ supersymmetry in the effective field theory. Because of these attractive features, intersecting brane model building has drawn considerable attention in recent years and several semi-realistic models with an MSSM like spectrum have been constructed [33].

To test these approximate clues and to begin to test string theory, only reproducing the SM

particle content is not enough. Numerical predictions must be made. In addition, a successful theory should not just explain existing data, it must also make predictions which can be tested in future experiments. For the brane models, if supersymmetry exists and is softly broken, soft SUSY breaking terms have to be calculated and tested by future experimental measurements. A fair amount of work on the low-energy effective action of intersecting D-brane models has been done. The stability of these kind of models has been discussed in [34]. The issues of tree level gauge couplings, gauge threshold corrections and gauge coupling unification has been addressed in [35, 36, 37, 38, 39, 40, 41]. Yukawa couplings and higher point scattering have been studied in [42, 43, 44, 45]. Some preliminary results for the Kähler metric have been obtained in [46]. A more complete derivation of the Kähler metric directly from open/closed string scattering amplitudes has been done in [47, 49], which we use in this section.

At present, the closely related issues of moduli stabilization and supersymmetry breaking such as to give rise to low energy supersymmetry have not been understood well enough in these compactifications. These can be better addressed in flux compactifications of type IIB string theory, which are T-dual to these compactifications. In this section, we have taken a phenomenological approach, parametrizing the effects of supersymmetry breaking in a self-consistent way and examining the consequences. Even though the supersymmetry breaking effects have not been derived from first principles, it should still be preferred to a blind parameterization of the mechanism of SUSY breaking and its transmission to the observable sector. In the absence of a complete supersymmetry-breaking model, such a parameterization, in terms of non-zero F -terms with the assumption of vanishing vacuum energy is useful as it gives us some idea about the low energy consequences of these constructions. Our main goal here is to use the results of [47] to calculate and analyze effective low energy soft supersymmetry breaking

terms. We also look at some of their dark matter applications.

4.1.1 General construction of intersecting brane models.

In this section, we will briefly review the basics of constructing these models. More comprehensive treatments can be found in [50, 51, 52, 53, 54]. The setup is as follows - we consider type *IIA* string theory compactified on a six dimensional manifold \mathcal{M} . It is understood that we are looking at the large volume limit of compactification, so that perturbation theory is valid. In general, there are K stacks of intersecting D6-branes filling four dimensional Minkowski space-time and wrapping internal homology 3-cycles of \mathcal{M} . Each stack P consists of N_P coincident D6 branes whose worldvolume is $M_4 \times \Pi_P$, where Π_P is the corresponding homology class of each 3-cycle. The closed string degrees of freedom reside in the entire ten dimensional space, which contain the geometric scalar moduli fields of the internal space besides the gravitational fields. The open string degrees of freedom give rise to the gauge theory on the D6-brane worldvolumes, with gauge group $\Pi_P U(N_P)$. In addition, there are open string modes which split into states with both ends on the same stack of branes as well as those connecting different stacks of branes. The latter are particularly interesting. If for example, the 3-cycles of two different stacks, say Π_P and Π_Q intersect at a single point in \mathcal{M} , the lowest open string mode in the Ramond sector corresponds to a chiral fermion localized at the four dimensional intersection of P and Q transforming in the bifundamental of $U(N_P) \times U(N_Q)$ [55]. The net number of left handed chiral fermions in the ab sector is given by the intersection number $I_{PQ} \equiv [\Pi_P] \cdot [\Pi_Q]$.

The propagation of massless closed string RR modes on the compact space \mathcal{M} under which the D-branes are charged, requires some consistency conditions to be fulfilled. These are known as the *RR* tadpole-cancellation conditions, which basically means that the net *RR* charge of

the configuration has to vanish [56]. In general, there could be additional RR sources such as orientifold planes or background fluxes. So they have to be taken into account too. Another desirable constraint which the models should satisfy is $\mathcal{N}=1$ supersymmetry. Imposing this constraint on the closed string sector requires that the internal manifold \mathcal{M} be a Calabi-Yau manifold. We will see shortly that imposing the same constraint on the open string sector leads to a different condition.

A technical remark on the practical formulation of these models is in order. Till now, we have described the construction in type *IIA* string theory. However, it is also possible to rephrase the construction in terms of type *IIB* string theory. The two pictures are related by T-duality. The more intuitive picture of type *IIA* intersecting D-branes is converted to a picture with type *IIB* D-branes having background magnetic fluxes on their world volume. It is useful to remember this equivalence as it turns out that in many situations, it is more convenient to do calculations in type *IIB*.

Most of the realistic models constructed in the literature involve toroidal (T^6) compactifications or orbifold/orientifold quotients of those. In particular, orientifolding introduces O6 planes as well as mirror branes wrapping 3-cycles which are related to those of the original branes by the orientifold action. For simplicity, the torus (T^6) is assumed to be factorized into three 2-tori, i.e $T^6 = T^2 \times T^2 \times T^2$. Many examples of the above type are known, especially with those involving orbifold groups - i) $Z_2 \times Z_2$ [57] ii) $Z_4 \times Z_2$ [58], iii) Z_4 [59], iv) Z_6 [60], etc.

4.1.2 A local MSSM-like model

In order to make contact with realistic low energy physics while keeping supersymmetry intact, we are led to consider models which give rise to a chiral spectrum close to that of the MSSM. In any case, it is a useful first step to analyze. It has been shown that this requires us to perform an orientifold twist. A stack of N_P D6 branes wrapping a 3-cycle not invariant under the orientifold projection will yield a $U(N_P)$ gauge group, otherwise we get a real ($SO(2N_P)$) or pseudoreal ($USp(2N_P)$) gauge group.

Using the above fact, the brane content for an MSSM-like chiral spectrum with the correct intersection numbers has been presented in [42]. Constructions with more than four stacks of branes can be found in [61]. In the simplest case, there are four stacks of branes which give rise to the initial gauge group : $U(3)_a \times Sp(2)_b \times U(1)_c \times U(1)_d$, where a, b, c & d label the different stacks. The intersection numbers $I_{PQ} = [\Pi_P] \cdot [\Pi_Q]$ between a D6-brane stack P and a D6-brane stack Q is given in terms of the 3-cycles $[\Pi_P]$ and $[\Pi_Q]$, which are assumed to be factorizable.

$$[\Pi_P] \equiv [(n_P^1, m_P^1) \otimes (n_P^2, m_P^2) \otimes (n_P^3, m_P^3)] \quad (4.1)$$

where (n_P^i, m_P^i) denote the wrapping numbers on the i^{th} 2-torus. The $O6$ planes are wrapped on 3-cycles :

$$[\Pi_{O6}] = \bigotimes_{r=1}^3 [(1, 0)]^r \quad (4.2)$$

Note that for stack b , the mirror brane b^* lies on top of b . So even though $N_b = 1$, it can be thought of as a stack of two D6 branes, which give an $USp(2) \cong SU(2)$ group under the orientifold projection.

The brane wrapping numbers are shown in Table 4.1 and the chiral particle spectrum from

Stack	Number of Branes	Gauge Group	(n_α^1, m_α^1)	(n_α^2, m_α^2)	(n_α^3, m_α^3)
<i>Baryonic</i>	$N_a = 3$	$U(3) = SU(3) \times U(1)_a$	$(1, 0)$	$(1/\rho, 3\rho)$	$(1/\rho, -3\rho)$
<i>Left</i>	$N_b = 1$	$USp(2) \cong SU(2)$	$(0, 1)$	$(1, 0)$	$(0, -1)$
<i>Right</i>	$N_c = 1$	$U(1)_c$	$(0, 1)$	$(0, -1)$	$(1, 0)$
<i>Leptonic</i>	$N_d = 1$	$U(1)_d$	$(1, 0)$	$(1/\rho, 3\rho)$	$(1/\rho, -3\rho)$

Table 4.1: Brane content for an MSSM-like spectrum. The mirror branes a^*, b^*, c^*, d^* are not shown. ρ can take values 1, $1/3$. For concreteness, we take $\rho = 1$ for calculating the soft terms. However, the parameter space for the soft terms remains the same for both $\rho = 1$ and $\rho = 1/3$.

these intersecting branes are shown in Table 4.2.

4.1.2.1 Getting the MSSM

The above spectrum is free of chiral anomalies. However, it has an anomalous $U(1)$ given by $U(1)_a + U(1)_d$. This anomaly is canceled by a generalized Green-Schwarz mechanism [51], which gives a Stueckelberg mass to the $U(1)$ gauge boson. The two nonanomalous $U(1)$ s are identified with $(B - L)$ and the third component of right-handed weak isospin $U(1)_R$ [42]. In orientifold models, it could sometimes happen that some nonanomalous $U(1)$ s also get a mass by the same mechanism, the details of which depend on the specific wrapping numbers. It turns out that in the above model, two massless $U(1)$ s survive. In order to break the two $U(1)$ s down to $U(1)_Y$, some fields carrying non-vanishing lepton number but neutral under $U(1)_Y$ are assumed to develop vevs. This can also be thought of as the geometrical process of brane recombination [62].

fields	sector	I	$SU(3)_c \times SU(2)_L$	$U(1)_a$	$U(1)_c$	$U(1)_d$	$U(1)_Y$
Q_L	(a, b)	3	$(3, 2)$	1	0	0	1/6
U_R	(a, c)	3	$(3, 1)$	-1	1	0	-2/3
D_R	(a, c^*)	3	$(3, 1)$	-1	-1	0	1/3
L	(d, b)	3	$(1, 2)$	0	0	1	-1/2
E_R	(d, c^*)	3	$(1, 1)$	0	-1	-1	1
N_R	(d, c)	3	$(1, 1)$	0	1	-1	0
H_u	(b, c)	1	$(1, 2)$	0	-1	0	1/2
H_d	(b, c^*)	1	$(1, 2)$	0	1	0	-1/2

Table 4.2: The MSSM spectrum from intersecting branes. The hypercharge normalization is given by $Q_Y = \frac{1}{6}Q_a - \frac{1}{2}Q_c - \frac{1}{2}Q_d$.

4.1.2.2 Global embedding and supersymmetry breaking

As can be checked from Table 1, the brane content by itself does not satisfy the RR tadpole cancellation conditions :

$$\sum_{\alpha} ([\Pi_{\alpha}] + [\Pi_{\alpha^*}]) = 32 [\Pi_{O6}] \quad (4.3)$$

Therefore, this construction has to be embedded in a bigger one, with extra RR sources included. There are various ways to do this such as including hidden D-branes or adding background closed string fluxes in addition to the open string ones. As a bonus, this could also give rise to spontaneous supersymmetry breaking. With extra D-branes, one might consider the possibility of gaugino condensation in the hidden sector [63]. Alternatively, one could consider turning on background closed string $NS-NS$ and RR fluxes which generate a non-trivial

effective superpotential for moduli, thereby stabilizing many of them.

In this work, we will leave open the questions of actually embedding the above model in a global one and the mechanism of supersymmetry breaking. We shall assume that the embedding has been done and also only *parametrize* the supersymmetry breaking, in the spirit of [64, 65, 66]. We are encouraged because there exists a claim of a concrete mechanism for the global embedding of (the T-dual of) this model as well as supersymmetry breaking [67].

4.1.2.3 Exotic matter and μ problem

The above local model is very simple in many respects, especially with regard to gauge groups and chiral matter. However, it also contains exotic matter content which is non-chiral. These non-chiral fields are related to the untwisted open string moduli - the D-brane positions and Wilson lines. The presence of these non-chiral fields is just another manifestation of the old moduli problem of supersymmetric string vacua. However, it has been argued [68] that mass terms for the above moduli can be generated by turning on a F - theory 4-form flux. One then expects that a proper understanding of this problem will result in a stabilization of all the moduli. As explained in [67], there could be $\mathcal{N}=1$ embeddings of this local model in a global construction. This requires additional D-brane sectors and background closed string 3-form fluxes. The other D-brane sectors add new gauge groups as well as chiral matter, some of which could be charged under the MSSM gauge group. This may introduce chiral exotics in the spectrum, an undesirable situation. However, many of these exotics uncharged under the MSSM gauge group can be made to go away by giving vevs to scalars parametrizing different flat directions. In this work, we assume that there exists an embedding such that there are no chiral exotics charged under the MSSM. Such exotics can cause two types of problems. It is

of course essential that no states exist that would already have been observed. It seems likely that can be arranged. In addition, states that would change the RGE running and details of the calculations have to be taken into account eventually.

The higgs sector in the local model arises from strings stretching between stacks b and c . However, the net chirality of the bc sector is zero, since the intersection number I_{bc} is zero. The higgs sector in the above model has a μ term, which has a geometrical interpretation. The real part of the μ parameter corresponds to the separation between stacks b and c in the first torus, while the imaginary part corresponds to a Wilson line phase along the 1-cycle wrapped on the first torus. These correspond to flat directions of the moduli space. Adding background closed string fluxes may provide another source of μ term [?], which will lift the flat direction in general. Thus, the effective μ term relevant for phenomenology is determined by the above factors and the problem of obtaining an electroweak scale μ term from a fundamental model remains open. In this work, therefore, we will not attempt to calculate μ , and fix it by imposing electroweak symmetry breaking (EWSB). It is important to study further the combined effect of the several contributions to μ and to EWSB.

4.1.2.4 Type IIA - type IIB equivalence

As mentioned earlier, it is useful to think about this model in terms of its T-dual equivalent. In type *IIB*, we are dealing with D9 branes wrapped on $T^2 \times T^2 \times T^2$ with an open string background magnetic flux \mathcal{F}^1 turned on. Therefore the D9-branes have in general mixed Dirichlet and Neumann boundary conditions. The flux has two parts - one coming from the antisymmetric tensor (b^j) and the other from the gauge flux (F^j) so that :

$$\mathcal{F}^j = b^j + 2\pi\alpha' F^j \tag{4.4}$$

The above compactification leads to the following closed string Kähler and complex structure moduli, each of which are three in number for this model:

$$T'^j = b^j + iR_1'^j R_2'^j \sin(\alpha'^j); \quad U'^j = \frac{R_2'^j}{R_1'^j} e^{i\alpha'^j}; \quad j = 1, 2, 3. \quad (4.5)$$

where $R_1'^j$ and $R_2'^j$ are lengths of the basis lattice vectors characterizing the torus $T^{2,j}$ and α^j is the angle between the two basis vectors of the torus $T^{2,j}$. By performing a T-duality in the y direction of each torus $T^{2,j}$, the D9 brane with flux \mathcal{F}^j is converted to a D6 brane with an angle θ^j with respect to the x-axis. This is given by [69]:

$$\tan(\pi \theta^j) = \frac{f^j}{\text{Im}(T'^j)} \quad (4.6)$$

where f^j is defined by the quantization condition for the net 2-form fluxes \mathcal{F}^j as

$$f^j \equiv \frac{1}{(2\pi)^2 \alpha'} \int_{T^{2,j}} \mathcal{F}^j = \frac{m^j}{n^j}; \quad m^j, n^j \in \mathbf{Z}, \quad (4.7)$$

Using the above equation and the relation between the type *IIA* and type *IIB*:

$$T^j = -\frac{\alpha'}{U'^j}, \quad U^j = -\frac{\alpha'}{T'^j}, \quad j = 1, 2, 3. \quad (4.8)$$

$$R_1^j = R_1'^j, \quad R_2^j = \frac{1}{R_2'^j} \quad (4.9)$$

we get the corresponding type *IIA* relation:

$$\tan(\pi \theta^j) = \frac{m^j}{n^j} \frac{|U^j|^2}{\text{Im}(U^j)}; \quad j = 1, 2, 3. \quad (4.10)$$

The unprimed symbols correspond to the type *IIA* version while the primed ones to the type *IIB*.

4.1.2.5 $\mathcal{N}=1$ *SUSY*

We now look at the $\mathcal{N}=1$ supersymmetry constraint on the open string sector. In type *IIA*, this leads to a condition on the angles θ^j [55]:

$$\begin{aligned} \theta^1 + \theta^2 + \theta^3 &= 0 \pmod{2} \quad \text{or} \\ \sum_{j=1}^3 \frac{m^j}{n^j} \frac{|U^j|^2}{\text{Im}(U^j)} &= \prod_{j=1}^3 \frac{m^j}{n^j} \frac{|U^j|^2}{\text{Im}(U^j)} \end{aligned} \quad (4.11)$$

which after T-duality leads to a condition on the fluxes in type *IIB*.

4.1.3 Low energy effective action and soft terms

We now analyze the issue of deriving the four dimensional $\mathcal{N}=1$ low energy effective action of these intersecting brane models. In the type *IIB* picture, this has been done in [70, 71] by Kaluza Klein reduction of the Dirac-Born-Infeld and Chern-Simons action. The effective action can also be obtained by explicitly computing disk scattering amplitudes involving open string gauge and matter fields as well as closed string moduli fields and deducing the relevant parts of the effective action directly. This has been done in [47]. We will follow the results of [47] in our analysis.

The $\mathcal{N}=1$ supergravity action thus obtained is encoded by three functions, the Kähler potential K , the superpotential W and the gauge kinetic function f [72]. Each of them will depend on the moduli fields describing the background of the model. One point needs to be emphasized. When we construct the effective action and its dependence on the moduli fields, we need to do so in terms of the moduli s , t and u in the field theory basis, in contrast to the S , T and U moduli in the string theory basis [47]. In type *IIA*, the real part of the field theory

s , u and t moduli are related to the corresponding string theory S , U and T moduli by :

$$\begin{aligned}
\text{Re}(s) &= \frac{e^{-\phi_4}}{2\pi} \left(\frac{\sqrt{\text{Im } U^1 \text{Im } U^2 \text{Im } U^3}}{|U^1 U^2 U^3|} \right) \\
\text{Re}(u^j) &= \frac{e^{-\phi_4}}{2\pi} \left(\sqrt{\frac{\text{Im } U^j}{\text{Im } U^k \text{Im } U^l}} \right) \left| \frac{U^k U^l}{U^j} \right| \quad (j, k, l) = (\overline{1, 2, 3}) \\
\text{Re}(t^j) &= \frac{i\alpha'}{T^j}
\end{aligned} \tag{4.12}$$

where j stands for the j^{th} 2-torus. The above formulas can be inverted to yield the string theory U moduli in terms of the field theory moduli s and u .

$$\frac{|U^j|^2}{\text{Im}(U^j)} = \sqrt{\frac{\text{Re}(u^k) \text{Re}(u^l)}{\text{Re}(u^j) \text{Re}(s)}} \quad (j, k, l) = (\overline{1, 2, 3}) \tag{4.13}$$

The holomorphic gauge kinetic function for a D6 brane stack P is given by :

$$\begin{aligned}
f_P &= \frac{1}{\kappa_P} (n_P^1 n_P^2 n_P^3 s - n_P^1 m_P^2 m_P^3 u^1 - n_P^2 m_P^1 m_P^3 u^2 - n_P^3 m_P^1 m_P^2 u^3) \\
g_{D6_P}^{-2} &= |\text{Re}(f_P)|
\end{aligned} \tag{4.14}$$

The extra factor κ_P is related to the difference between the gauge couplings for $U(N_P)$ and $Sp(2N_P)$, $SO(2N_P)$. $\kappa_P = 1$ for $U(N_P)$ and $\kappa_P = 2$ for $Sp(2N_P)$ or $SO(2N_P)$ [73].

The SM hypercharge $U(1)_Y$ gauge group is a linear combination of several $U(1)$ s:

$$Q_Y = \frac{1}{6} Q_a - \frac{1}{2} Q_c - \frac{1}{2} Q_d. \tag{4.15}$$

Therefore the gauge kinetic function for the $U(1)_Y$ gauge group is determined to be [40]:

$$f_Y = \frac{1}{6} f_{D_a} + \frac{1}{2} f_{D_c} + \frac{1}{2} f_{D_d}. \tag{4.16}$$

The Kähler potential to the second order in open string matter fields is given by :

$$K(M, \bar{M}, C, \bar{C}) = \hat{K}(M, \bar{M}) + \sum_{\text{untwisted } i, j} \tilde{K}_{C_i \bar{C}_j}(M, \bar{M}) C_i \bar{C}_j + \sum_{\text{twisted}, \theta} \tilde{K}_{C_\theta \bar{C}_\theta}(M, \bar{M}) C_\theta \bar{C}_\theta \tag{4.17}$$

where M collectively denote the moduli; C_i denote untwisted open string moduli which comprise the D-brane positions and the Wilson line moduli which arise from strings with both ends on the same stack; and C_θ denote twisted open string states arising from strings stretching between different stacks.

The open string moduli fields could be thought of as matter fields from the low energy field theory point of view. The untwisted open string moduli represent non-chiral matter fields and so do not correspond to the MSSM. For the model to be realistic, they have to acquire large masses by some additional mechanism, as already explained in section 4.1.2.3.

Let's now write the Kähler metric for the twisted moduli arising from strings stretching between stacks P and Q , and comprising 1/4 BPS brane configurations. In the type IIA picture, this is given by [44, 47]:

$$\tilde{K}_{C_{\theta_{PQ}} \bar{C}_{\theta_{PQ}}} \equiv \tilde{K}_{PQ} = e^{\phi_4} \left(e^{\gamma_E \sum_{j=1}^3 \theta_{PQ}^j} \prod_{j=1}^3 \left[\sqrt{\frac{\Gamma(1 - \theta_{PQ}^j)}{\Gamma(\theta_{PQ}^j)}} (t^j + \bar{t}^j)^{-\theta_{PQ}^j} \right] \right) \quad (4.18)$$

where $\theta_{PQ}^j = \theta_P^j - \theta_Q^j$ is the angle between branes in the j^{th} torus and ϕ_4 is the four dimensional dilaton. From (4.12), ϕ_4 can be written as $(\text{Re}(s) \text{Re}(u_1) \text{Re}(u_2) \text{Re}(u_3))^{-1/4}$. String-loop corrections to the Kähler metric have been calculated for some orientifolds in [48]. The above Kähler metric depends on the field theory dilaton and complex structure moduli u^j through ϕ_4 and θ_{PQ} . It is to be noted that (4.18) is a product of two factors, one which explicitly depends on the field theory s and u moduli (e^{ϕ_4}), and the other which implicitly depends on the s and u moduli (through the dependence on θ_{PQ}^j). Thus, \tilde{K}_{PQ} can be symbolically written as :

$$\tilde{K}_{PQ} = e^{\phi_4} \tilde{K}_{PQ}^0 \quad (4.19)$$

The Kähler metric for 1/2 BPS brane configurations is qualitatively different from that of the 1/4 BPS brane configurations mentioned above. Generically, these cases arise if both branes P

and Q have a relative angle $\theta_{PQ}^j = 0, 1$ in the same complex plane j . It is worthwhile to note that the higgs fields in Table 4.2 form a 1/2 BPS configuration and are characterized by the following Kähler metric [74]:

$$\tilde{K}_{PQ}^{higgs} = ((s + \bar{s})(u^1 + \bar{u}^1)(t^2 + \bar{t}^2)(t^3 + \bar{t}^3))^{-1/2} \quad (4.20)$$

An important point about the above expressions needs to be kept in mind. These expressions for the Kähler metric has been derived using *tree level* scattering amplitudes and with Wilson line moduli turned *off*. Carefully taking the Wilson lines into account as in [43], we see that the Kähler metric has another multiplicative factor which depends on the Wilson line moduli as well as t moduli in type *IIA*. If the Wilson line moduli do not get a vev, then our analysis goes through. However, if they do, they change the dependence of the metric on the t moduli. As will be explained later, we only choose the u moduli dominated case for our phenomenological analysis, so none of our results will be modified.

The superpotential is given by:

$$W = \hat{W} + \frac{1}{2}\mu_{\alpha\beta}(M) C^\alpha C^\beta + \frac{1}{6}Y_{\alpha\beta\gamma}(M) C^\alpha C^\beta C^\gamma + \dots \quad (4.21)$$

In our phenomenological analysis, we have not included the Yukawa couplings for simplicity. But as explained later, in the u moduli dominant SUSY breaking case, the soft terms are independent of the Yukawa couplings and will not change the phenomenology.

4.1.3.1 Soft terms in general soft broken $\mathcal{N}=1$, $D = 4$ supergravity Lagrangian

From the gauge kinetic function, Kähler potential and the superpotential, it is possible to find formulas for the *normalized* soft parameters - the gaugino mass parameters, mass squared

parameter for scalars and the trilinear parameters respectively. These are given by [66]:

$$\begin{aligned}
M_P &= \frac{1}{2 \operatorname{Re} f_P} (F^M \partial_M f_P) \\
m_{PQ}^2 &= (m_{3/2}^2 + V_0) - \sum_{M,N} \bar{F}^{\bar{M}} F^N \partial_{\bar{M}} \partial_N \log(\tilde{K}_{PQ}) \\
A_{PQR} &= F^M [\hat{K}_M + \partial_M \log(Y_{PQR}) - \partial_M \log(\tilde{K}_{PQ} \tilde{K}_{QR} \tilde{K}_{RP})]
\end{aligned} \tag{4.22}$$

For our purposes, P, Q and R denote brane stacks. So M_P denotes the gaugino mass parameter arising from stack P ; m_{PQ}^2 denotes mass squared parameters arising from strings stretching between stacks P and Q and Y_{PQR} denotes Yukawa terms arising from the triple intersection of stacks P, Q and R . The terms on the RHS without the indices P, Q and R are flavor independent. Also, M and N run over the closed string moduli. F^M stands for the auxiliary fields of the moduli in general. Supersymmetry is spontaneously broken if these fields get non-vanishing vevs. It is assumed here that the auxiliary fields D have vanishing vevs. Their effect on the soft terms can be calculated as in [77], which we assume to be zero. These formulas have been derived for the case when the Kähler metric for the observable (MSSM) fields is diagonal and universal in flavor space. In principle, there are also off-diagonal terms in the Kähler metric. They relate twisted open string states at different intersections and therefore are highly suppressed. We neglect the off-diagonal terms in our study. If the separations between the intersections are very small, the off-diagonal terms or non-universal diagonal terms may have observable effects leading to interesting flavor physics.

The effective $\mathcal{N} = \infty, 4d$ field theory is assumed to be valid at some high scale, presumably the string scale. The string scale in our analysis is taken to be the unification scale ($\sim 2 \times 10^{16}$ GeV). We then need to use the renormalization group equations (RGE) to evaluate these parameters at the electroweak scale. In this work, as mentioned before, it is assumed that the

non-chiral exotics have been made heavy by some mechanism and there are no extra matter fields at any scale between the electroweak scale and the unification scale. This is also suggested by gauge coupling unification at the unification scale.

One might wonder whether including the Yukawas in the analysis may lead to significant modifications in the spectrum at low energies because of their presence in the formulas for the soft terms (4.22). However, this does not happen. This is because the Yukawa couplings ($Y_{\alpha\beta\gamma}$) appearing in the soft terms are *not* the physical Yukawa couplings ($Y_{\alpha\beta\gamma}^{\text{ph}}$). The two are related by:

$$Y_{\alpha\beta\gamma}^{\text{ph}} = Y_{\alpha\beta\gamma} \frac{\hat{W}^*}{|\hat{W}|} e^{\hat{K}/2} (\tilde{K}_\alpha \tilde{K}_\beta \tilde{K}_\gamma)^{-1/2} \quad (4.23)$$

The Yukawa couplings ($Y_{\alpha\beta\gamma}$) between fields living at brane intersections in intersecting D-brane models arise from worldsheet instantons involving three different boundary conditions [50]. These semi-classical instanton amplitudes are proportional to e^{-A} where A is the worldsheet area. They have been shown to depend on the Kähler (t) moduli (complexified area) and the Wilson line moduli [42] in type *IIA*. Although the physical Yukawas ($Y_{\alpha\beta\gamma}^{\text{ph}}$) depend on the u moduli through their dependence on the Kähler potential, the fact that $Y_{\alpha\beta\gamma}$ do not depend on the u moduli in type *IIA* ensures that in the F^u dominant supersymmetry breaking case, the soft terms are independent of $Y_{\alpha\beta\gamma}$.

Thus our analysis is similar in spirit to those in the case of the heterotic string, where dilaton dominated supersymmetry breaking and moduli dominated supersymmetry breaking are analyzed as extreme cases. It should be remembered however, that T-duality interchanges the field theory (t) and (u) moduli. Thus what we call u moduli in type *IIA*, become t moduli in type *IIB* and vice versa. In a general situation, in which the F -terms of all the moduli get vevs, the situation is much more complicated and a more general analysis needs to be done.

This is left for the future.

4.1.3.2 Soft terms in intersecting brane models

We calculate the soft terms in type IIA picture. As already explained, we assume that only F -terms for u moduli get non-vanishing vevs. In terms of the goldstino angle θ as defined in [66], we have $\theta = 0$. We assume the cosmological constant is zero and introduce the following parameterization of F^{u^i} :

$$F^{u^i} = \sqrt{3}m_{3/2}(u^i + \bar{u}^i)\Theta_i e^{-i\gamma_i} \quad \text{for } i = 1, 2, 3 \quad (4.24)$$

with $\sum |\Theta_i|^2 = 1$. To calculate the soft terms, we need to know the derivatives of the Kähler potential with respect to u . For a chiral field C arising from open strings stretched between stacks P and Q , we denote its Kähler potential as \tilde{K}_{PQ} . From (4.19), we see that their derivatives with respect to u^i are

$$\frac{\partial \log \tilde{K}_{PQ}}{\partial u^i} = \sum_{j=1}^3 \frac{\partial \log \tilde{K}_{PQ}^0}{\partial \theta_{PQ}^j} \frac{\partial \theta_{PQ}^j}{\partial u^i} + \frac{-1}{4(u^i + \bar{u}^i)} \quad (4.25)$$

$$\frac{\partial^2 \log \tilde{K}_{PQ}}{\partial u^i \partial \bar{u}^j} = \sum_{k=1}^3 \left(\frac{\partial \log \tilde{K}_{PQ}^0}{\partial \theta_{PQ}^k} \frac{\partial^2 \theta_{PQ}^k}{\partial u^i \partial \bar{u}^j} + \frac{\partial^2 \log \tilde{K}_{PQ}^0}{\partial (\theta_{PQ}^k)^2} \frac{\partial \theta_{PQ}^k}{\partial u^i} \frac{\partial \theta_{PQ}^k}{\partial \bar{u}^j} + \frac{\delta_{ij}}{4(u^i + \bar{u}^i)^2} \right) \quad (4.26)$$

From the Kähler potential in eq.(4.18), we have

$$\Psi(\theta_{PQ}^j) \equiv \frac{\partial \log \tilde{K}_{PQ}^0}{\partial \theta_{PQ}^j} = \gamma_E + \frac{1}{2} \frac{d}{d\theta_{PQ}^j} \ln \Gamma(1 - \theta_{PQ}^j) - \frac{1}{2} \frac{d}{d\theta_{PQ}^j} \ln \Gamma(\theta_{PQ}^j) - \log(t^j + \bar{t}^j) \quad (4.27)$$

$$\Psi'(\theta_{PQ}^j) \equiv \frac{\partial^2 \log \tilde{K}_{PQ}^0}{\partial (\theta_{PQ}^j)^2} = \frac{d\Psi(\theta_{PQ}^j)}{d\theta_{PQ}^j} \quad (4.28)$$

The angle $\theta_{PQ}^j \equiv \theta_P^j - \theta_Q^j$ can be written in terms of u moduli as:

$$\tan(\pi\theta_P^j) = \frac{m_P^j}{n_P^j} \sqrt{\frac{\text{Re}u^k \text{Re}u^l}{\text{Re}u^j \text{Re}s}} \quad \text{where } (j, k, l) = (\overline{1, 2, 3}) \quad (4.29)$$

Then we have

$$\theta_{PQ}^{j,k} \equiv (u^k + \bar{u}^k) \frac{\partial \theta_{PQ}^j}{\partial u^k} = \begin{cases} [-\frac{1}{4\pi} \sin(2\pi\theta^j)]_Q^P & \text{when } j = k \\ [\frac{1}{4\pi} \sin(2\pi\theta^j)]_Q^P & \text{when } j \neq k \end{cases} \quad (4.30)$$

where we have defined $[f(\theta^j)]_Q^P = f(\theta_P^j) - f(\theta_Q^j)$. The second order derivatives are

$$\theta_{PQ}^{j,k\bar{l}} \equiv (u^k + \bar{u}^k)(u^l + \bar{u}^l) \frac{\partial^2 \theta_{PQ}^j}{\partial u^k \partial \bar{u}^l} = \begin{cases} \frac{1}{16\pi} [\sin(4\pi\theta^j) + 4 \sin(2\pi\theta^j)]_Q^P & \text{when } j = k = l \\ \frac{1}{16\pi} [\sin(4\pi\theta^j) - 4 \sin(2\pi\theta^j)]_Q^P & \text{when } j \neq k = l \\ -\frac{1}{16\pi} [\sin(4\pi\theta^j)]_Q^P & \text{when } j = k \neq l \text{ or } j = l \neq k \\ \frac{1}{16\pi} [\sin(4\pi\theta^j)]_Q^P & \text{when } j \neq k \neq l \neq j \end{cases} \quad (4.31)$$

Now, one can substitute eq.(4.24-4.31) to the general formulas of soft terms in eq.(4.22). The formulas for the soft parameters in terms of the wrapping numbers of a general intersecting D-brane model are given by:

- Gaugino mass parameters

$$M_P = \frac{-\sqrt{3}m_{3/2}}{\text{Ref}_P} \sum_{j=1}^3 (\text{Re}u^j \Theta_j e^{-i\gamma_j} n_P^j m_P^k m_P^l) \quad (j, k, l) = (\overline{1, 2, 3}) \quad (4.32)$$

As an example, the $M_{\tilde{g}}$ can be obtained by putting $P = a$ and using the appropriate wrapping numbers, as in Table 4.1.

- Trilinears :

$$A_{PQR} = -\sqrt{3}m_{3/2} \sum_{j=1}^3 \left[\Theta_j e^{-i\gamma_j} \left(1 + \left(\sum_{k=1}^3 \theta_{PQ}^{k,j} \Psi(\theta_{PQ}^k) - \frac{1}{4} \right) + \left(\sum_{k=1}^3 \theta_{RP}^{k,j} \Psi(\theta_{RP}^k) - \frac{1}{4} \right) \right) \right] + \frac{\sqrt{3}}{2} m_{3/2} \Theta_1 e^{-i\gamma_1} \quad (4.33)$$

This arises in general from the triple intersections PQ , QR and RP , where PQ and RP are 1/4 BPS sector states and QR is a 1/2 BPS state. QR being the higgs field, has a special contribution to the trilinear term compared to PQ and RP . So as an example, $A_{Q_L H_u U_R}$ can be obtained as a triple intersection of ab , bc and ca , as seen from Table 4.2.

- Scalar mass squared (1/4 BPS) :

$$m_{PQ}^2 = m_{3/2}^2 \left[1 - 3 \sum_{m,n=1}^3 \Theta_m \Theta_n e^{-i(\gamma_m - \gamma_n)} \left(\frac{\delta_{mn}}{4} + \sum_{j=1}^3 (\theta_{PQ}^{j,m\bar{n}} \Psi(\theta_{PQ}^j) + \theta_{PQ}^{j,m} \theta_{PQ}^{j,\bar{n}} \Psi'(\theta_{PQ}^j)) \right) \right] \quad (4.34)$$

By using the definitions in eq.(4.30, 4.31), we see that $\theta_{PQ}^{j,k}$ and $\theta_{PQ}^{j,k\bar{l}}$ do not depend on the vevs of u moduli: u^j . As an example, the squark mass squared $m_{\tilde{Q}}^2$ can be obtained by putting $P, Q = a, b$; as can be seen again from Table 4.2.

We can now use the wrapping numbers in Table 4.1 to get explicit expressions for the soft terms for the particular model in terms of the s, t and u moduli and the parameters $m_{3/2}$, γ_i and Θ_i , $i = 1, 2, 3$. The expressions for the trilinear A parameters and scalar mass squared parameters (except those for the up and down type higgs) are provided in the Appendix A. Using Table 4.1, the formula for the gaugino mass parameters and the mass squared parameters for the up and down higgs are given by:

- Gaugino mass parameters:

$$M_{\tilde{B}} = 3\sqrt{3}m_{3/2} \frac{12e^{-i\gamma_1} \text{Re}u_1 \Theta_1 + e^{-i\gamma_3} \text{Re}u_3 \Theta_3}{3\text{Re}u_3 + 4\text{Re}s + 36\text{Re}u_1} \quad (4.35)$$

$$M_{\tilde{W}} = \sqrt{3}m_{3/2} e^{-i\gamma_2} \Theta_2 \quad (4.36)$$

$$M_{\tilde{g}} = \sqrt{3}m_{3/2} \frac{9e^{-i\gamma_1} \text{Re}u_1 \Theta_1}{\text{Re}s + 9\text{Re}u_1} \quad (4.37)$$

Stack	Number of Branes	Gauge Group	(θ_P^1)	(θ_P^2)	(θ_P^3)
<i>Baryonic</i>	$N_a = 3$	$U(3) = SU(3) \times U(1)_a$	0	α	$-\alpha$
<i>Left</i>	$N_b = 1$	$USp(2) \cong SU(2)$	$\frac{1}{2}$	0	$-\frac{1}{2}$
<i>Right</i>	$N_c = 1$	$U(1)_c$	$\frac{1}{2}$	$-\frac{1}{2}$	0
<i>Leptonic</i>	$N_d = 1$	$U(1)_d$	0	α	$-\alpha$

Table 4.3: Angles between a brane P and the orientifold plane on the j th torus: θ_P^j .

It is important to note that there is no gaugino mass degeneracy at the unification scale, unlike other models such as mSUGRA. This will lead to interesting experimental signatures.

- Higgs mass parameters

$$m_{H_u}^2 = m_{H_d}^2 = m_{3/2}^2 \left(1 - \frac{3}{2} |\Theta_1|^2\right) \quad (4.38)$$

The Higgs mass parameters are equal because they are characterized by the same Kähler metric \tilde{K}_{PQ}^{higgs} in (4.20).

For completeness, we would also like to list the relative angles between a brane P and the orientifold plane on the j th torus are denoted by θ_P^j in Table 4.3. The soft terms depend on these angles.

The only non-trivial angle is α , which is given by

$$\tan(\pi\alpha) = 3\rho^2 \sqrt{\frac{\text{Re}u^1 \text{Re}u^3}{\text{Re}u^2 \text{Re}s}}. \quad (4.39)$$

as can be seen from eq.(4.10,4.13) and Table 4.1.

We would now like to compare our setup and results for the soft terms with those obtained in [75]. The setup considered in [75] is very similar to ours, but with a few differences. It is a type *IIB* setup with three stacks of D7 branes wrapping four cycles on T^6 . The last stack is equipped with a non-trivial open string flux, to mimic the intersecting brane picture in type *IIA*, as explained in section 3.4. There is also a particular mechanism of supersymmetry breaking through closed string 3-form fluxes. Thus, there is an explicit superpotential generated for the closed string moduli, which leads to an explicit dependence of the gravitino mass ($m_{3/2}$), F^{s,t^i,u^i} and the cosmological constant (V) on the moduli s , t^i and u^i . The cosmological constant is zero if the goldstino angle (θ) is zero which is the same in our case. It turns out that using these formulas, in order for the gravitino mass to be small, the string scale is sufficiently low for reasonable values ($\mathcal{O}(1)$ in string units) of the flux. We have not assumed any particular mechanism of supersymmetry breaking, so we do not have an explicit expression for ($m_{3/2}$), F^{s,t^i,u^i} and (V) in terms of the moduli and have taken the string scale to be of the order of the unification scale.

The model considered in [75] considers non-zero (0,3) and (3,0) form fluxes only, which leads to non-vanishing F^s and F^{t^i} . In the T-dual version, this means that F^s and F^{u^i} are non-zero, which is the case we examined in detail. However, in [75], an isotropic compactification is considered, while we allow a more general situation.

For the calculation of soft terms, we have used the updated form of the 1/4 BPS sector Kähler metric as in [76], which we have also explicitly checked. In [75], the *un-normalized* general expression for calculating the soft terms has been used following [65], whereas we use the *normalized* general expression for the soft terms in eq.(4.22) [66]. In contrast to [75] which has a left-right symmetry, we have also provided an expression for the Bino mass parameter, since

we have the SM gauge group (possibly augmented by $U(1)'s$) and the exact linear combination of $U(1)'s$ giving rise to $U(1)_Y$ is known.

4.1.4 Some phenomenological implications

Using the formulas for the soft terms given in the previous section, we can study some aspects of the phenomenology of the model that has the brane setup shown in Table 4.1.

Although ideally the theory should generate μ of order the soft terms and $\tan\beta$ should be calculated, that is not yet possible in practice as explained before. Therefore we will not specify the mechanism for generating the μ term. We will take $\tan\beta$ and m_Z as input and use EWSB to fix μ and b terms.

Unlike the heterotic string models where the gauge couplings are automatically unified¹, generic brane models don't have this nice feature. This is simply because in brane models different gauge groups originate from different branes and they do not necessarily have the same volume in the compactified space. Therefore to ensure gauge coupling unification at the scale $M_X \approx 2 \times 10^{16} \text{GeV}$, the vev of some moduli fields need to take certain values. In our models, the gauge couplings are determined according to eq.(4.14). Thus the unification relations

$$g_s^2 = g_w^2 = \frac{5}{3}g_Y^2 \approx 0.5. \quad (4.40)$$

lead to three conditions on the four variables: $\text{Re } s$ and $\text{Re } u^i$ where $i = 1, 2, 3$. One of the solutions is

$$\text{Re } s = 2 - 9\text{Re } u_1 \quad \text{Re } u_2 = 4 \quad \text{Re } u_3 = 4. \quad (4.41)$$

It's interesting to note that $\mathcal{N}=1$ SUSY condition actually requires $\text{Re } u_2 = \text{Re } u_3$. There-

¹But usually unified at a higher scale than the true GUT scale.

fore although at first sight it seems that the three gauge couplings are totally unrelated in brane models, in this case requiring $\mathcal{N}=1$ SUSY actually guarantees one of the gauge coupling unification conditions [40].

After taking into account the gauge coupling unification constraint, the undetermined parameters we are left with are $m_{3/2}$, $\tan\beta$, $\text{Re}u^1$, $\text{Re}t^2$, $\text{Re}t^3$, Θ_i and γ_i , where $i = 1, 2, 3$. The phases $\gamma_{1,2,3}$ enter both gaugino masses and trilinears and in general can not be rotated away, leading to EDMs and a variety of other interesting phenomena for colliders, dark matter, etc. in principle. However, for simplicity, in this work we set all phases to be zero: $\gamma_{1,2,3} = 0$. The only dependence on $\text{Re}t^2$ and $\text{Re}t^3$ is in the scalar mass squared terms and is logarithmic. For simplicity, we set them equal: $\text{Re}t^2 = \text{Re}t^3$. Using the relation $\sum |\Theta_i|^2 = 1$, we can eliminate the magnitude of one of the Θ_i s but its sign is free to vary. Thus we are left with the following six free parameters and two signs:

$$m_{3/2}, \tan\beta, \text{Re}u^1, \text{Re}t^2, \Theta_1, \Theta_2, \text{sign}(\mu), \text{sign}(\Theta_3). \quad (4.42)$$

Instead of scanning the full parameter space, we show here three representative models which correspond to three interesting points in the parameter space. In order to reduce fine tuning, we require that the gluino be not too heavy. We also require that the higgs mass is about 114 GeV, that all other experimental bounds are satisfied and that the universe is not overclosed. These requirements strongly constrains the free parameters. The parameters of these three points are shown in Table 4.4.

Using the values of the moduli, one can calculate the string scale M_S . It is indeed between the unification scale and the Planck scale. Notice that since $t \sim 1/T$, we are in the large radius limit of compactification and perturbation theory holds good.

From the parameters shown in Table 4.4, we can calculate the soft terms at high scale.

LSP	$m_{3/2}$	$\tan\beta$	$\text{Re}u^1$	$\text{Re}t^2$	Θ_1	Θ_2	$\text{sign}(\mu)$	$\text{sign}(\Theta_3)$	$\Omega_{\tilde{N}_1}^{\text{thermal}}$
\tilde{W}	1500	20	0.025	0.01	0.50	0.060	+	-	~ 0
\tilde{H}	2300	30	0.025	0.01	-0.75	0.518	+	+	~ 0
\tilde{B} - \tilde{H} mixture	2300	30	0.025	0.01	-0.75	0.512	+	+	~ 0.23

Table 4.4: Parameter choices for three particular models. All masses are in GeV. We set $\text{Re}t^3 = \text{Re}t^2$. $|\Theta_3|$ will be fixed by the condition $\sum |\Theta_i|^2 = 1$. $\text{Re}s$, $\text{Re}u^2$ and $\text{Re}u^3$ are determined by requiring gauge coupling unification.

They are shown in Table 4.5. We use SUSPECT [120] to run the soft terms from the high scale

	M_1	M_2	M_3	A_t	m_0
\tilde{W} LSP	-1288	156	146	-728	$\sim m_{3/2}$
\tilde{H} LSP	849	2064	-336	633	$\sim m_{3/2}$
\tilde{B} - \tilde{H}	866	2040	-336	640	$\sim m_{3/2}$

Table 4.5: Soft terms at the unification scale. The input parameters for calculating the soft terms are shown in Table 4.4. m_0 denotes the average of scalar masses. In both models, they are roughly the gravitino mass. The sign of the trilinears is according to the convention used by SUSPECT. It should be kept in mind that this is opposite to the convention used in supergravity formulas.

to the weak scale and calculate the sparticle spectrum. Most string-based models that have been analyzed in such detail have had Bino LSPs. The three models we examine give wino, higgsino and mixed bino-higgsino LSP, respectively. The gluino masses² in the three models are $\mathcal{O}(500\text{GeV})$. They are significantly lighter than the gluinos in most of existing supergravity

²The radiative contributions to the gluino pole mass from squarks are included.

and superstring based MSSM models. These three models satisfy all current experimental constraints. If the LSP is a pure bino, usually the relic density is too large to satisfy the WMAP[79] constraint. For the third model, the LSP is a mixture of bino and higgsino such that its thermal relic density is just the measured Ω_{CDM} . For the first two models, LSPs annihilate quite efficiently such that their thermal relic density is negligible. Thus if only thermal production is taken into account, the LSP can not be the cold dark matter (CDM) candidate. But in general, there are non-thermal production mechanisms for the LSP, for example the late gravitino decay[80] or Q-ball decays [81, 82]. These non-thermal production mechanisms have usually been neglected but could have important effects on predicting the relic density of the LSP. Since at present, it is not known whether non-thermal production mechanisms were relevant in the early universe, we have presented examples of both possibilities.

Late gravitino decay actually can not generate enough LSPs to explain the observed Ω_{CDM} for the first two models. This is because the gravitino decays after nucleosynthesis. Thus to avoid destroying the successful nucleosynthesis predictions, the gravitino should not be produced abundantly during the reheating process. Therefore, LSPs from the gravitino decay can not be the dominant part of CDM.

Another mechanism for non-thermal production is by the late Q-ball decay. Q-balls are non-topological solitons[83]. At a classical level, their stability is guaranteed by some conserved charge, which could be associated with either a global or a local $U(1)$ symmetry. At a quantum level, since the field configuration corresponding to Q-balls does not minimize the potential globally and in addition Q-balls by definition do not carry conserved topological numbers, they will ultimately decay. Q-balls can be generated in the Affleck-Dine mechanism of baryogenesis[84]. Large amounts of supersymmetric scalar particles can be stored in Q-balls.

Final Q-ball decay products will include LSPs, assuming R-parity is conserved. If Q-balls decay after the LSP freezes out and before nucleosynthesis, the LSP could be the CDM candidate and explain the observed Ω_{CDM} . The relic density of \tilde{N}_1 can be estimated as[81]

$$\Omega_{\tilde{N}_1} \approx 0.5 \times \left(\frac{0.7}{h}\right)^2 \times \left(\frac{m_{\tilde{N}_1}}{100\text{GeV}}\right) \left(\frac{10^{-7}\text{GeV}^2}{\langle\sigma v\rangle}\right) \left(\frac{100\text{MeV}}{T_d}\right) \left(\frac{10}{g_*(T_d)}\right)^{1/2} \quad (4.43)$$

For our first two models, $\langle\sigma v\rangle \sim 10^{-7}\text{GeV}^2$. Thus if the temperature (T_d) when Q-balls decay is about 100 MeV, we will have $\Omega_{\tilde{N}_1} \approx 0.22$. One may attempt to relate this number to the baryon number of the universe since Q-balls may also carry baryon number. But probably, this wouldn't happen in these models at least at the perturbative level, because then baryon number is a global symmetry. Therefore Q-balls wouldn't carry net baryon number. They may carry lepton number because of lepton number violation. But since T_d is well below the temperature of the electroweak (EW) phase transition, sphaleron effects are well suppressed so that the net lepton number cannot be transferred to baryon number. Hence, in the Q-ball scenario, baryon number probably is not directly related to $\Omega_{\tilde{N}_1}$.

If we assume $\Omega_{\tilde{N}_1} \approx 0.23$ by either thermal (for the third model) or non-thermal production (for the first two models), then there will be interesting experimental signatures. One of them is a positron excess in cosmic rays. Such an excess has been reported by the HEAT experiment[85] and two other experiments (AMS and PAMELA) [86] have been planned which will give improved results in the future. In fact the HEAT excess is currently the only reported dark matter signal that is consistent with other data. In both the wino LSP and the higgsino LSP models, LSPs annihilate to W bosons quite efficiently. In particular, W^+ decays to a positron (and a neutrino). We used DARKSUSY[87] to fit the HEAT experiment measurements[88]. The fitted curves are shown in Figure 4.1. The ‘‘boost’’ factors, which characterize the local CDM density fluctuation against the averaged halo CDM density, in both models are not large. Small

changes in other parameters could give boost factors very near unity. Thus both models give a nice explanation for the measured positron excess in the cosmic ray data. For the mixed LSP model, because the LSPs do not annihilate efficiently, one needs a “boost” factor of $\mathcal{O}(100)$ to get a good fit, which may be a bit too high.

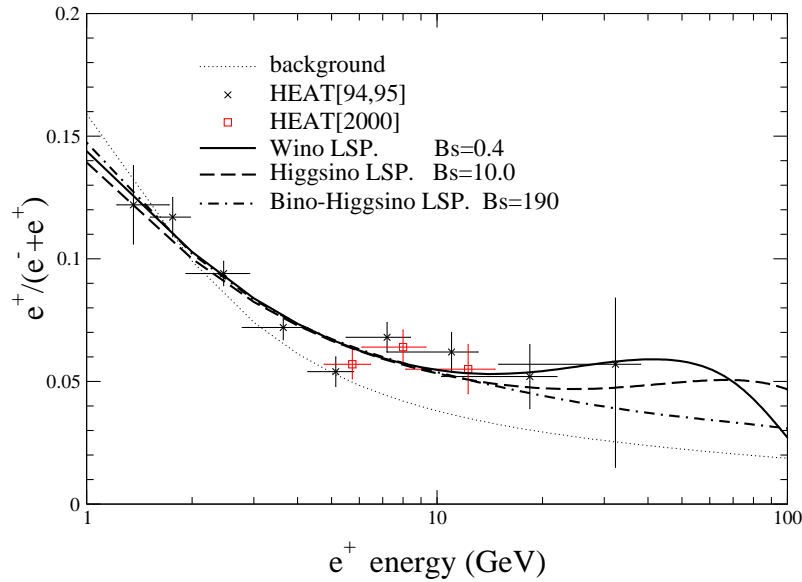


Figure 4.1: Cosmic ray positron excess due to LSP annihilations. Crossed points are HEAT experimental data. The dotted line is from the standard cosmological model without taking into account the LSP annihilation contributions. The solid line is for the \tilde{W} LSP model, the dashed line is for the \tilde{H} LSP model and the dashed-dotted line is for the mixed $\tilde{B}-\tilde{H}$ LSP model. B_s is the boost factor.

4.1.5 Summary of Results

We have investigated some phenomenological implications of intersecting D-brane models, with emphasis on dark matter. We calculated the soft SUSY breaking terms in these models focussing on the u moduli dominated SUSY breaking scenario in type IIA string theory, in which

case the results do not depend on the Yukawa couplings and Wilson lines. The results depend on the brane wrapping numbers as well as SUSY breaking parameters. Our main result is providing in detail the soft-breaking Lagrangian for intersecting brane models, which provides a new set of soft parameters to study phenomenologically. In the absence of a satisfactory mechanism of supersymmetry breaking and moduli stabilization in these compactifications, we use a general self consistent parameterization of F-term vevs, based on [66]. We applied our results to a particular intersecting brane model[42] which gives an MSSM-like particle spectrum, and then selected three representative points in the parameter space with relatively light gluinos, in order to reduce fine-tuning, and calculated the weak scale spectrum for them. The phenomenology of the three models corresponding to the three points is very interesting. The LSPs have different properties. They can be either wino-like, higgsino-like, or a mixture of bino and higgsino. All of them can be good candidates for the CDM.

4.2 M Theory compactifications on singular G_2 Holonomy Manifolds

In the previous section, we saw that it is possible to construct type IIA orientifold models giving rise to MSSM-like chiral spectra in a natural way. However, the issues of moduli stabilization and supersymmetry breaking such as to generate the hierarchy have not been well understood in this picture, which led us to parametrize the effects of supersymmetry breaking in a self-consistent manner and then examine their phenomenological consequences.

In this section, we will focus on another corner of the entire M theory moduli space, that of M theory compactifications on singular G_2 holonomy manifolds, where the issues of moduli stabilization and supersymmetry breaking can be solved in a natural manner such as to give rise to a stable hierarchy between the Planck and electroweak scales. Thus far, there has been

essentially one good idea proposed to explain the relatively small value of the weak scale. This is that the weak scale might be identified with, or related to, the strong coupling scale of an asymptotically free theory which becomes strongly coupled at low energies and exhibits a mass gap at that strong coupling scale. Holographically dual to this is the idea of warped extra dimensions [89]. Strong dynamics (or its dual) can certainly generate a small scale in a natural manner, but can it also be compatible with the stabilization of all the moduli fields?

One context for this question, which we will see is particularly natural, is M theory compactification on manifolds X of G_2 -holonomy without fluxes. In these vacua, the only moduli one has are zero modes of the metric on X , whose bosonic superpartners are axions. Thus each moduli supermultiplet has a Peccei-Quinn shift symmetry (which originates from 3-form gauge transformations in the bulk 11d supergravity). Since such symmetries can only be broken by non-perturbative effects, the entire moduli superpotential W is non-perturbative. In general W can depend on all the moduli. Therefore, in addition to the small scale generated by the strong dynamics we might expect that all the moduli are actually stabilized. This work will demonstrate in detail that this is indeed the case.

Having established that the basic idea works well, the next question we address is “what are the phenomenological implications?” Since string/ M theory has many vacua, it would be extremely useful if we could obtain a general prediction from *all* vacua or at least some well-defined subset of vacua. Remarkably, we are able to give such a prediction for all the fluxless M theory vacua (at least within the supergravity approximation to which we are restricted for calculability): *gaugino masses are generically suppressed relative to the gravitino mass.*

A slightly more detailed elucidation of this result is that in all de Sitter vacua within this class, gaugino masses are always suppressed. In AdS vacua - which are obviously less interesting

phenomenologically - the gaugino masses are suppressed in ‘most’ of the vacua. This will be explained in more detail later.

The reason why we are able to draw such a generic conclusion is the following: any given non-perturbative contribution to the superpotential depends on various constants which are determined by a specific choice of G_2 -manifold X . *These constants determine entirely the moduli potential.* They are given by the one-loop beta-function coefficients b_k , the normalization of each term A_k and the constants a_i (see (4.45)) which characterize the Kähler potential for the moduli. Finally, there is a dependence on the gauge kinetic function, and in M theory this is determined by a set of integers N_i which specify the homology class of the 3-cycle on which the non-Abelian gauge group is localized. Rather than study a particular X which fixes a particular choice for these constants we have studied the effective potential as a function of the (A_k, b_k, a_i, N_i) . The result of gaugino mass suppression holds essentially for arbitrary values of the (A_k, b_k, a_i, N_i) , at least in the supergravity regime where we have been able to calculate. Thus, any G_2 -manifold which has hidden sectors with strong gauge dynamics will lead to suppressed gaugino masses.

At a deeper level, however, the reason that this works is that the idea of strong gauge dynamics to solve the hierarchy problem is a good and simple idea which guides us to the answers directly. If one’s theory does not provide a simple mechanism for how the hierarchy is generated, then it is difficult to see how one could obtain a reliable prediction for, say, the spectrum of beyond the Standard Model particles. In a particular subset of Type IIB compactifications, Conlon and Quevedo have also discovered some general results [90]. In fact, they remarkably also find that gaugino masses are suppressed at tree level, though the nature of the suppression is not quite the same. Some heterotic compactifications also exhibit

a suppression of tree-level gaugino masses [91].

The suppression of gaugino masses relative to $m_{3/2}$ applies for all the vacua, independent of the value of $m_{3/2}$. However, in a generic vacuum the cosmological constant is too large. If we therefore consider only those vacua in which the cosmological constant is acceptable at leading order, this constrains the scale of $m_{3/2}$ further. Remarkably, we find evidence that for such vacua, $m_{3/2}$ is of order 1 – 100 TeV. This result certainly deserves much further investigation. The fact that such general results emerge from these studies makes the task of predicting implications for various collider observables as well as distinguishing among different vacua with data from the LHC (or any other experiment) easier. A more detailed study of the collider physics and other phenomenology is currently being worked out and will appear in the future.

4.2.1 The Moduli Potential

In this section we quickly summarize the basic relevant features of G_2 -compactifications, setup the notation and calculate the potential for the moduli generated by strong hidden sector gauge dynamics.

In M theory compactifications on a manifold X of G_2 -holonomy the moduli are in correspondence with the harmonic 3-forms. Since there are $N \equiv b_3(X)$ such independent 3-forms there are N moduli $z_i = t_i + is_i$. The real parts of these moduli t_i are axion fields which originate from the 3-form field C in M theory and the imaginary parts s_i are zero modes of the metric on X and characterize the size and shape of X . Roughly speaking, one can think of the s_i 's as measuring the volumes of a basis of the N independent three dimensional cycles in X .

Non-Abelian gauge fields are localized on three dimensional submanifolds Q of X along

which there is an orbifold singularity [30] while chiral fermions are localized at point-like conical singularities [31, 32, 29]. Thus these provide M theory realizations of theories with localized matter. A particle localized at a point p will be charged under a gauge field supported on Q if $p \in Q$. Since generically, two three dimensional submanifolds do not intersect in a seven dimensional space, there will be no light matter fields charged under both the standard model gauge group and any hidden sector gauge group. *Supersymmetry breaking is therefore gravity mediated in these vacua.*³

In general the Kähler potentials for the moduli are difficult to determine in these vacua. However a set of Kähler potentials, consistent with G_2 -holonomy and known to describe accurately some explicit examples of G_2 moduli dynamics were given in [93]. These models are given by

$$K = -3 \ln(4\pi^{1/3} V_X) \tag{4.44}$$

where the volume as a function of s_i is

$$V_X = \prod_{i=1}^N s_i^{a_i}, \quad \text{with} \quad \sum_{i=1}^N a_i = 7/3 \tag{4.45}$$

We will assume that this N -parameter family of Kähler potentials represents well the moduli dynamics. More general Kähler potentials outside this class have the volume functional multiplied by a function invariant under rescaling of the metric. It would be extremely interesting to investigate the extension of our results to these cases.

As motivated in the introduction, we are interested in studying moduli stabilization induced

³This is an example of the sort of general result one is aiming for in string/ M theory. We can contrast this result with Type IIA vacua. Here the non-Abelian gauge fields are again localized on 3-cycles, but since generically a pair of three cycles intersect at points in six extra dimensions, *In Type IIA supersymmetry breaking will generically be gauge mediated.*

via strong gauge dynamics. We will begin by considering hidden sector gauge groups with no chiral matter. Later sections will describe the cases with hidden sector chiral matter.

In this ‘no matter’ case, a superpotential of the following form is generated

$$W = \sum_{k=1}^M A_k e^{ib_k f_k} \quad (4.46)$$

where M is the number of hidden sectors undergoing gaugino condensation, $b_k = \frac{2\pi}{c_k}$ with c_k being the dual coxeter numbers of the hidden sector gauge groups, and A_k are numerical constants. The A_k are RG-scheme dependent and also depend upon the threshold corrections to the gauge couplings; the work of [176] shows that their ratios (which should be scheme independent) can in fact take a reasonably wide range of values in the space of M theory vacua. We will only consider the ratios to vary from $\mathcal{O}(0.1-10)$ in what follows.

The gauge coupling functions f_k for these singularities are integer linear combinations of the z_i , because a 3-cycle Q along which a given non-Abelian gauge field is localized is a supersymmetric cycle, whose volume is linear in the moduli.

$$f_k = \sum_{i=1}^N N_i^k z_i. \quad (4.47)$$

Notice that, given a particular G_2 -manifold X for the extra dimensions, the constants (a_i, b_k, A_k, N_i^k) are determined. Then, the Kähler potential and superpotential for that particular X are *completely determined* by the constants (a_i, b_k, A_k, N_i^k) . This is as it should be, since M theory has no free dimensionless parameters.

We are ultimately aiming for an answer to the question, “do M theory vacua in general make a prediction for the beyond the standard model spectrum?”. For this reason, since a fluxless M theory vacuum is completely specified by the constants (a_i, b_k, A_k, N_i^k) we will try as much as possible *not* to pick a particular value for the constants and try to first evaluate

whether or not there is a prediction for *general values of the constants*. Our results will show that at least within the supergravity approximation there is indeed a general prediction: the suppression of gaugino masses relative to the gravitino mass.

At this point the simplest possibility would be to consider a single hidden sector gauge group. Whilst this does in fact stabilize all the moduli, it is a) non-generic and b) fixes the moduli in a place which is strictly beyond the supergravity approximation. Therefore we will begin, for simplicity, by considering two such hidden sectors, which is more representative of a typical G_2 compactification as well as being tractable enough to analyze. The superpotential therefore has the following form

$$W^{np} = A_1 e^{ib_1 f_1} + A_2 e^{ib_2 f_2} . \quad (4.48)$$

The metric corresponding to the Kähler potential (4.44) is given by

$$K_{i\bar{j}} = \frac{3a_i}{4s_i^2} \delta_{i\bar{j}} . \quad (4.49)$$

The $\mathcal{N} = 1$ supergravity scalar potential given by

$$V = e^K (K^{i\bar{j}} F_i \bar{F}_{\bar{j}} - 3|W|^2) , \quad (4.50)$$

where

$$F_i = \partial_i W + (\partial_i K) W , \quad (4.51)$$

can now be computed. The full expression for the scalar potential is given by

$$\begin{aligned} V = & \frac{1}{48\pi V_X^3} \left[\sum_{k=1}^2 \sum_{i=1}^N a_i \nu_i^k (\nu_i^k b_k + 3) b_k A_k^2 e^{-2b_k \vec{\nu}^k \cdot \vec{a}} + 3 \sum_{k=1}^2 A_k^2 e^{-2b_k \vec{\nu}^k \cdot \vec{a}} \right. \\ & + 2 \cos[(b_1 \vec{N}^1 - b_2 \vec{N}^2) \cdot \vec{t}] \sum_{i=1}^N a_i \prod_{k=1}^2 \nu_i^k b_k A_k e^{-b_k \vec{\nu}^k \cdot \vec{a}} \\ & \left. + 3 \cos[(b_1 \vec{N}^1 - b_2 \vec{N}^2) \cdot \vec{t}] \left(2 + \sum_{k=1}^2 b_k \vec{\nu}^k \cdot \vec{a} \right) \prod_{j=1}^2 A_j e^{-b_j \vec{\nu}^j \cdot \vec{a}} \right] \end{aligned} \quad (4.52)$$

where we introduced a variable

$$\nu_i^k \equiv \frac{N_i^k s_i}{a_i} \quad (\text{no sum}) \quad (4.53)$$

such that

$$\text{Im} f_k = \vec{\nu}^k \cdot \vec{a}. \quad (4.54)$$

By extremizing (4.52) with respect to the axions t_i we obtain an equation

$$\sin[(b_1 \vec{N}^1 - b_2 \vec{N}^2) \cdot \vec{t}] = 0, \quad (4.55)$$

which fixes only one linear combination of the axions. In this case

$$\cos[(b_1 \vec{N}^1 - b_2 \vec{N}^2) \cdot \vec{t}] = \pm 1. \quad (4.56)$$

It turns out that in order for the potential (4.52) to have minima, the axions must take on the values such that $\cos[(b_1 \vec{N}^1 - b_2 \vec{N}^2) \cdot \vec{t}] = -1$ for $A_1, A_2 > 0$. Otherwise the potential has a runaway behavior. After choosing the minus sign, the potential takes the form

$$\begin{aligned} V = & \frac{1}{48\pi V_X^3} \left[\sum_{k=1}^2 \sum_{i=1}^N a_i \nu_i^k (\nu_i^k b_k + 3) b_k A_k^2 e^{-2b_k \vec{\nu}^k \cdot \vec{a}} + 3 \sum_{k=1}^2 A_k^2 e^{-2b_k \vec{\nu}^k \cdot \vec{a}} \right. \\ & \left. - 2 \sum_{i=1}^N a_i \prod_{k=1}^2 \nu_i^k b_k A_k e^{-b_k \vec{\nu}^k \cdot \vec{a}} - 3 \left(2 + \sum_{k=1}^2 b_k \vec{\nu}^k \cdot \vec{a} \right) \prod_{j=1}^2 A_j e^{-b_j \vec{\nu}^j \cdot \vec{a}} \right] \end{aligned} \quad (4.57)$$

In the next section we will go on to analyze the vacua of this potential with unbroken supersymmetry. The vacua in which supersymmetry is spontaneously broken are described in sections 4.2.4 and 4.2.5.

4.2.2 Supersymmetric Vacua

In this section we will discuss the existence and properties of the supersymmetric vacua in our theory. This is comparatively easy to do since such vacua can be obtained by imposing the

supersymmetry conditions instead of extremizing the full scalar potential (4.57). Therefore, we will study this case with the most detail. Experience has also taught us that potentials possessing rigid isolated supersymmetric vacua, also typically have other non-supersymmetric vacua with many qualitatively similar features.

The conditions for a supersymmetric vacuum are:

$$F_i = 0,$$

which implies

$$\begin{aligned} (b_1 N_i^1 + \frac{3a_i}{2s_i})A_1 + (b_2 N_i^2 + \frac{3a_i}{2s_i})A_2 [\cos[(b_1 \vec{N}^1 - b_2 \vec{N}^2) \cdot \vec{t}] e^{(b_1 \vec{N}^1 - b_2 \vec{N}^2) \cdot \vec{s}} \\ + i \sin[(b_1 \vec{N}^1 - b_2 \vec{N}^2) \cdot \vec{t}] e^{(b_1 \vec{N}^1 - b_2 \vec{N}^2) \cdot \vec{s}}] = 0 \end{aligned} \quad (4.58)$$

Equating the imaginary part of (4.58) to zero, one finds that

$$\sin[(b_1 \vec{N}^1 - b_2 \vec{N}^2) \cdot \vec{t}] = 0,$$

$$\text{which implies } \cos[(b_1 \vec{N}^1 - b_2 \vec{N}^2) \cdot \vec{t}] = \pm 1. \quad (4.59)$$

For $A_1, A_2 > 0$, a solution with positive values for the moduli (s_i) exists when the axions take on the values such that $\cos[(b_1 \vec{N}^1 - b_2 \vec{N}^2) \cdot \vec{t}] = -1$. Now, equating the real part of (4.58) to zero, one obtains

$$(b_1 N_i^1 + \frac{3a_i}{2s_i})A_1 + (b_2 N_i^2 + \frac{3a_i}{2s_i})A_2 e^{(b_1 \vec{N}^1 - b_2 \vec{N}^2) \cdot \vec{s}} = 0. \quad (4.60)$$

This is a system of N transcendental equations with N unknowns. As such, it can only be solved numerically, in which case, it is harder to get a good understanding of the nature of solutions obtained. Rather than doing a brute force numerical analysis of the system (4.60)

it is very convenient to introduce a new auxiliary variable α to recast (4.60) into a system of *linear* equations with N unknowns coupled to a single transcendental constraint as follows:

$$\alpha(b_1 N_i^1 + \frac{3a_i}{2s_i}) - (b_2 N_i^2 + \frac{3a_i}{2s_i}) = 0 \quad (4.61)$$

$$\frac{A_2}{A_1} = \frac{1}{\alpha} e^{-(b_1 \vec{N}^1 - b_2 \vec{N}^2) \cdot \vec{s}}. \quad (4.62)$$

The system of linear equations (4.61) can then be formally solved for s_i in terms of $\{b_1, b_2, N_i^1, N_i^2, a_i\}$ and α :

$$s_i = -\frac{3a_i(\alpha - 1)}{2(b_1 N_i^1 \alpha - b_2 N_i^2)}; \quad i = 1, 2, \dots, N. \quad (4.63)$$

One can then substitute the solutions for s_i into the constraint (4.62) and self-consistently solve for the parameter α in terms of the input quantities $\{A_1, A_2, b_1, b_2, N_i^1, N_i^2, a_i\}$. This, of course, has to be done numerically, but we have indeed verified that solutions exist. Thus, we have shown explicitly that the moduli can be stabilized. We now go on to discuss the solutions, in particular those which lie within the supergravity approximation.

4.2.2.1 Solutions and the Supergravity Approximation

Not all choices of the constants $\{A_1, A_2, b_1, b_2, N_i^1, N_i^2, a_i\}$ lead to solutions consistent with the approximation that in the bulk of spacetime, eleven dimensional supergravity is valid. Although this is not a precisely (in the numerical sense) defined approximation, a reasonable requirement would seem to be that the values of the stabilized moduli (s_i) obtained from (4.63) are greater than 1. It is an interesting question, certainly worthy of further study, whether or not this is the correct criterion. In any case, this is the criterion that we will use and discuss further.

From (4.63) and (4.62), and requiring the s_i to be greater than 1, we get the following two

branches of conditions on parameter α :

$$\begin{aligned}
 a) \quad & \frac{A_2}{A_1} > 1; \quad \min \left\{ \frac{b_2 N_i^2}{b_1 N_i^1}; i = \overline{1, N} \right\} > \alpha > \max \left\{ \frac{b_2 N_i^2 + 3a_i/2}{b_1 N_i^1 + 3a_i/2}; i = \overline{1, N} \right\} \\
 b) \quad & \frac{A_2}{A_1} < 1; \quad \max \left\{ \frac{b_2 N_i^2}{b_1 N_i^1}; i = \overline{1, N} \right\} < \alpha < \min \left\{ \frac{b_2 N_i^2 + 3a_i/2}{b_1 N_i^1 + 3a_i/2}; i = \overline{1, N} \right\}
 \end{aligned} \tag{4.64}$$

Notice that the solution for s_i (4.63) has a singularity at $\alpha = \frac{b_2 N_i^2}{b_1 N_i^1}$. This can be seen clearly from Figure (4.2). We see that the modulus $s_1 (> 0)$ falls very rapidly as one moves away from the vertical asymptote representing the singularity and can become smaller than one very quickly, where the supergravity approximation fails to be valid. The relative location of the

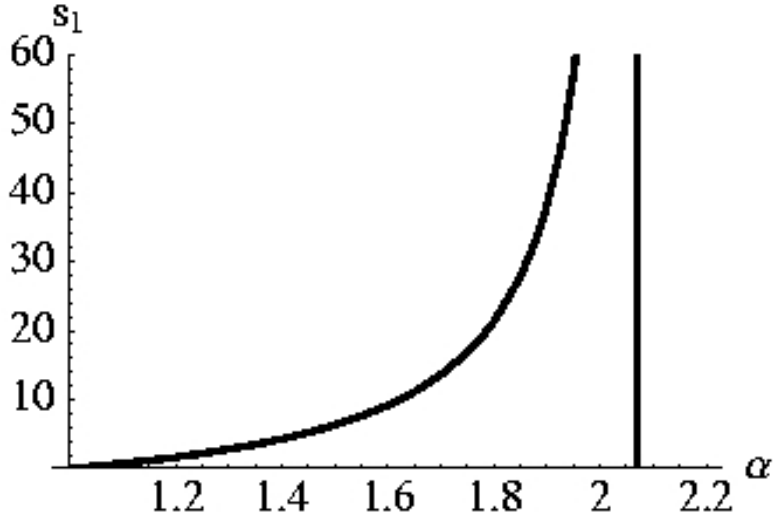


Figure 4.2: Positive values of s_1 plotted as a function of α for a case with two condensates and three bulk moduli for the following choice of constants $b_1 = \frac{2\pi}{30}, b_2 = \frac{2\pi}{29}, N_i^1 = \{1, 2, 2\}, N_i^2 = \{2, 3, 5\}, a_i = \{1, 1/7, 25/21\}$. The qualitative feature of this plot remains the same for different choices of constants as well as for different i . The vertical line is the locus for $\alpha = \frac{b_2 N_i^2}{b_1 N_i^1}$, where the denominator of (4.63) vanishes.

singularities for different moduli will turn out to be very important as we will see shortly. From (4.64), we know that there are two branches for allowed values of α . Here we consider branch a) for concreteness, branch b) can be analyzed similarly. Figure (4.3) shows plots for A_2/A_1

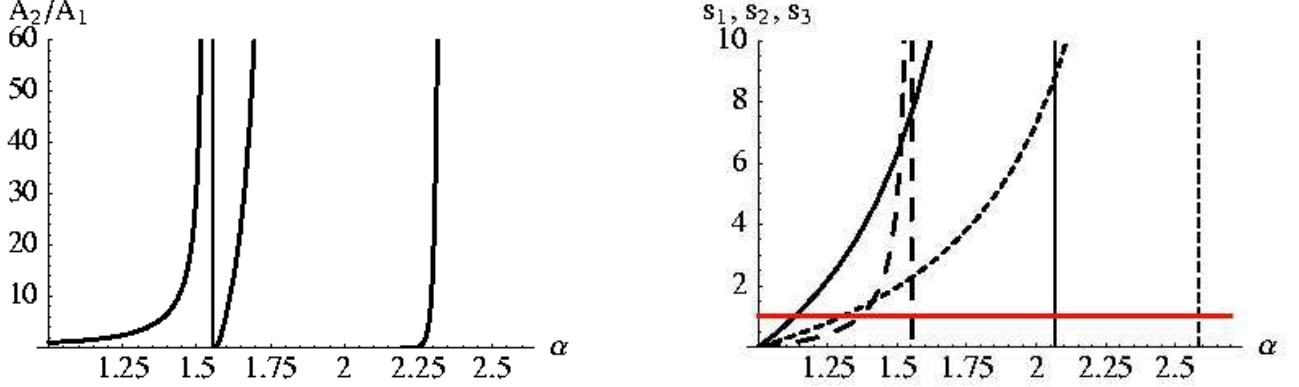


Figure 4.3: Left - A_2/A_1 plotted as a function of α for a case with two condensates and three bulk moduli. The function diverges as it approaches the loci of singularities of (4.63), *viz.* $\alpha = \frac{b_2 N_i^2}{b_1 N_i^1}$.

Right - Positive s_i , $i = 1, 2, 3$ for the same case plotted as functions of α . s_1 is represented by the solid curve, s_2 by the long dashed curve and s_3 by the short dashed curve. The vertical lines again represent the loci of singularities of (4.63) which the respective moduli s_i asymptote to. The horizontal solid (red) line shows the value unity for the moduli, below which the supergravity approximation is not valid.

Both plots are for $b_1 = \frac{2\pi}{30}$, $b_2 = \frac{2\pi}{29}$, $N_i^1 = \{1, 2, 2\}$, $N_i^2 = \{2, 3, 5\}$, $a_i = \{1, 1/7, 25/21\}$.

and s_i as functions of α for a case with two condensates and three bulk moduli. The plots are for a given choice of the constants $\{b_1, b_2, N_i^1, N_i^2, a_i, i = 1, 2, 3\}$. The qualitative feature of the plots remains the same even if one has a different value for the constants.

Since the s_i fall very rapidly as one goes to the left of the vertical asymptotes, there is a small region of α between the origin and the leftmost vertical asymptote which yields allowed values for all $s_i > 1$. Thus, for a solution in the supergravity regime all (three) vertical lines representing the loci of singularities of the (three) moduli s_i should be (sufficiently) close to each other. This means that the positions of the vertical line for the i th modulus ($\alpha = \frac{b_2 N_i^2}{b_1 N_i^1}$) and the j th modulus ($\alpha = \frac{b_2 N_j^2}{b_1 N_j^1}$) can not be too far apart. This in turn implies that the ratio of

integer coefficients (N_i^1/N_i^2) and (N_j^1/N_j^2) for the i th and j th modulus cannot be too different from each other in order to remain within the approximation. Effectively, this means that the integer combinations in the gauge kinetic functions (4.47) of the two hidden sector gauge groups in (4.48) can not be too linearly independent. We will give explicit examples of G_2 manifolds in which (N_i^1/N_i^2) and (N_j^1/N_j^2) are the same for all i and j , so the constraint of being within the supergravity approximation is satisfied. We now turn to the effect of the other constants on

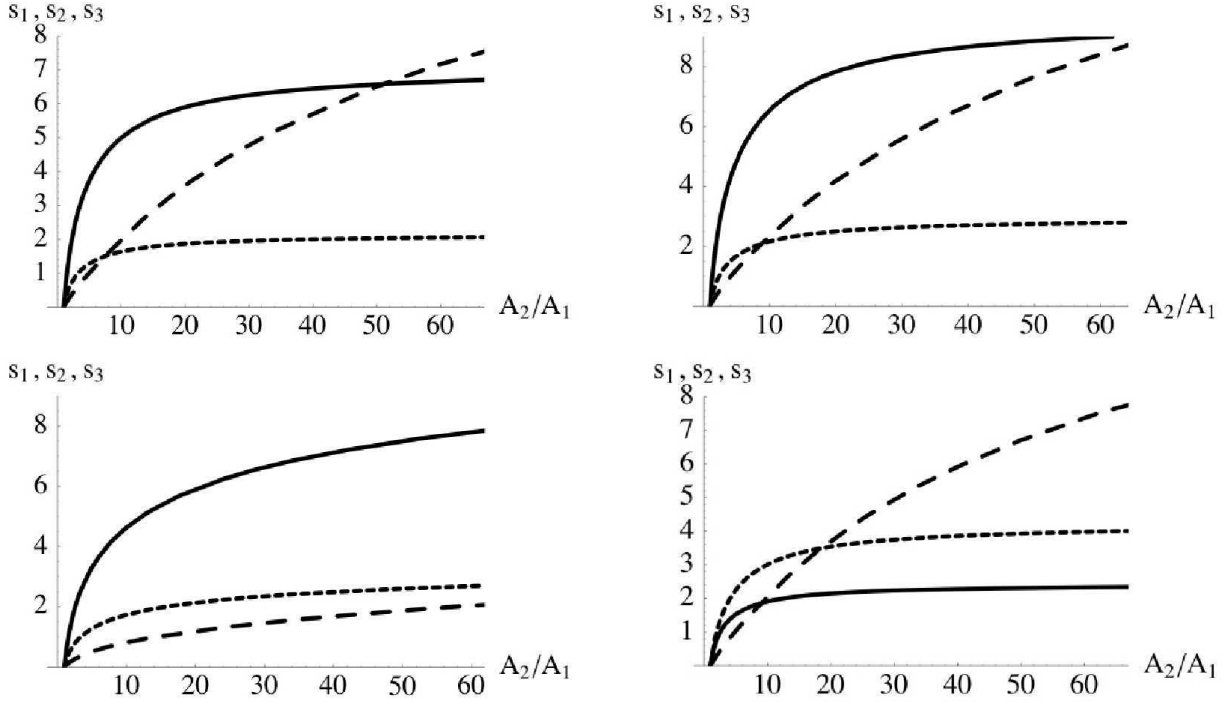


Figure 4.4: Plots of positive $s_i, i = 1, 2, 3$ as functions of A_2/A_1 .

Top Left: Same choice of constants as in Figure(4.3), i.e. $b_1 = \frac{2\pi}{30}, b_2 = \frac{2\pi}{29}, N_i^1 = \{1, 2, 2\}, N_i^2 = \{2, 3, 5\}, a_i = \{1, 1/7, 25/21\}$.

Top Right: We increase the ranks of the gauge groups but keep them close (keeping everything else same) - $b_1 = \frac{2\pi}{40}, b_2 = \frac{2\pi}{38}$.

Bottom Left: We introduce a large difference in the ranks of the gauge groups (with everything else same) - $b_1 = \frac{2\pi}{40}, b_2 = \frac{2\pi}{30}$.

Bottom Right: We keep the ranks of the gauge groups as in Top Left but change the integer coefficients to $N_i^1 = \{1, 2, 2\}, N_i^2 = \{3, 3, 4\}$.

the nature of solutions obtained. From the top right plot in Figure (4.4), we see that increasing the ranks of the gauge groups while keeping them close to each other (with all other constants fixed) increases the size of the moduli in general. On the other hand, from the bottom left plot we see that introducing a large difference in the ranks leads to a decrease in the size of the moduli in general. Hence, typically it is easier to find solutions with comparatively large rank gauge groups which are close to each other. The bottom right plot shows the sizes of the moduli as functions of A_2/A_1 while keeping the ranks of the gauge groups same as in the top left plot but changing the integer coefficients. We typically find that if the integer coefficients are such that the two gauge kinetic functions are almost dependent, then it is easier to find solutions with values of moduli in the supergravity regime.

The above analysis performed for three moduli can be easily extended to include many more moduli. Typically, as the number of moduli grows, the values of a_i in (4.63) decrease because of (4.45). Therefore the ranks of the gauge groups should be increased in order to remain in the supergravity regime as one can see from the structure of (4.63). At the same time, for reasons described above, the integer combinations for the two gauge kinetic functions should not be too linearly independent. In addition, the integers N_i^k should not be too large as they also decrease the moduli sizes in (4.63).

What happens if some of the integers N_i^1 or N_i^2 are zero. Figure 4.5 corresponds to this type of a situation when the integer combinations are given by $N_i^1 = \{1, 0, 1\}$, $N_i^2 = \{1, 1, 1\}$. As we can see from the plots, all the moduli can still be stabilized although one of the moduli, namely s_2 is stabilized at values less than one in 11-dim Planck units. This gets us back to the previous discussion as to when the supergravity approximation can be valid. We will not have too much to say about this point, except to note that a) the volume of X can still be large ((4.45) is

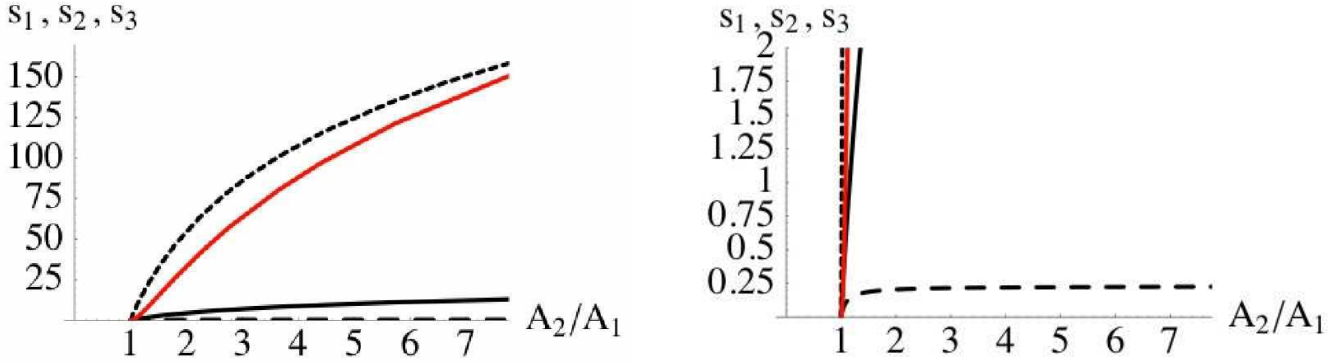


Figure 4.5: Plots of positive $s_i, i = 1, 2, 3$ as functions of A_2/A_1 . The constants are $b_1 = \frac{2\pi}{30}, b_2 = \frac{2\pi}{29}, N_i^1 = \{1, 0, 1\}, N_i^2 = \{1, 1, 1\}, a_i = \{1/10, 1, 37/30\}$. s_1 is represented by the solid curve, s_2 by the long dashed curve and s_3 by the short dashed curve. The red curve represents the volume of the internal manifold as a function of A_2/A_1 . Right - the same plot with the vertical plot range decreased.

large, greater than one in 11-dim Plank units), b) the volumes of the associative three-cycles Q_k which appear in the gauge kinetic function (4.47), i.e. $Vol(Q_k) = \sum_{i=1}^n N_i^k s_i$ can also be large and c) that the top Yukawa in these models comes from a small modulus vev [31]. From Figure 4.5 we see that although the modulus s_2 is always much smaller than one, the overall volume of the manifold V_X represented by the solid red curve is much greater than one. Likewise, the volumes of the associative three cycles $Vol(Q_1) = s_1 + s_3$ and $Vol(Q_2) = s_1 + s_2 + s_3$ are also large. Therefore if one interprets the SUGRA approximation in this way, it seems possible to have zero entries in the gauge kinetic functions for some of the moduli and still stabilize all the moduli, as demonstrated by the explicit example given above. In general, however, there is no reason why any of the integers should vanish in the basis in which the Kähler metric is given by (4.49).

4.2.2.2 Special Case

A very interesting special case arises when the gauge kinetic functions f_1 and f_2 in (4.48) are equal. Recall, that since, in this case $N_i^1 = N_i^2$, the moduli vevs are larger in the supersymmetric vacuum and hence this case is representative of the vacua to be found within the supergravity approximation.

Even though this is a special case, in section 4.2.3, we will describe explicit examples of G_2 manifolds in which $N_i^1 = N_i^2$.

In the special case, we have

$$N_i^1 = N_i^2 \equiv N_i, \quad (4.65)$$

and therefore

$$\nu_i^1 = \nu_i^2 = \nu_i \equiv \frac{N_i s_i}{a_i} \quad (4.66)$$

For this special case, the system of equations (4.60) can be simplified even further. We have

$$(b_1 \nu_i + \frac{3}{2})A_1 - (b_2 \nu_i + \frac{3}{2})A_2 e^{(b_1 - b_2)\vec{\nu} \cdot \vec{a}} = 0 \quad (4.67)$$

with ν_i actually *independent* of i . Thus, we are left with just *one* simple algebraic equation and one transcendental constraint. The solution for ν_i is given by :

$$\nu_i \equiv \nu = -\frac{3(\alpha - 1)}{2(\alpha b_1 - b_2)}, \quad (4.68)$$

with

$$\frac{A_2}{A_1} = \frac{1}{\alpha} e^{-\frac{7}{3}(b_1 - b_2)\nu}. \quad (4.69)$$

Since ν_i is independent of i , it is also independent of the number of moduli N . In Figure (4.6) we plotted ν as a function of A_2/A_1 when the hidden sector gauge groups are $SU(5)$ and

$SU(4)$. Notice that here the ranks of the gauge groups don't have to be large for the moduli to be greater than one. This is in contrast with the linearly independent cases plotted in Figure (4.4). Once ν is determined in terms of A_2/A_1 , the moduli are given by:

$$s_i = \frac{a_i \nu}{N_i}. \quad (4.70)$$

Therefore, the hierarchy between the moduli sizes is completely determined by the ratios a_i/N_i for different values of i . In addition, from Figure 4.6 it can be seen that ν keeps increasing

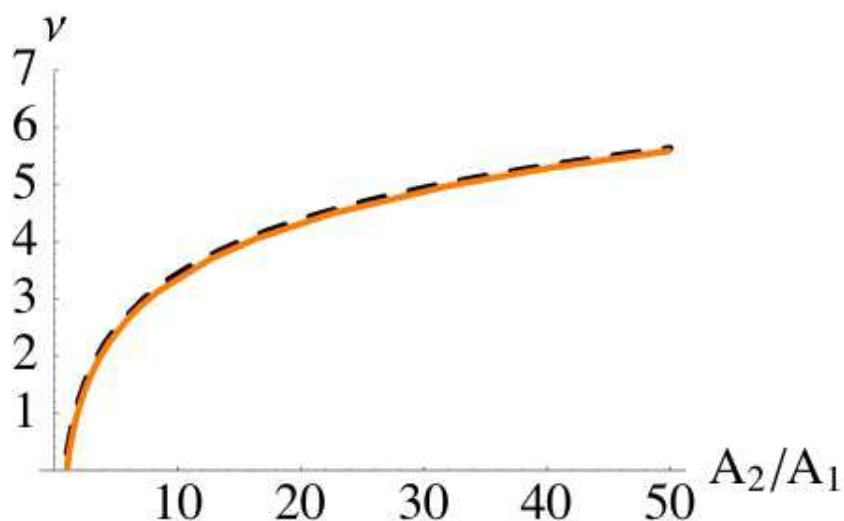


Figure 4.6: Plot of ν as a function of A_2/A_1 for the choice $b_1 = \frac{2\pi}{5}$, $b_2 = \frac{2\pi}{4}$. The red solid curve represents the exact numerical solution whereas the black dashed curve is the leading order approximation given by (4.72).

indefinitely if we keep increasing A_2/A_1 (though theoretically there may be a reasonable upper limit for A_2/A_1), which is not possible for the general case as there are N ν_i 's. This implies that it is possible to have a wide range of the constants which yield a solution in the supergravity regime.

Although the numerical solutions to the system (4.68-4.69) described above are easy to

generate, having an explicit analytic solution, even an approximate one, which could capture the dependence of ν on the constants A_2/A_1 , b_1 and b_2 would be very useful.

Fortunately there exists a good approximation, namely a large ν limit, which allows us to find an analytical solution for ν in a straightforward way. Expressing α from (4.68), in the leading order approximation when ν is large we obtain

$$\alpha^{(0)} = \frac{b_2}{b_1}. \quad (4.71)$$

After substituting (4.71) into (4.69) we obtain the approximate solution for ν in the leading order:

$$\nu^{(0)} = \frac{3}{7} \frac{1}{b_2 - b_1} \ln \left(\frac{A_2 b_2}{A_1 b_1} \right) = \frac{3}{14\pi} \frac{PQ}{P - Q} \ln \left(\frac{A_2 P}{A_1 Q} \right), \quad (4.72)$$

where the last expression corresponds to $SU(P)$ and $SU(Q)$ hidden sector gauge groups. For the moduli to be positive either of the two following conditions have to be satisfied

$$\begin{aligned} a) \quad & A_1 Q < A_2 P; \quad P > Q \\ b) \quad & A_1 Q > A_2 P; \quad P < Q. \end{aligned} \quad (4.73)$$

From the plots in Figure 4.6 we notice that the above approximation is fairly accurate even when ν is $O(1)$. This is very helpful and can be seen once we compute the first subleading contribution. By substituting (4.72) back into (4.68) and solving for α we now have up to the first subleading order:

$$\alpha = \alpha^{(0)} + \alpha^{(1)} = \frac{P}{Q} - \frac{7}{2 \ln \left(\frac{A_2 P}{A_1 Q} \right)} \left(\frac{P - Q}{Q} \right)^2. \quad (4.74)$$

It is then straightforward to compute ν which includes the first subleading order contribution

$$\nu = \nu^{(0)} + \nu^{(1)} = \frac{3}{14\pi} \frac{PQ}{P - Q} \ln \left(\frac{A_2 P}{A_1 Q} \right) - \frac{3}{4\pi} \frac{P - Q}{\ln \left(\frac{A_2 P}{A_1 Q} \right)}. \quad (4.75)$$

We can now examine the accuracy of the leading order approximation when ν is $O(1)$ by considering the region where the ratio A_2/A_1 is small. A quick check for the $SU(5)$ and $SU(4)$ hidden sector gauge groups chosen in the case presented in Figure 4.6 yields for $A_2/A_1 = 4$:

$$\alpha = \alpha^{(0)} + \alpha^{(1)} = 1.25 - 0.136, \quad (4.76)$$

$$\nu = \nu^{(0)} + \nu^{(1)} = 2.195 - 0.148. \quad (4.77)$$

which results in a 12% and 7% error for $\alpha^{(0)}$ and $\nu^{(0)}$ respectively. The errors get highly suppressed when ν becomes $O(10)$ and larger. Also, when the ranks of the gauge groups $SU(P)$ and $SU(Q)$ are $O(10)$ and $P - Q$ is small, the ratio A_2/A_1 can be $O(1)$ and still yield a large ν . The dependence of ν on the constants in (4.72) is very similar to the moduli dependence obtained for SUSY Minkowski vacua in the Type IIB racetrack models [95].

We have demonstrated that there exist isolated supersymmetric vacua in M theory compactifications on G_2 -manifolds with two strongly coupled hidden sectors which give non-perturbative contributions to the superpotential. Given the existence of supersymmetric vacua, it is very likely that the potential also contains non-supersymmetric critical points. Previous examples have certainly illustrated this [93]. Before analyzing the non-supersymmetric critical points, however, we will now present some examples of vacua which give rise to two strongly coupled hidden sectors.

4.2.3 Examples of G_2 Manifolds

Having shown that the potential stabilizes all the moduli, it is of interest to construct explicit examples of G_2 -manifolds realizing these vacua. To demonstrate the existence of a G_2 -holonomy metric on a compact 7-manifold is a difficult problem in solving non-linear equations [96]. There is no analogue of Yau's theorem for Calabi-Yau manifolds which allows an "alge-

braic” construction. However, Joyce and Kovalev have successfully constructed many smooth examples [96]. Furthermore, dualities with heterotic and Type IIA string vacua also imply the existence of many singular examples. The vacua of interest to us here are those with two or more hidden sector gauge groups. These correspond to G_2 -manifolds which have two three dimensional submanifolds Q_1 and Q_2 along which there are orbifold singularities. In order to describe such examples we will a) outline an extension of Kovalev’s construction to include orbifold singularities and b) use duality with the heterotic string.

Kovalev constructs G_2 manifolds which can be described as the total space of a fibration. The fibres are four dimensional $K3$ surfaces, which vary over a three dimensional sphere. Kovalev considers the case in which the $K3$ fibers are generically smooth, but it is reasonably straightforward to also consider cases in which the (generic) $K3$ fiber has orbifold singularities. This gives G_2 -manifolds which also have orbifold singularities along the sphere and give rise to Yang-Mills fields in M theory. For example if the generic fibre has both an $SU(4)$ and an $SU(5)$ singularity, then the G_2 manifold will have two such singularities, both parameterized by disjoint copies of the sphere. In this case N_i^1 and N_i^2 are equal because Q_1 and Q_2 are in the same homology class, which is precisely the special case that we consider both above and below.

We arrive at a very similar picture by considering the M theory dual of the heterotic string on a Calabi-Yau manifold at large complex structure. In this limit, the Calabi-Yau is T^3 fibered and the M theory dual is $K3$ -fibered, again over a three-sphere (or a discrete quotient thereof). Then, if the hidden sector E_8 is broken by the background gauge field to, say, $SU(5) \times SU(2)$ the $K3$ -fibers of the G_2 -manifold generically have $SU(5)$ and $SU(2)$ singularities, again with $N_i^1 = N_i^2$. More generally, in $K3$ fibered examples, the homology class of Q_1 could be k times

that of Q_2 and in this case $N_i^1 = kN_i^2$. As a particularly interesting example, the M theory dual of the heterotic vacua described in [97] include a G_2 manifold whose singularities are such that they give rise to an observable sector with precisely the matter content of the MSSM whilst the hidden sector has gauge group $G = E_8$.

Finally, we also note that Joyce's examples typically can have several sets of orbifold singularities which often fall into the special class [96]. We now go on to describe the vacua in which supersymmetry is spontaneously broken.

4.2.4 Vacua with spontaneously broken Supersymmetry

The potential (4.52) also possesses vacua in which supersymmetry is spontaneously broken. Again these are isolated, so the moduli are all fixed. These all turn out to have negative cosmological constant. We will see in section 4.2.5 that adding matter in the hidden sector can give a potential with de Sitter vacua.

Since the scalar potential (4.52) is extremely complicated, finding solutions is quite a non-trivial task. As for the supersymmetric solution, it is possible to simplify the system of N transcendental equations obtained. However, unlike the supersymmetric solution, we have only been able to do this so far for the special case as in 4.2.2.2. Therefore, for simplicity we analyze the special case in detail. As we described above, there are examples of vacua which fall into this special class. Moreover, as explained previously, we expect that typically vacua not in the special class are beyond the supergravity approximation.

By extremizing (4.57) with respect to s_k we obtain the following system of equations

$$\begin{aligned}
& 2\nu_k^2(b_1\alpha - b_2)^2 - \nu_k[2(b_1\alpha - b_2)(b_1^2\alpha - b_2^2) \sum_{i=1}^N a_i\nu_i^2 + 3(\alpha - 1)(b_1^2\alpha - b_2^2)\vec{\nu} \cdot \vec{a} \\
& + 3(b_1\alpha - b_2)^2\vec{\nu} \cdot \vec{a} + 3(\alpha - 1)(b_1\alpha - b_2)] - 3[(b_1\alpha - b_2)^2 \sum_{i=1}^N a_i\nu_i^2 \\
& + 3(\alpha - 1)(b_1\alpha - b_2)\vec{\nu} \cdot \vec{a} + 3(\alpha - 1)^2] = 0,
\end{aligned} \tag{4.78}$$

where we have again introduced an auxiliary variable α defined by

$$\frac{A_2}{A_1} \equiv \frac{1}{\alpha} e^{-(b_1 - b_2)\vec{\nu} \cdot \vec{a}}. \tag{4.79}$$

similar to that in section 4.2.2.2. The definition (4.79) together with the system of polynomial equations (4.78) can be regarded as a coupled system of equations for α and ν_k . We introduce the following notation:

$$x \equiv (\alpha - 1), \quad y \equiv (b_1\alpha - b_2), \quad z \equiv (b_1^2\alpha - b_2^2), \quad w \equiv \frac{xz}{y^2}. \tag{4.80}$$

In this notation, from (4.78) (divided by x^2) we obtain the following system of coupled equations

$$2\frac{y^2}{x^2}\nu_k^2 - \left(2\frac{y^2}{x^2}w \sum_{i=1}^N a_i\nu_i^2 + 3\frac{y}{x}(w + 1)\vec{\nu} \cdot \vec{a} + 3 \right) \frac{y}{x}\nu_k - 3 \left(\frac{y^2}{x^2} \sum_{i=1}^N a_i\nu_i^2 + 3\frac{y}{x}\vec{\nu} \cdot \vec{a} + 3 \right) = 0. \tag{4.81}$$

It is convenient to recast this system of N *cubic* equations into a system of N *quadratic* equations plus a constraint. Namely, by introducing a new variable T as

$$4T \equiv 2\frac{y^2}{x^2}w \sum_{i=1}^N a_i\nu_i^2 + 3\frac{y}{x}(w + 1)\vec{\nu} \cdot \vec{a} + 3, \tag{4.82}$$

where the factor of four has been introduced for future convenience, the system in (4.81) can be expressed as

$$2\frac{y^2}{x^2}\nu_k^2 - 4T\frac{y}{x}\nu_k - 3 \left(\frac{y^2}{x^2} \sum_{i=1}^N a_i\nu_i^2 + 3\frac{y}{x}\vec{\nu} \cdot \vec{a} + 3 \right) = 0. \tag{4.83}$$

An important property of the system (4.83) is that *all of its equations are the same independent of the index k* . However, since the combination in the round brackets in (4.83) is not a constant with respect to $\vec{\nu}$ this system of quadratic equations does not decouple. Nevertheless, because both the first and the second monomials in (4.83) with respect to ν_k are *independent of $\vec{\nu}$* , the standard solution of a quadratic equation dictates that the solutions for ν_k of (4.83) have the form

$$\nu_k = \frac{x}{y} (T + m_k H) , \text{ with } m_k = \pm 1 , k = \overline{1, N} , \quad (4.84)$$

where we introduced another variable H and pulled out the factor of x/y for future convenience.

We have now reduced the task of determining ν_k for each $k = \overline{1, N}$ to finding *only two* quantities - T and H . By substituting (4.84) into equations (4.82-4.83) and using (4.45), we obtain a system of two coupled quadratic equations

$$\begin{aligned} \frac{14w}{3} (T_A^2 + 2AT_A H_A + H_A^2) + 7(w+1) (T_A + AH_A) + 3 - 4T_A &= 0 \\ 9 (T_A^2 + 2AT_A H_A + H_A^2) - 4H_A (H_A + AT_A) + 21 (T_A + AH_A) + 9 &= 0 , \end{aligned} \quad (4.85)$$

where parameter A defined by

$$A \equiv \frac{3}{7} \vec{m} \cdot \vec{a} , \quad (4.86)$$

is now labelling each solution. Note that by factoring out x/y in (4.84), the system obtained in (4.85) is independent of either x or y . However, it does couple to the constraint (4.79) via w . In subsection 4.2.4.3 we will see that there exists a natural limit when the system (4.85) completely decouples from the constraint (4.79). Since both T_A and H_A both depend on the parameter A , the solution in (4.84) is now written as

$$\nu_k^A = \frac{x}{y} (T_A + m_k H_A) . \quad (4.87)$$

Since $k = \overline{1, N}$ and $m_k = \pm 1$, vector \vec{m} represents one of 2^N possible combinations. Thus, parameter $\vec{m} \cdot \vec{a}$ can take on 2^N possible rational values within the range:

$$-\frac{7}{3} \leq \vec{m} \cdot \vec{a} \leq \frac{7}{3}, \quad (4.88)$$

so that parameter A defined in (4.86) labelling each solution can take on 2^N rational values in the range:

$$-1 \leq A \leq 1. \quad (4.89)$$

For example, when $N = 2$, there are four possible combinations for $\vec{m} = (m_1, m_2)$, namely

$$(m_1, m_2) = \{(-1, -1), (1, -1), (-1, 1), (1, 1)\}. \quad (4.90)$$

These combinations result in the following four possible values for A :

$$A = \left\{-1, \frac{3}{7}(a_1 - a_2), \frac{3}{7}(-a_1 + a_2), 1\right\}, \quad (4.91)$$

where we used (4.45) for the first and last combinations.

In general, for an arbitrary value of A , system (4.85) has four solutions. However, with the exception of the case when $A = 1$, out of the four solutions only two are actually real, as we will see later in subsection 4.2.4.3. The way to find those solutions is the following:

Having found ν_k^A analytically in terms of α and the other constants, we can substitute it into the transcendental constraint (4.79) to determine α numerically for particular values of $\{A_1, A_2, b_1, b_2, N_k, a_k\}$. Again, in general there will be more than one solution for α . We can then substitute those values back into the analytical solution for ν_k^A to find the corresponding extrema, having chosen only those α , obtained numerically from (4.79), which result in real values of ν_k^A . We thus have 2^{N+1} real extrema. However, after a closer look at the system of equations (4.85) we notice that when $A \rightarrow -A$, equations remain invariant if $H_{-A} \rightarrow -H_A$,

and $T_{-A} \rightarrow T_A$, thus simply exchanging the solutions $\nu_{(k,+)}^A$ where $m_k = 1$ with $\nu_{(k,-)}^A$ where $m_k = -1$, i.e.

$$\nu_{(k,+)}^{-A} = \nu_{(k,-)}^A, \quad (4.92)$$

which implies that the scalar potential (4.57) in general has a total number of 2^N real independent extrema. However, as we will see later in section 4.2.4.3, many of those vacua will be incompatible with the supergravity approximation.

For general values of A , equations (4.85) have analytical solutions that are too complicated to be presented here. In addition to restricting to the situation with the same gauge kinetic function f in both hidden sectors, we now further restrict to special situations where A takes special values, so that the expressions are simple. However, it is important to understand that they still capture the main features of the general solution. In the following, we provide explicit solutions (in the restricted situation as mentioned above) for M theory compactifications on G_2 manifolds with one and two moduli respectively. In subsection 4.2.4.3 we will generalize our results to the case with many moduli and give a complete classification of all possible solutions. We will then consider the limit when the volume of the associative cycle $Vol(Q) = \vec{v} \cdot \vec{a}$ is large and obtain explicit analytic solutions for the moduli.

4.2.4.1 One modulus case

The first, and the simplest case is to consider a manifold with only one modulus, i.e. $N = 1$, $a = \frac{7}{3}$. In this case, $A = \pm 1$. From the previous discussion we only need to consider the case $A = 1$. It turns out that this is a special case for which the system (4.85) degenerates to yield three solutions instead of four. All three are real, however, only two of them result in positive

values of the modulus:

$$T_1^{(1)} = -\frac{15}{8}, \quad H_1^{(1)} = \frac{3}{8} \quad (4.93)$$

and

$$\begin{aligned} T_1^{(2)} &= \frac{3}{28(243 - 441w + 196w^2)} \left(-13419 + \frac{3645}{w} + 15288w - 5488w^2 \right. \\ &\quad \left. - 329\sqrt{729 - 1701w + 1323w^2 - 343w^3} \right. \\ &\quad \left. + \frac{135}{w}\sqrt{729 - 1701w + 1323w^2 - 343w^3} \right. \\ &\quad \left. + 196w\sqrt{729 - 1701w + 1323w^2 - 343w^3} \right) \\ H_1^{(2)} &= \frac{3}{28w} \left(-27 + 28w - \sqrt{729 - 1701w + 1323w^2 - 343w^3} \right), \end{aligned} \quad (4.94)$$

which give the following two values for the modulus

$$\begin{aligned} s^{(1)} &= \frac{a}{N_1} \frac{x}{y} \left(T_1^{(1)} + H_1^{(1)} \right) = -\frac{7x}{2Ny} \\ s^{(2)} &= \frac{a}{N_1} \frac{x}{y} \left(T_1^{(2)} + H_1^{(2)} \right) = -\frac{x}{Ny} \left(\frac{3 + \sqrt{9 - 7w}}{w} \right). \end{aligned} \quad (4.95)$$

In addition, each solution in (4.95) is a function of the auxiliary variable α defined in (4.79).

By substituting (4.95) into (4.79) we obtain two equations for $\alpha^{(1)}$ and $\alpha^{(2)}$

$$\frac{A_2}{A_1} = \frac{1}{\alpha^{(1)}} e^{-(b_1 - b_2)s^{(1)}N_1}, \quad \frac{A_2}{A_1} = \frac{1}{\alpha^{(2)}} e^{-(b_1 - b_2)s^{(2)}N_1}. \quad (4.96)$$

The transcendental equations (4.96) can only be solved numerically. Here we will choose the following values for this simple toy model

$$A_1 = 0.12, \quad A_2 = 2, \quad b_1 = \frac{2\pi}{8}, \quad b_2 = \frac{2\pi}{7}, \quad N_1 = 1. \quad (4.97)$$

By solving (4.96) numerically and keeping only those solutions that result in real positive values for the modulus s in (4.95) we get

$$s^{(1)} = 26.101, \quad s^{(2)} = 27.185. \quad (4.98)$$

with

$$\alpha^{(1)} = 1.122, \quad \alpha^{(2)} = 1.267. \quad (4.99)$$

In figure (4.7) we see that the two solutions in (4.98) correspond to an AdS minimum and

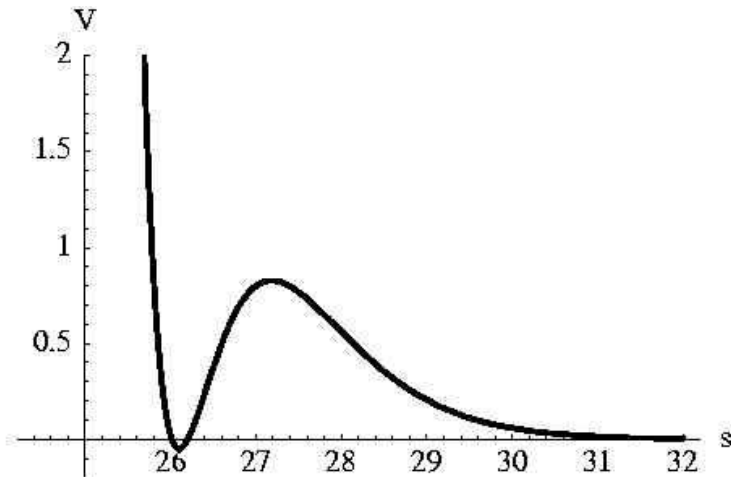


Figure 4.7: Potential multiplied by 10^{32} plotted as a function of one modulus s . For our particular choice of constants in (4.97), the modulus is stabilized at the supersymmetric AdS minimum $s^{(1)} = 26.101$. The maximum is de Sitter, given by $s^{(2)} = 27.185$.

a de Sitter maximum. In fact, the AdS minimum at $s^{(1)}$ is supersymmetric. The general solution for $s^{(1)}$ given in (4.95) can also be obtained by methods of section 4.2.2, imposing the SUSY condition on the corresponding F -term by setting it to zero, while introducing the same auxiliary constraint as in (4.79).

4.2.4.2 Two moduli case

While the previous example with one modulus is interesting, it does not capture some very important properties of the vacua which arise when two or more moduli are considered. In particular, in this subsection we will see that the supersymmetric AdS minimum, obtained in the one-dimensional case, actually turns into a saddle point whereas the stable minima are AdS

with spontaneously broken supersymmetry. Let us now consider a particularly simple example with two moduli. Here we will choose both moduli to appear on an equal footing in the Kähler potential (4.44) by choosing

$$a_1 = \frac{7}{6}, \quad a_2 = \frac{7}{6}. \quad (4.100)$$

We now have four possible combinations for $\vec{m} = (m_1, m_2)$:

$$(1, 1), \quad (1, -1), \quad (-1, 1), \quad (-1, -1), \quad (4.101)$$

corresponding to the following possible values of A :

$$1, \quad 0, \quad 0, \quad -1, \quad (4.102)$$

where only two of the four actually produce independent solutions. The case when $A = 1$ has been solved in the previous subsection with $T_1^{(1)}$, $H_1^{(1)}$ and $T_1^{(2)}$, $H_1^{(2)}$ given by (4.93-4.94) with the moduli taking on the following values for the supersymmetric AdS extremum

$$\begin{aligned} s_1^{(1)} &= \frac{a_1 x}{N_1 y} \left(-\frac{3}{2} \right) = -\frac{7x}{4N_1 y}, \\ s_2^{(1)} &= \frac{a_2 x}{N_2 y} \left(-\frac{3}{2} \right) = -\frac{7x}{4N_2 y}, \end{aligned} \quad (4.103)$$

and the de Sitter extremum

$$\begin{aligned} s_1^{(2)} &= \frac{a_1 x}{N_1 y} \left(-\frac{3}{7w} (3 + \sqrt{9 - 7w}) \right) = -\frac{x}{2N_1 y} \left(\frac{3 + \sqrt{9 - 7w}}{w} \right), \\ s_2^{(2)} &= \frac{a_2 x}{N_2 y} \left(-\frac{3}{7w} (3 + \sqrt{9 - 7w}) \right) = -\frac{x}{2N_2 y} \left(\frac{3 + \sqrt{9 - 7w}}{w} \right). \end{aligned} \quad (4.104)$$

As mentioned earlier, the supersymmetric solution can also be obtained by the methods of section 4.2.2. Now, we also have a new case when $A = 0$. The corresponding two real solutions

for T_0 and H_0 are

$$\begin{aligned} T_0^{(1)} &= \frac{3}{112w}(15 - 63w - D), \\ H_0^{(1)} &= \frac{1}{4\sqrt{5}}\sqrt{-\frac{585}{8} - \frac{18225}{392w^2} + \frac{3915}{28w} + \frac{1215}{392w^2}D - \frac{225}{56w}D}, \end{aligned} \quad (4.105)$$

and

$$\begin{aligned} T_0^{(2)} &= \frac{3}{112w}(15 - 63w - D), \\ H_0^{(2)} &= -\frac{1}{4\sqrt{5}}\sqrt{-\frac{585}{8} - \frac{18225}{392w^2} + \frac{3915}{28w} + \frac{1215}{392w^2}D - \frac{225}{56w}D}, \end{aligned} \quad (4.106)$$

where we defined

$$D \equiv \sqrt{225 - 770w + 833w^2}. \quad (4.107)$$

The moduli are then extremized at the values given by

$$\begin{aligned} s_1^{(3)} &= \frac{a_1x}{N_1y} \left(T_0^{(1)} + H_0^{(1)} \right), \\ s_2^{(3)} &= \frac{a_2x}{N_2y} \left(T_0^{(1)} - H_0^{(1)} \right), \end{aligned} \quad (4.108)$$

and

$$\begin{aligned} s_1^{(4)} &= \frac{a_1x}{N_1y} \left(T_0^{(2)} + H_0^{(2)} \right), \\ s_2^{(4)} &= \frac{a_2x}{N_2y} \left(T_0^{(2)} - H_0^{(2)} \right). \end{aligned} \quad (4.109)$$

To completely determine the extrema we again need to substitute the solutions given above into the constraint equation (4.79) and choose a particular set of values for A_1 , A_2 , b_1 , and b_2 to find numerical solutions that result in real positive values for the moduli s_1 and s_2 . Here we again use the same values as we chose in the previous case given by

$$A_1 = 0.12, \quad A_2 = 2, \quad b_1 = \frac{2\pi}{8}, \quad b_2 = \frac{2\pi}{7}, \quad N_1 = 1, \quad N_2 = 1. \quad (4.110)$$

For the SUSY extremum we have

$$s_1^{(1)} = 13.05, \quad s_2^{(1)} = 13.05. \quad (4.111)$$

The de Sitter extremum is given by

$$s_2^{(2)} = 13.59, \quad s_2^{(2)} = 13.59. \quad (4.112)$$

The other two extrema are at the values

$$s_1^{(3)} = 2.61, \quad s_2^{(3)} = 23.55, \quad \text{and} \quad s_1^{(4)} = 23.55, \quad s_2^{(4)} = 2.61 \quad (4.113)$$

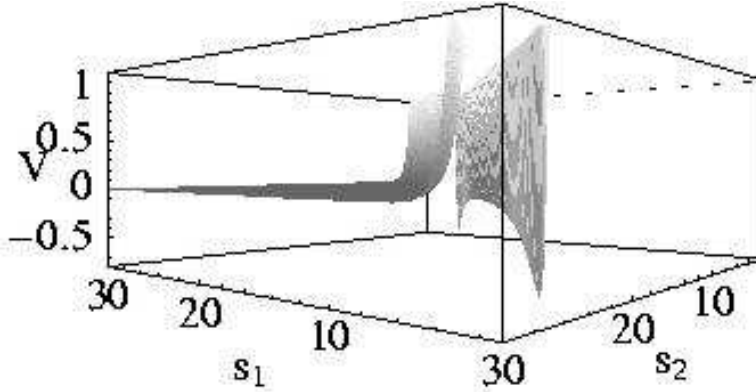


Figure 4.8: Potential multiplied by 10^{32} plotted as a function of two moduli s_1 and s_2 for the values in (4.110). The SUSY AdS extremum given by (4.111) is a saddle point, located between the non-supersymmetric AdS minima given by (4.113).

It is interesting to note that the supersymmetric extremum in (4.111) is no longer a stable minimum but instead, a saddle point. The two symmetrically located stable minima seen in figure (4.8) are non-supersymmetric. Thus we have an explicit illustration of a potential where spontaneous breaking of supersymmetry can be realized. The stable minima appear

symmetrically since both moduli were chosen to be on an equal footing in the scalar potential. With a slight deviation where $a_1 \neq a_2$ and/or $N_1 \neq N_2$ one of the minima will be deeper than the other. It is important to note that at both minima, the volume given by (4.45) is stabilized at the value $V_X = 122.28$ which is large enough for the supergravity analysis presented here to be valid.

4.2.4.3 Generalization to many moduli

In the previous section we demonstrated the existence of stable vacua with broken SUSY for the special case with two moduli. Here we will extend the analysis to include cases with an arbitrary number of moduli for any value of the parameter A . It was demonstrated in section 4.2.2.2 that the SUSY extremum has an approximate analytical solution given by (4.72). Therefore, it would be highly desirable to obtain approximate analytical solutions for the other extrema in a similar way. We will start with the observation that for the SUSY extremum (4.103) obtained for the special case when $A = 1$, both $T_1^{(1)}$ and $H_1^{(1)}$ given by (4.93) are independent of w . On the other hand, if in the leading order parameter α is given by (4.71), from the definitions in (4.80) it follows that in this case

$$y \rightarrow 0, \text{ and } w \rightarrow -\infty. \quad (4.114)$$

Thus, if we consider the system (4.85) in the limit when $w \rightarrow -\infty$, we should be able to still obtain the SUSY extremum exactly. In addition, one might also expect that the solutions for the vacua with broken SUSY may also be located near the loci where $y \rightarrow 0$. With this in mind we will take the limit (4.114) which results in the following somewhat simplified system

of equations for T_A and H_A :

$$2(T_A^2 + 2AT_A H_A + H_A^2) + 3(T_A + AH_A) = 0 \quad (4.115)$$

$$9(T_A^2 + 2AT_A H_A + H_A^2) - 4H_A(H_A + AT_A) + 21(T_A + AH_A) + 9 = 0.$$

It is straightforward to see that (4.93) is an exact solution to the above system when $A = 1$. Moreover, unlike the general case when w is finite, where the system had three real solutions two of which resulted in positive moduli, system (4.115) above completely degenerates when $A = 1$ yielding only one solution corresponding to the SUSY extremum. On the other hand, for an arbitrary $0 \leq A < 1$ the system has four solutions. One can check that at every point A in the range $0 \leq A < 1$ exactly two out of these four solutions are real. The corresponding plots are presented in Figure 4.9. Before we discuss the plots we would like to introduce some new notation:

$$L_{A,k}^{(c)} = T_A^{(c)} + m_k H_A^{(c)}, \quad (4.116)$$

where $c = \overline{1, 2}$ corresponding to the two real solutions. In this notation (4.87) can be reexpressed as:

$$\nu_{A,k}^{(c)} = \frac{x}{y} L_{A,k}^{(c)}. \quad (4.117)$$

The volume of the associative three cycle Q for these vacua is then:

$$\mathcal{T}_A^{(c)} \equiv Vol(Q)_A^{(c)} = Im(f_A^{(c)}) = \sum_{i=1}^N N_i s_{A,i}^{(c)} = \sum_{i=1}^N a_i \nu_{A,i}^{(c)} = \frac{x}{y} \vec{a} \cdot \vec{L}_A^{(c)}. \quad (4.118)$$

For future convenience we will also introduce

$$B_A^{(c)} \equiv \vec{a} \cdot \vec{L}_A^{(c)} = \frac{7}{3} (T_A^{(c)} + AH_A^{(c)}). \quad (4.119)$$

Constraint (4.79) is then given by:

$$\alpha_A^{(c)} = \frac{A_1}{A_2} e^{-(b_1 - b_2) \mathcal{T}_A^{(c)}}, \quad (4.120)$$

which is coupled to

$$\frac{x}{y} = \frac{\alpha_A^{(c)} - 1}{b_1 \alpha_A^{(c)} - b_2} = \frac{\mathcal{T}_A^{(c)}}{B_A^{(c)}}, \quad (4.121)$$

where definitions (4.80) were used to substitute for x and y . Both $L_{A,k}^{(c)}$ and $B_A^{(c)}$ are completely determined by the system (4.115), whereas $\mathcal{T}_A^{(c)}$ is determined from (4.120-4.121). Then solution (4.117) can be conveniently expressed as

$$\nu_{A,k}^{(c)} = \frac{\mathcal{T}_A^{(c)}}{B_A^{(c)}} L_{A,k}^{(c)}. \quad (4.122)$$

Recall that $m_k = \pm 1$. Thus the only two possibilities for $L_{A,k}^{(c)}$ for any $k = \overline{1, N}$ are

$$L_{A,\pm}^{(c)} = T_A^{(c)} \pm H_A^{(c)}. \quad (4.123)$$

As we vary parameter A over the range $0 \leq A < 1$ point by point, system (4.115) always has exactly two real solutions. In Figure 4.9 we present plots of $L_{A,+}^{(c)}$, $L_{A,-}^{(c)}$ and $B_A^{(c)}$, where $c = \overline{1, 2}$ as functions of A . We only need to consider the positive range $0 \leq A < 1$ because of the symmetry (4.92). What happens to these solutions when $A = 1$? We already know from the previous discussion that the system (4.115) obtained in the limit $w \rightarrow -\infty$ degenerates for $A = 1$ and one obtains the solution that corresponds to the SUSY extremum explicitly. The solutions plotted in Figure 4.9 were obtained assuming $A \neq 1$ and therefore have an apparent singularity when $A = 1$. Thus they cannot capture either the SUSY or the de Sitter extrema that arise in this special case. To explain what happens to the de Sitter extremum we need to examine the exact solution in (4.94), in the same limit. Indeed, bearing in mind that w is negative, from (4.94) we have

$$L_{A,+}^{(2)} = T_1^{(2)} + H_1^{(2)} = -\frac{3}{7} \left(\frac{3 + \sqrt{9 - 7w}}{w} \right). \quad (4.124)$$

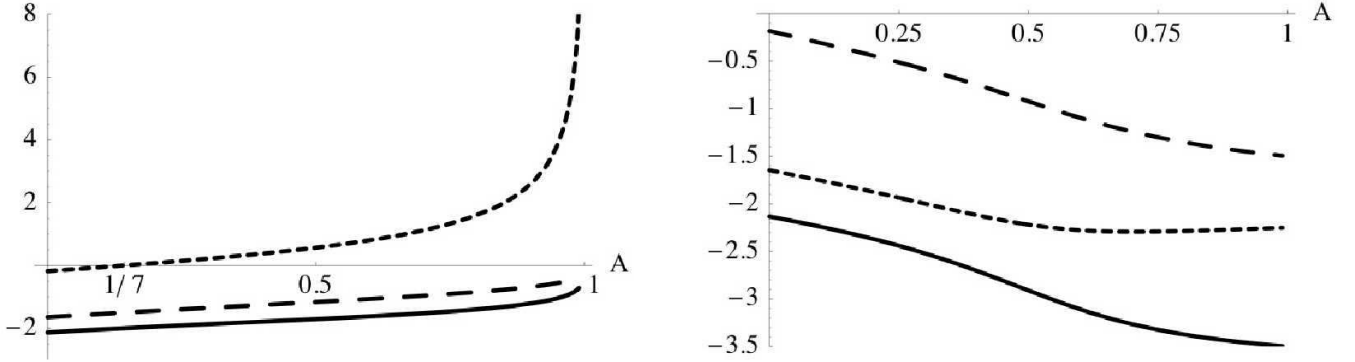


Figure 4.9: Plots of $L_{A,+}^{(c)}$, $L_{A,-}^{(c)}$ and $B_A^{(c)}$, where $c = \overline{1,2}$, corresponding to the two real solutions of the system (4.115) as functions of parameter A in the range $0 \leq A < 1$. Both left and right graphs have $L_{A,+}^{(c)}$ - long dashed line, $L_{A,-}^{(c)}$ - short dashed line, $B_A^{(c)}$ - solid line.

Left: Plots of $L_{A,+}^{(1)}$, $L_{A,-}^{(1)}$ and $B_A^{(1)}$ corresponding to the first real solution at each A . There is a critical value $A = 1/7$ where $L_{A,-}^{(1)} = 0$ and becomes positive for $A > 1/7$.

Right: Plots of $L_{A,+}^{(2)}$, $L_{A,-}^{(2)}$ and $B_A^{(2)}$ corresponding to the second real solution at each A .

Here we see immediately that in the limit $w \rightarrow -\infty$ for the solution above $L_{A,+}^{(2)} \rightarrow 0$. Therefore we conclude that the de Sitter extremum cannot be obtained from (4.115) which correlates with the previous observation that for $A = 1$ (4.115) has only one solution - the SUSY extremum. Nevertheless, as we will see in the next subsection the real solutions plotted in Figure 4.9 are a very good approximation to the exact numerical solutions corresponding to the AdS vacua with spontaneously broken supersymmetry.

Now we would like to classify which of these AdS vacua have all the moduli stabilized at positive values. Indeed if some of the moduli are fixed at negative values we can automatically exclude such vacua from further consideration since the supergravity approximation assumes that all the moduli are positive. Since the volume $\mathcal{T}_A^{(c)}$ is always positive by definition, from

(4.122) we see immediately that for all moduli to be stabilized in the positive range, all three quantities $L_{A,+}^{(c)}$, $L_{A,-}^{(c)}$ and $B_A^{(c)}$ must have the same sign. In Figure 4.9 the plots on the right satisfy this requirement for the entire range $0 \leq A < 1$. On the other hand, the short-dashed curve corresponding to $L_{A,-}^{(1)}$ on the left plot is negative when $0 \leq A < 1/7$, features a zero at $A = 1/7$ and becomes positive for $1/7 < A < 1$. Yet, both $L_{A,+}^{(1)}$ and $B_A^{(1)}$ remain negative throughout the entire range. Moreover, it is easy to verify that the solution with $T_{1/7}^{(1)} = -3/4$ and $H_{1/7}^{(1)} = -3/4$, such that $L_{1/7,-}^{(1)} = 0$ is also an exact solution for the general case (4.85) when w is finite. Therefore, all solutions compatible with the SUGRA approximation can be classified as follows:

Given a set of $\{a_i\}$ with $i = \overline{1, N}$, there are 2^N possible values of A , including the negative ones. From the symmetry in (4.92), only half of those give independent solutions. This narrows the possibilities to 2^{N-1} positive combinations that fall in the range $0 \leq A \leq 1$. For each A in the range $0 \leq A < 1/7$ there exist exactly two solutions describing AdS vacua with broken SUSY with all the moduli fixed at positive values.

For each A in the range $1/7 \leq A < 1$ there exists exactly one solution describing an AdS vacuum with broken SUSY with all the moduli stabilized in the positive range of values. For $A = 1$ there are exactly two solutions with all the moduli stabilized in the positive range - de Sitter extremum in (4.94) and the SUSY AdS extremum in (4.93). These two solutions are always present for any set of $\{a_i\}$.

4.2.4.4 Explicit approximate solutions

In this section we will complete our analysis of the AdS vacua and obtain explicit analytic solutions for the moduli. We will take an approach similar to the one we employed in section

4.2.2.2 when we obtained an approximate formula (4.72). Expressing $\alpha^{(c)}$ from (4.121) we obtain

$$\alpha_A^{(c)} = \frac{b_2 \mathcal{T}_A^{(c)} - B_A^{(c)}}{b_1 \mathcal{T}_A^{(c)} - B_A^{(c)}}. \quad (4.125)$$

There exists a natural limit when the volume of the associative cycle $\mathcal{T}_A^{(c)}$ is large. Just like in the approximate SUSY case in (4.71), the leading order solution to (4.125) in this limit is given by

$$\alpha_A^{(c)} = \frac{b_2}{b_1}, \quad (4.126)$$

independent of A and c . Plugging this into (4.120) and solving for $\mathcal{T}_A^{(c)}$ we have in the leading order

$$\mathcal{T}_A^{(c)} = \frac{1}{b_2 - b_1} \ln \left(\frac{A_2 b_2}{A_1 b_1} \right) = \frac{1}{2\pi} \frac{PQ}{P - Q} \ln \left(\frac{A_2 P}{A_1 Q} \right), \quad (4.127)$$

where we again assumed the hidden sector gauge groups to be $SU(P)$ and $SU(Q)$. Notice that this approximation automatically results in the limit $w \rightarrow -\infty$ and therefore, $L_{A,+}^{(c)}$, $L_{A,-}^{(c)}$ and $B_A^{(c)}$ computed by solving (4.115) and plotted in Figure 4.9 are consistent with this approximation. Thus, combining (4.127) with (4.122) and (4.66) we have the following approximate analytic solution for the moduli in the leading order:

$$s_{A,k}^{(c)} = \frac{1}{2\pi} \left(\frac{a_k}{N_k} \right) \left(\frac{L_{A,k}^{(c)}}{B_A^{(c)}} \right) \frac{PQ}{P - Q} \ln \left(\frac{A_2 P}{A_1 Q} \right). \quad (4.128)$$

To verify the approximation we can check it for the previously considered special case with two moduli when $a_1 = a_2 = 7/6$, i.e. the case when $A = 0$. By solving (4.115) we obtain:

$$\begin{aligned} L_{0,+}^{(1)} = L_{0,-}^{(2)} &= \frac{3}{16} \left(-9 + \sqrt{17} + \sqrt{-26 + 10\sqrt{17}} \right), \\ L_{0,-}^{(1)} = L_{0,+}^{(2)} &= \frac{3}{16} \left(-9 + \sqrt{17} - \sqrt{-26 + 10\sqrt{17}} \right), \\ B_0^{(1)} = B_0^{(2)} &= \frac{7}{16} \left(-9 + \sqrt{17} \right). \end{aligned} \quad (4.129)$$

Thus, we have the following two solutions for the moduli for the AdS vacua with broken SUSY:

$$\begin{aligned} s_{0,1}^{(1)} &= \left(1 - \frac{\sqrt{-26 + 10\sqrt{17}}}{9 - \sqrt{17}}\right) \frac{1}{4\pi N_1} \frac{PQ}{P-Q} \ln\left(\frac{A_2 P}{A_1 Q}\right) \sim \frac{0.016}{N_1} \frac{PQ}{P-Q} \ln\left(\frac{A_2 P}{A_1 Q}\right) \\ s_{0,2}^{(1)} &= \left(1 + \frac{\sqrt{-26 + 10\sqrt{17}}}{9 - \sqrt{17}}\right) \frac{1}{4\pi N_2} \frac{PQ}{P-Q} \ln\left(\frac{A_2 P}{A_1 Q}\right) \sim \frac{0.143}{N_2} \frac{PQ}{P-Q} \ln\left(\frac{A_2 P}{A_1 Q}\right). \end{aligned} \quad (4.130)$$

and

$$\begin{aligned} s_{0,1}^{(2)} &= \left(1 + \frac{\sqrt{-26 + 10\sqrt{17}}}{9 - \sqrt{17}}\right) \frac{1}{4\pi N_1} \frac{PQ}{P-Q} \ln\left(\frac{A_2 P}{A_1 Q}\right) \sim \frac{0.143}{N_2} \frac{PQ}{P-Q} \ln\left(\frac{A_2 P}{A_1 Q}\right) \\ s_{0,2}^{(2)} &= \left(1 - \frac{\sqrt{-26 + 10\sqrt{17}}}{9 - \sqrt{17}}\right) \frac{1}{4\pi N_2} \frac{PQ}{P-Q} \ln\left(\frac{A_2 P}{A_1 Q}\right) \sim \frac{0.016}{N_1} \frac{PQ}{P-Q} \ln\left(\frac{A_2 P}{A_1 Q}\right). \end{aligned} \quad (4.131)$$

The choice of the constants given in (4.110) results the following values:

$$s_{0,1}^{(1)} = s_{0,2}^{(2)} = 2.62, \quad s_{0,1}^{(2)} = s_{0,2}^{(1)} = 23.64. \quad (4.132)$$

A quick comparison with the exact values in (4.113) obtained numerically leads us to believe that the approximate analytical solutions presented here are highly accurate. This is especially true when the volume of the associative cycle $\mathcal{T}_A^{(c)}$ is large. For the particular choice above the approximate value is:

$$\mathcal{T}_0^{(1)} = \mathcal{T}_0^{(2)} = 26.16, \quad (4.133)$$

which is indeed fairly large. To complete the picture, we also would like to include the first subleading order contributions to the approximate solutions presented here. After a straightforward computation we have the following:

$$\alpha_A^{(c)} = \frac{P}{Q} + \frac{B_A^{(c)}}{\ln\left(\frac{A_2 P}{A_1 Q}\right)} \left(\frac{P-Q}{Q}\right)^2, \quad (4.134)$$

and

$$\mathcal{T}_A^{(c)} = \frac{1}{2\pi} \frac{PQ}{P-Q} \ln\left(\frac{A_2 P}{A_1 Q}\right) + \frac{B_A^{(c)}}{2\pi} \left(\frac{P-Q}{\log\left(\frac{A_2 P}{A_1 Q}\right)}\right). \quad (4.135)$$

By combining (4.135) with (4.122) and (4.66) it is easy to obtain the corresponding expressions for the moduli that include the first subleading order correction:

$$s_{A,k}^{(c)} = \frac{1}{2\pi} \left(\frac{a_k}{N_k} \right) \left(\frac{L_{A,k}^{(c)}}{B_A^{(c)}} \right) \frac{PQ}{P-Q} \ln \left(\frac{A_2 P}{A_1 Q} \right) + \frac{L_{A,k}^{(c)}}{2\pi} \left(\frac{a_k}{N_k} \right) \left(\frac{P-Q}{\ln \left(\frac{A_2 P}{A_1 Q} \right)} \right). \quad (4.136)$$

4.2.5 Vacua with charged matter in the Hidden Sector

Thus far, we have studied in reasonable detail, the vacuum structure in the cases when the hidden sector has two strongly coupled gauge groups without any charged matter. It is of interest to study how the addition of matter charged under the hidden sector gauge group changes the conclusions, as done for type IIB compactifications in [98]. We argue that the addition of charged matter can give rise to Minkowski or metastable de Sitter (dS) vacua. This is due to the additional F -term's of the matter fields. Moreover, we explain why it is reasonable to expect that for a given choice of G_2 -manifold, the dS vacuum obtained is *unique*.

4.2.5.1 Scalar Potential

Generically we would expect that a hidden sector gauge theory can possess a fairly rich particle spectrum which, like the visible sector, may include chiral matter. For example, an $SU(N_c)$ gauge theory apart from the “pure glue” may also include massless quark states Q and \tilde{Q} transforming in N_c and \bar{N}_c of $SU(N_c)$. When embedded into M theory the effective superpotential due to gaugino condensation for such a hidden sector with N_f quark flavors has the following form [99]:

$$W = A_1 e^{i \frac{2\pi}{N_c - N_f} \sum_{i=1}^N N_i^{(1)} z_i} \det(Q\tilde{Q})^{-\frac{1}{N_c - N_f}}. \quad (4.137)$$

We can introduce an effective meson field ϕ to replace the quark bilinear

$$\phi \equiv \left(Q\tilde{Q}\right)^{1/2} = \phi_0 e^{i\theta}, \quad (4.138)$$

and for notational brevity we define

$$b_1 \equiv \frac{2\pi}{N_c - N_f}, \quad a \equiv -\frac{2}{N_c - N_f}. \quad (4.139)$$

Here we will consider the case when the hidden sector gauge groups are $SU(N_c)$ and $SU(Q)$ with N_f flavors of the quarks Q (\tilde{Q}) transforming as N_c (\bar{N}_c) under $SU(N_c)$ and as singlets under $SU(Q)$. In this case, when $N_f = 1$, the effective nonperturbative superpotential has the following form:

$$W = A_1 \phi^a e^{ib_1 f} + A_2 e^{ib_2 f}. \quad (4.140)$$

One serious drawback of considering hidden sector matter is that we cannot explicitly calculate the moduli dependence of the matter Kähler potential. Therefore we will have to make some (albeit reasonable) assumptions, unlike the cases studied in the previous sections. In what follows we will assume that we work in a particular region of the moduli space where the Kähler metric for the matter fields in the hidden sector is a very slowly varying function of the moduli, essentially a constant. This assumption is based on the fact that the chiral fermions are localized at point-like conical singularities so that the bulk moduli s_i should have very little effect on the local physics. In general, a singularity supporting a chiral fermion has no local moduli, since there are no flat directions constructed from a single chiral matter representation. Our assumption is further justified by the M theory lift of some calculable Type IIA matter metrics as described in the Appendix B. It is an interesting and extremely important problem to properly derive the matter Kähler potential in M theory and test our assumptions.

Thus we will consider the case when the hidden sector chiral fermions have “modular weight zero” and assume a canonically normalized Kähler potential. Furthermore, for the sake of simplicity, we will only study the case $N_f = 1$. Since the potential is invariant under $Q \leftrightarrow \tilde{Q}$ we will focus only on vacua with $Q = \tilde{Q}$. With these assumptions, the meson field $\phi \equiv (Q\tilde{Q})^{1/2}$ is such that the corresponding Kähler potential for ϕ is canonical. Therefore, the total Kähler potential, i.e. moduli plus matter takes the form:

$$K = -3 \ln(4\pi^{1/3} V_X) + \phi\bar{\phi}. \quad (4.141)$$

The moduli F -terms are then given by

$$\begin{aligned} F_k &= ie^{ib_2\vec{N}\cdot\vec{t}} [N_k (b_1 A_1 \phi_0^a e^{-b_1\vec{N}\cdot\vec{s} + i(b_1-b_2)\vec{N}\cdot\vec{t} + ia\theta} + b_2 A_2 e^{-b_2\vec{N}\cdot\vec{s}}) \\ &\quad + \frac{3a_k}{2s_k} (A_1 \phi_0^a e^{-b_1\vec{N}\cdot\vec{s} + i(b_1-b_2)\vec{N}\cdot\vec{t} + ia\theta} + A_2 e^{-b_2\vec{N}\cdot\vec{s}})]. \end{aligned} \quad (4.142)$$

In addition, an F -term due to the meson field is also generated

$$F_\phi = \phi_0 e^{-i\theta + ib_2\vec{N}\cdot\vec{t}} \left[\left(\frac{a}{\phi_0^2} + 1 \right) A_1 \phi_0^a e^{-b_1\vec{N}\cdot\vec{s} + i(b_1-b_2)\vec{N}\cdot\vec{t} + ia\theta} + A_2 e^{-b_2\vec{N}\cdot\vec{s}} \right]. \quad (4.143)$$

The supergravity scalar potential is then given by:

$$\begin{aligned}
V &= \frac{e^{\phi_0^2}}{48\pi V_X^3} [(b_1^2 A_1^2 \phi_0^{2a} e^{-2b_1 \vec{\nu} \cdot \vec{a}} + b_2^2 A_2^2 e^{-2b_2 \vec{\nu} \cdot \vec{a}} + 2b_1 b_2 A_1 A_2 \phi_0^a e^{-(b_1+b_2) \vec{\nu} \cdot \vec{a}} \cos((b_1 - b_2) \vec{N} \cdot \vec{t} + a\theta)) \\
&\times \sum_{i=1}^N a_i (\nu_i)^2 + 3(\vec{\nu} \cdot \vec{a})(b_1 A_1^2 \phi_0^{2a} e^{-2b_1 \vec{\nu} \cdot \vec{a}} + b_2 A_2^2 e^{-2b_2 \vec{\nu} \cdot \vec{a}} + (b_1 + b_2) A_1 A_2 \phi_0^a e^{-(b_1+b_2) \vec{\nu} \cdot \vec{a}} \\
&\times \cos((b_1 - b_2) \vec{N} \cdot \vec{t} + a\theta)) + 3(A_1^2 \phi_0^{2a} e^{-2b_1 \vec{\nu} \cdot \vec{a}} + A_2^2 e^{-2b_2 \vec{\nu} \cdot \vec{a}} + 2A_1 A_2 \phi_0^a e^{-(b_1+b_2) \vec{\nu} \cdot \vec{a}} \quad (4.144) \\
&\times \cos((b_1 - b_2) \vec{N} \cdot \vec{t} + a\theta)) + \frac{3}{4} \phi_0^2 (A_1^2 \phi_0^{2a} \left(\frac{a}{\phi_0^2} + 1\right)^2 e^{-2b_1 \vec{\nu} \cdot \vec{a}} + A_2^2 e^{-2b_2 \vec{\nu} \cdot \vec{a}} \\
&+ 2A_1 A_2 \phi_0^a \left(\frac{a}{\phi_0^2} + 1\right) e^{-(b_1+b_2) \vec{\nu} \cdot \vec{a}} \cos((b_1 - b_2) \vec{N} \cdot \vec{t} + a\theta)].
\end{aligned}$$

Minimizing this potential with respect to the axions and θ we obtain the following condition:

$$\sin((b_1 - b_2) \vec{N} \cdot \vec{t} + a\theta) = 0. \quad (4.145)$$

The potential has local minima with respect to the moduli s_i when

$$\cos((b_1 - b_2) \vec{N} \cdot \vec{t} + a\theta) = -1. \quad (4.146)$$

In this case (4.144) reduces to

$$\begin{aligned}
V &= \frac{e^{\phi_0^2}}{48\pi V_X^3} [(b_1 A_1 \phi_0^a e^{-b_1 \vec{\nu} \cdot \vec{a}} - b_2 A_2 e^{-b_2 \vec{\nu} \cdot \vec{a}})^2 \sum_{i=1}^N a_i (\nu_i)^2 \\
&+ 3(\vec{\nu} \cdot \vec{a})(A_1 \phi_0^a e^{-b_1 \vec{\nu} \cdot \vec{a}} - A_2 e^{-b_2 \vec{\nu} \cdot \vec{a}})(b_1 A_1 \phi_0^a e^{-b_1 \vec{\nu} \cdot \vec{a}} - b_2 A_2 e^{-b_2 \vec{\nu} \cdot \vec{a}}) \quad (4.147) \\
&+ 3(A_1 \phi_0^a e^{-b_1 \vec{\nu} \cdot \vec{a}} - A_2 e^{-b_2 \vec{\nu} \cdot \vec{a}})^2 + \frac{3}{4} (A_1 \phi_0^a \left(\frac{a}{\phi_0} + \phi_0\right) e^{-b_1 \vec{\nu} \cdot \vec{a}} - A_2 \phi_0 e^{-b_2 \vec{\nu} \cdot \vec{a}})^2].
\end{aligned}$$

4.2.5.2 Supersymmetric extrema

Here we consider a case when the scalar potential (4.147) possess SUSY extrema and find approximate solutions for the moduli and the meson field vevs. Taking into account (4.146) and setting the moduli F -terms (4.142) to zero we obtain

$$\nu_k = \nu = -\frac{3}{2} \frac{\tilde{\alpha} - 1}{b_1 \tilde{\alpha} - b_2}, \quad (4.148)$$

together with the constraint

$$\tilde{\alpha} \equiv \frac{A_1}{A_2} \phi_0^a e^{-\frac{7}{3}(b_1 - b_2)\nu}. \quad (4.149)$$

At the same time, setting the matter F -term (4.143) to zero results in the following condition:

$$\left(\frac{a}{\phi_0^2} + 1 \right) \tilde{\alpha} - 1 = 0. \quad (4.150)$$

Expressing $\tilde{\alpha}$ from (4.148) and substituting it into (4.150) we obtain the following solution for the meson vev at the SUSY extremum:

$$\phi_0^2 = a \frac{b_2 + 3/(2\nu)}{b_1 - b_2}. \quad (4.151)$$

Recall that in our analysis we are considering the case when $P \equiv N_c - N_f > 0$, which implies that parameter a defined in (4.139) is negative. Thus, since the left hand side of (4.151) is positive, for the SUSY solution to exist, it is necessary to satisfy

$$b_2 > b_1 \quad \Rightarrow \quad P > Q. \quad (4.152)$$

Recall that for the moduli to be positive, the constants have to satisfy certain conditions resulting in two possible branches (4.73). Therefore, condition (4.152) implies that the SUSY AdS extremum exists only for branch a) in (4.73). In the limit, when ν is large, the approximate

solution is given by:

$$\begin{aligned}\tilde{\alpha} &= \frac{P}{Q}, \\ s_i &= \frac{a_i \nu}{N_i}, \quad \text{with} \quad \nu = \frac{3}{14\pi} \frac{PQ}{P-Q} \ln \left(\frac{A_2 P}{A_1 Q} \right), \\ \phi_0^2 &= \frac{2}{P-Q} + \frac{7}{P \ln \left(\frac{A_2 P}{A_1 Q} \right)},\end{aligned}\tag{4.153}$$

where we also assumed that $P \sim \mathcal{O}(10)$, such that $\phi_0^a \approx 1$. For the case with two moduli where $a_1 = a_2 = 7/6$ and the choice

$$A_1 = 4.1, \quad A_2 = 30, \quad b_1 = \frac{2\pi}{30}, \quad b_2 = \frac{2\pi}{27}, \quad N_1 = 1, \quad N_2 = 1,\tag{4.154}$$

the numerical solution for the SUSY extremum obtained by minimizing the scalar potential (4.147) gives

$$s_1 \approx 44.5, \quad s_2 \approx 44.5, \quad \phi_0 \approx 0.883,\tag{4.155}$$

whereas the approximate analytic solution obtained in (4.153) yields

$$s_1 \approx 45.0, \quad s_2 \approx 45.0, \quad \phi_0 \approx 0.882.\tag{4.156}$$

This vacuum is very similar to the SUSY AdS extremum obtained previously for the potential arising from the ‘‘pure glue’’ Super Yang-Mills (SYM) hidden sector gauge theory. Thus, we will not discuss it any further and instead move to the more interesting case, for which condition (4.152) is not satisfied.

4.2.5.3 Metastable de Sitter (dS) minima

Below we will use the same approach and notation we used in section 4.2.4, to describe AdS vacua with broken SUSY. Again, for brevity we denote

$$\tilde{x} \equiv (\tilde{\alpha} - 1), \quad \tilde{y} \equiv (b_1 \tilde{\alpha} - b_2), \quad \tilde{z} \equiv (b_1^2 \tilde{\alpha} - b_2^2), \quad \tilde{w} \equiv \frac{\tilde{x} \tilde{z}}{\tilde{y}^2}.\tag{4.157}$$

Extremizing (4.147) with respect to the moduli s_i and dividing by \tilde{x}^2 we obtain the following system of coupled equations

$$\begin{aligned} 2\frac{\tilde{y}^2}{\tilde{x}^2}\nu_k^2 &- \left(2\frac{\tilde{y}^2}{\tilde{x}^2}\tilde{w}\sum_{i=1}^N a_i\nu_i^2 + 3\frac{\tilde{y}}{\tilde{x}}(\tilde{w}+1)\vec{\nu}\cdot\vec{a} + 3 + \frac{3}{2}\phi_0^2\left(\frac{a\tilde{\alpha}}{\phi_0^2\tilde{x}} + 1\right)\left(\frac{a\tilde{\alpha}b_1}{\phi_0^2\tilde{y}} + 1\right)\right)\frac{\tilde{y}}{\tilde{x}} \\ &- 3\left(\frac{\tilde{y}^2}{\tilde{x}^2}\sum_{i=1}^N a_i\nu_i^2 + 3\frac{\tilde{y}}{\tilde{x}}\vec{\nu}\cdot\vec{a} + 3 + \frac{3}{4}\phi_0^2\left(\frac{a\tilde{\alpha}}{\phi_0^2\tilde{x}} + 1\right)^2\right) = 0, \end{aligned} \quad (4.158)$$

plus the constraint (4.149). Next, we extremize (4.147) with respect to ϕ_0 and divide it by $2\phi_0\tilde{x}^2$ to obtain:

$$\begin{aligned} \frac{\tilde{y}^2}{\tilde{x}^2}\sum_{i=1}^N a_i\nu_i^2 + \frac{3}{2}\frac{\tilde{y}}{\tilde{x}}\vec{\nu}\cdot\vec{a} + \frac{3}{4}\left(2\frac{\tilde{y}}{\tilde{x}}\vec{\nu}\cdot\vec{a} + \frac{a\tilde{\alpha}}{\tilde{x}}\left(\frac{a-1}{\phi_0^2} + 2\right) + 5 + \phi_0^2\right)\left(\frac{a\tilde{\alpha}}{\phi_0^2\tilde{x}} + 1\right) \\ + \frac{a\tilde{\alpha}b_1}{\phi_0^2\tilde{x}}\left(\frac{\tilde{y}}{\tilde{x}}\sum_{i=1}^N a_i\nu_i^2 + \frac{3}{2}\vec{\nu}\cdot\vec{a}\right) = 0. \end{aligned} \quad (4.159)$$

To solve the system of N cubic equations (4.158), we introduce a quadratic constraint

$$4\tilde{T} \equiv 2\frac{\tilde{y}^2}{\tilde{x}^2}\tilde{w}\sum_{i=1}^N a_i\nu_i^2 + 3\frac{\tilde{y}}{\tilde{x}}(\tilde{w}+1)\vec{\nu}\cdot\vec{a} + 3 + \frac{3}{2}\phi_0^2\left(\frac{a\tilde{\alpha}}{\phi_0^2\tilde{x}} + 1\right)\left(\frac{a\tilde{\alpha}b_1}{\phi_0^2\tilde{y}} + 1\right), \quad (4.160)$$

such that (4.158) turns into a system of N coupled quadratic equations:

$$2\frac{\tilde{y}^2}{\tilde{x}^2}\nu_k^2 - 4\tilde{T}\frac{\tilde{y}}{\tilde{x}}\nu_k - 3\left(\frac{\tilde{y}^2}{\tilde{x}^2}\sum_{i=1}^N a_i\nu_i^2 + 3\frac{\tilde{y}}{\tilde{x}}\vec{\nu}\cdot\vec{a} + 3 + \frac{3}{4}\phi_0^2\left(\frac{a\tilde{\alpha}}{\phi_0^2\tilde{x}} + 1\right)^2\right) = 0. \quad (4.161)$$

Again, the standard solution of a quadratic equation dictates that the solutions for ν_k of (4.161) have the form

$$\nu_k = \frac{\tilde{x}}{\tilde{y}}\left(\tilde{T} + m_k\tilde{H}\right), \quad \text{with } m_k = \pm 1, \quad k = \overline{1, N}. \quad (4.162)$$

We have now reduced the task of determining ν_k for each $k = \overline{1, N}$ to finding *only two* quantities - \tilde{T} and \tilde{H} . By substituting (4.162) into equations (4.159-4.161) and using (4.45), we obtain a

system of three coupled equations

$$\begin{aligned}
& \frac{7}{3} \left(\tilde{T}_A^2 + 2A\tilde{T}_A\tilde{H}_A + \tilde{H}_A^2 \right) + \frac{7}{2} \left(\tilde{T}_A + A\tilde{H}_A \right) + \frac{3}{4} \left[\frac{14}{3} \left(\tilde{T}_A + A\tilde{H}_A \right) + \right. \\
& \left. \frac{a\tilde{\alpha}}{x} \left(\frac{a-1}{\phi_0^2} + 2 \right) + 5 + \phi_0^2 \right] \times \left(\frac{a\tilde{\alpha}}{\phi_0^2 \tilde{x}} + 1 \right) + \\
& \frac{a\tilde{\alpha}b_1}{\phi_0^2} \frac{7}{3\tilde{y}} \left(\left(\tilde{T}_A^2 + 2A\tilde{T}_A\tilde{H}_A + \tilde{H}_A^2 \right) + \frac{3}{2} \left(\tilde{T}_A + A\tilde{H}_A \right) \right) = 0 \\
& \frac{14w}{3} \left(\tilde{T}_A^2 + 2A\tilde{T}_A\tilde{H}_A + \tilde{H}_A^2 \right) + 7(w+1) \left(\tilde{T}_A + A\tilde{H}_A \right) + 3 + \\
& \frac{3}{2} \phi_0^2 \left(\frac{a\tilde{\alpha}}{\phi_0^2 \tilde{x}} + 1 \right) \left(\frac{a\tilde{\alpha}b_1}{\phi_0^2 \tilde{y}} + 1 \right) - 4\tilde{T}_A = 0 \\
& 9 \left(\tilde{T}_A^2 + 2A\tilde{T}_A\tilde{H}_A + \tilde{H}_A^2 \right) - 4\tilde{H}_A \left(\tilde{H}_A + A\tilde{T}_A \right) + 21 \left(\tilde{T}_A + A\tilde{H}_A \right) + 9 + \\
& \frac{9}{4} \phi_0^2 \left(\frac{a\tilde{\alpha}}{\phi_0^2 \tilde{x}} + 1 \right)^2 = 0,
\end{aligned} \tag{4.163}$$

plus the constraint (4.149). Note that each solution is again labelled by parameter A so that (4.162) becomes

$$\nu_k^A = \frac{\tilde{x}}{\tilde{y}} \left(\tilde{T}_A + m_k \tilde{H}_A \right). \tag{4.164}$$

Let us consider the case when $A = 1$. In this case, the solution is given by

$$\nu_k^1 = \nu = \frac{\tilde{x}}{\tilde{y}} \left(\tilde{T}_1 + \tilde{H}_1 \right) = \frac{\tilde{x}}{\tilde{y}} \tilde{L}_{1,+}. \tag{4.165}$$

and (4.163) is reduced to

$$\begin{aligned}
& \frac{7}{3} \left(\tilde{T}_1 + \tilde{H}_1 \right)^2 + \frac{7}{2} \left(\tilde{T}_1 + \tilde{H}_1 \right) + \frac{3}{4} \left(\frac{14}{3} \left(\tilde{T}_1 + \tilde{H}_1 \right) + \frac{a\tilde{\alpha}}{x} \left(\frac{a-1}{\phi_0^2} + 2 \right) + \phi_0^2 + 5 \right) \\
& \left(\frac{a\tilde{\alpha}}{\phi_0^2 \tilde{x}} + 1 \right) + \frac{a\tilde{\alpha}b_1}{\phi_0^2} \frac{7}{3\tilde{y}} \left(\left(\tilde{T}_1 + \tilde{H}_1 \right)^2 + \frac{3}{2} \left(\tilde{T}_1 + \tilde{H}_1 \right) \right) = 0 \\
& \frac{14w}{3} \left(\tilde{T}_1 + \tilde{H}_1 \right)^2 + 7(w+1) \left(\tilde{T}_1 + \tilde{H}_1 \right) + 3 + \frac{3}{2} \phi_0^2 \left(\frac{a\tilde{\alpha}}{\phi_0^2 \tilde{x}} + 1 \right) \left(\frac{a\tilde{\alpha}b_1}{\phi_0^2 \tilde{y}} + 1 \right) - 4\tilde{T}_1 = 0 \\
& 9 \left(\tilde{T}_1 + \tilde{H}_1 \right)^2 - 4\tilde{H}_1 \left(\tilde{H}_1 + \tilde{T}_1 \right) + 21 \left(\tilde{T}_1 + \tilde{H}_1 \right) + 9 + \frac{9}{4} \phi_0^2 \left(\frac{a\tilde{\alpha}}{\phi_0^2 \tilde{x}} + 1 \right)^2 = 0.
\end{aligned} \tag{4.166}$$

In the notation introduced in (4.157), the SUSY condition (4.150) can be written as

$$\frac{a\tilde{\alpha}}{\phi_0^2} + \tilde{x} = 0. \quad (4.167)$$

It is then straightforward to check that in the SUSY case, the system (4.166) yields

$$\tilde{T}_1 = -\frac{15}{8}, \quad \tilde{H}_1 = \frac{3}{8}, \quad \tilde{L}_{1,+} = -\frac{3}{2}, \quad (4.168)$$

as expected. We will now consider branch b) in (4.73) for which (4.167) is not satisfied. Moreover, in order to obtain analytical solutions for the moduli and the meson vev ϕ_0 we will again consider the large three cycle volume approximation. Recall that in this case we take $\tilde{y} \rightarrow 0$ and $\tilde{w} \rightarrow -\infty$ limit to obtain the following reduced system of equations when $A = 1$ for $\tilde{L}_{1,+}$ and ϕ_0 :

$$\begin{aligned} \frac{7}{3} \left(\tilde{L}_{1,+} \right)^2 + \frac{7}{2} \tilde{L}_{1,+} + \frac{3}{4} \left(\frac{14}{3} \tilde{L}_{1,+} + \frac{a\tilde{\alpha}}{x} \left(\frac{a-1}{\phi_0^2} + 2 \right) + \phi_0^2 + 5 \right) \left(\frac{a\tilde{\alpha}}{\phi_0^2 \tilde{x}} + 1 \right) \\ + \frac{a\tilde{\alpha}b_1}{\phi_0^2} \frac{7}{3\tilde{y}} \left(\left(\tilde{L}_{1,+} \right)^2 + \frac{3}{2} \tilde{L}_{1,+} \right) = 0 \\ \frac{2}{3} \left(\tilde{L}_{1,+} \right)^2 + \tilde{L}_{1,+} + \frac{3a\tilde{\alpha}b_1\tilde{y}}{14\tilde{x}\tilde{z}} \left(\frac{a\tilde{\alpha}}{\phi_0^2 \tilde{x}} + 1 \right) = 0, \end{aligned} \quad (4.169)$$

Note that in (4.169), we have dropped the third equation since for $A = 1$ we only need to know $\tilde{L}_{1,+}$ and the third equation in (4.166) determines $\tilde{H}_{1,+}$ in terms of $\tilde{L}_{1,+}$. We also kept the first subleading term in the second equation. Note that the term in the second line of the first equation proportional to $\sim 1/\tilde{y}$ appears to blow up as $\tilde{y} \rightarrow 0$. However, from the second equation one can see that the combination $\left(\tilde{L}_{1,+} \right)^2 + \frac{3}{2} \tilde{L}_{1,+}$ is proportional to \tilde{y} which makes the corresponding term finite. By keeping the subleading term in the second equation, we can express

$$\left(\tilde{L}_{1,+} \right)^2 = -\frac{3}{2} \tilde{L}_{1,+} - \frac{9a\tilde{\alpha}b_1\tilde{y}}{28\tilde{x}\tilde{z}} \left(\frac{a\tilde{\alpha}}{\phi_0^2 \tilde{x}} + 1 \right) \quad (4.170)$$

from the second equation to substitute into the first equation to obtain in the leading order

$$\left(\frac{14}{3} \tilde{L}_{1,+} + 5 + \phi_0^2 + \frac{a\tilde{\alpha}}{x} \left(\frac{a-1}{\phi_0^2} + 2 \right) - \frac{1}{\tilde{z}\tilde{x}} \left(\frac{a\tilde{\alpha}b_1}{\phi_0} \right)^2 \right) \left(\frac{a\tilde{\alpha}}{\phi_0^2 \tilde{x}} + 1 \right) = 0. \quad (4.171)$$

Since we are now considering branch b) in (4.73), the second factor in (4.171) is automatically non-zero. Therefore, the first factor in (4.171) must be zero. Thus, after substituting

$$\tilde{L}_{1,+} \approx -\frac{3}{2} + \frac{3a\tilde{\alpha}b_1\tilde{y}}{14\tilde{x}\tilde{z}} \left(\frac{a\tilde{\alpha}}{\phi_0^2 \tilde{x}} + 1 \right), \quad (4.172)$$

obtained from (4.170), we have the following equation for ϕ_0

$$\phi_0^2 - 2 + \frac{a\tilde{\alpha}b_1\tilde{y}}{\tilde{x}\tilde{z}} \left(\frac{a\tilde{\alpha}}{\phi_0^2 \tilde{x}} + 1 \right) + \frac{a\tilde{\alpha}}{x} \left(\frac{a-1}{\phi_0^2} + 2 \right) - \frac{1}{\tilde{z}\tilde{x}} \left(\frac{a\tilde{\alpha}b_1}{\phi_0} \right)^2 = 0. \quad (4.173)$$

Also, since in the leading order $\tilde{L}_{1,+} = -3/2$, using the definitions in (4.157) we can express $\tilde{\alpha}$ from (4.165) in the limit when ν is large, including the first subleading term

$$\tilde{\alpha} \approx \frac{b_2}{b_1} + \frac{3(b_1 - b_2)}{2b_1^2 \nu}. \quad (4.174)$$

By combining (4.149) with the leading term in (4.174) and taking into account that $\phi_0^a \sim 1$ we again obtain

$$s_i = \frac{a_i \nu}{N_i}, \quad \text{with} \quad \nu \approx \frac{3}{14\pi} \frac{PQ}{Q-P} \ln \left(\frac{A_1 Q}{A_2 P} \right). \quad (4.175)$$

Thus, from (4.174) we have

$$\tilde{\alpha} \approx \frac{P}{Q} + \frac{7(Q-P)^2}{2Q^2 \ln \left(\frac{A_1 Q}{A_2 P} \right)}. \quad (4.176)$$

Finally, using (4.176) along with the definitions of \tilde{x} , \tilde{y} and \tilde{z} in (4.157) in terms of $\tilde{\alpha}$ we can solve for ϕ_0^2 from (4.173) and assuming that $Q - P \sim \mathcal{O}(1)$, in the limit when P is large we obtain

$$\phi_0^2 \approx 1 - \frac{2}{Q-P} + \sqrt{1 - \frac{2}{Q-P}} - \frac{7}{P \ln \left(\frac{A_1 Q}{A_2 P} \right)} \left(\frac{3}{2} + \sqrt{1 - \frac{2}{Q-P}} \right). \quad (4.177)$$

We notice immediately that since ϕ_0^2 is real and positive it is necessary that

$$Q - P > 2. \quad (4.178)$$

We will show shortly that the extremum we found above corresponds to a metastable minimum. Also, for a simple case with two moduli, via an explicit numerical check we have confirmed that if $Q - P \leq 2$ the local minimum is completely destabilized yielding a runaway potential. Also note that for (4.177) to be accurate, it is not only P which has to be large but also the product $P \ln\left(\frac{A_1 Q}{A_2 P}\right)$ has to stay large to keep the subleading terms suppressed. To check the accuracy of the solution we again consider a manifold with two moduli where $a_1 = a_2 = 7/6$ and $P = 27$, $Q = 30$, $A_1 = 27$, $A_2 = 4$, $N_1 = N_2 = 1$. The exact values obtained numerically are:

$$s_1 \approx 43.2917, \quad s_2 \approx 43.2917, \quad \phi_0 \approx 0.809. \quad (4.179)$$

The approximate equations above yield the following values:

$$s_1 \approx 43.292, \quad s_2 \approx 43.292, \quad \phi_0 \approx 0.802. \quad (4.180)$$

Note the high accuracy of the leading order approximation for the moduli s_i .

It is now straightforward to compute the vacuum energy using the approximate solution obtained above. First, we compute

$$K^{i\bar{j}} F_i \bar{F}_{\bar{j}} - 3|W|^2 = 4(A_2 \tilde{x})^2 \left(\frac{7}{9} (L_{1,+})^2 + \frac{7}{3} L_{1,+} + 1 \right) \left(\frac{A_1 Q}{A_2 P} \right)^{-\frac{2P}{Q-P}} \quad (4.181)$$

and

$$K^{\phi\bar{\phi}} F_\phi \bar{F}_{\bar{\phi}} = (A_2 \tilde{x} \phi_0)^2 \left(\frac{a\tilde{\alpha}}{\phi_0^2 \tilde{x}} + 1 \right)^2 \left(\frac{A_1 Q}{A_2 P} \right)^{-\frac{2P}{Q-P}} \quad (4.182)$$

Using (4.172), (4.181) and (4.182) we obtain the following expression for the potential at the extremum with respect to the moduli s_i as a function of ϕ_0

$$V_0 = \frac{(A_2 \tilde{x})^2}{64\pi V_X^3} \left[\phi_0^4 + \left(\frac{2a\tilde{\alpha}}{\tilde{x}} - 3 \right) \phi_0^2 + \left(\frac{a\tilde{\alpha}}{\tilde{x}} \right)^2 \right] \frac{e^{\phi_0^2}}{\phi_0^2} \left(\frac{A_1 Q}{A_2 P} \right)^{-\frac{2P}{Q-P}}, \quad (4.183)$$

where the terms linear in \tilde{y} cancelled and the quadratic terms were dropped. A quick look at the structure of the potential (4.183) as a function of ϕ_0^2 , where $\phi_0^2 > 0$, is enough to see that there is a single extremum with respect to ϕ_0^2 which is indeed, a minimum. The polynomial in the square brackets is quadratic with respect to ϕ_0^2 . Moreover, the coefficient of the ϕ_0^4 monomial is equal to unity and therefore is always positive. This implies that for the minimum of such a biquadratic polynomial to be positive, it is necessary for the corresponding discriminant to be negative, which results in the following condition:

$$3 - 4 \frac{a\tilde{\alpha}}{\tilde{x}} < 0. \quad (4.184)$$

Again, since in the leading order $\tilde{L}_{1,+} = -3/2$, using the definitions in (4.175), we can express $\tilde{\alpha}$ from (4.165) in terms of ν to get

$$\frac{\tilde{\alpha}}{\tilde{x}} = \frac{\tilde{\alpha}}{\tilde{\alpha} - 1} = \frac{P}{P - Q} + \frac{3PQ}{4\pi\nu(P - Q)}. \quad (4.185)$$

We then substitute ν from (4.175) into (4.185) and use it together with $a = -2/P$ we obtain from (4.184) the following condition

$$3 - \frac{8}{Q - P} - \frac{28}{P \ln\left(\frac{A_1 Q}{A_2 P}\right)} < 0. \quad (4.186)$$

The above equation is the leading order requirement for the energy density at the minimum to be positive. It is also clear that the minimum is *metastable*, as in the decompactification limit ($V_X \rightarrow \infty$), the scalar potential vanishes from above, leading to an absolute Minkowski minimum.

4.2.5.4 The uniqueness of the dS vacuum

In the previous subsection we found a particular solution of the system in (4.163) corresponding to $A = 1$. Here we would like to investigate if solutions for $0 \leq A < 1$ are possible

when the vacuum for $A = 1$ is de Sitter. Just like for the pure Super Yang-Mills (SYM) case, we can recast (4.164) as

$$\nu_k^A = \frac{\mathcal{T}_A}{\tilde{B}_A} \tilde{L}_{A,k}, \quad (4.187)$$

where the volume of the associative three cycle Q is again

$$\mathcal{T}_A \equiv Vol(Q)_A = \vec{a} \cdot \vec{\nu}^A = \frac{\tilde{x}}{\tilde{y}} \tilde{B}_A, \quad (4.188)$$

and we have introduced

$$\tilde{B}_A \equiv \vec{a} \cdot \vec{L}_A = \frac{7}{3} \left(\tilde{T}_A + A\tilde{H}_A \right). \quad (4.189)$$

Just like we did in equation (4.125) for the pure SYM case, we can also express $\tilde{\alpha}_A$ as

$$\tilde{\alpha}_A = \frac{b_2 \mathcal{T}_A - \tilde{B}_A}{b_1 \mathcal{T}_A - \tilde{B}_A}. \quad (4.190)$$

If we again consider the large associative cycle volume limit and take $\tilde{y} \rightarrow 0$ and $\tilde{w} \rightarrow -\infty$, the second and third equations in (4.163) in the leading order reduce to

$$\begin{aligned} 2 \left(\tilde{T}_A^2 + 2A\tilde{T}_A\tilde{H}_A + \tilde{H}_A^2 \right) + 3 \left(\tilde{T}_A + A\tilde{H}_A \right) &= 0 \\ 9 \left(\tilde{T}_A^2 + 2A\tilde{T}_A\tilde{H}_A + \tilde{H}_A^2 \right) - 4\tilde{H}_A \left(\tilde{H}_A + A\tilde{T}_A \right) + 21 \left(\tilde{T}_A + A\tilde{H}_A \right) + 9 + \frac{9}{4}\phi_0^2 \left(\frac{a\tilde{\alpha}}{\phi_0^2 \tilde{x}} + 1 \right)^2 &= 0. \end{aligned} \quad (4.191)$$

Note that the only difference between (4.115) and (4.191) is the presence of the term

$$\delta \equiv \frac{9}{4}\phi_0^2 \left(\frac{a\tilde{\alpha}}{\phi_0^2 \tilde{x}} + 1 \right)^2, \quad (4.192)$$

which couples the system (4.191) to the first equation in (4.163) which determines ϕ_0 . Instead of solving the full system to determine \tilde{T}_A , \tilde{H}_A and ϕ_0 and analyzing the solutions we choose a quicker strategy for our further analysis. Namely, we can solve the system of two equations in (4.191) and regard δ as a continuous deformation parameter. One may object to this proposition

because $\tilde{\alpha}$ and therefore $\tilde{x} = \tilde{\alpha} - 1$ are not independent of parameter A . However, in the limit when \mathcal{T}_A is large, we notice from (4.190) that in the leading order, $\tilde{\alpha}_A$ is indeed *independent* of A .

Recall that in the pure SYM case the system (4.115) corresponding to the case when $\delta = 0$ has two *real* solutions for all $0 \leq A \leq 1$. Thus, one may expect that as we continuously dial δ , the system may still yield real solutions for $A < 1$. Let us first determine the range of possible values of parameter δ . A quick calculation yields that the combination in (4.192) is the smallest with respect to ϕ_0 when $\phi_0^2 = \frac{a\tilde{\alpha}}{\tilde{x}}$. In this case

$$\delta = 9 \frac{a\tilde{\alpha}}{\tilde{x}}. \quad (4.193)$$

Now, recall from the previous subsection that for the solution corresponding to $A = 1$ to have a positive vacuum energy, condition (4.184) must hold. Since $\tilde{\alpha}$ and \tilde{x} are independent of A in the leading order, condition (4.184) implies that

$$\delta > \frac{27}{4}. \quad (4.194)$$

Again, since the volume \mathcal{T}_A is always positive, from (4.187) we see that for all moduli to be stabilized in the positive range, all three quantities $\tilde{L}_{A,+}$, $\tilde{L}_{A,-}$ and \tilde{B}_A must have the same sign. For $\delta = 27/4$, the system (4.191) has two real solutions when $0.877781 < A < 1$. However, from the left plot in Figure 4.10 corresponding to the minimum value $\delta = 27/4$ we see that neither of the two solutions satisfy the above requirement since both short-dashed curves corresponding to $\tilde{L}_{A,-}$ for the two solutions are *always* positive for the entire range $0.877781 < A < 1$, whereas both $\tilde{L}_{A,+}$ and \tilde{B}_A remain negative. Therefore for $\delta = 27/4$ and $A < 1$ there are no solutions for which all the moduli are stabilized at positive values. Moreover, as parameter δ is further increased, the range of possible values of A for which the system has two real solutions gets

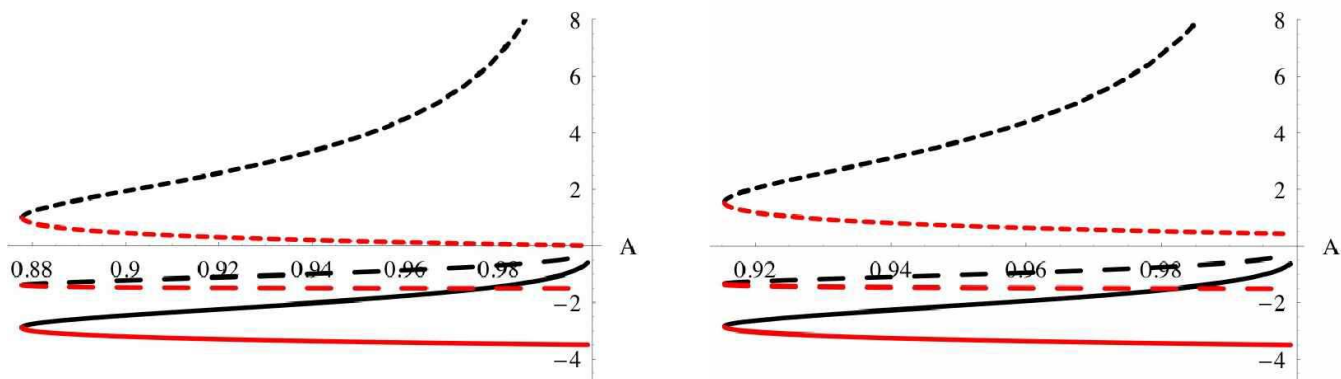


Figure 4.10: Plots of $\tilde{L}_{A,+}^{(c)}$, $\tilde{L}_{A,-}^{(c)}$ and $\tilde{B}_A^{(c)}$, where $c = \overline{1,2}$, corresponding to the two real solutions of the system (4.191) as functions of parameter A . $\tilde{L}_{A,+}^{(c)}$ - long dashed curve, $\tilde{L}_{A,-}^{(c)}$ - short dashed curve, $\tilde{B}_A^{(c)}$ - solid curve. Black color: $\tilde{L}_{A,+}^{(1)}$, $\tilde{L}_{A,-}^{(1)}$ and $\tilde{B}_A^{(1)}$ corresponding to the first real solution. Red color: $\tilde{L}_{A,+}^{(2)}$, $\tilde{L}_{A,-}^{(2)}$ and $\tilde{B}_A^{(2)}$ corresponding to the second real solution. Left plot: when $\delta = 27/4$ the real solutions exist in the range $0.877781 < A < 1$. Right plot: when $\delta = 8$ the real solutions exist st in the range $0.915342 < A < 1$.

smaller and more importantly, the values of $\tilde{L}_{A,-}$ remain positive and only increase while both $\tilde{L}_{A,+}$ and \tilde{B}_A remain negative, which can be seen from the right plot in Figure 4.10, where $\delta = 8$. This trend continues as we increase δ .

Thus, we can make the following general claim: If the solution for $A = 1$ has a positive vacuum energy, condition (4.194) must hold. When this condition is satisfied the system (4.191) has no solutions in the range $0 \leq A < 1$ for which all the moduli are stabilized at positive values. Therefore, if the vacuum found for $A = 1$ is de Sitter it is the only possible vacuum where all the moduli are stabilized at positive values. Although the above analysis was done in the limit when \mathcal{T}_A is large, we have run a number of explicit numerical checks for a manifold with two moduli and various values of the constants confirming the above claim. In addition, although we have not proved it, it seems plausible from many numerical checks we carried out that it is

also not possible to have a metastable dS minimum for values of A different from unity, even if the dS condition on the $A = 1$ vacuum is *not* imposed.

Finally, it should be noted that the situation with a “unique” dS vacuum is in sharp contrast to that when one obtains anti-de Sitter vacua, where there are between 2^{N-1} and 2^N solutions for N moduli depending on the value of A (see section 4.2.4). Let us explain this in a bit more detail. Since the dS solution found for $A = 1$ is located right in the vicinity of the “would be AdS SUSY extremum”⁴ where the moduli F -terms are nearly zero, it is the large contribution from the matter F -term (4.182) which cancels the $-3|W|^2$ term in the scalar potential resulting in a positive vacuum energy. Recall that in the leading order all the AdS vacua with the moduli vevs $s_{A,i}^{(c)}$ are located within the hyperplane⁵

$$\sum_{i=1}^N s_{A,i}^{(c)} N_i = \frac{1}{2\pi} \frac{PQ}{P-Q} \ln \left(\frac{A_2 P}{A_1 Q} \right) = \text{constant}. \quad (4.195)$$

The matter F -term contribution to the scalar potential $K^{\phi\bar{\phi}} F_\phi \bar{F}_{\bar{\phi}}$ evaluated at the same $s_{A,i}^{(c)}$ but arbitrary ϕ_0 is therefore also *constant* along the hyperplane (4.195). Thus, while the matter F -term contribution stays constant, as we move along the hyperplane (4.195) away from the dS minimum, where the moduli F -terms are the smallest, the moduli F -term contributions can only get larger so that the scalar potential becomes even more positive. This implies that the AdS minima with broken SUSY found in Section 4.2.4 completely disappear, as the AdS SUSY extremum becomes a minimum.

⁴This can be seen by comparing the leading order expression for the moduli vevs in the dS case (4.175) with the corresponding formula for the SUSY AdS extremum (4.74).

⁵ $c=1,2$ labels the two real solutions of the system (4.115).

4.2.6 Relevant Scales

We have demonstrated above that in fluxless M theory vacua, strong gauge dynamics can generate a potential which stabilizes all the moduli. Since the entire potential is generated by this dynamics, and the strong coupling scale is below the Planck scale, we also have a hierarchy of scales. In this section we will calculate some of the basic scales in detail. In particular, the gravitino mass, which typically controls the scale of supersymmetry breaking is calculated. By uniformly scanning over the constants (N, P, Q, A_k) with N_i order one, we demonstrate in 4.2.6.3 that a reasonable fraction of choices of constants have a TeV scale gravitino mass. We do not know if the space of G_2 -manifolds uniformly scans the (P, Q, A_k, N_i) or not, and more importantly, the scale of variation of the A_k 's in the space of manifolds is not clear. The variation of the A_k 's is the most important issue here, since one can certainly vary P and Q over an order of magnitude. We begin with a discussion of the basic scales in the problem. We will begin with the AdS vacua, then go on to discuss the de Sitter case. In particular, in the dS case, requiring a small vacuum energy seems to lead to superpartners at around the TeV scale.

4.2.6.1 Scales: AdS Vacua

As an example, we consider one of the non-SUSY minima in our toy model given by (4.113) and compute some of the quantities relevant for phenomenology. Namely, the vacuum energy

$$\Lambda_0 = -(5.1 \times 10^{10} \text{ GeV})^4, \quad (4.196)$$

the gravitino mass

$$M_{3/2} = m_p e^{K/2} |W| \approx 2.081 \text{ TeV}, \quad (4.197)$$

the 11-dimensional Planck scale

$$M_{11} = \frac{\sqrt{\pi} m_p}{V_X^{1/2}} \approx 3.9 \times 10^{17} \text{ GeV}, \quad (4.198)$$

the scale of gaugino condensation in the hidden sectors

$$\Lambda_g^{(1)} = m_p e^{-\frac{b_1}{3} \Sigma_i N_i s^i} \approx 2.6 \times 10^{15} \text{ GeV} \quad (4.199)$$

$$\Lambda_g^{(2)} \approx 9.7 \times 10^{14} \text{ GeV} \quad (4.200)$$

where $m_p = (8\pi G_N)^{-1/2} = 2.43 \times 10^{18} \text{ GeV}$ is the reduced four-dimensional Planck mass.

From (4.197) and (4.198), we see that it is possible to have a TeV scale gravitino mass together with $M_{11} \geq M_{unif}(2 \times 10^{16} \text{ GeV})$. This feature survives in more general cases as well, *implying that standard gauge unification is compatible with low scale SUSY in these vacua.*

4.2.6.2 Gravitino mass

By definition, the gravitino mass is given by:

$$m_{3/2} = m_p e^{K/2} |W|. \quad (4.201)$$

For the particular M theory vacua with Kähler potential given by (4.44) and the non-perturbative superpotential as in (4.48) with $SU(P)$ and $SU(Q)$ hidden sector gauge groups we have:

$$m_{3/2} = \frac{m_p}{8\sqrt{\pi} V_X^{3/2}} \left| A_1 e^{-\frac{2\pi}{P} \text{Im}f} - A_2 e^{-\frac{2\pi}{Q} \text{Im}f} \right|, \quad (4.202)$$

where the relative minus sign inside the superpotential is due to the axions. Before we get to the gravitino mass we first compute the volume of the compactified manifold V_X for the AdS vacua with broken SUSY. By plugging the approximate leading order solution for the moduli (4.128) into the definition (4.45) of V_X we obtain:

$$(V_X)_A^{(c)} = \left[\frac{1}{2\pi} \frac{PQ}{P-Q} \ln \left(\frac{A_2 P}{A_1 Q} \right) \right]^{7/3} \prod_{i=1}^N \left(\frac{a_i L_{A,i}^{(c)}}{N_i B_A^{(c)}} \right)^{a_i}. \quad (4.203)$$

Recalling the definition (4.118) of $\mathcal{T}_A^{(c)}$ and using (4.127) together with (4.203) to plug into (4.202) the gravitino mass for these vacua in the leading order approximation is given by:

$$(m_{3/2})_A^{(c)} = \sqrt{2}\pi^3 A_2 P \left| \frac{P-Q}{PQ} \right| \left[\frac{PQ}{P-Q} \ln \left(\frac{A_2 P}{A_1 Q} \right) \right]^{-\frac{7}{2}} \left[\frac{A_2 P}{A_1 Q} \right]^{-\frac{P}{P-Q}} \prod_{i=1}^N \left(\frac{N_i B_A^{(c)}}{a_i L_{A,i}^{(c)}} \right)^{\frac{3a_i}{2}}. \quad (4.204)$$

For the special case with two moduli when $a_1 = a_2 = 7/6$, considered in the previous sections we obtain the following:

$$\begin{aligned} (m_{3/2})_0^{(1,2)} &= m_p 2^{1/2} \pi^3 \left(7 + \sqrt{17} \right)^{\frac{7}{4}} (N_1 N_2)^{\frac{7}{4}} A_2 P \left| \frac{P-Q}{PQ} \right| \left(\frac{A_2 P}{A_1 Q} \right)^{-\frac{P}{P-Q}} \left(\frac{PQ}{P-Q} \ln \frac{A_2 P}{A_1 Q} \right)^{-\frac{7}{2}} \\ &\sim m_p 2.97 \times 10^3 (N_1 N_2)^{\frac{7}{4}} A_2 P \left| \frac{P-Q}{PQ} \right| \left(\frac{A_2 P}{A_1 Q} \right)^{-\frac{P}{P-Q}} \left(\frac{PQ}{P-Q} \ln \frac{A_2 P}{A_1 Q} \right)^{-\frac{7}{2}} \end{aligned} \quad (4.205)$$

For the choice of constants as in (4.110) the leading order approximation (4.205) yields:

$$(m_{3/2})_0^{(1,2)} = 2061 \text{GeV}, \quad (4.206)$$

whereas the exact value computed numerically for the same choice of constants is:

$$m_{3/2} = 2081 \text{GeV}. \quad (4.207)$$

Again, we see a good agreement between the leading order approximation and the exact values.

4.2.6.3 Scanning the Gravitino mass

In previous sections we found explicit solutions describing vacua with spontaneously broken supersymmetry. Moreover, we also demonstrated that for a particular set of the constants these solutions can result in $m_{3/2} \sim O(1)$ TeV. It would be extremely interesting and worthwhile to estimate (even roughly) the fraction of all possible solutions which exhibit spontaneously broken SUSY at the scales of $O(1)$ - $O(10)$ TeV. We would first like to do this for generic AdS/dS vacua

with a large magnitude of the cosmological constant ($\sim m_{3/2}^2 m_p^2$). The analysis for the AdS vacua is given below but as we will see, the results obtained for the fraction of vacua are virtually the same for the dS case as well. In the next subsection, we impose the requirement of a small cosmological constant as a constraint and try to understand its repercussions for the gravitino mass.

We do not yet know the range that the constants (N, P, Q, A_1, A_2) take in the space of all G_2 manifolds. Nevertheless, we do have a rough idea about some of them. For example, we expect that the quantity given by the ratio

$$\rho \equiv \frac{A_2 P}{A_1 Q}, \quad (4.208)$$

which appears in several equations, does deviate from unity. One reason for this may be due the threshold corrections [176] which in turn depend on the properties of a particular G_2 -holonomy manifold. On the other hand, since we do not expect large threshold corrections, we might guess that the range of possible values of ρ should not be much greater than one. Thus, an upper limit $\rho \leq 10$ is probably reasonable. Also, based on the duality with the Heterotic String we can get some idea on the possible range of integers P and Q corresponding to the dual coxeter numbers of the hidden sector gauge groups. Namely, since for both $SO(32)$ and E_8 gauge groups appearing in the Heterotic String theories the dual coxeter numbers are $h^v = 30$, we can tentatively assume that both P and Q can be at least as large as 30. Of course, we do not rule out any values higher than 30 but in this section we will assume an upper bound $P, Q \leq 30$.

We now turn our attention to equation (4.204) which will be used to estimate the gravitino mass scale. It is clear from the structure of the formula that $m_{3/2}$ is extremely sensitive to P , Q as well as the ratio ρ , given by (4.208). On the other hand it is less sensitive to the other

constants appearing in the equation such as N_i , a_i and the ratios $B_A^{(c)}/L_{A,i}^{(c)}$. This is because the powers $3a_i/2$ for each term under the product get much less than one as the number of moduli increases because of the constraint on a_i in (4.45). This will smooth any differences between the contributions coming from the individual factors inside the product. Since for $0 \leq A \leq 1$ (A is defined in (4.87)), the ratios $B_A^{(c)}/L_{A,i}^{(c)}$ vary only in the range $O(1)$ - $O(10)$, for our purposes it will be sufficient to simply consider (4.204) for the case when $A = 1$ corresponding to the SUSY extremum so that $B_1^{(1)}/L_{1,i}^{(1)} = 7/3$ for all i . This is certainly good enough for the order of magnitude estimates we are interested in. It also seems reasonable to assume that the integers N_i are all of $O(1)$. Yet, even if some N_i are unnaturally large, their individual contributions are generically washed out since they are raised to the powers that are much less than one. Thus, for simplicity we will take $N_i = 1$ for all $i = \overline{1, N}$. Finally, from field theory computations [100], $A_2 = Q$ (in a particular RG scheme) up to threshold corrections. We therefore take $A_2 \sim Q$ for simplicity, allowing A_1 to vary.

Thus, the gravitino mass in our analysis is given by

$$m_{3/2} \sim \sqrt{2}\pi^3 PQ \left(\frac{P-Q}{PQ} \right)^{\frac{9}{2}} [\ln \rho]^{-\frac{7}{2}} (\rho)^{-\frac{P}{P-Q}} \prod_{i=1}^N \left(\frac{7}{3a_i} \right)^{\frac{3a_i}{2}}. \quad (4.209)$$

Finally, with regard to the constants a_i which are a subject to the constraint

$$\sum_{i=1}^N a_i = \frac{7}{3}, \quad (4.210)$$

we will narrow our analysis to two opposite cases. For the first case we make the following choice

$$1) \quad a_1 = 2, \text{ and } a_i = \frac{1}{3(N-1)}, \text{ for } i = \overline{2, N}, \quad (4.211)$$

such that one modulus is generically large and all the other moduli are much smaller. This is

a highly anisotropic G_2 -manifold. The second case is

$$2) \quad a_i = \frac{7}{3N}, \quad \text{for all } i = \overline{1, N}, \quad (4.212)$$

with all the moduli being on an equal footing. Therefore, by considering these opposite cases we expect that most other possible sets of a_i will give similar results that are somewhere in between. For each set of a_i above, equation (4.209) gives

$$1) \quad m_{3/2}^{(1)} \sim \frac{343\sqrt{14}\pi^3}{216} PQ \left(\frac{P-Q}{PQ} \right)^{\frac{9}{2}} [\ln \rho]^{-\frac{7}{2}} (\rho)^{-\frac{P}{P-Q}} (N-1)^{\frac{1}{2}}, \quad (4.213)$$

$$2) \quad m_{3/2}^{(2)} \sim \sqrt{2}\pi^3 PQ \left(\frac{P-Q}{PQ} \right)^{\frac{9}{2}} [\ln \rho]^{-\frac{7}{2}} (\rho)^{-\frac{P}{P-Q}} (N)^{\frac{7}{2}}. \quad (4.214)$$

For a typical compactification we expect $N \sim O(100)$, therefore the variation of $m_{3/2}$ due to an $O(1)$ change in the number of moduli for the first case is $O(1)$ whereas in the second case it can be as large as $O(10)$. Thus, if we choose $N = 100$, we expect that our order of magnitude analysis will be fairly robust for case 1). For case 2), however, we will perform the same analysis for $N = 100$ and $N = 50$ to see how different the results will be. Before we proceed further we need to impose a restriction on the possible solutions to remain within the SUGRA framework. Using (4.203), condition that V_X must remain greater than one for the two cases under consideration translates into the following two conditions:

$$1) \quad \frac{3}{7} \left(\frac{64}{3(N-1)} \right)^{\frac{1}{7}} \frac{1}{2\pi} \frac{PQ}{P-Q} \ln \rho > 1, \quad (4.215)$$

$$2) \quad \frac{1}{2\pi N} \frac{PQ}{P-Q} \ln \rho > 1. \quad (4.216)$$

Then, as long as conditions (4.215-4.216) hold, volume of the associative cycle \mathcal{T} is greater than one is satisfied automatically - a necessary condition for the validity of supergravity. This

is obvious from comparing the right hand side of (4.127) with each condition above. From (4.215-4.216) we can find a critical value of $\rho = \rho_{crit}$ for both cases at which $V_X = 1$:

$$1) \quad \rho_{crit}^{(1)} \equiv \text{Exp} \left[\frac{14\pi}{3} \left(\frac{3(N-1)}{64} \right)^{\frac{1}{7}} \frac{P-Q}{PQ} \right], \quad (4.217)$$

$$2) \quad \rho_{crit}^{(2)} \equiv \text{Exp} \left[2\pi N \left(\frac{P-Q}{PQ} \right) \right]. \quad (4.218)$$

By substituting (4.217-4.218) into (4.213-4.214) we can find the corresponding upper limits on $m_{3/2}$ as functions of P and Q , below which our solutions are going to be consistent with the SUGRA approximation.

In Figure 4.11 we present plots of $\log_{10}(m_{3/2})$ for both cases as a function of P in the range where $\rho_{crit} \leq \rho \leq 10$ for different values of $P - Q$. On all the plots the light grey area represents possible values of $\log_{10}(m_{3/2})$ consistent with the supergravity framework. For the sake of completeness we have also included the formal plot of $\log_{10}(m_{3/2})$ corresponding to $\rho = 1.01$ represented by the dashed curve. From the plots it is clear that as the difference $P - Q$ is increased from 1 to 3 - top and from 1 to 2 - bottom, both the light grey area representing all possible values of $\log_{10}(m_{3/2})$ consistent with the SUGRA approximation and the dark area corresponding to $-16 \leq \log_{10}(m_{3/2}) \leq -14$ get significantly smaller. If we further increase $P - Q$, the light grey region shrinks even more for case 1), and does not exist for case 2), while the dark region completely disappears in both cases. Therefore, for case 2) the plots on the bottom of Figure 4.11 are the only possibilities where solutions for $P \leq 30$ and $N = 100$ consistent with the SUGRA approximation are possible, implying an upper bound $(P - Q)_{max} = 2$. It turns out that for case 1) the upper bound on $(P - Q)$ where such solutions are possible is much higher $(P - Q)_{max} = 23$.

Assuming that all values of the constants such as P , Q and ρ are equally likely to occur

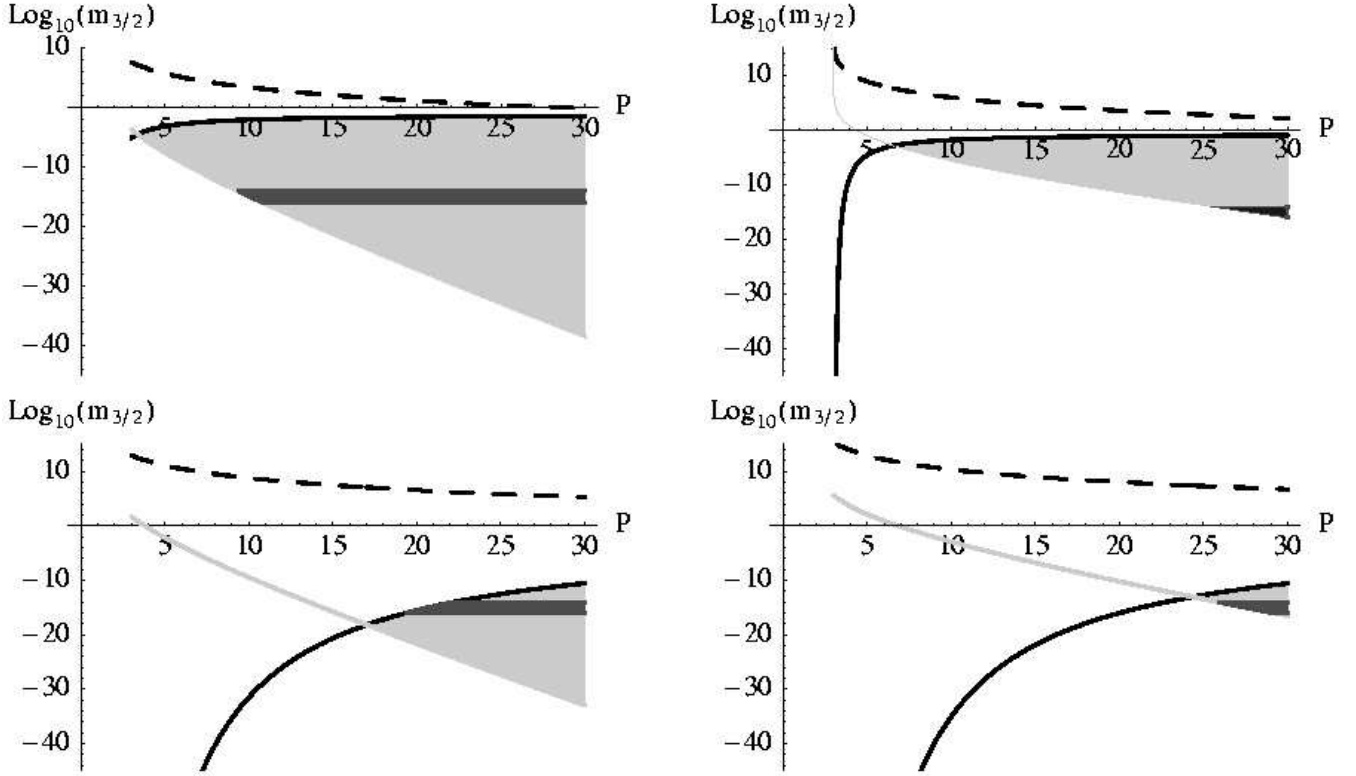


Figure 4.11: $\log_{10}(m_{3/2})$ as a function of P for case 1) - top plots and case 2) - bottom plots. The light grey area represents possible values of $\log_{10}(m_{3/2})$ in the range where $\rho_{crit} \leq \rho \leq 10$ consistent with the SUGRA approximation. The dark area indicates the region of interest where $-16 \leq \log_{10}(m_{3/2}) \leq -14$ such that $240 \text{ GeV} \leq m_{3/2} \leq 24 \text{ TeV}$. The dark solid curve corresponds to $\log_{10}(m_{3/2})$ when $\rho = \rho_{crit}$. The lower boundary of the light grey area represents the $\log_{10}(m_{3/2})$ curve when $\rho = 10$. The dashed curve corresponds to $\rho = 1.01$. Top left: Case 1) when $P - Q = 1$. Top right: Case 1) when $P - Q = 3$. Bottom left: Case 2) when $P - Q = 1$. Bottom right: Case 2) when $P - Q = 2$.

in the ranges chosen above we can perform a crude estimate of the number of solutions with $-16 \leq \log_{10}(m_{3/2}) \leq -14$ relative to the total number of possible solutions consistent with the SUGRA approximation. In doing so we will use the following approach. For each value of $(P - Q)$ in the range $1 \leq (P - Q) \leq (P - Q)_{max}$ we compute the area of the grey region for each plot and then add all of them to find the total volume corresponding to all possible values

of $\log_{10}(m_{3/2})$ consistent with the supergravity approximation.

$$\Omega_{tot} = \sum_{(P-Q)=1}^{(P-Q)_{max}} \int_{P_{min}}^{30} dP \log_{10}(m_{3/2})|_{\{\rho_{crit} \leq \rho \leq 10\}}. \quad (4.219)$$

Likewise, we add all the dark areas for each plot to find the volume corresponding to the region where $-16 \leq \log_{10}(m_{3/2}) \leq -14$

$$\Omega_0 = \sum_{(P-Q)=1}^{(P-Q)_{max}^*} \int dP \log_{10}(m_{3/2})|_{\left\{ \begin{array}{l} \rho_{crit} \leq \rho \leq 10 \\ -16 \leq \log_{10}(m_{3/2}) \leq -14 \end{array} \right\}}, \quad (4.220)$$

where $(P-Q)_{max}^*$ is an upper bound before the dark region completely disappears. From the previous discussion, for case 1): $(P-Q)_{max}^* = 3$; for case 2): $(P-Q)_{max}^* = 2$. Then, the fraction of the volume where $240 \text{ GeV} \leq m_{3/2} \leq 24 \text{ TeV}$ is given by the ratio

$$\Delta = \frac{\Omega_0}{\Omega_{tot}}. \quad (4.221)$$

Numerical computations yield the following values for the two cases when $N = 100$:

$$1) \quad \Delta_1 = 3.5\%, \quad (4.222)$$

$$2) \quad \Delta_2 = 13.6\%. \quad (4.223)$$

Because of the significant difference in the dependence of ρ_{crit} on the number of moduli N in (4.217) versus (4.218), the number of solutions consistent with the SUGRA approximation is cut down dramatically in case 2) compared to case 1). This also occurs because of the different dependence of $m_{3/2}$ in (4.213) and (4.214) on N . Namely, for $N \sim O(100)$, the values of $m_{3/2}$ for case 2) in (4.214) are $\sim O(10^6)$ greater than those for case 1). Furthermore, for the same reasons, it turns out that if we keep increasing the number of moduli N , for case 2) there is an upper bound $N \leq 157$ for the solutions with $240 \text{ GeV} \leq m_{3/2} \leq 24 \text{ TeV}$ compatible with the

SUGRA approximation to exist at all. Of course, this upper bound can be higher if we allow P to be greater than 30.

By performing the same analysis for $N = 50$ we get the following estimates

$$1) \quad \Delta_1 = 3.4\%, \quad (4.224)$$

$$2) \quad \Delta_2 = 10.7\%. \quad (4.225)$$

As expected, decreasing the number of moduli by a half has produced little effect on Δ_1 while decreasing Δ_2 by a few percent. These numbers coming from our somewhat crude analysis already demonstrate that a comparatively large fraction of vacua in M theory generate the desired hierarchy between the Planck and the electroweak scale physics. Also, one can easily check that all the solutions consistent with the SUGRA framework for which $240 \text{ GeV} \leq m_{3/2} \leq 24 \text{ TeV}$ for any number of moduli N satisfy the following bound on the eleven dimensional scale

$$3.6 \times 10^{16} \text{ GeV} \leq m_{11} \leq 4.3 \times 10^{18} \text{ GeV}, \quad (4.226)$$

which makes them compatible with the standard unification at $M_{GUT} \sim 2 \times 10^{16} \text{ GeV}$. This is also a nice feature. Of course, apart from determining the upper and lower bounds on the constants, it would be desirable to know their distribution for all possible manifolds of G_2 holonomy. In this case instead of using the flat statistical measure as we did here, each solution would be assigned a certain weight making the sampling analysis more accurate. However, this is an extremely challenging task which goes beyond the scope of this work.

The simple analysis presented in this section clearly points to a very restrictive nature of the solutions. Namely, the requirement of consistency with the supergravity regime results in very strict bounds on the properties of the compactification manifold. Further requirements

coming from the SUSY breaking scale to be in the range required for supersymmetry to solve the hierarchy problem narrows down the class of possible G_2 holonomy manifolds even more. It would be extremely interesting to know to what extent these results extend into the small volume, "stringy" regime, about which we have nothing to say here.

4.2.6.4 Results for dS Vacua

We will now show that the results obtained in the previous subsection also hold true for dS vacua with Kähler potential given by (4.141) and the non-perturbative superpotential as in (4.140) with $SU(N_c)$ and $SU(Q)$ hidden sector gauge groups. For this case, we have :

$$m_{3/2} = m_p \frac{e^{\phi_0^2/2}}{8\sqrt{\pi}V_X^{3/2}} \left| A_1 \phi_0^a e^{-\frac{2\pi}{P}\text{Im}f} - A_2 e^{-\frac{2\pi}{Q}\text{Im}f} \right|, \quad (4.227)$$

where the relative minus sign inside the superpotential is due to the axions and $P \equiv N_c - 1$. Before we get to the gravitino mass we first compute the volume of the compactified manifold V_X for the metastable dS vacuum with broken SUSY. By substituting the approximate leading order solution for the moduli (4.175) into the definition (4.45) of V_X we obtain:

$$V_X = \left(\frac{1}{2\pi} \right)^{7/3} \left[\frac{PQ}{Q-P} \ln \left(\frac{A_1 Q}{A_2 P} \right) \right]^{7/3} \prod_{i=1}^N \left(\frac{3a_i}{7N_i} \right)^{a_i}. \quad (4.228)$$

Recalling the definition of $\text{Im}(f)$ in terms of ν and using the solution for ν (eqn.(4.175)) together with (4.228), the gravitino mass for the dS vacuum in the leading order approximation is given by:

$$m_{3/2} = m_p \sqrt{2\pi}^3 A_2 \left| \frac{P}{Q} \phi_0^{-\frac{2}{P}} - 1 \right| \left(\frac{PQ}{Q-P} \ln \left(\frac{A_1 Q}{A_2 P} \right) \right)^{-\frac{7}{2}} \left(\frac{A_1 Q}{A_2 P} \right)^{-\frac{P}{Q-P}} \prod_{i=1}^N \left(\frac{7N_i}{3a_i} \right)^{\frac{3a_i}{2}} e^{\phi_0^2/2}, \quad (4.229)$$

where ϕ_0^2 is given by (4.177). Since $\phi_0^{-2/P} \sim 1$ from section 4.2.5 and $A_2 \sim Q$, we see that the expression for the gravitino mass for dS vacua is almost the same as that for the AdS vacua

(eqn. 4.209) provided we replace ρ in (4.209) by $\tilde{\rho} = A_1 Q/A_2 P$ in (4.229) and $P - Q$ in (4.209) by $Q - P$ in (4.229). Therefore, the results obtained for the fraction of vacua with a gravitino mass in the $O(1 - 10)$ TeV range also hold for this case.

4.2.6.5 Small Cosmological Constant implies Low-scale Supersymmetry in dS Vacua

In this subsection we will study the distribution of SUSY breaking scales in the de Sitter vacua which as we showed earlier, can arise when the hidden sector has chiral matter. In particular we will see that the requirement of a small cosmological constant leads to a scale of SUSY breaking of $\mathcal{O}(1 - 100)$ TeV.

In section VI, we saw that the minimum obtained is de Sitter if the discriminant of the quadratic polynomial with respect to ϕ_0^2 in eqn. (4.183) is negative, while it is anti-de Sitter if the discriminant in (4.183) is positive. For $m_{3/2} \sim \mathcal{O}(1 - 10 \text{ TeV})$ the magnitude of the vacuum energy in both cases can be estimated to be

$$|V_0| \sim m_p^2 m_{3/2}^2 \sim (10^{10} \text{ GeV})^4 - (10^{11} \text{ GeV})^4. \quad (4.230)$$

On the other hand, if the discriminant in (4.183) vanishes, one obtains a vanishing cosmological constant (to leading order in the approximation). At present it is not known if there is a physical principle which imposes this condition. However, one can still use it as an observational constraint since the observed value of the cosmological constant is known to be extremely small. For instance, if the space of G_2 manifolds scans the constants (A_i, P, Q, N) finely enough there could simply exist vacua for which the vacuum energy is acceptably low.

By setting the left hand side in (4.186) to zero we can then express

$$P \ln \left(\frac{A_1 Q}{A_2 P} \right) = \frac{28(Q - P)}{3(Q - P) - 8}, \quad (4.231)$$

Of course, since the above constraint was obtained in the leading order, the vacuum energy is only zero in the leading order in our analytic expansion. The subleading contributions we neglected in (225) although smaller than the leading contributions, are still much larger than the observed value of the cosmological constant. However, one can *in principle* take into account all the subleading corrections and tune the ratio A_1Q/A_2P inside the logarithm to set the vacuum energy to a very small value compatible with the observations. As will be seen later, since the expression in the R.H.S. of (4.231) turns out to be large, the subleading corrections which affect the value of the cosmological constant will have little effect on the phenomenological quantities calculated by imposing the constraint to leading order.

We would now like to analyze in detail the phenomenological implications of the solutions obtained by imposing (4.231) as a constraint. The most important phenomenological quantity in this regard is the gravitino mass as it sets the scale of all soft supersymmetry breaking parameters. We focus on the gravitino mass in this section. The soft supersymmetry breaking parameters will be discussed in section 4.2.7.

4.2.6.6 Gravitino mass with a small positive cosmological constant

By substituting the constraint (4.231) into the gravitino mass formula (4.229), we obtain:

$$m_{3/2} = m_p \sqrt{2} \pi^3 A_2 \left| \frac{P}{Q} \phi_0^{-\frac{2}{P}} - 1 \right| \left(\frac{28Q}{3(Q-P)-8} \right)^{-\frac{7}{2}} e^{-\frac{28}{3(Q-P)-8}} \prod_{i=1}^N \left(\frac{7N_i}{3a_i} \right)^{\frac{3a_i}{2}} e^{\phi_0^2/2}, \quad (4.232)$$

where the meson vev is now given by:

$$\phi_0^2 \approx -\frac{1}{8} + \frac{1}{Q-P} + \frac{1}{4} \sqrt{1 - \frac{2}{Q-P}} + \frac{2}{Q-P} \sqrt{1 - \frac{2}{Q-P}}. \quad (4.233)$$

In this case, the moduli vevs are given by

$$s_i = \frac{a_i \nu}{N_i}, \quad \text{with} \quad \nu \approx \frac{6Q}{\pi(3(Q-P)-8)}. \quad (4.234)$$

From (4.232), one notes that the gravitino mass (when the cosmological constant is made tiny) is completely determined by the dual coxeter numbers of the hidden sector gauge groups N_c and Q , the rational numbers a_i (see (4.45)) characterizing the volume of the G_2 manifold and the integers N_i .⁶

The rationals a_i are subject to the constraint $\sum_{i=1}^N a_i = 7/3$. It is reasonable to consider a “democratic” choice for a_i , $a_i = 7/(3N)$ for all $i = \overline{1, N}$ and also to take for simplicity all the integers $N_i = 1$. The integers N_i will generically be of $\mathcal{O}(1)$; even if some of the N_i are unnaturally large, their individual contributions will be typically washed out as they are raised to powers that are much less than unity (see (4.229) and the expression for a_i for the democratic choice). In this case, after setting $A_2 = Q C_2$, the gravitino mass formula is given by

$$m_{3/2} = m_p \sqrt{2} \pi^3 C_2 \left| P \phi_0^{-\frac{2}{P}} - Q \right| \left(\frac{N(3(Q-P)-8)}{28Q} \right)^{\frac{7}{2}} e^{-\frac{28}{3(Q-P)-8} \phi_0^2/2}, \quad (4.235)$$

and the moduli vevs are

$$s_i = \frac{14Q}{\pi N(3(Q-P)-8)}. \quad (4.236)$$

From (4.235), the gravitino mass depends on just four constants - C_2 , P , Q and N (the total number of moduli), determined by the topology of the manifold. It should be kept in mind that for the solution to exist, it is necessary that $Q - P > 2$ (see (4.178)). For the smallest possible value $(Q - P)_{min} = 3$, the expression for $m_{3/2}$ simplifies even further

$$m_{3/2} = m_p \sqrt{2} \pi^3 C_2 \left| P(\phi_0^{-\frac{2}{P}} - 1) - 3 \right| \left(\frac{N}{28(P+3)} \right)^{\frac{7}{2}} e^{-28} e^{\phi_0^2/2} \approx m_p 3\sqrt{2} \pi^3 C_2 \left(\frac{N}{28(P+3)} \right)^{\frac{7}{2}} e^{-28} e^{\phi_0^2/2}. \quad (4.237)$$

⁶From field theory computations [100], $A_1 = N_c - N_f = P$ and $A_2 = Q$ (in a particular RG scheme), up to threshold corrections. We can therefore express A_1 , A_2 as $A_1 = P C_1$ and $A_2 = Q C_2$, where coefficients C_1 and C_2 depend *only* on the threshold corrections and are constant with respect to the moduli [176]. In this case, the quantity $\ln(A_1 Q / A_2 P) = \ln(C_1 / C_2)$ is fixed by imposing (4.231).

together with

$$\phi_0^2 \approx \frac{1}{72} \left(15 + 22\sqrt{3} \right) \approx 0.7376, \quad s_i = \frac{14(P+3)}{\pi N}.$$

Note that the dependence on N and P in (4.237) is due solely to the volume V_X dependence on those parameters. The expression for the gravitino mass has a more transparent form if we don't substitute the expression for the volume (4.228) into (4.227). For $Q - P = 3$ we obtain

$$m_{3/2} \approx m_p \frac{3 e^{\phi_0^2/2}}{8\sqrt{\pi}V_X^{3/2}} e^{-28} C_2 \approx 514 \text{ TeV} \frac{C_2}{V_X^{3/2}}, \quad (4.238)$$

where the detailed dependence on a_i , N_i , P and the number of moduli N is completely encoded inside the seven-dimensional volume V_X which appears to be the more relevant physical quantity. Furthermore, in the supergravity approximation the volume $V_X > 1$, which translates into an upper bound on the gravitino mass when $Q - P = 3$

$$m_{3/2} < \mathcal{O}(100 \text{ TeV}). \quad (4.239)$$

4.2.6.7 The Gravitino mass Distribution and its consequences

The gravitino mass (4.235) depends on three integers: the two gauge group dual coxeter numbers N_c , Q and the number of moduli N .⁷ This will give us an idea about the distribution of the gravitino mass (which sets the superpartner masses) obtained after imposing the constraint (4.231) that the vacuum energy is acceptable. Besides from only considering the vacua within the supergravity approximation (ie $s_i > 1$) we expect an upper bound on the dual coxeter numbers of the hidden sector gauge groups P and Q . Based on duality with the heterotic string, it seems reasonable to assume that they can be at least as large as 30 - the dual coxeter number of E_8 . Of course, values of P, Q larger than 30 cannot be ruled out, and here we assume an upper bound $P \leq 100$.

⁷We can set $C_2 = 1$ for the order of magnitude estimates we are doing here.

The distribution can be constructed as follows. The three integers: P , $Q - P$ and N are varied subject to (4.178) and the supergravity constraint $s_i > 1$. For each point in the resulting two dimensional subspace, $\log_{10}(m_{3/2})$ can be computed and rounded off to the closest integer value. One can then count how many times each integer value is encountered in the entire scan and plot the corresponding distribution. In the first three scans we cover a broad range of

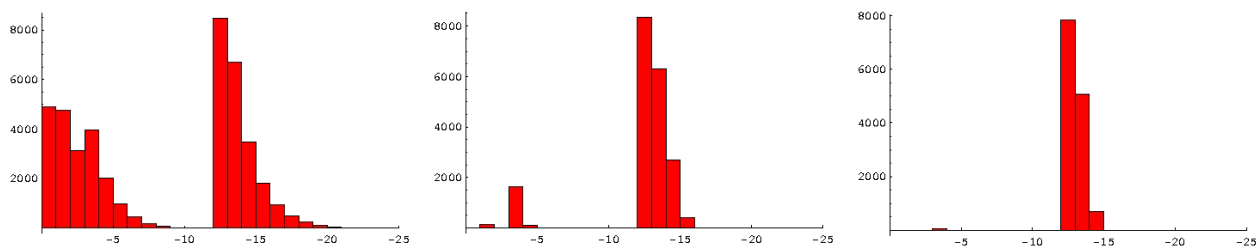


Figure 4.12: The gravitino mass distribution with the x-axis denoting the logarithm of the gravitino mass (to base 10). Left: Distribution corresponding to scan one in (4.240). Middle: Distribution corresponding to scan two in (4.241) for which manifolds with the number of moduli $N < 50$ were excluded from the scan. Right: Distribution corresponding to scan three in (4.242) for which manifolds with the number of moduli $N < 100$ were excluded from the scan.

values by choosing $P_{max} = 100$. Taking into account the SUGRA constraint ($s_i > 1$), we have the following ranges of integers for the first scan:

$$3 \leq P \leq 100; \quad 3 \leq (Q - P) \leq 100 - P; \quad 2 \leq N < \frac{14(P + (Q - P))}{\pi(3(Q - P) - 8)}. \quad (4.240)$$

In the second scan we have excluded the small N region and considered only the manifolds with $N \geq 50$. Thus we have the following ranges of constants for the second scan:

$$3 \leq P \leq 100; \quad 3 \leq (Q - P) \leq 100 - P; \quad 50 \leq N < \frac{14(P + (Q - P))}{\pi(3(Q - P) - 8)}. \quad (4.241)$$

In the third scan we have only considered manifolds with $N \geq 100$. Thus we have the following

ranges of integers for the second scan:

$$3 \leq P \leq 100; \quad 3 \leq (Q - P) \leq 100 - P; \quad 100 \leq N < \frac{14(P + (Q - P))}{\pi(3(Q - P) - 8)}. \quad (4.242)$$

The first two distributions in Figure 4.12 clearly have several prominent peaks. Amazingly, in all three plots one of the peaks landed right in the $m_{3/2} \sim \mathcal{O}(1 - 100)$ TeV range! The high scale peaks on the left plot appear to be around $m_{3/2} \sim 10^{14}$ GeV and the GUT scales. However, for the middle plot the GUT scale peak almost disappears. Recall that the middle plot corresponds to scan two in (4.241) where we excluded all the manifolds for which the number of moduli N is less than 50. Therefore, the high scale peaks are largely dominated by contributions from the G_2 manifolds with a small number of moduli $N < 50$. As seen from the right plot, when G_2 manifolds with $N < 100$ are excluded from the scan, the peak at the $m_{3/2} \sim 10^{14}$ GeV scale has all but disappeared, whereas the peak at $m_{3/2} \sim \mathcal{O}(1 - 100)$ TeV remains virtually unchanged.

In Figure 4.13 we included three more scans for which the upper bound on P was reduced to $P_{max} = 30$. The fourth scan has the following ranges:

$$3 \leq P \leq 30; \quad 3 \leq (Q - P) \leq 30 - P; \quad 2 \leq N < \frac{14(P + (Q - P))}{\pi(3(Q - P) - 8)}. \quad (4.243)$$

In the fifth scan we again excluded the small N region and considered only the manifolds with $N \geq 50$ and considered $P_{max} = 30$:

$$3 \leq P \leq 30; \quad 3 \leq (Q - P) \leq 30 - P; \quad 50 \leq N < \frac{14(P + (Q - P))}{\pi(3(Q - P) - 8)}. \quad (4.244)$$

In the sixth scan we considered only the manifolds with $N \geq 100$ and $P_{max} = 30$:

$$3 \leq P \leq 30; \quad 3 \leq (Q - P) \leq 30 - P; \quad 100 \leq N < \frac{14(P + (Q - P))}{\pi(3(Q - P) - 8)}. \quad (4.245)$$

Again, in Figure 4.13 we notice that the $\mathcal{O}(1 - 100)$ TeV peak narrows around $m_{3/2} \sim$

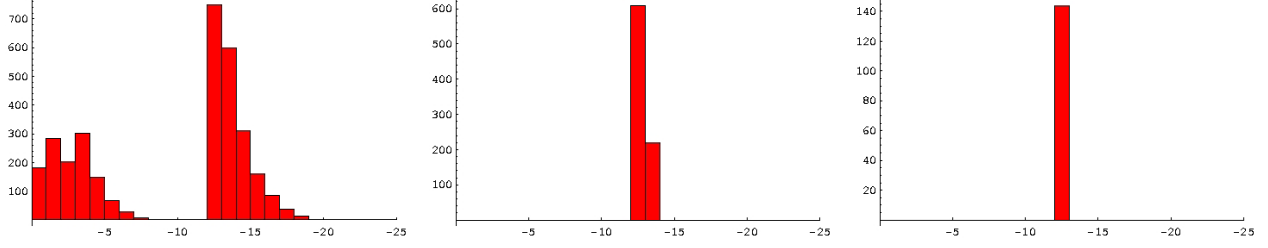


Figure 4.13: The gravitino mass distribution with the x-axis denoting the logarithm of the gravitino mass (to base 10). Left: Distribution corresponding to scan four in (4.243). Middle: Distribution corresponding to scan five in (4.244) for which manifolds with the number of moduli $N < 50$ were excluded from the scan. Right: Distribution corresponding to scan six in (4.245) for which manifolds with the number of moduli $N < 100$ were excluded from the scan.

$\mathcal{O}(100)$ TeV, as we exclude manifolds with small number of moduli. As the same time, the peaks at the high scale completely disappear for G_2 manifolds with $N > 50$. Finally, in Figure 4.14 we chose the smallest possible value $Q - P = 3$ and scanned integers P and N in the

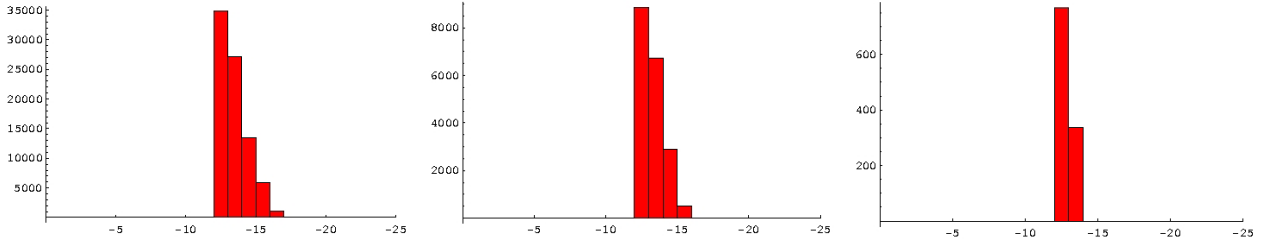


Figure 4.14: The gravitino mass distribution with the x-axis denoting the logarithm of the gravitino mass (to base 10). Scans for the smallest possible choice $(Q - P)_{min} = 3$. Left: Distribution corresponding to the scan with $P_{max} = 200$. Middle: Distribution corresponding to the scan with $P_{max} = 100$. Right: Distribution corresponding to the scan with $P_{max} = 30$.

following ranges:

$$\begin{aligned}
3 \leq P \leq 200; \quad 50 \leq N < \frac{14(P+3)}{\pi}, \\
3 \leq P \leq 100; \quad 50 \leq N < \frac{14(P+3)}{\pi}, \\
3 \leq P \leq 30; \quad 50 \leq N < \frac{14(P+3)}{\pi}.
\end{aligned} \tag{4.246}$$

In all three plots in Figure 4.14 we see the same peak at $m_{3/2} \sim \mathcal{O}(1-100)$ TeV, which narrows around $m_{3/2} \sim \mathcal{O}(100)$ TeV as P_{max} is decreased.

Therefore, from the above distributions we conclude that the peak corresponding to $m_{3/2} \sim (1-100)$ TeV is entirely due to the smallest possible value $(Q-P)_{min} = 3$. This can be explained if we examine the gravitino mass formula in (4.237). In particular the constant factor $e^{-28} \sim 10^{-12}$ is most crucial in lowering the gravitino mass to the TeV scale. It is easy to trace the origin of this factor to the constraint (4.231), imposed by the requirement to have a zero cosmological constant (to leading order). When (4.231) is used along with the requirement $Q-P=3$ we simply get

$$P \ln \left(\frac{A_1 Q}{A_2 P} \right) = 84. \tag{4.247}$$

When this is substituted into the gravitino mass (4.229), the corresponding suppression factor turns into the constant

$$\left(\frac{A_1 Q}{A_2 P} \right)^{-\frac{P}{Q-P}} = e^{-28}. \tag{4.248}$$

Physically, this suppression factor corresponds to the hidden sector gaugino condensation scale (cubed). Recall that for an $SU(Q)$ hidden sector gauge group, the scale of gaugino condensation is given by

$$\Lambda_g = m_p e^{-\frac{8\pi^2}{3Qg^2}} = m_p e^{-\frac{2\pi}{3Q} \text{Im}f}. \tag{4.249}$$

The moduli vevs in (4.234) completely determine the gauge kinetic function. Taking $Q - P = 3$ we obtain

$$\text{Im}f = \sum_{i=1}^N N_i s_i = \frac{14Q}{\pi}. \quad (4.250)$$

Substituting (4.250) into (4.249) we obtain the following scale of gaugino condensation

$$\Lambda_g = m_p e^{-28/3} \approx 2.15 \times 10^{14} \text{ GeV}. \quad (4.251)$$

It is important to note that the expression in the R.H.S. of (4.231) is quite large ($= 84$, when $Q - P = 3$) in the leading order, and the quantity $(A_1 Q / A_2 P)$ which is fixed by imposing the vacuum energy constraint is inside a logarithm. Therefore, even when one incorporates all the higher order corrections and tunes the ratio $A_1 Q / A_2 P$ inside the logarithm to set the cosmological constant equal to the observed value, the constant on the R.H.S. ($=84$), crucial in obtaining the $\mathcal{O}(100)$ TeV scale peak, is hardly affected.

The dominance of the $\mathcal{O}(1 - 100)$ TeV range also becomes clear from Figure 4.15, where $\log_{10}(m_{3/2})$ as a function of P for $Q - P = 3$ is plotted for a manifold with $N = 50$ moduli - short-dashed curve, and a manifold with $N = 500$ moduli - long-dashed curve. Indeed, even when we do not impose the SUGRA constraint, from the above plot we can see that the $\mathcal{O}(1 - 100)$ TeV range is covered by a large swath of the vacuum space and it is not so surprising that the corresponding distribution peaks at that scale. This essentially follows from the formula for the gravitino mass in (4.237).

An important point which should be emphasized is that for $Q - P = 3$, the gravitino mass dependence on P and N appears *only* through the volume V_X , as can be seen from (4.238). Thus, the distribution in Figure 4.14 directly correlates with the corresponding distribution of the stabilized volume of the seven-dimensional manifold V_X as a function of P and N .

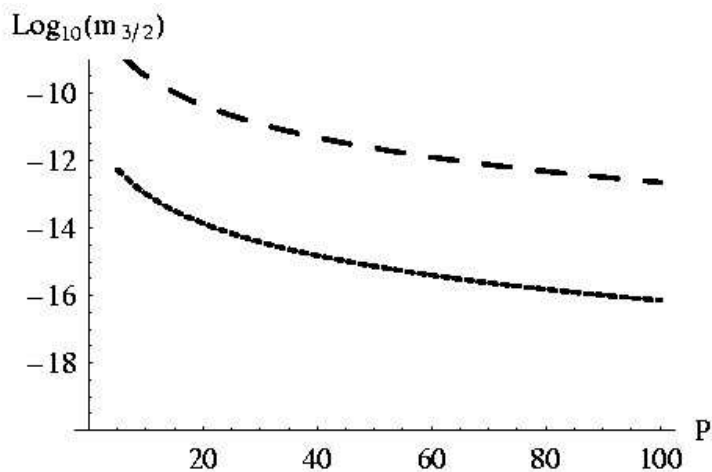


Figure 4.15: Plot of $\log_{10}(m_{3/2})$ as a function of P for $Q - P = 3$. Short-dashed curve corresponds to $N = 50$. Long-dashed curve corresponds to $N = 500$.

Therefore, it is the dominance of the vacua with a relatively small volume, which results in the peak at $\mathcal{O}(100)$ TeV.

Also note that in the above analysis we simply set the constant coefficient due to the threshold corrections C_2 to unity. It would be interesting to get a handle on this quantity and include its variation into the gravitino mass distribution study.

One could argue that even though $Q - P = (Q - P)_{min} = 3$ gives a peak for the gravitino mass distribution at around $\mathcal{O}(100)$ TeV scale, it seems plausible from a theoretical point of view to have many examples of gauge singularities in G_2 manifolds such that $Q - P > 3$. However, by imposing the supergravity constraint that all moduli s_i are larger than unity (which is the regime in which the entire analysis is valid), one sees that having $Q - P > 3$ drastically reduces the upper bound on N compared to that for $Q - P = 3$ (see eqn(4.234)). Therefore, the peaks in the gravitino mass distribution obtained for $-2 \leq \log_{10}(m_{3/2}) \leq -5$ in Figures 4.12 and 4.13 come from vacua with a *small* number of moduli as well as $Q - P > 3$,

compatible with the analysis in the supergravity regime. Since it is presumably true that the number of G_2 manifolds with the required gauge singularities which have a large number of moduli is much larger than those with a small number of moduli, it seems reasonable to expect that the peak of the gravitino mass distribution obtained at around $\mathcal{O}(100)$ TeV scale is quite robust and is representative of the most generic class of G_2 manifolds with the appropriate gauge singularities.

One could also contrast the results obtained above with those obtained for the Type IIB flux vacua. In Type IIB flux vacua, one has to *independently* tune both the gravitino mass to a TeV scale (if one requires low scale supersymmetry to solve the hierarchy problem) as well as the cosmological constant to its observed value. This is quite different to what we are finding here.

Finally, we should emphasize that imposing the supergravity approximation was crucial in obtaining low scale SUSY breaking. Plausibly, the vacua which exist in the M theoretic, small volume regime will have a much higher SUSY breaking scale. However, such vacua presumably also have the incorrect electroweak scale (either zero or M_{11}).

4.2.6.8 Including more than one flavor of quarks in the hidden sector

In the previous analysis we assumed a single flavor for the quarks in the hidden sector, i.e $N_f = 1$. In order to check that the way we obtain a dS metastable minimum is robust and not dependent on a particular choice of chiral hidden sector matter spectrum, we would like to extend our analysis to include more than one flavor so that the meson fields are given by:

$$\phi_{\bar{\sigma}}^{\sigma} \equiv \left(Q^{\sigma} \tilde{Q}_{\bar{\sigma}} \right)^{1/2}, \quad (4.252)$$

where $\sigma, \bar{\sigma} = \overline{1, N_f}$. It is convenient to keep the effective Kähler potential for the hidden sector mesons in canonical form. For this purpose we assume that the flavor space matrix $\phi_{\bar{\sigma}}^{\sigma}$ is diagonal, i.e.

$$\langle Q^{\sigma} \tilde{Q}_{\bar{\sigma}} \rangle = 0, \quad \text{for } \sigma \neq \bar{\sigma} \quad (4.253)$$

$$\langle Q^{\sigma} \tilde{Q}_{\bar{\sigma}} \rangle \neq 0, \quad \text{for } \sigma = \bar{\sigma}.$$

In this case, the determinant appearing in (4.137) is simplified

$$\det(\phi_{\bar{\sigma}}^{\sigma}) = \prod_{\sigma=1}^{N_f} \phi_{\sigma}, \quad \text{where } \phi_{\sigma} \equiv \phi_{\sigma}^{\sigma}. \quad (4.254)$$

Thus, the nonperturbative superpotential and the Kähler potential are then given by

$$W = A_1 \prod_{\sigma=1}^{N_f} \phi_{\sigma}^a e^{ib_1 f} + A_2 e^{ib_2 f} \quad (4.255)$$

$$K = -3 \ln(4\pi^{1/3} V_X) + \sum_{\sigma=1}^{N_f} \phi_{\sigma} \bar{\phi}_{\sigma},$$

where we again denoted $b_1 \equiv 2\pi/P$, $b_2 \equiv 2\pi/Q$, $P \equiv N_c - N_f$ and $a \equiv -2/P$. After minimizing with respect to the axions, the scalar potential is given by

$$V = \frac{e^{\sum_{\sigma=1}^{N_f} (\phi_0)_{\sigma}^2}}{48\pi V_X^3} \left[(b_1 A_1 \prod_{\sigma=1}^{N_f} (\phi_0)_{\sigma}^a e^{-b_1 \vec{\nu} \cdot \vec{a}} - b_2 A_2 e^{-b_2 \vec{\nu} \cdot \vec{a}})^2 \sum_{i=1}^N a_i (\nu_i)^2 + \right. \quad (4.256)$$

$$3(A_1 \prod_{\sigma=1}^{N_f} (\phi_0)_{\sigma}^a e^{-b_1 \vec{\nu} \cdot \vec{a}} - A_2 e^{-b_2 \vec{\nu} \cdot \vec{a}})^2 + 3(\vec{\nu} \cdot \vec{a}) (A_1 \prod_{\sigma=1}^{N_f} (\phi_0)_{\sigma}^a e^{-b_1 \vec{\nu} \cdot \vec{a}} - A_2 e^{-b_2 \vec{\nu} \cdot \vec{a}})$$

$$(b_1 A_1 \prod_{\sigma=1}^{N_f} (\phi_0)_{\sigma}^a e^{-b_1 \vec{\nu} \cdot \vec{a}} - b_2 A_2 e^{-b_2 \vec{\nu} \cdot \vec{a}}) + \sum_{\gamma=1}^{N_f} \frac{3}{4} (\phi_0)_{\gamma}^2 \times$$

$$\left. \left(\left(\frac{a}{(\phi_0)_{\gamma}^2} + 1 \right) A_1 \prod_{\sigma=1}^{N_f} (\phi_0)_{\sigma}^a e^{-b_1 \vec{\nu} \cdot \vec{a}} - A_2 e^{-b_2 \vec{\nu} \cdot \vec{a}} \right)^2 \right].$$

Instead of presenting a full analysis of this more general case we would simply like to check that we have a metastable dS vacuum, and that the main feature of the dS vacuum, namely the

emergence of the TeV scale when the tree-level cosmological constant is set to zero, survives when $N_f > 1$. For this purpose we need to compute the scalar potential at the minimum with respect to the moduli s_i as a function of the meson fields ϕ_σ .

The generalization of the equations minimizing the scalar potential is fairly straightforward. In particular, in the limit when the size of the associative cycle $\text{Im}f = \vec{\nu} \cdot \vec{a}$ is large, for $A = 1$ the generalization of the second equation in (4.169), which determines $\tilde{L}_{1,+}$ takes on the following form

$$\frac{2}{3} \left(\tilde{L}_{1,+} \right)^2 + \tilde{L}_{1,+} + \sum_{\sigma=1}^{N_f} \frac{3a\beta b_1 \hat{y}}{14\hat{x}\hat{z}} \left(\frac{a\beta}{(\phi_0)_\sigma^2 \hat{x}} + 1 \right) = 0$$

where we again defined $\beta \equiv \frac{A_1}{A_2} \prod_{\sigma=1}^{N_f} (\phi_0)_\sigma^a e^{-(b_1-b_2)\vec{\nu} \cdot \vec{a}}$, $\hat{x} \equiv \beta - 1$, $\hat{y} \equiv b_1\beta - b_2$ and $\hat{z} \equiv b_1^2\beta - b_2^2$. Thus, in the large three-cycle limit we again have $\beta \approx b_2/b_1 = P/Q$ so that $\hat{y} \rightarrow 0$ and the leading order solution for $L_{1,+}$ is again given by

$$L_{1,+} \approx -\frac{3}{2}. \quad (4.257)$$

In this case the moduli are stabilized at the same values given by (4.175). Since both the superpotential and the Kähler potential are completely symmetric with respect to the meson fields, it seems reasonable to expect that there is a vacuum where all ϕ_σ are stabilized at the same value, i.e. $(\phi_0)_\sigma = \tilde{\phi}_0$ for all $\sigma = \overline{1, N_f}$. Using the solution for the moduli vevs (4.175) and the above assumption we obtain the following expression for the potential at the extremum with respect to the moduli s_i as a function of $\tilde{\phi}_0$

$$V_0 = N_f \frac{(A_2 \hat{x})^2}{64\pi V_X^3} \left[\tilde{\phi}_0^4 + \left(\frac{2a\beta}{\hat{x}} - \frac{3}{N_f} \right) \tilde{\phi}_0^2 + \left(\frac{a\beta}{\hat{x}} \right)^2 \right] \frac{e^{N_f \tilde{\phi}_0^2}}{\tilde{\phi}_0^2} \left(\frac{A_1 Q}{A_2 P} \right)^{-\frac{2P}{Q-P}}. \quad (4.258)$$

By setting the discriminant of the biquadratic polynomial in the square brackets to zero we

again obtain the leading order condition on the tree-level cosmological constant to vanish:

$$\frac{3}{N_f} - \frac{8}{Q-P} - \frac{28}{P \ln\left(\frac{A_1 Q}{A_2 P}\right)} = 0. \quad (4.259)$$

Since the solutions for the moduli in the dS case correspond to branch b) where $Q > P$ and $A_1 Q > A_2 P$, zero vacuum energy condition (4.259) can be satisfied only when

$$\frac{3}{N_f} > \frac{8}{Q-P} \Rightarrow (Q-P) > \frac{8}{3} N_f. \quad (4.260)$$

Therefore, a vanishing tree-level cosmological constant in the leading order results in the following set of conditions:

$$P \ln\left(\frac{A_1 Q}{A_2 P}\right) = \frac{28(Q-P)N_f}{3(Q-P) - 8N_f}, \quad \text{and} \quad (Q-P) > \frac{8}{3} N_f. \quad (4.261)$$

Recall that the key to obtaining the TeV scale gravitino mass was the exponential suppression factor e^{-28} when $Q-P = (Q-P)_{min} = 3$, related to the scale of gaugino condensation. In the present case, up a factor of order one, we have

$$m_{3/2} \sim \frac{m_p}{V_X^{3/2}} \left(\frac{A_1 Q}{A_2 P}\right)^{-\frac{P}{Q-P}} = \frac{m_p}{V_X^{3/2}} e^{-\frac{28N_f}{3(Q-P) - 8N_f}} \quad (4.262)$$

Consider a few examples where $N_f > 1$. From (4.261) we have the following set

$$N_f = 2, \quad (Q-P)_{min} = 6, \quad P \ln\left(\frac{A_1 Q}{A_2 P}\right) = 168, \quad m_{3/2} \sim \frac{m_p}{V_X^{3/2}} e^{-\frac{28N_f}{3(Q-P) - 8N_f}} = \frac{m_p}{V_X^{3/2}} e^{-128} \quad (4.263)$$

$$N_f = 3, \quad (Q-P)_{min} = 9, \quad P \ln\left(\frac{A_1 Q}{A_2 P}\right) = 252, \quad m_{3/2} \sim \frac{m_p}{V_X^{3/2}} e^{-\frac{28N_f}{3(Q-P) - 8N_f}} = \frac{m_p}{V_X^{3/2}} e^{-28}$$

$$N_f = 4, \quad (Q-P)_{min} = 11, \quad P \ln\left(\frac{A_1 Q}{A_2 P}\right) = 1232, \quad m_{3/2} \sim \frac{m_p}{V_X^{3/2}} e^{-\frac{28N_f}{3(Q-P) - 8N_f}} = \frac{m_p}{V_X^{3/2}} e^{-112}$$

$$N_f = 4, \quad Q-P = 12, \quad P \ln\left(\frac{A_1 Q}{A_2 P}\right) = 336, \quad m_{3/2} \sim \frac{m_p}{V_X^{3/2}} e^{-\frac{28N_f}{3(Q-P) - 8N_f}} = \frac{m_p}{V_X^{3/2}} e^{-28}$$

Remarkably, in all but one cases listed above we obtain *the same* suppression factor $e^{-28} \approx 7 \times 10^{-13}$ which was the reason for the peak at $m_{3/2} \sim \mathcal{O}(1 - 100)\text{TeV}$! Note that the only example which did not fall into this range was the third case for which the condition on the cosmological constant to vanish was $P \ln \left(\frac{A_1 Q}{A_2 P} \right) = 1232$, which is too unrealistic anyway, as it requires either extremely large dual coxeter numbers for the gauge groups $N_c, Q \sim \mathcal{O}(1000)$ or an exponentially large ratio inside the logarithm. On a similar note, as can be seen from the third entry in each line in (4.263), increasing the number of flavors N_f even further would again require either $P, Q > 300$ or an extremely large ratio $\left(\frac{A_1 Q}{A_2 P} \right)$, which appears inside the logarithm. Therefore, limiting our analysis to the cases with $N_f < 5$ seems quite reasonable.

Recall that for $N_f = 1$ the TeV scale appeared for the minimum value $(Q - P)_{min} = 3$ whereas the vacua corresponding to the higher values of $Q - P$ generally failed to satisfy the SUGRA constraint for more generic G_2 manifolds with a large number of moduli. For this reason, considering larger values of $Q - P$ for the examples listed above is probably unnecessary.

Thus, given that the assumptions we made in the beginning of this subsection are reasonable, it appears that the connection of the TeV scale SUSY breaking to the requirement that the tree-level vacuum energy is very small is a fairly robust feature of these vacua, independent of the number of flavors.

4.2.6.9 Including matter in both hidden sectors

In the previous analysis we tried to be minimalistic and included chiral matter in only one of the hidden sectors. Due to this asymmetry, we obtained two types of solutions - a supersymmetric AdS extremum when $P > Q$ corresponding to branch a) and a dS minimum when $Q > P$ (when condition (4.186) holds), corresponding to branch b). Using this result it

is then fairly straightforward to figure out what happens when both hidden sectors produce F -terms due to chiral matter. For the sake of simplicity, we will again consider the case when $N_f = 1$ in both hidden sectors. In this case, the Kähler potential is given by

$$K = -3 \ln(4\pi^{1/3} V_X) + \phi\bar{\phi} + \psi\bar{\psi}. \quad (4.264)$$

After minimizing with respect to the axions, the non-perturbative superpotential (up to a phase) is given by

$$W = -A_1 \phi^{a_1} e^{-\frac{2\pi}{P} \text{Im}f} + A_2 \psi^{a_2} e^{-\frac{2\pi}{Q} \text{Im}f}, \quad (4.265)$$

where $a_1 \equiv -2/P$ and $a_2 \equiv -2/Q$. We will now check to see if it is still possible to obtain SUSY extrema when both hidden sectors have chiral matter. Setting the moduli F -terms to zero we obtain

$$\nu_k = \nu = -\frac{3PQ}{4\pi} \frac{\tilde{\beta} - 1}{Q\tilde{\beta} - P}, \quad (4.266)$$

where $\tilde{\beta} \equiv \frac{A_1 \phi^{a_1}}{A_2 \psi^{a_2}} e^{-(\frac{2\pi}{P} - \frac{2\pi}{Q}) \text{Im}f}$. At the same time, setting the matter F -terms to zero results in the following conditions:

$$\left(\frac{a_1}{\phi_0^2} + 1 \right) \tilde{\beta} - 1 = 0. \quad (4.267)$$

$$-\frac{a_2}{\psi_0^2} + \tilde{\beta} - 1 = 0. \quad (4.268)$$

Expressing $\tilde{\beta}$ from (4.266) and substituting it into (4.267-4.268) and using the definitions for a_1 and a_2 , we obtain the following expressions for the meson field vevs:

$$\phi_0^2 = \frac{2 + 3Q/(2\pi\nu)}{P - Q}, \quad (4.269)$$

$$\psi_0^2 = \frac{2 + 3P/(2\pi\nu)}{Q - P}. \quad (4.270)$$

Since ν as well as both ϕ_0^2 and ψ_0^2 are positive definite, we have the following two possibilities:

$$\begin{aligned} a) \quad P > Q : & \Rightarrow F_\phi = 0 \text{ and } F_\psi \neq 0, \\ b) \quad P < Q : & \Rightarrow F_\phi \neq 0 \text{ and } F_\psi = 0. \end{aligned} \tag{4.271}$$

Thus, when both hidden sectors have chiral matter, supersymmetric extrema are absent. Instead, when condition (4.186) holds (for branch a) we simply swap P and Q , A_1 and A_2 in (4.186)), for each branch we obtain a dS vacuum where only one of the matter F -terms is non-zero. Keep in mind that although in the above analysis we used condition (4.266) obtained by setting the moduli F -terms to zero, even in the dS case when the moduli F -terms are non-zero, one of the two mesons will be stabilized at a value such that the corresponding matter F -term is zero. The zero F -term has no effect on the analysis of the dS solution and apart from replacing $\tilde{\alpha}$ with $\tilde{\beta}$ defined above, the same solution obtained previously for the dS vacuum applies. In this case, the only difference will be in the meson field vevs:

$$\begin{aligned} a) \quad \phi_0^2 &\approx \frac{2}{P-Q} + \frac{7}{P \ln\left(\frac{A_2 P}{A_1 Q}\right)}, \quad \psi_0^2 \approx 1 - \frac{2}{P-Q} + \sqrt{1 - \frac{2}{P-Q}} - \\ &\quad \frac{7}{Q \ln\left(\frac{A_2 P}{A_1 Q}\right)} \left(\frac{3}{2} + \sqrt{1 - \frac{2}{P-Q}}\right) \\ b) \quad \psi_0^2 &\approx \frac{2}{Q-P} + \frac{7}{Q \ln\left(\frac{A_1 Q}{A_2 P}\right)}, \quad \phi_0^2 \approx 1 - \frac{2}{Q-P} + \sqrt{1 - \frac{2}{Q-P}} - \\ &\quad \frac{7}{P \ln\left(\frac{A_1 Q}{A_2 P}\right)} \left(\frac{3}{2} + \sqrt{1 - \frac{2}{Q-P}}\right) \end{aligned} \tag{4.272}$$

Therefore, the dS solution obtained for the minimal case when only one of the hidden sectors has chiral matter does not change even when we include chiral matter in both hidden sectors.

4.2.7 Phenomenology

In this section, we will begin the analysis of more detailed particle physics features of the vacua, with emphasis on the soft supersymmetry breaking parameters, since we are particularly interested in predicting collider physics observables that will be measured at the LHC.

The low energy physics observables are determined by the kähler potential, superpotential and the gauge kinetic function of the effective $\mathcal{N} = 1, d = 4$ supergravity. The gauge kinetic function (f) has already been discussed. The Kähler potential and the superpotential can be written in general as follows:

$$\begin{aligned} K &= \hat{K}(s^i) + \tilde{K}_{\bar{\alpha}\beta}(s^i) \bar{\Phi}^{\bar{\alpha}} \Phi^{\beta} + Z_{\alpha\beta}(s^i, \phi^h) \Phi^{\alpha} \Phi^{\beta} + \dots \\ W &= \hat{W}(z^i) + \mu' \Phi^{\alpha} \Phi^{\beta} + Y'_{\alpha\beta\gamma} \Phi^{\alpha} \Phi^{\beta} \Phi^{\gamma} + \dots \end{aligned} \quad (4.273)$$

where Φ^{α} are the visible sector chiral matter fields, $\tilde{K}_{\bar{\alpha}\beta}$ is their Kähler metric and $Y'_{\alpha\beta\gamma}$ are their *unnormalized* Yukawa couplings. ϕ^h denote the hidden sector matter fields. The first terms in K and W depend only on the bulk moduli and have been already studied earlier. In general there can be a mass term (μ') in the superpotential, but as explained in [101], natural discrete symmetries can exist which forbid it, in order to solve the doublet-triplet splitting problem. The quantity $Z_{\alpha\beta}$ in the Kähler potential will be important for generating an effective μ term as we will see later.

Since the vacua have low scale supersymmetry, the effective lagrangian must be equivalent to the MSSM plus couplings involving possibly additional fields beyond the MSSM. For simplicity in this section we will assume an observable sector which is precisely the MSSM, although it would also be interesting to consider natural M theoretic extensions. The MSSM lagrangian is characterized by the Yukawa and gauge couplings of the standard model and the

soft supersymmetry breaking couplings. These are the scalar squared masses m_i^2 , the trilinear couplings A_{ijk} , the μ and $B\mu$ mass parameters and the gaugino masses. In M theory all of these couplings become functions of the various constants (A_i, N, P, Q, N_k) which are determined by the *particular* G_2 -manifold X . In addition, because we are now discussing the observable sector, we have to explain the origin of observable sector gauge, Yukawa and other couplings in M theory. As we have already explained, all gauge couplings are integer linear combinations of the N moduli, the N integers determining the homology class of the three dimensional subspace of X which supports that particular gauge group. Furthermore, the entire superpotential is generated by membrane instantons, as we have already discussed. Therefore mass terms and Yukawa couplings in the superpotential are also determined by integer linear combinations of the moduli fields. Hence, in addition to the constants (A_i, N, P, Q, N_k) which determine the moduli potential, additional integers enter in determining the observable sector superpotential. Generically, though, we do not expect these integers to be large in the basis that the moduli Kähler metric is given by (6).

We determine the values of the soft SUSY breaking couplings at M_{unif} in the standard way : The moduli fields, hidden sector matter fields as well as their auxiliary fields are replaced by their *vevs* in the $\mathcal{N} = 1, d = 4$ SUGRA lagrangian. One then takes the flat limit $M_p \rightarrow \infty$ with $m_{3/2}$ fixed. This gives a global SUSY lagrangian with soft SUSY breaking terms [64]. Unfortunately, in M theory the matter Kähler potential is difficult to compute. This leads to theoretical uncertainties in the calculation of the scalar masses and A , B and μ parameters. Fortunately though we are able to calculate the gaugino masses. Our main phenomenological result is that the tree level gaugino masses are suppressed relative to the gravitino mass. After explaining this, we will go on to discuss the other soft terms in a certain, calculable limit.

4.2.7.1 Suppression of Gaugino masses

Grand Unification is particularly natural in G_2 vacua of M theory [176]. This implies that the gaugino masses at tree level (at the unification scale) are *universal*, i.e. the gauginos of the three SM gauge groups have the same mass. In order to compute the SM sector gaugino mass scale at tree-level we need the Standard Model gauge kinetic function, f_{sm} . In general this will be an integer linear combination of the moduli, with integers N_i^{sm} , which is linearly independent of the hidden sector gauge kinetic function in general. The expression for the tree-level MSSM gaugino masses in general $\mathcal{N} = 1, d = 4$ SUGRA is given by:

$$M_{1/2} = m_p \frac{e^{\hat{K}/2} K^{n\bar{m}} F_{\bar{m}} \partial_n f_{sm}}{2i \operatorname{Im} f_{sm}}, \quad (4.274)$$

Note that the gauge kinetic function is independent of the hidden sector matter fields. Therefore, the large hidden sector matter F term responsible for the dS minimum does not contribute to the gaugino masses at tree level. We will now proceed to evaluate this expression explicitly both for the AdS and dS vacua. We will find that generically, the gaugino masses are suppressed relative to the gravitino mass.

4.2.7.2 Gaugino masses in AdS Vacua

Choosing the hidden sector to be pure SYM with gauge groups $SU(P)$ and $SU(Q)$, the normalized gaugino mass in these compactifications can be expressed as

$$M_{1/2} = -\frac{m_p e^{-i\gamma_W}}{8\sqrt{\pi} V_X^{3/2}} \left[\frac{4\pi}{3} \left(\frac{A_1}{P} e^{-\frac{2\pi}{P} \operatorname{Im} f} - \frac{A_2}{Q} e^{-\frac{2\pi}{Q} \operatorname{Im} f} \right) \frac{\sum_{i=1}^N N_i^{sm} s_i \mathcal{V}_i}{\sum_{i=1}^N N_i^{sm} s_i} + A_1 e^{-\frac{2\pi}{P} \operatorname{Im} f} - A_2 e^{-\frac{2\pi}{Q} \operatorname{Im} f} \right] \quad (4.275)$$

where γ_W is the phase of the superpotential W . In the leading order, the last two terms in the brackets can be combined as

$$A_1 e^{-\frac{2\pi}{P} \text{Im}f} - A_2 e^{-\frac{2\pi}{Q} \text{Im}f} = A_2 \left[\frac{P-Q}{Q} \right] \left[\frac{A_2 P}{A_1 Q} \right]^{-\frac{P}{P-Q}}. \quad (4.276)$$

On the other hand, the two terms in the round brackets coming from the partial derivative of the superpotential cancel in the leading order. Therefore we need to take into account the first subleading order contribution (4.135). In this order, we obtain ⁸:

$$\left(\frac{A_1}{P} e^{-\frac{2\pi}{P} \text{Im}f} - \frac{A_2}{Q} e^{-\frac{2\pi}{Q} \text{Im}f} \right) = \frac{1}{2\pi} A_2 \left[\frac{P-Q}{Q} \right] \left[\frac{A_2 P}{A_1 Q} \right]^{-\frac{P}{P-Q}} \frac{B_A^{(c)}}{\mathcal{T}_A^{(c)}}. \quad (4.277)$$

From (4.276) and (4.277) we notice that the absolute value of gaugino mass can now be conveniently expressed in terms of the gravitino mass (for a given value of A and c , as discussed in previous sections) as

$$|M_{1/2}|_A^{(c)} = \frac{2 \sum_{i=1}^N a_i L_{A,k}^{(c)} \left(L_{A,k}^{(c)} + 3/2 \right) (N_i^{sm}/N_i)}{3 \sum_{i=1}^N a_i L_{A,k}^{(c)} (N_i^{sm}/N_i)} \times (m_{3/2})_A^{(c)}, \quad (4.278)$$

where we also used (4.122) and (4.128). Finally, using (4.116) and the first equation in (4.115), after some algebra we arrive at the following expression for the gaugino mass:

$$|M_{1/2}|_A^{(c)} = \left(\frac{4}{3} T_A^{(c)} + 1 \right) \frac{q - A}{q + \frac{T_A^{(c)}}{H_A^{(c)}}} \times (m_{3/2})_A^{(c)}, \quad (4.279)$$

where we have introduced a new quantity

$$q = \frac{\sum_{i=1}^N m_i a_i (N_i^{sm}/N_i)}{\sum_{i=1}^N a_i (N_i^{sm}/N_i)}, \quad (4.280)$$

such that the range of possible values for q is

$$-1 \leq q \leq 1. \quad (4.281)$$

⁸Recall that $\text{Im}(f)_A^{(c)} \equiv \mathcal{T}_A^{(c)}$ (see (4.118)).

Note that the general formula (4.279) which relates the gravitino and gaugino masses is completely independent of the number of moduli.

When all m_k have the same sign the gaugino mass in (4.279) automatically vanishes. This is expected since the solution when $A = \pm 1$ is the SUSY extremum. In Figure 4.16 we have plotted absolute values of $(M_{1/2})_A^{(1)}$ and $(M_{1/2})_A^{(2)}$ as functions of q .

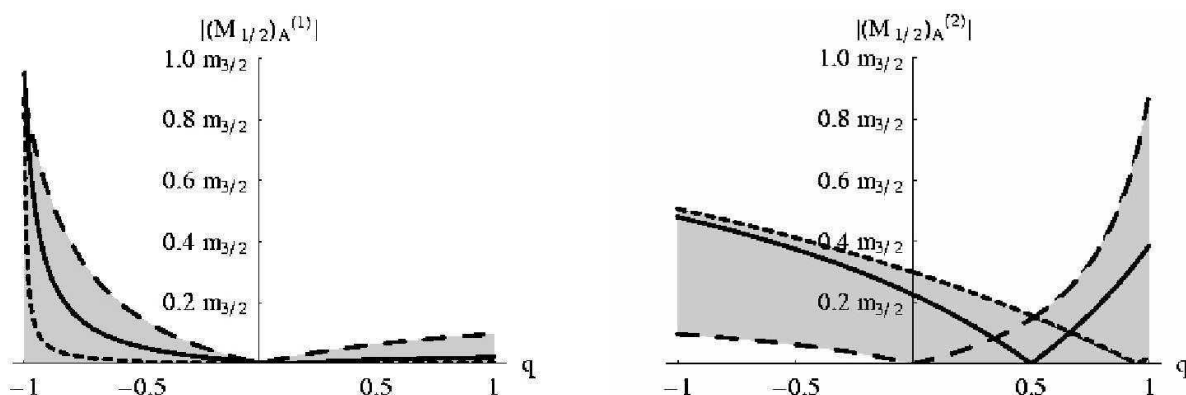


Figure 4.16: Absolute values of $(M_{1/2})_A^{(1)}$ -left and $(M_{1/2})_A^{(2)}$ -right in units of gravitino mass as functions of q . As parameter A varies over $0 \leq A < 1/7$ - on the left and $0 \leq A \leq 1$ - on the right the whole light grey region is covered.

Left plot: $A = 0$ - long dashed line, $A = 1/9$ - solid line, $A = 5/36$ - short dashed line.

Right plot: $A = 0$ -long dashed line, $A = 0.5$ - solid line, $A = 0.95$ - short dashed line.

For a significant fraction of the space in both plots we have $(M_{1/2})_A^{(1,2)} \leq 0.2 (m_{3/2})_A^{(1,2)}$, so the gaugino masses are typically suppressed compared to the gravitino mass for these AdS vacua. Note also that the suppression factor in (4.279) is independent of the gravitino mass. This result is different from the small hierarchy between $M_{1/2}$ and $m_{3/2}$ in the Type IIB flux vacua [90], where the gaugino mass is generically suppressed by $\ln(m_{3/2})$.

For the special case $A = 0$, system (4.115) yields two solutions with positive moduli. Therefore, there will be two different values for the gaugino mass corresponding to these solutions.

After some algebra we obtain

$$\begin{aligned}
|M_{1/2}|_0^{(1,2)} &= \left(\frac{5 - \sqrt{17}}{4} \right) \left| \frac{q}{q \pm \frac{-9 + \sqrt{17}}{\sqrt{-26 + 10\sqrt{17}}}} \right| \times (m_{3/2})_0^{(1,2)} \\
&\sim 0.22 \left| \frac{q}{q \mp 1.25} \right| \times (m_{3/2})_0^{(1,2)}. \tag{4.282}
\end{aligned}$$

Again, this relation is valid for any AdS vacuum with broken SUSY with $A = 0$ with an arbitrary number of moduli.

To check the accuracy of the approximate gaugino mass formula we again try the special case with two moduli $a_1 = a_2 = 7/6$ with the same choice of the constants as in (4.110) and the integer combination for the Standard Model gauge kinetic function $\{N_1^{sm} = 2, N_2^{sm} = 1\}$. In this case equation (4.282) for the absolute value of $M_{1/2}$ yields:

$$(M_{1/2})_0^{(1)} = 164.4 \text{ GeV}, \quad (M_{1/2})_0^{(2)} = 95 \text{ GeV}, \tag{4.283}$$

whereas the exact values computed numerically for the same choice of constants are:

$$(M_{1/2})_0^{(1)} = 165.4 \text{ GeV}, \quad (M_{1/2})_0^{(2)} = 97 \text{ GeV}. \tag{4.284}$$

This demonstrates a high degree of accuracy of our approximation, similar to that for the gravitino mass.

4.2.7.3 Gaugino masses in dS Vacua

From the formula for the gaugino mass in (4.274), the gaugino mass for the dS vacua in general can be expressed as

$$\begin{aligned}
M_{1/2} &= \frac{e^{-i\gamma w} m_p e^{\phi_0^2/2}}{8\sqrt{\pi} V_X^{3/2}} \left[\frac{2}{3} \tilde{y} \frac{\sum_{i=1}^N N_i^{sm} s_i \mathcal{V}_i}{\sum_{i=1}^N N_i^{sm} s_i} + \tilde{x} \right] A_2 e^{-b_2 \vec{v} \cdot \vec{a}} \\
\Rightarrow M_{1/2} &= -e^{-i\gamma w} \left(\frac{2}{3} L_{1,+} + 1 \right) m_{3/2}, \tag{4.285}
\end{aligned}$$

where in the second equality we used (4.165) and the fact that for these vacua $\nu_i = \nu$ for all $i = \overline{1, N}$, independent of i . Also, by including the minus sign we took into account that $m_{3/2} = e^{K/2} |\tilde{x}| A_2 e^{-b_2 \tilde{v} \tilde{a}}$ but $\tilde{x} < 0$, since $Q - P \geq 3$. From (4.170) we can find $\tilde{L}_{1,+}$ including the first subleading contribution

$$\tilde{L}_{1,+} \approx -\frac{3}{2} + \frac{3a\tilde{\alpha}b_1\tilde{y}}{14\tilde{x}\tilde{z}} \left(\frac{a\tilde{\alpha}}{\phi_0^2 \tilde{x}} + 1 \right). \quad (4.286)$$

For \tilde{x} , \tilde{y} and \tilde{z} in (4.286) we use the definitions (4.157) and substitute the approximate result (4.176) for $\tilde{\alpha}$. Then after substituting (4.286) into (4.285) and assuming that $Q - P \sim \mathcal{O}(1)$, in the limit when P is large the approximate tree level MSSM gaugino mass is given by

$$M_{1/2} \approx -\frac{e^{-i\gamma_W}}{P \ln\left(\frac{A_1 Q}{A_2 P}\right)} \left(1 + \frac{2}{\phi_0^2 (Q - P)} + \frac{7}{\phi_0^2 P \ln\left(\frac{A_1 Q}{A_2 P}\right)} \right) \times m_{3/2}, \quad (4.287)$$

where we use (4.177) to substitute for ϕ_0^2 . It is important to note some features of the above equation. First, equation (4.287) is completely independent of the choice of integers N_i^{sm} for the Standard Model gauge kinetic function as well as the integers N_i for the hidden sector. Second, it is independent of the number of moduli N and moreover, it is also independent of the particular details of the internal manifold described by the rational numbers a_i appearing in the Kähler potential (4.45). These properties imply that relation (4.287) is universal for all G_2 holonomy compactifications consistent with our approximations, independent of many internal details of the manifold. Furthermore, since the denominator $P \ln(A_1 Q/A_2 P)$ is typically of $\mathcal{O}(10-100)$ and since the expression in the round brackets in (4.287) is slowly varying and for the range under consideration is of $\mathcal{O}(1)$, we see that *gaugino masses are always suppressed relative to the gravitino for these dS vacua.*

After one imposes the constraint equation (4.231) ((4.247) when $Q - P = 3$) to make the cosmological constant very small, one can get rid of one of the constants in (4.287), and further

simplify the expression for the universal tree level gaugino mass parameters for the dS vacuum with a very small cosmological constant:

$$M_{1/2} \approx -\frac{e^{-i\gamma w}}{84} \left(1 + \frac{2}{3\phi_0^2} + \frac{7}{84\phi_0^2} \right) \times m_{3/2} = -e^{-i\gamma w} \frac{139 + 396\sqrt{3}}{34356} \times m_{3/2} \approx -e^{-i\gamma w} 0.024 \times m_{3/2}. \quad (4.288)$$

As in the more general case (eqn.(4.287)), the tree level gaugino mass is suppressed compared to the gravitino mass, and the suppression factor can also be predicted.

One would like to understand the physical origin of the suppression of the gaugino masses at tree level, especially for the dS vacua which are phenomenologically relevant. As mentioned earlier, since the matter F term does not contribute to the gaugino masses, the gaugino masses can only get contributions from the moduli F terms, which, as explained in the last paragraph in section 4.2.5.4, vanish in the leading order of our approximation. The first subleading contribution is suppressed by the inverse power of the volume of the associative three-cycle, causing the gaugino masses to be suppressed relative to the gravitino. Since the inverse volume of this three-cycle is essentially α_{hidden} - the hidden sector gauge coupling in the UV - the suppression is due to the fact that the hidden sector is asymptotically free. In large volume type IIB compactifications, the moduli F terms also vanish in the leading order, leading to suppressed gaugino masses as well [90]. However, in contrast to our case, there the subleading contribution is suppressed by the inverse power of the volume of the compactification manifold. Note that a large associative cycle on a G_2 manifold does *not* translate into a large volume compactification manifold. Thus, unlike the large volume type IIB compactifications, these M theory vacua are consistent with standard gauge coupling unification.

4.2.7.4 Other parameters and Flavor issues

The trilinears, scalars, anomaly mediated contributions to gaugino masses and the $B\mu$ parameter depend more on the microscopic details of the theory – the Yukawa couplings, the μ' parameter and the Kähler metric for visible sector matter fields. The flavor structure of the Yukawa matrices as well as that of the Kähler metric for matter fields is crucial for estimating flavor changing effects. We will comment on these at appropriate places.

The (un-normalized) Yukawa couplings in these vacua arise from membrane instantons which connect singularities where chiral superfields are supported (if some singularities coincide, there could also be order one contributions). They are given by:

$$Y'_{\alpha\beta\gamma} = C_{\alpha\beta\gamma} e^{i2\pi \sum_i l_i^{\alpha\beta\gamma} z^i} \quad (4.289)$$

where $C_{\alpha\beta\gamma}$ is an $\mathcal{O}(1)$ constant and $l_i^{\alpha\beta\gamma}$ are integers.

The moduli dependence of the matter Kähler metric is notoriously difficult to compute in generic string and M theory vacua, and the vacua under study here are no exception. The best we can do here is to consider the Type IIA limit of these vacua. The matter Kähler metric has been computed in type IIA intersecting $D6$ -brane vacua on toroidal orientifolds [49] building on earlier work [47]. Since chiral fermions living at intersections of $D6$ -branes lift to chiral fermions supported at conical singularities in M theory [31, 102], we will simply uplift the IIA calculation to M theory. Thus the results of this section are strictly only valid in the Type IIA limit.

Lifting the Type IIA result to M theory, one gets (see Appendix for details):

$$\begin{aligned} \tilde{K}_{\bar{\alpha}\beta} &= \delta_{\bar{\alpha}\beta} \prod_{i=1}^n \left(\frac{\Gamma(1 - \theta_i^\alpha)}{\Gamma(\theta_i^\alpha)} \right)^{1/2} \\ \tan(\pi\theta_i^\alpha) &= c_i^\alpha (s_i)^l; \quad c_i^\alpha = \text{constant}; \quad l = \text{rational number of } \mathcal{O}(1). \end{aligned} \quad (4.290)$$

In the type IIA toroidal orientifolds, the underlying symmetries always allow us to have a diagonal Kähler metric [49]. We have assumed for simplicity the Kähler metric to be diagonal in the analysis below. Now, we will write down the general expressions for the physical Yukawa couplings and the soft parameters - the trilinears and the scalars and then estimate these in M theory compactifications. The μ and $B\mu$ parameters will be discussed in section 4.2.7.7.

The Kähler potential for the chiral matter fields is non-canonical for any compactification in general. In determining physical implications however, it is much simpler to work in a basis with a canonical Kähler potential. So, to canonically normalize the matter field Kähler potential, we introduce the normalization matrix \mathcal{Q} :

$$\Phi \rightarrow \mathcal{Q} \cdot \Phi, \quad s.t. \quad \mathcal{Q}^\dagger \tilde{K} \mathcal{Q} = 1. \quad (4.291)$$

The \mathcal{Q} s are themselves only defined up to a unitary transformation, i.e. $\mathcal{Q}' = \mathcal{Q} \cdot \mathcal{U}$ is also an allowed normalization matrix if \mathcal{U} is unitary. If the Kähler metric is already diagonal ($\tilde{K}_{\bar{\alpha}\beta} = \tilde{K}_\alpha \delta_{\bar{\alpha}\beta}$), the normalization matrix can be simplified : $\mathcal{Q}_{\bar{\alpha}\beta} = (\tilde{K}_\alpha)^{-\infty/\epsilon} \delta_{\bar{\alpha}\beta}$. The normalized (physical) Yukawa couplings are [64]:

$$Y_{\alpha\beta\gamma} = e^{\hat{K}/2} \frac{\hat{W}^*}{|\hat{W}|} Y'_{\alpha'\beta'\gamma'} \mathcal{Q}_{\alpha'\alpha} \mathcal{Q}_{\beta'\beta} \mathcal{Q}_{\gamma'\gamma} \quad (4.292)$$

It was shown in [103] that in the class of theories with a hierarchical structure of the un-normalized Yukawa couplings (in the superpotential), the Kähler corrections to both masses and mixing angles of the SM particles are subdominant. Since in these compactifications, it is very natural to obtain a hierarchical structure of the un-normalized Yukawa couplings due to their exponential dependence on the various moduli and also because of some possible family symmetries, therefore one expects the effects of the Kähler corrections which are less under control, to be subdominant. The expressions for the *un-normalized* trilinears and scalar masses

are given by [64]:

$$\begin{aligned}
m_{\tilde{\alpha}\beta}^{\prime 2} &= (m_{3/2}^2 + V_0) \tilde{K}_{\tilde{\alpha}\beta} - e^{\hat{K}} F^{\tilde{m}} (\partial_{\tilde{m}} \partial_n \tilde{K}_{\tilde{\alpha}\beta} - \partial_{\tilde{m}} \tilde{K}_{\tilde{\alpha}\gamma} \tilde{K}^{\gamma\tilde{\delta}} \partial_n \tilde{K}_{\tilde{\delta}\beta}) F^n \\
A'_{\alpha\beta\gamma} &= \frac{\hat{W}^*}{|\hat{W}|} e^{\hat{K}/2} F^m [\hat{K}_m Y'_{\alpha\beta\gamma} + \partial_m Y'_{\alpha\beta\gamma} - (\tilde{K}^{\tilde{\delta}\tilde{\rho}} \partial_n \tilde{K}_{\tilde{\rho}\alpha} Y'_{\alpha\beta\gamma} + \alpha \leftrightarrow \gamma + \alpha \leftrightarrow \beta)]
\end{aligned} \tag{4.293}$$

The *normalized* scalar masses and trilinears are thus given by:

$$\begin{aligned}
m_{\tilde{\alpha}\beta}^2 &= (\mathcal{Q}^\dagger \cdot \Downarrow'^\epsilon \cdot \mathcal{Q})_{\tilde{\alpha}\beta} \\
\tilde{A}_{\alpha\beta\gamma} &= A'_{\alpha'\beta'\gamma'} \mathcal{Q}_{\alpha'\alpha} \mathcal{Q}_{\beta'\beta} \mathcal{Q}_{\gamma'\gamma}
\end{aligned} \tag{4.294}$$

Let us discuss the implications for the soft terms, beginning with the Anomaly mediated corrections to gaugino masses.

Anomaly mediated contributions to Gaugino Masses

We saw in section 4.2.7.1 that the gauginos are generically suppressed relative to the gravitino. Since anomaly mediated gaugino masses are also suppressed relative to the gravitino (by a loop factor), they are non-negligible compared to the tree level contributions and have to be taken into account. Also, since anomaly mediated contributions for the three gauge groups are *non-universal*, these introduce non-universality in the gaugino masses at the unification scale.

The general expression for the anomaly mediated contributions is given by [104]:

$$(M)_a^{am} = -\frac{g_a^2}{16\pi^2} \left[-(3C_a - \sum_\alpha C_a^\alpha) e^{\hat{K}/2} W^* + (C_a - \sum_\alpha C_a^\alpha) e^{\hat{K}/2} F^m K_m + 2 \sum_\alpha (C_a^\alpha e^{\hat{K}/2} F^m \partial_m \ln(\tilde{K}_\alpha)) \right] \tag{4.295}$$

where C_a and C_a^α are the casimir invariants of the a^{th} gauge group and α runs over the number of fields charged under the a^{th} gauge group. For a given spectrum such as that of the MSSM, C_a and C_a^α are known.

We first compute the F-term contributions

$$e^{\hat{K}/2} F^i K_i = \frac{14}{3} e^{-i\gamma w} \left(L_{1,+} + \frac{3}{2} \right) \times m_{3/2} \quad (4.296)$$

$$e^{\hat{K}/2} F^\phi K_\phi = e^{-i\gamma w} \left(\frac{a\tilde{\alpha}}{\tilde{x}} + \phi_0^2 \right) \times m_{3/2}.$$

Then, equation (4.295) gives

$$(M)_a^{am} = -e^{-i\gamma w} \frac{\alpha_{GUT}}{4\pi} \left[-(3C_a - \sum_\alpha C_a^\alpha) + \frac{14}{3} (C_a - \sum_\alpha C_a^\alpha) \left(\tilde{L}_{1,+} + \frac{3}{2} \right) \right. \quad (4.297)$$

$$\left. + (C_a - \sum_\alpha C_a^\alpha) \left(\frac{a\tilde{\alpha}}{\tilde{x}} + \phi_0^2 \right) - \frac{4}{3} \left(\tilde{L}_{1,+} + \frac{3}{2} \right) \sum_\alpha C_a^\alpha \sum_i \frac{1}{2\pi} (l \psi_i^\alpha \sin(2\pi\theta_i^\alpha)) \right] \times m_{3/2}.$$

where

$$(\alpha_{GUT})^{-1} = \sum_{i=1}^N s_i N_i^{sm}, \quad (4.298)$$

and we have defined the quantity:

$$\psi_i^\alpha(\theta_i^\alpha) \equiv \frac{d \ln(\tilde{K}_\alpha)}{d \theta_i^\alpha}, \quad (4.299)$$

where θ_i^α implicitly depends on the moduli. However, it is much simpler to keep the dependence as a function of θ_i^α , as is explained in the Appendix. Depending on the values of the Casimir invariants C_a and C_a^i for the three gauge groups, the anomaly mediated contribution can either add to or cancel the tree level contributions. Here we also took into account that $m_{3/2} = e^{K/2} |\tilde{x}| A_2 e^{-b_2 \tilde{v} \cdot \tilde{a}}$ but $\tilde{x} < 0$, since $Q - P \geq 3$. Using the expression for $L_{1,+}$ in (4.172) along with the definitions of \tilde{x} , \tilde{y} and \tilde{z} in (4.157) in terms of $\tilde{\alpha}$ in (4.176) and assuming that $Q - P \sim \mathcal{O}(1)$, in the limit when P is large we obtain

$$\tilde{L}_{1,+} = -\frac{3}{2} + \frac{3}{2P \ln\left(\frac{A_1 Q}{A_2 P}\right)} \left(1 + \frac{2}{(Q-P)\phi_0^2} + \frac{7}{\phi_0^2 P \ln\left(\frac{A_1 Q}{A_2 P}\right)} \right). \quad (4.300)$$

Using (4.185) and substituting for ν from (4.175) into (4.185) together with $a = -2/P$ we can express

$$\frac{a\tilde{\alpha}}{\tilde{x}} + \phi_0^2 = \phi_0^2 \left(1 + \frac{2}{(Q-P)\phi_0^2} + \frac{7}{\phi_0^2 P \ln\left(\frac{A_1 Q}{A_2 P}\right)} \right). \quad (4.301)$$

Substituting (4.300) and (4.301) into (4.297) we obtain

$$\begin{aligned} (M)_a^{am} &= -e^{-i\gamma w} \frac{\alpha_{GUT}}{4\pi} \left[-(3C_a - \sum_{\alpha} C_a^{\alpha}) + \left(1 + \frac{2}{(Q-P)\phi_0^2} + \frac{7}{\phi_0^2 P \ln\left(\frac{A_1 Q}{A_2 P}\right)} \right) \right. \\ &\quad \left. \times \left((C_a - \sum_{\alpha} C_a^{\alpha}) \left(\phi_0^2 + \frac{7}{P \ln\left(\frac{A_1 Q}{A_2 P}\right)} \right) - \frac{2 \sum_{\alpha} C_a^{\alpha} \sum_i \frac{1}{2\pi} (l \psi_i^{\alpha} \sin(2\pi\theta_i^{\alpha}))}{P \ln\left(\frac{A_1 Q}{A_2 P}\right)} \right) \right] \times m_{3/2}. \end{aligned} \quad (4.302)$$

Note that these M theory vacua do not have a no-scale structure. Therefore, the anomaly mediated gaugino masses are only suppressed by loop effects, in contrast to the type IIB compactifications, which exhibit a no-scale structure in the leading order [90], leading to an additional suppression of the anomaly mediated gaugino masses.

As before, when one imposes the constraint (4.247), the anomaly mediated gaugino mass contribution can be simplified further and is given by:

$$\begin{aligned} (M)_a^{am} &= -\frac{\alpha_{GUT}(e^{-i\gamma w})}{4\pi} \left[-(3C_a - \sum_{\alpha} C_a^{\alpha}) + \frac{29055 + 11374\sqrt{3}}{29448} (C_a - \sum_{\alpha} C_a^{\alpha}) \right. \\ &\quad \left. - \frac{139 + 396\sqrt{3}}{17178} \sum_{\alpha} C_a^{\alpha} \sum_i \frac{1}{2\pi} (l \psi_i^{\alpha} \sin(2\pi\theta_i^{\alpha})) \right] \times \bar{m}_{3/2} \\ (M)_a^{am} &\approx -\frac{\alpha_{GUT}(e^{-i\gamma w})}{4\pi} \left[-(3C_a - \sum_{\alpha} C_a^{\alpha}) + 1.6556 (C_a - \sum_{\alpha} C_a^{\alpha}) \right. \\ &\quad \left. - 0.048 \sum_{\alpha} C_a^{\alpha} \sum_i \frac{1}{2\pi} (l \psi_i^{\alpha} \sin(2\pi\theta_i^{\alpha})) \right] \times m_{3/2}. \end{aligned} \quad (4.303)$$

From the left plot in Figure B.0.2 of the Appendix we note that $|\frac{1}{2\pi} (l \psi_i^{\alpha} \sin(2\pi\theta_i^{\alpha}))| < 0.5$. In a generic case, we expect that parameters θ_i^{α} are all different and, as a result, the terms appearing inside the corresponding sum over i partially cancel each other. Thus, in a typical

case we expect that

$$\left| \sum_{\alpha} C_a^{\alpha} \sum_i \frac{1}{2\pi} (l \psi_i^{\alpha} \sin(2\pi\theta_i^{\alpha})) \right| < 1. \quad (4.304)$$

Neglecting the corresponding contribution in (4.303), taking $\alpha_{GUT} = 1/25$, and substituting the Casimirs for an MSSM spectrum, we obtain the following values in the leading order, up to an overall phase $e^{-i\gamma w}$:

$$(M)_{U(1)}^{am} \approx 0.01377 \times m_{3/2}, \quad (M)_{SU(2)}^{am} \approx 0.02317 \times m_{3/2}, \quad (M)_{SU(3)}^{am} \approx 0.02536 \times m_{3/2}. \quad (4.305)$$

Finally, combining the tree-level (4.288) plus anomaly mediated (4.305) contributions, we obtain the following *non-universal* gaugino masses at the unification scale:

$$M_1 \approx -10.24 \times 10^{-3} m_{3/2}, \quad M_2 \approx -0.84 \times 10^{-3} m_{3/2}, \quad M_3 \approx +1.35 \times 10^{-3} m_{3/2}. \quad (4.306)$$

We immediately notice remarkable cancellations for M_2 and M_3 between the tree-level and the anomaly mediated contributions. Recall that since the distribution of $m_{3/2}$ peaked at $m_{3/2} \sim \mathcal{O}(100)$ TeV, the possible range of gaugino masses is in the desirable range $m_{1/2} \sim \mathcal{O}(0.1 - 1)$ TeV. One of the consequences of these cancellations is a comparatively lighter gluino. Furthermore, since M_2 is a lot smaller than M_1 , the neutralino LSP is wino-like.

One should be extremely cautious however, since the predictive expressions above are only true if (4.304) is satisfied. The extra contribution neglected in the above estimates is given by:

$$\Delta_a = 0.15 \times 10^{-3} \sum_{\alpha} C_a^{\alpha} \sum_i \frac{1}{2\pi} (l \psi_i^{\alpha} \sin(2\pi\theta_i^{\alpha})) \times m_{3/2}. \quad (4.307)$$

Because of the large cancellations between the tree-level and anomaly mediated contributions, it may happen that these corrections become important in a relatively small region of the overall parameter space, leading to a deviation from the above result thereby altering the pattern of

gaugino masses. Further corrections may also come from varying α_{GUT} as well as taking into account the subleading corrections to the condition for the cosmological constant to be very small. We will study these issues in detail in [92].

Trilinears

The normalized trilinear can be written as :

$$\begin{aligned} \tilde{A}_{\alpha\beta\gamma} &= \frac{\hat{W}^*}{|\hat{W}|} e^{\hat{K}/2} (\tilde{K}_\alpha \tilde{K}_\beta \tilde{K}_\gamma)^{-1/2} \left(\sum_i e^{\hat{K}/2} F^m [\hat{K}_m Y'_{\rho\delta\kappa} + \partial_m Y'_{\rho\delta\kappa} - \partial_m \ln(\tilde{K}_\alpha \tilde{K}_\beta \tilde{K}_\gamma)] \right) \\ &= Y_{\alpha\beta\gamma} \left(\sum_i e^{\hat{K}/2} F^m [\hat{K}_m + \partial_m \ln(Y'_{\alpha\beta\gamma}) - \partial_m \ln(\tilde{K}_\alpha \tilde{K}_\beta \tilde{K}_\gamma)] \right) \end{aligned} \quad (4.308)$$

As stated earlier, the subscripts $\{\alpha, \beta, \gamma\}$ stand for the visible chiral matter fields. For example, α can be the left-handed up quark doublet, β can be the right-handed up quark singlet and γ can be the up-type higgs doublet. Our present understanding of the microscopic details of these constructions does not allow us to compute the three individual trilinear parameters – corresponding to the up-type Yukawa, the down-type Yukawa and the lepton Yukawa matrices, explicitly. One can only estimate the rough overall scale of the trilinears.

We see from (4.308) that the normalized trilinears are proportional to the Yukawas since the Kähler metric is diagonal. If instead the off-diagonal entries in the kähler metric are small but non-zero, it would lead to a slight deviation from the proportionality of the trilinears to the Yukawa couplings. In most phenomenological analyzes, the trilinears \tilde{A} are taken to be proportional to the Yukawas and the *reduced* trilinear couplings $A_{\alpha\beta\gamma} \equiv \tilde{A}_{\alpha\beta\gamma}/Y_{\alpha\beta\gamma}$ are used. We expect this to be true in these compactifications from above. If the Yukawa couplings are those of the Standard Model, then from (4.308) the normalized reduced trilinear coupling $A_{\alpha\beta\gamma}$

for de Sitter vacua in general is given by

$$\begin{aligned}
A_{\alpha\beta\gamma} &= e^{-i\gamma w} \left(1 + \frac{2}{(Q-P)\phi_0^2} + \frac{7}{\phi_0^2 P \ln\left(\frac{A_1 Q}{A_2 P}\right)} \right) \left(\phi_0^2 + \frac{1}{P \ln\left(\frac{A_1 Q}{A_2 P}\right)} [7 + 2 \ln \left| \frac{C_{\alpha\beta\gamma}}{Y'_{\alpha\beta\gamma}} \right| \right. \\
&\quad \left. + \sum_i \frac{1}{2\pi} (l \psi_i^\alpha \sin(2\pi\theta_i^\alpha) + \alpha \rightarrow \beta + \alpha \rightarrow \gamma) \right] \times m_{3/2}. \tag{4.309}
\end{aligned}$$

If we then use (4.292) together with (4.290) and $\mathcal{Q}_{\bar{\alpha}\beta} = (\tilde{\mathcal{K}}_\alpha)^{-\infty/\epsilon} \delta_{\bar{\alpha}\beta}$, we obtain the following expression for the trilinears

$$\begin{aligned}
A_{\alpha\beta\gamma} &= m_{3/2} e^{-i\gamma w} \left(1 + \frac{2}{(Q-P)\phi_0^2} + \frac{7}{\phi_0^2 P \ln\left(\frac{A_1 Q}{A_2 P}\right)} \right) \left(\phi_0^2 + \frac{1}{P \ln\left(\frac{A_1 Q}{A_2 P}\right)} \times \right. \\
&\quad \left. [7 + 2 \ln \left| \frac{C_{\alpha\beta\gamma}}{Y_{\alpha\beta\gamma}} \right| - 3 \ln(4\pi^{1/3} V_X) + \phi_0^2 - \sum_i \left[\left\{ \frac{1}{2} \ln \left(\frac{\Gamma(1-\theta_i^\alpha)}{\Gamma(\theta_i^\alpha)} \right) - \frac{1}{2\pi} l \psi_i^\alpha \sin(2\pi\theta_i^\alpha) \right\} \right. \right. \\
&\quad \left. \left. + \alpha \rightarrow \beta + \alpha \rightarrow \gamma \right] \right] \right). \tag{4.310}
\end{aligned}$$

Imposing the constraint equation (4.247) on the expression above, the reduced trilinears for a dS vacuum with a tiny cosmological constant are simplified to:

$$\begin{aligned}
A_{\alpha\beta\gamma} &= e^{-i\gamma w} \left(\frac{69 + 22\sqrt{3}}{72} + \frac{139 + 396\sqrt{3}}{34356} [7 + 2 \ln \left| \frac{C_{\alpha\beta\gamma}}{Y_{\alpha\beta\gamma}} \right| - 7 \ln \left(\frac{14(P+3)}{N} \right) \right. \\
&\quad \left. + \frac{1}{72} (15 + 22\sqrt{3}) - 6 \ln \left(\frac{2}{\pi} \right) - \sum_i \left[\left\{ \frac{1}{2} \ln \left(\frac{\Gamma(1-\theta_i^\alpha)}{\Gamma(\theta_i^\alpha)} \right) - \frac{1}{2\pi} l \psi_i^\alpha \sin(2\pi\theta_i^\alpha) \right\} \right. \right. \\
&\quad \left. \left. + \alpha \rightarrow \beta + \alpha \rightarrow \gamma \right] \right] \times m_{3/2} \\
A_{\alpha\beta\gamma} &\approx e^{-i\gamma w} (1.4876 + 0.024 [10.45 + 2 \ln \left| \frac{C_{\alpha\beta\gamma}}{Y_{\alpha\beta\gamma}} \right| - 7 \ln \left(\frac{14(P+3)}{N} \right) \tag{4.311} \\
&\quad - \sum_i \left(\left\{ \frac{1}{2} \ln \left(\frac{\Gamma(1-\theta_i^\alpha)}{\Gamma(\theta_i^\alpha)} \right) - \frac{1}{2\pi} l \psi_i^\alpha \sin(2\pi\theta_i^\alpha) \right\} + \alpha \rightarrow \beta + \alpha \rightarrow \gamma \right)] \times m_{3/2}.
\end{aligned}$$

We see that compared to the gauginos, the trilinears depend on more constants. The quantity $\left\{ \frac{1}{2} \ln \left(\frac{\Gamma(1-\theta_i^\alpha)}{\Gamma(\theta_i^\alpha)} \right) - \frac{1}{2\pi} (l \psi_i^\alpha \sin(2\pi\theta_i^\alpha)) \right\}$ is of $\mathcal{O}(1)$. Therefore, in a generic situation, we expect the terms inside the sum in $\sum_i \left\{ \frac{1}{2} \ln \left(\frac{\Gamma(1-\theta_i^\alpha)}{\Gamma(\theta_i^\alpha)} \right) - \frac{1}{2\pi} (l \psi_i^\alpha \sin(2\pi\theta_i^\alpha)) \right\}$ to partially cancel each other and give an overall contribution much smaller than the first three terms inside the

square brackets. Then, for known values of the physical Yukawa couplings and reasonable values of P and N , the trilinears generically turn out to slightly larger than $m_{3/2}$.

Scalar Masses

For an (almost) diagonal Kähler metric, the normalized scalar masses reduce to :

$$(m_{\bar{\alpha}\beta}^2) = [m_{3/2}^2 + V_0 - e^{\tilde{K}} F^{\bar{m}} F^n \partial_{\bar{m}} \partial_n \ln(\tilde{K}_\alpha)] \delta_{\bar{\alpha}\beta} \quad (4.312)$$

where we have used (4.291). Using (4.300) in (4.312), we obtain the following expression for the scalar mass squared

$$(m_\alpha^2) = V_0 + (m_{3/2}^2) \left[1 - \frac{9}{4P^2 \left(\ln \left(\frac{A_1 Q}{A_2 P} \right) \right)^2} \left(1 + \frac{2}{(Q-P)\phi_0^2} + \frac{7}{\phi_0^2 P \ln \left(\frac{A_1 Q}{A_2 P} \right)} \right)^2 \right. \\ \left. \times \frac{1}{4\pi} \sum_i \{ l^2 \psi_{ii}^\alpha \sin^2(2\pi\theta_i^\alpha) + l^2 \psi_i^\alpha \sin(4\pi\theta_i^\alpha) - 2l \psi_i^\alpha \sin(2\pi\theta_i^\alpha) \} \right]. \quad (4.313)$$

where we have defined another quantity:

$$\psi_{ii}^\alpha(\theta_i^\alpha) \equiv \frac{d\psi_i^\alpha}{d\theta_i^\alpha} \quad (4.314)$$

As in the case of the trilinears, only the overall scale of the scalars can be estimated, not the individual masses of different flavors of squarks and sleptons. Once the cosmological constant is made small by imposing the constraint (4.247), the scalars are given by

$$(m_\alpha^2) = (m_{3/2}^2) \left[1 - \frac{(139 + 396\sqrt{3})^2}{524593216} \frac{1}{4\pi} \sum_i \{ l^2 \psi_{ii}^\alpha \sin^2(2\pi\theta_i^\alpha) + l^2 \psi_i^\alpha \sin(4\pi\theta_i^\alpha) \right. \\ \left. - 2l \psi_i^\alpha \sin(2\pi\theta_i^\alpha) \} \right] \\ \approx (m_{3/2}^2) \left[1 - \frac{0.0013}{4\pi} \sum_i \{ l^2 \psi_{ii}^\alpha \sin^2(2\pi\theta_i^\alpha) + l^2 \psi_i^\alpha \sin(4\pi\theta_i^\alpha) - 2l \psi_i^\alpha \sin(2\pi\theta_i^\alpha) \} \right] \\ \approx m_{3/2}^2. \quad (4.315)$$

Thus, to a high degree of accuracy, in the IIA limit, the scalar masses for de Sitter vacua are flavor universal as well as flavor diagonal and independent of the details of the matter Kähler metric described by parameters θ_i . Moreover, to a very good approximation, they are equal to the gravitino mass. A natural expectation away from the IIA limit is that the squark and slepton masses are always of order $m_{3/2}$. Since $m_{3/2}$ is of several TeV, the scalars are quite heavy, naturally suppressing flavor changing neutral currents (FCNCs).

4.2.7.5 Effects of tuning the cosmological constant on the phenomenology

In this subsection we would like to give a rough estimate of how the amount of tuning of the cosmological constant might affect the values of the soft parameters. In fact, the constraint (4.247) which sets the cosmological constant to zero in the leading order still results in a very large value of the cosmological constant $V_0 \sim 0.01 \times m_{3/2}^2 m_p^2$, once the subleading terms are taken into account. Exact numerical computations for a manifold with two moduli reveal that the subleading order corrections can change the right hand side in (4.247) by as much as $\sim 5\%$.

The quantity most sensitive to such corrections is the gravitino mass, since it is proportional to $\left(\frac{A_1 Q}{A_2 P}\right)^{-\frac{P}{Q-P}}$ and can therefore change by a factor of order one. Of course, this hardly affects the distributions of scales of $m_{3/2}$ and the emergence of the TeV scale peak remains very robust.

Since the tree-level gaugino mass is suppressed in the leading order as $m_{1/2} \sim \frac{m_{3/2}}{P \ln\left(\frac{A_1 Q}{A_2 P}\right)}$, it is somewhat sensitive to the above corrections and can change by a few percent. However, such variation in $m_{1/2}$ is very mild, considering that as these corrections are taken into account the cosmological constant changes by many orders of magnitude.

Finally, the anomaly mediated gaugino mass contribution (4.302), the trilinear couplings (4.310) and especially the scalar mass squares (4.313) stay virtually unaffected by the few

percent corrections to (4.247). This happens because the dominant contributions to these soft parameters are completely *independent* of $P \ln \left(\frac{A_1 Q}{A_2 P} \right)$ and therefore stay the same, whereas the contributions which do get affected by the corrections are largely subdominant since they are proportional to either $\frac{1}{P \ln \left(\frac{A_1 Q}{A_2 P} \right)}$ or $\frac{1}{P^2 \ln^2 \left(\frac{A_1 Q}{A_2 P} \right)}$.

These considerations indicate that one should not be concerned that tuning of the cosmological constant will affect particle physics phenomenology.

4.2.7.6 Radiative Electroweak Symmetry Breaking (REWSB)

It is very important to check whether the soft supersymmetry breaking parameters in these vacua naturally give rise to radiative electroweak symmetry breaking (REWSB) at low scales. In order to check that, one has to first RG evolve the scalar higgs mass parameters $m_{H_u}^2$ and $m_{H_d}^2$ from the high scale to low scales. Then one has to check whether for a given $\tan \beta$, there exists a value of μ which satisfies the EWSB conditions. At the one-loop level, we find that EWSB occurs quite generically in the parameter space. This can be understood as follows. The gaugino mass contributions to the RGE equation for $m_{H_u}^2$ push the value of $m_{H_u}^2$ up while the top Yukawa coupling, third generation squark masses and the top trilinear pull it down. The suppression of the gaugino mass relative to the gravitino mass causes it to have a negligible effect on the RGE evolution of $m_{H_u}^2$. On the other hand, the masses of squarks and A -terms are both of $\mathcal{O}(m_{3/2})$, which guarantees that $m_{H_u}^2$ is negative at the low scale. Typically, $m_{H_u}^2$ is proportional to $-m_{3/2}^2$, up to a factor less than one depending on $\tan \beta$. Thus, the EWSB condition can be easily satisfied with a μ parameter also of the order $m_{3/2}$. Note that large A -terms (of $\mathcal{O}(m_{3/2})$) are crucial for obtaining EWSB. Having large squark masses and small A -terms cannot guarantee EWSB, as is known from the focus point region in mSUGRA. By low

scale effective theory criteria, the EWSB maybe fine-tuned, but those criteria may change with an underlying theory. Also, one has to ensure that the third generation squarks have positive squared masses, which we have checked. We will report a detailed analysis of these issues in [92].

4.2.7.7 The μ and $B\mu$ problem

We will not have much to say about the μ terms here, leaving a detailed phenomenological study for our future work [92]. We will however, take this opportunity to highlight the main theoretical issues.

The normalized μ and $B\mu$ parameters are :

$$\begin{aligned}\mu &= \left(\frac{\hat{W}^\star}{|\hat{W}|} e^{\hat{K}/2} \mu' + m_{3/2} Z - e^{\hat{K}/2} F^{\bar{m}} \partial_{\bar{m}} Z\right) (\tilde{K}_{H_u} \tilde{K}_{H_d})^{-1/2} \\ B\mu &= (\tilde{K}_{H_u} \tilde{K}_{H_d})^{-1/2} \left\{ \frac{\hat{W}^\star}{|\hat{W}|} e^{\hat{K}/2} \mu' (e^{\hat{K}/2} F^m [\hat{K}_m + \partial_m \ln \mu'] - m_{3/2}) + (2m_{3/2}^2 + V_0) Z \right\}\end{aligned}\tag{4.316}$$

We see from above that the value of the physical μ and $B\mu$ parameters depend crucially on many of the microscopic details eg. if the theory gives rise to a non-zero superpotential μ' parameter and/or if a non-zero bilinear coefficient Z is present in the Kähler potential for the Higgs fields. From section 4.2.7.6, we see that one requires a μ term of $\mathcal{O}(m_{3/2})$ to get consistent radiative EWSB. This is possible for eg. when one has a vanishing μ' parameter and an $\mathcal{O}(1)$ higgs bilinear coefficient Z , among other possibilities.

4.2.7.8 Dark Matter

For dS vacua with a small cosmological constant, $M_2 \ll M_1$ at low scale. In addition, since μ should be of $\mathcal{O}(m_{3/2})$ for consistent EWSB as seen in section 4.2.7.6, both M_2 and M_1 are much less than μ . Hence, the LSP is wino-like. As was discussed in section 4.2.7.5, the tuning of

the cosmological constant has little effect on the gaugino masses, thereby preserving the gaugino mass hierarchy. It is well known that winos coannihilate quite efficiently as the universe cools down. Since the wino masses in these vacua are $\mathcal{O}(100)$ GeV, the corresponding relic density after they freeze out is very small. However there could be non-thermal contributions to the dark matter as well, e.g. the decay of moduli fields into the LSP after the LSP freezes out. In addition, one should remember that the above result for a wino LSP is obtained after imposing the requirement of a small cosmological constant. It would be interesting to analyze the more general case where the results may change. We leave a full analysis of these possibilities for the future [92].

4.2.7.9 Correlations

As we have seen, the parameters of the MSSM depend on the “microscopic constants” determined by a given G_2 manifold and can be explicitly calculated in principle. Therefore, the parameters obtained are correlated with each other in general. For instance we saw that the gaugino and gravitino masses are related. By scanning over the allowed values of the “microscopic constants”, by scanning the space of G_2 manifolds, one obtains a particular subspace of the parameter space of the MSSM at the unification scale. For a given spectrum and gauge group, the RG evolution of these parameters to low scales can also be determined unambiguously, leading to correlations in soft parameters at the low scale. Finally, these correlations in the soft parameters will lead to correlations in the space of actual observables (for eg, the LHC signature space) as well. In other words, the predictions of these vacua will only occupy a *finite* region of the observable signature space at say the LHC. Since two different theoretical constructions will have different correlations in general, this will in turn lead to different patterns

of signatures at the LHC, allowing us to distinguish among different classes of string/ M theory vacua (at least in principle). These issues, in particular the systematics of the distinguishing procedure have been explained in detail in [105].

4.2.7.10 Signatures at the LHC

The subject of predicting signatures at the LHC for a given class of string vacua requires considerable analysis. Here, we will make some preliminary comments, with a detailed analysis to appear in [92].

The scale of soft parameters is determined by the gravitino mass. We saw in section 4.2.6.5 that requiring the cosmological constant to be very small by imposition of a constraint equation (eqn. (4.231)) fixes the overall scale of superpartner masses to be of $\mathcal{O}(1 - 100)\text{TeV}$. Once the overall scale is fixed, the pattern of soft parameters at M_{unif} is crucial in determining the signatures at the LHC. As explained earlier, these M theory vacua give rise to a specific pattern of soft parameters at M_{unif} . We find non-universal gaugino masses which are suppressed relative to the gravitino mass. We furthermore expect that the scalar masses and trilinears are of the same order as the gravitino. The μ and $B\mu$ parameters are not yet understood. For phenomenological analysis however, we may fix them by imposing consistent EWSB.

One can get a sense of the broad pattern of signatures at the LHC from the pattern of soft parameters. Since gaugino masses are suppressed and the fact that the anomaly contribution to the gluino mass parameter approximately *cancel*s the tree-level contribution, one would generically get comparatively light gluinos in these constructions, much lighter than the scalars, which would give rise to a large number of events for many signatures, in particular many events with same-sign dileptons and trileptons in excess of the SM and many events with large missing

energy, even for a modest luminosity of 10 fb^{-1} . Since the gauginos are lighter than the squarks and sleptons, gluino pair production is likely to be the dominant production mechanism. The LSP will be a neutralino for the same reason.

It is also possible to distinguish the class of vacua obtained above from those obtained in Type IIB compactifications, by the pattern of signatures at the LHC. For the large volume type IIB vacua, the scalars are lighter than the gluino [106] while for the KKLT type IIB vacua, the scalars are comparable to the gluino [107]. This implies that squark pair production and squark-gluino production are respectively the dominant production mechanisms at the LHC. Since the LHC is a pp collider, up-type squarks are preferentially produced when they are kinematically allowed, leading to a charge asymmetry which is preserved in cascade decays all the way to the final state with leptons. On the other hand, for the class of M theory vacua described here, since gluino pair production is the dominant mechanism and the decays of the gluino are charge symmetric (it is a Majorana particle), the M theory vacua predict a much smaller charge asymmetry in the number of events with one or two leptons and ≥ 2 jets compared to the Type IIB vacua.

4.2.7.11 The Moduli and Gravitino Problems

The cosmological moduli and gravitino problems can exist if moduli and gravitino masses are too light in gravity mediated SUSY breaking theories. Naively, after the end of inflation, the moduli fields coherently oscillate dominating the energy density of the universe. Since the interactions of the moduli are suppressed by the Planck scale (m_p), their decay rates are extremely small leading to the onset of a radiation dominated universe at very low temperature ($T_R \sim \mathcal{O}(10^{-3})$ MeV for moduli of $\mathcal{O}(100 \text{ GeV}-5\text{TeV})$), compared to what is required for

successful BBN.

To check if the moduli and gravitino problem can be resolved in these M theory compactifications, one has to first compute the masses of the moduli. After doing this, we will use the results to discuss the moduli and gravitino problems.

The geometric moduli s_i appear in the lagrangian with a kinetic term given by

$$\sum_{i=1}^N \frac{3 a_i}{4 s_i^2} \partial_\mu s_i \partial^\mu s_i, \quad (4.317)$$

which is non canonical. The canonically normalized moduli χ_i are

$$\chi_i \equiv \sqrt{\frac{3 a_i}{2}} \ln s_i. \quad (4.318)$$

Their mass matrix is

$$(m_\chi^2)_{ij} = \frac{2 \nu^2 (a_i a_j)^{\frac{1}{2}}}{3 N_i N_j} \frac{\partial^2 V}{\partial s_i \partial s_j}, \quad (4.319)$$

where we took into account the fact that $\frac{\partial V}{\partial s_i} = 0$ at the extremum and that $\nu_i = \nu$ for all $i = \overline{1, N}$. A fairly straightforward but rather tedious computation yields the following structure of the mass matrix

$$(m_\chi^2)_{ij} = \left((a_i a_j)^{\frac{1}{2}} K_1 + \delta_{ij} K_2 \right) \times m_{3/2}^2, \quad (4.320)$$

where, in the large Q approximation keeping $Q - P \sim \mathcal{O}(1)$, K_1 and K_2 are given by

$$K_1 \approx \frac{112}{27} \left(\frac{\tilde{z}}{\tilde{x}} \right)^2 \nu^4 \approx \frac{48 \left(Q \ln \left(\frac{A_1 Q}{A_2 P} \right) \right)^4}{343 (Q - P)^4} \quad (4.321)$$

$$K_2 = -\frac{40}{9} \left(\tilde{L}_{1,+} \right)^2 - \frac{56}{3} L_{1,+} - 8 - 2\phi_0^2 \left(\frac{a\tilde{\alpha}}{\tilde{x}\phi_0^2} + 1 \right)^2 \approx 10 - \frac{8}{Q - P} - \frac{8}{(Q - P)^2 \phi_0^2} - 2\phi_0^2.$$

Using condition $Q - P = 3$, we obtain from (4.177) in the leading order

$$\phi_0^2 \approx (1 + \sqrt{3})/3, \quad (4.322)$$

which results in

$$K_1 \approx \frac{16}{9261} \left(Q \ln \left(\frac{A_1 Q}{A_2 P} \right) \right)^4 \quad (4.323)$$

$$K_2 \approx 8 - 2\sqrt{3}.$$

Diagonalizing the $N \times N$ matrix $(m_\chi^2)_{ij}$ in (4.320) is hard in general. However, for the “all equal” choice when $a_i = 7/(3N)$ for all $i = \overline{1, N}$ this task actually becomes quite simple.

We use the fact that for an $N \times N$ matrix A whose elements are

$$A_{ij} = a \text{ for } i \neq j, \text{ and } A_{ii} = a + b, \quad (4.324)$$

the eigenvalues are given by

$$\lambda_i = b \text{ for } i = 1, \dots, N - 1, \quad (4.325)$$

$$\lambda_N = N a + b. \quad (4.326)$$

For the “all equal” choice the mass matrix (4.320) is precisely of the form (4.324) and therefore we can explicitly determine the entire moduli mass spectrum. The $N - 1$ equal masses are smaller than the remaining mass. All eigenvalues are positive, confirming we have a de Sitter minimum. The $N - 1$ equal moduli masses are given by

$$(m_\chi)_k \approx \sqrt{8 - 2\sqrt{3}} \times m_{3/2} \approx 2 m_{3/2}, \quad k = 1, \dots, N - 1, \quad (4.327)$$

The remaining heavier modulus has

$$M_\chi \approx \frac{4}{63} \left(Q \ln \left(\frac{A_1 Q}{A_2 P} \right) \right)^2 \times m_{3/2}. \quad (4.328)$$

Note that these masses are independent of the number of moduli N .

After imposing the constraint (4.247) to make the cosmological constant small, the mass of the heavy modulus is given by

$$M_\chi \approx 448 m_{3/2} \tag{4.329}$$

Since the gravitino mass distribution peaks at $\mathcal{O}(100)$ TeV, which is also in the phenomenologically relevant range, and the light moduli are roughly twice as heavy compared to the gravitino, the moduli masses are heavy enough to be consistent with BBN constraints.

4.2.8 Summary of Results

We have shown that in fluxless M theory vacua the entire effective potential is generated by non-perturbative effects and depends upon all the moduli. In this work we have studied such this potential in detail when the non-perturbative effects are dominated by strong gauge dynamics in the hidden sector and when such vacua are amenable to the supergravity approximation. In the simplest case, we studied G_2 -manifolds giving rise to two hidden sectors. The resulting scalar potential has AdS vacua - most of them with broken supersymmetry and one supersymmetric one. Then we studied the cases in which there was also charged matter in the hidden sector under the plausible assumption that the matter Kähler potential has weak moduli dependence. In these cases the potential receives positive contributions from non-vanishing F -term vevs for the hidden sector matter leading to a unique de Sitter minimum. In all cases we have explicitly shown that all moduli are stabilized by the potential generated by strong dynamics.

In the de Sitter minimum we computed $m_{3/2}$ and found that a significant fraction of solutions have $m_{3/2}$ in the TeV region, even though the Planck scale is the only dimensionful parameter in the theory. The suppression of $m_{3/2}$ is due to the traditional dimensional transmutation as in the heterotic theory; what is different here is that the moduli are all stabilized, which has

been difficult in the heterotic case. No small parameters or fine-tunings occur, and the eleven dimensional M theory scale is slightly above the gauge unification scale but below the Planck scale. The absence of fluxes is significant for having $m_{3/2} \sim \text{TeV}$ with no small parameters or tuning, and simultaneously M_{11} not far below the Planck scale.

The problem of why the cosmological constant is not large is of course not solved by this approach. We do however understand to a certain extent what properties of G_2 -manifolds are required in order to solve it and we suggest that one can set the value of the potential at the minimum to zero at tree level and proceed to do phenomenology with the superpartners whose masses are described by the softly broken Lagrangian. One particularly nice feature is that we are able to explicitly demonstrate that the soft-breaking terms are not sensitive to the value of the potential at the minimum.

When we set the value of the potential at the minimum to zero at tree level a surprising result occurs. Doing so gives a non-trivial condition on the solutions. When this condition is imposed on $m_{3/2}$, for generic G_2 manifolds it turns out that the resulting values of $m_{3/2}$ are all in the TeV region. Thus we do not have to independently set V_0 to zero *and* set $m_{3/2}$ to the TeV region as has been required in previous approaches.

A more detailed study of the phenomenology of these vacua, particularly for LHC and for dark matter, is underway and will be reported in the future. In the present work we presented the relevant soft-breaking Lagrangian parameters and mentioned a few broad and generic features of the phenomenology, for both our generic solutions and for the case where V_0 is set to zero at tree level. We presented a standard supergravity calculation of the soft breaking Lagrangian parameters, and found that the scalar masses m_α , and also the trilinears, are approximately equal to $m_{3/2}$, to the extent that our assumptions about the matter Kahler

potential are valid. Remarkably, the tree-level gaugino masses are suppressed by a factor of $\mathcal{O}(10 - 100)$. This suppression is present for all G_2 -manifolds giving the de Sitter minimum. For calculating the tree level gaugino masses the matter Kähler potential does not enter, so the obtained values at tree level are reliable. Because the gaugino suppression is large, the anomaly mediated mass contributions are comparable to the tree level ones, and significant cancellations can occur. Gluinos are generically quite light, and should be produced copiously at LHC and perhaps even at the Tevatron – this is an unavoidable prediction of our approach. We have also checked that radiative electroweak symmetry breaking occurs over a large part of the space of G_2 manifolds, and that the lightest neutralino is a good dark matter candidate. It will be exciting to pursue a number of additional phenomenological issues in our approach, including inflation, baryogenesis, flavor and CP-violation physics, Yukawa couplings and neutrino masses.

The approach we describe here apparently offers a framework that can simultaneously address many important questions, from formal ones to cosmological ones to phenomenological ones (apart from the cosmological constant problem, which might be solved in a different way). Clearly, however much work remains to be done. In particular, a much deeper understanding of G_2 -manifolds is required to understand better some of the assumptions we made about the Kähler potential of these vacua.

CHAPTER V

Distinguishing String Constructions from Experimental Observables

In the previous sections, we studied two different regions of the full M theory moduli space from a top-down perspective and looked at some of their consequences for low energy physics. However, with the arrival of the LHC, as well as forthcoming data from other fields such as cosmology, flavor physics, etc. it is imperative to analyze underlying theoretical models to the extent that one could make predictions for real physics observables, signatures at the LHC in particular. Therefore, in the future, we plan to study the two constructions to the extent that predictions for physics observables could be made. Moreover, once we have data, the problem facing us would be the “Inverse Problem”, *viz.*, “how to go from data to underlying theory?” One has to first answer some “zeroth order” questions in order to address the Inverse Problem meaningfully, as was explained in the Introduction. We would like to propose and explore an approach which allows us to answer them successfully for many specific classes of string constructions. The basic idea was first proposed in [108]. Our study here shows that the idea is very promising and it is possible to realize it in a concrete way.

By studying the pattern of signatures (signatures that are real experimental observables) for

many classes of realistic microscopic constructions, one may be able to rule out some classes of underlying theory constructions giving rise to the observed physics beyond the standard model, and be pointed towards others. Our results suggest that a lot of this can be done with limited data and systematically improved with more data and better techniques.

For concreteness, we focus on traditional low-scale supersymmetry as new physics beyond the standard model and the underlying theoretical framework of string theory with different constructions giving rise to low-scale supersymmetry. While there exist other possibilities for new physics beyond the standard model such as technicolor [109], large extra dimensions [110], warped extra dimensions [111], higgsless models [112], composite higgs models [113], little higgs models [114], split supersymmetry [115], etc., low-scale supersymmetry remains the most appealing - both theoretically and phenomenologically. In addition, even though some of these other possibilities may be embedded in the framework of string theory, low-scale supersymmetry is perhaps the most natural and certainly the most popular possibility arising from string constructions. Having said the above, we would like to emphasize that the proposed technique is completely general and can be used for any new physics arising from any theoretical framework whatsoever.

5.1 Examples

We want to focus on compactifications to four dimensions preserving $\mathcal{N}=1$ supersymmetry, which stabilize all (most) moduli and have a mechanism of generating the electroweak scale, allowing us to connect these constructions to real experimental observables. In addition, we want to focus on compactifications which are valid within the supergravity approximation, so that effective four dimensional supergravity techniques are valid. The motivations for all the

above were already explained in section III. Two very good examples which show the above features as well as illustrate our approach, are – KKLT compactifications [116] and Large Volume compactifications [22]. These compactifications preserve $\mathcal{N} = 1$ supersymmetry, so they can be described by a superpotential, kähler potential and gauge kinetic function. Even though both examples fall under the broad class of Type IIB flux compactifications, they arise in two very different regions of the flux superpotential, resulting in rather distinct phenomenological consequences. So, for the purposes of this work, they will be treated differently. In the following, we briefly list their main features relevant for phenomenology.

Type IIB KKLT compactifications (IIB-K)

This class of constructions is a part of the IIB landscape with all moduli stabilized [116]. Closed string fluxes are used to stabilize the dilaton and complex structure moduli at a high scale and non-perturbative corrections to the superpotential are used to stabilize the lighter Kähler moduli. One obtains a supersymmetric anti-deSitter vacuum and D terms [117] or anti D-branes are used to break supersymmetry and to lift the vacuum to a deSitter one. Supersymmetry breaking is then mediated to the visible sector by gravity. The flux superpotential (W_0) has to be tuned very small to get a gravitino mass of $\mathcal{O}(1-10 \text{ TeV})$. By parameterizing the lift from a supersymmetric anti-deSitter vacuum to a non-supersymmetric deSitter vacuum, one can calculate the soft terms [118]. The soft terms depend on the following microscopic input parameters – $\{W_0, \alpha, n_i\}$ or equivalently $\{m_{3/2}, \alpha, n_i\}$, where α is the ratio $\frac{F^T/(T+\bar{T})}{m_{3/2}}$ and n_i are the modular weights of the matter fields [118]. In addition, $\tan(\beta)$ and $\text{sign}(\mu)$ are fixed by electroweak symmetry breaking. A feature of this class of constructions is that the tree level soft terms are comparable to the anomaly mediated contributions, which are always present

and have been calculated in [119].

Type IIB Large Volume Compactifications (IIB-L)

This class of constructions also form part of the IIB landscape with all moduli stabilized. In this case, the internal manifold admits a large volume limit with the overall volume modulus very large and all the remaining moduli small [22]. Fluxes again stabilize the complex structure and dilaton moduli at a high scale, but the flux superpotential W_0 in this case can be $\mathcal{O}(1)$. Higher order corrections in Large Volume compactifications have been computed in [23]. One also incorporates perturbative contributions to the Kähler potential in addition to non-perturbative contributions to the superpotential to stabilize the Kähler moduli. A consequence of $W_0 = \mathcal{O}(1)$ is that the conclusions are qualitatively different compared to the KKLT case. Now one gets a non-supersymmetric anti-de Sitter vacuum in contrast to the KKLT case, which can be lifted to a de Sitter one by similar mechanisms as in the previous case. Since the volume is very large, the string scale turns out to be quite low. Assuming a natural value of W_0 to be $\mathcal{O}(1)$ ¹, to get a gravitino mass of $\mathcal{O}(1-10 \text{ TeV})$, one needs the string scale of $\sim 10^{11} \text{ GeV}$. Since the string scale is much smaller than the unification scale, one cannot have standard gauge unification in these compactifications with W_0 as $\mathcal{O}(1)$. Supersymmetry breaking is again mediated to the visible sector by gravity and soft terms can be calculated [90]. Anomaly mediated contributions turn out to be important for some soft parameters and have to be accounted for. The soft terms depend on the following microscopic input parameters - $\{\mathcal{V}, n_i\}$ or equivalently $\{m_{3/2}, n_i\}$, where \mathcal{V} denotes the volume of the internal manifold and n_i denote the modular weight of the matter fields. $\tan(\beta)$ and $\text{sign}(\mu)$ are fixed by electroweak

¹we actually varied it roughly from 0.1 to 10.

symmetry breaking.

These two classes of compactifications are good for the following two reasons :

- These compactifications stabilize *all* the moduli, making them massive at acceptable scales. This is good for two reasons – a) Light scalars (moduli) are in conflict with astrophysical observations, and b) Since particle physics masses and couplings explicitly depend on the moduli, one cannot compute these couplings unless the moduli are stabilized.
- They have a mechanism for generating a small gravitino mass ($O(1 - 10)$ TeV). This is essential to deal with the *hierarchy problem*. The mechanisms available for generating a small gravitino mass may not be completely satisfactory though. For example, the KKLT vacua require an enormous amount of tuning, while the Large Volume vacua (with $W_0 = O(1)$) do not have standard gauge unification at 2×10^{16} GeV. The class of M theory vacua discussed in the previous chapter though, stabilize all the moduli, naturally explain the hierarchy and are also consistent with standard gauge unification [19].

There do not exist MSSM-like matter embeddings in the KKLT and Large Volume classes of vacua at present. However, since many examples of MSSM-like matter embeddings have been constructed in simpler type II orientifold constructions, one hopes that it will be possible to also construct explicit MSSM-like matter embeddings in these vacua as well in the future. Therefore, we take the following approach in our analysis – we *assume* the existence of an MSSM matter embedding on stacks of D7 branes² in these vacua and analyze the consequences for low energy observables. Having said that, it is important to understand that the assumption of an

²for concreteness.

MSSM-like matter embedding has been made only for conceptual and computational simplicity – a) Any model of low energy supersymmetry must at least have the MSSM matter spectrum for consistency, so assuming the MSSM seems to be a reasonable starting point. b) In addition, most of the software tools and packages available are optimized for the MSSM. In principle, the approach advocated is completely general and can be applied to any theoretical construction. The main point we want to emphasize is that *it is possible to complete the first steps towards addressing the deeper inverse problem*. Choosing a different class of vacua or the above vacua with a different matter embedding will change the results, but not the properties that it is possible to go from classes of semi-realistic string vacua to experimental observables and that classes of string vacua can be distinguished on the basis of their experimental observables.

In order to illustrate better the fact that our approach works for any given theoretical construction, we also include some other classes of constructions in our analysis. These constructions are *inspired* from microscopic string constructions and include some of their model building and some of their moduli stabilization features, although not in a completely convincing and comprehensive manner. Also, in these constructions the supersymmetry breaking mechanism is not specified explicitly, it is only parameterized. These constructions serve as nice toy constructions making it easy to connect these constructions to low energy phenomenology quickly and efficiently. Therefore, even though from a strictly technical point of view they only have educational significance, they are still very helpful in bringing home the point we want to emphasize.

All the string constructions studied in this work have a thing in common – the soft supersymmetry breaking terms at the string scale are determined in terms of a few parameters. This is in stark contrast to completely phenomenological models such as mSUGRA or minimal

gauge mediation, where the soft supersymmetry breaking terms are chosen *by hand* instead of being determined from a few underlying parameters.

Although for all studied string constructions the soft terms are determined in terms of a few underlying parameters, the KKLT and Large Volume constructions differ from the others in the sense that for these constructions, the parameters which determine the soft terms are intimately connected to the underlying microscopic theoretical structure compared to the other constructions. From a practical point of view though, once the soft terms are determined, then one can treat all the constructions at par as far as the analysis of low energy observables is concerned. This also applies if one is only interested in understanding the origin of the specific pattern of signatures of a given construction from its spectrum and soft parameters, as is done in sections 5.4.3 and 5.4.4. However, in order to understand the origin of the soft parameters from the structure of the underlying theoretical construction, it makes more sense to analyze the KKLT and Large Volume constructions as they are microscopically better defined³ and because they provide a better representation of phenomenological characteristics of classes of string vacua. This will be done in section 5.4.5.

The string-motivated constructions considered in the analysis are the following:

- HM-A – Heterotic M theory constructions with one modulus.
- HM-B – Heterotic M theory constructions with five-branes.
- HM-C – Heterotic M theory constructions with more than one moduli.
- PH-A – Weakly coupled heterotic string constructions with non-perturbative corrections to the Kähler potential.
- PH-B – Weakly coupled heterotic string constructions with a tree level Kähler potential and multiple gaugino condensates.
- II-A – Type IIA constructions on toroidal orientifolds with Intersecting D branes.

³in the sense that they provide an explicit mechanism of supersymmetry breaking and moduli stabilization.

5.2 The “String” Benchmark Pattern Table - Results

Before we explain, we briefly summarize the results so that the reader can see the goals. The results for the pattern table are summarized in Table 5.1. The rows and columns constitute eight “string” constructions⁴ analyzed in our study.

	HM-A	HM-B	HM-C	PH-A	PH-B	II-A	IIB-K	IIB-L
HM-A	–	PY	PY	Yes	Yes	Yes	Yes	Yes
HM-B		–	PY	Yes	Yes	Yes	Yes	Yes
HM-C			–	PY	Yes	Yes	PY	PY
PH-A				–	Yes	Yes	Yes	PY
PH-B					–	Yes	Yes	Yes
II-A						–	Yes	Yes
IIB-K							–	Yes
IIB-L								–

Table 5.1: **The String Pattern Table Results**

A “Yes” for a given pair of constructions indicates that the two constructions are distinguishable in a robust way, while a “No” indicates that the two models are not distinguishable with available data ($5 fb^{-1}$ in this case). A “Probably Yes (No)” means that the two models are (aren’t) distinguishable in large regions of their parameter spaces.

For each construction, we go from the ten or eleven dimensional string/M theory to its four dimensional effective theory and then to its LHC signatures. For the string constructions we study, the task of deducing the effective four-dimensional lagrangian has already been accom-

⁴One should be aware of the qualifications made in the previous section.

plished. Therefore, we use results for the description of the effective four-dimensional theories from literature. However, barring the KKLT constructions ⁵, none of the other constructions have been studied to the extent that predictions for LHC observables can be made. In this work, we have studied the phenomenological consequences of each of these constructions in detail, and computed their LHC signatures. An LHC signature by definition is one that is really observable at a hadron collider, e.g. number of events for n leptons, m jets and \cancel{E}_T and various ratios of numbers of events, but not (for example) masses of superpartners or $\tan\beta$. Signatures are typically of two kinds - counting signatures, as mentioned in the examples above and distribution signatures, e.g. the effective mass distribution, invariant mass distribution of various objects, etc.

The results shown in Table 5.1 are deduced by calculating signatures for the various constructions and looking for signatures that are particularly useful in distinguishing different constructions, shown in Table 5.2. The details of the procedure involved and the kind of signatures used will be explained unambiguously in later sections. The results are shown here so that the interested reader can see the goals. The rows depict the string constructions used in our study while the columns consist of useful signatures, which will be defined precisely later. The *pattern table* (Table 5.2) has been constructed for $5 fb^{-1}$ of data at the LHC, which is roughly two years' worth of initial LHC running. Since everyone is eager to make progress, we focus on getting early results. More data will allow doing even better. From Table 5.1, it can be seen that most of the pairs can be distinguished from each other, encouraging optimism about the power and usefulness of this analysis.

The logically simplest way to distinguish constructions on the basis of their signature pat-

⁵The collider phenomenology of Large Volume constructions had not been studied at the time of writing, it was studied soon afterwards.

Signature	A	B	C	D	E	F	G
Condition	> 1200	> 25	> 1.6	> 0.54	> 0.05	> 160GeV	> 0.58
HM-A	OC	OC	OC	OC	OC	Both	OC
HM-B	Both	Both	Both	Both	Both	Both	Both
HM-C	Both	Both	OC	Both	Both	Both	Both
PH-A	ONC	N.O.	OC	Both	ONC	ONC	Both
PH-B	N.O.	N.O.	N.O.	N.O.	N.O.	Both	N.O.
II-A	ONC	N.O.	ONC	OC	ONC	ONC	ONC
IIB-K	ONC	ONC	OC	ONC	Both	OC	ONC
IIB-L	ONC	N.O.	OC	Both	ONC	ONC	Both

Table 5.2: **The String Pattern Table**

An “OC” for the i^{th} row and j^{th} column means that the signature is observable for many models of the i^{th} construction. The value of the j^{th} signature for the i^{th} construction is (almost) always consistent with the condition in the second row and j^{th} column of the Table. An “ONC” also means that the signature is observable for many models of i^{th} construction. However, the value of the signature (almost) always does *not* consistent with the condition as specified in the second row and j^{th} column of the Table. A “Both” means that some models of the i^{th} construction have values of the j^{th} signature which are consistent the condition in the second row and the j^{th} column while other models of the i^{th} construction have values of the j^{th} signature which are not consistent with the condition. An “N.O.” for the i^{th} row and j^{th} column implies that the j^{th} signature is *not* observable for the i^{th} construction, i.e. the values of the observable for all (most) models of the construction are always below the observable limit as defined by (5.1), for the given luminosity ($5 fb^{-1}$). So, the construction is not observable in the j^{th} signature channel with the given amount of “data”.

tern would be to construct a multi-dimensional plot which shows that all constructions occupy different regions in the multi-dimensional space. Since this is not practically feasible, we construct two dimensional projection plots for various pairs of signatures. For simplicity in this initial analysis, each observable signature has been divided into two classes, based on the value the observable takes. The observable value dividing the two classes is chosen so as to yield good results. For a given two dimensional plot for two signatures, we will have clusters of points representing various constructions. Each point will represent a set of parameters for a given construction, which we call a “model”. The cluster of points representing a given construction may form a connected or disconnected region. To distinguish any two given constructions, we essentially look for conditions in this two dimensional plane which are satisfied by all (most) models of one construction (represented by one cluster of points) but not satisfied by all (most) models of the other construction (represented by the other cluster of points). In this way, it will be possible to distinguish the two given constructions.

The cartoon in Figure 5.1 illustrates the above point in a clear way. In a given two dimensional plot with axes given by signatures A and B , we will in general have two clusters of points for two given constructions a and b , as shown by the light and dark regions respectively. If we define a condition Φ on the signatures A and B such that it is given by the line (or curve in general) shown in the cartoon, then it is possible to distinguish constructions a and b by the above set of signatures. To be clear, the above method of distinguishing theoretical constructions has some possible technical limitations, which will be addressed in section 5.6. Since the purpose here is to explain the overall approach in a simple manner, we have used the above method. One can make the approach more sophisticated to tackle more complicated situations, as is mentioned in section 5.6.

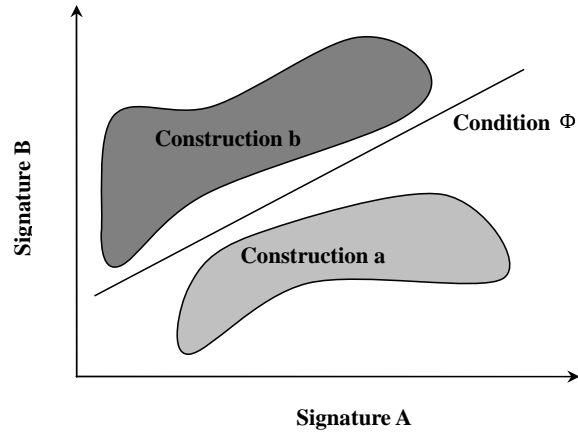


Figure 5.1: Cartoon to illustrate the method used to distinguish constructions.

The counting signatures in Table 5.2 denote numbers of events in excess of the Standard Model (SM). A description of some of the SM backgrounds included is in the next section.

Simple Criterion for Distinguishing Constructions

Based on the above pattern table, our criterion for distinguishing any given pair of constructions (a “Yes” in the pattern table) is that their respective entries are very different in at least one column, such as an *OC* for one construction while an *ONC* or *N.O.* for another construction. A *Both* for one construction while an *OC* or *ONC* or *N.O.* for another does not distinguish the constructions cleanly. If there is only a small region of overlap between the two constructions for all signatures, then the two constructions can be distinguished in the regions in which they don’t overlap. This would give a “Probably Yes (PY)” in the pattern table, otherwise it would give a “Probably No (PN)”. Similarly, an *ONC* for one construction and an *N.O.* for another also does not distinguish the two constructions cleanly, and would give a “PY” or “PN” depending on their overlap. Carrying out this procedure for all constructions

and signatures gives the result in Table 5.1. It should be kept in mind though that the result shown in Table 5.1 is only for a simple set of signatures. Using more sophisticated signatures and analysis techniques could give better results. Also, there are typically other useful signatures present than what is listed in the Table. We have only shown the most useful ones. In section 5.4, we give a description of the useful signatures and explain why these particular signatures are useful in distinguishing the various constructions in terms of the spectrum, the soft terms and in turn from the underlying theoretical structure.

5.3 Procedural Details

In this section we enumerate the procedure to answer question (A) in the Introduction, namely, how to go from a string construction to the space of LHC signatures.

The first step concerns the spectrum of a given construction. Many of the string-motivated constructions considered give a semi-realistic spectrum which contains the MSSM, and perhaps also some exotics. However for simplicity, in this initial analysis we only consider the MSSM fields because mechanisms may exist which project the exotic fields out or make them heavy. As already explained, for the KKLT and Large Volume vacua, we just assume the existence of an MSSM matter embedding. The weakly and strongly coupled heterotic string constructions are naturally compatible with gauge coupling unification at $M_{unif} \sim 2 \times 10^{16}$ GeV, but type II-A and type II-B constructions are not in general. One can however try to impose that as an additional constraint even for type II constructions since gauge unification provides a very important clue to beyond-the-Standard Model physics. Therefore, all constructions except the Large Volume compactifications (IIB-L) used in our analysis either naturally predict or consistently assume the existence of gauge coupling unification at M_{unif} . The IIB-L construction does not have

the possibility of gauge coupling unification at M_{unif} compatible with having a supersymmetry breaking scale of $\mathcal{O}(\text{TeV})$ [22]. The string scale for the IIB-L constructions is taken to be of $\mathcal{O}(10^{10} - 10^{11})$ GeV in order to have a supersymmetry breaking scale of $\mathcal{O}(\text{TeV})$, making it incompatible with standard gauge unification.

In order to connect to low energy four-dimensional physics, one has to write the effective four dimensional action at the String scale /11 dim Planck scale, which we will denote by M_s . M_s will be equated to M_{unif} for all constructions except for the Large Volume compactifications (IIB-L). The four-dimensional effective action for each of these constructions is determined by a set of microscopic “input” parameters of the underlying theory. Soft supersymmetry breaking parameters for the MSSM fields are calculated at M_s as functions of these underlying input parameters. The input parameters are taken to vary within appropriate ranges, as determined by theoretical and phenomenological considerations. In a more realistic construction, some of these parameters may actually be fixed by the theory. Our approach therefore is broad in the sense that we include a wide range of possibilities without restricting too much to a particular one.

Each of the “models” for a particular construction is thus defined by a list of input parameters which in turn translate to a *parameter space* of soft parameters at the unification scale. In other words, the boundary conditions for the soft parameters are determined by the underlying microscopic constructions. As emphasized earlier, this is very different from an *ad hoc* choice of boundary conditions for the soft parameters, as in many models like mSUGRA or minimal gauge mediation.

Once the soft parameters are *determined* from the underlying microscopic parameters, then the procedure to connect these soft parameters to low-scale physics is standard, namely, the soft

parameters are evolved through the Renormalization Group (RG) evolution programs (SuSPECT [120] and SOFTSUSY [121]) to the electroweak scale, and the spectrum of particles produced is calculated. For concreteness and simplicity, we assume that no intermediate scale physics exists between the electroweak scale and the unification scale, though we wish to study constructions with intermediate scale physics and other subtleties in the future.

Of all the models thus generated, only some will be consistent with low energy experimental and observational constraints. Some of the most important low energy constraints are :

- Electroweak symmetry breaking (EWSB).
- Experimental bounds for superpartner masses.
- Experimental bound for the Higgs mass.
- Constraints from flavor and CP physics.
- Upper bound on the relic density from WMAP.

In this analysis, we use $\tan\beta$ as an input parameter and the RGE software package determines μ and $B\mu$ by requiring consistent EWSB. This is because none of the constructions studied are sufficiently well developed so as to predict these quantities *a priori*. In the future, we hope to consider constructions which predict μ , $B\mu$ and the Yukawa couplings allowing us to deduce $\tan\beta$ at the electroweak scale and explain EWSB. The models we consider are consistent with constraints on particle spectra, $b \rightarrow s\gamma$ [122], $(g_\mu - 2)$ [123] and the upper bound on relic density. One should not impose the lower bound on relic density since non-thermal mechanisms can turn a small relic density into a larger one. Also, the usually talked about lower bound on the LSP mass (~ 50 GeV) is only present for models with gaugino mass unification. There is no general lower bound on the LSP mass, especially if one also relaxes the constraint of a thermal relic density. In our analysis, we have not imposed any lower bound on the LSP mass. In our study at present, we have generated ~ 50 models for most constructions (~ 100

models for the PH-A construction)⁶. This might seem too small at first. However from our analysis it seems that the results we obtain are robust and do not change when more points are added. For a purely statistical analysis this could be a weak point, but because in each case we know the connection between the theory and signatures and understand why the points populate the region they do, we expect stable results. We simulated many more models for two particular constructions and found that the qualitative results do not change, confirming our expectations. This will be explained in section 5.6.

Once one obtains the spectrum of superpartners at the low scale, one calculates matrix elements for relevant physics processes at parton level which are then evolved to “long-distance” physics, accounting for the conversion of quarks and gluons into jets of hadrons, decays of tau leptons, etc. We carry out this procedure using PYTHIA 6.324 [124]. The resulting hadrons, leptons and photons have to be then run through a detector simulation program which simulates a real detector. This was done by piping the PYTHIA output to a modified CDF fast detector simulation program PGS [125]. The modified version was developed by John Conway, Stephen Mrenna and others and approximates an ATLAS or CMS-like detector. The output of the PGS program is in a format which is also used in the LHC Olympics [126]. It consists of a list of objects in each event labelled by their identity and their four-vector. Lepton objects are also labelled by their charges and b-jets are tagged. With this help of these, one can construct a wide variety of signatures.

The precise definitions of jets and isolated leptons, criteria for hadronically decaying taus, efficiencies for heavy flavor tagging as well as trigger-level cuts imposed on objects are the same as used for the “blackbox” data files in the LHC Olympics [126]. In addition, we impose event

⁶However, not all 50 (or 100) models will be above the observable limit in general.

selection cuts as the following:

- If the event has photons, electrons, muons or hadronic taus, we only select the particles which satisfy the following – Photon $P_T > 10$ GeV; Electron, Muon $P_T > 10$ GeV; (hadronic) Tau $P_T > 100$ GeV.
- For any event with jets, we only select jets with $P_T > 100$ GeV.
- Only those events are selected with \cancel{E}_T in the event > 100 GeV.

These selection cuts are quite simple and standard. We have used a simple and relatively “broad-brush” set of cuts since for a preliminary analysis, we want to analyze many constructions simultaneously. As mentioned before, we have simulated 5 fb^{-1} of data at the LHC for each model. A small luminosity was chosen for two reasons – first, in the interest of computing time and second, in order to argue that our proposed technique is powerful enough to distinguish between different constructions even with a limited amount of data. Of course, to go further than distinguishing classes of constructions broadly from relatively simple signatures, such as getting more insights about particular models within a given construction, one would in general require more data and could sharpen the approach by imposing more exclusive cuts and signatures.

In order to be realistic, one has to take the effects of the standard model background into account. In our analysis, we have simulated the $t\bar{t}$ background and the diboson (WW, ZZ)+jets background. We have not included the uniboson (W, Z) + jets background in the interest of time. However, from [127] we know that for a \cancel{E}_T threshold of 100 GeV, as has been used in our analysis, the $t\bar{t}$ background is either the largest background or comparable to the largest one (W + jets typically). Therefore, we expect our analysis and results to be robust against

addition of the $W + \text{jets}$ background. The criteria we employ for an observable signature is :

$$\frac{N_{signal}}{\sqrt{N_{bkgd}}} > 4; \quad \frac{N_{signal}}{N_{bkgd}} > 0.1; \quad N_{signal} > 5. \quad (5.1)$$

These conditions are quite standard. A signature is observable only when the most stringent of the three constraints is satisfied.

Although the steps used in our analysis are quite standard, there are at least two respects in which our analysis differs from that of previous ones in the literature. First, our work shows for the first time that with a few reasonable assumptions, one can study string theory constructions to the extent that reliable predictions for experimental observables can be made, and more importantly, different string constructions give rise to overlapping but distinguishable footprints in signature space. Moreover, it is possible to understand *why* particular combinations of signatures are helpful in distinguishing different constructions, from the underlying theoretical structure of the constructions. Therefore, even though we have done a simplified (but reasonably realistic) analysis in terms of trigger and selection level cuts, detection efficiencies of particles, detector simulation and calculation of backgrounds, we expect that doing a more sophisticated analysis will only change some of the details but not the qualitative results. In particular, it will not affect the properties that predictions for experimental observables can be made for many classes of realistic string constructions, and that patterns of signatures are sensitive to the structure of the underlying string constructions, making it possible to distinguish among various classes of string constructions.

5.4 Distinguishability of Constructions

5.4.1 General Remarks

For convenience, we present the signature pattern table again. As was also mentioned in section 5.2, each signature has been broadly divided into two main classes for simplicity. The value of the observable dividing the two classes is chosen so as to yield the best results. A description of the most useful signatures is given below:

- A – Number of events with trileptons and ≥ 2 jets. The value of the observable dividing the signature into two classes is 1200.
- B – Number of events with clean (not accompanied by jets) dileptons. The value of the observable dividing the signature into two classes is 25.
- C – (Y/X) ⁷; Y= Number of events with 2 leptons, 0 b jets and ≥ 2 jets, X= Number of events with 0 leptons, 1 or 2 b jets and ≥ 6 jets⁸. The value of the observable dividing the signature into two classes is 1.6.
- D – (Y/X) ; Y= Number of events with 2 leptons, 1 or 2 b jets and ≥ 2 jets, X= Number of events with 2 leptons, 0 b jets and ≥ 2 jets. The value of the observable dividing the signature into two classes is 0.54.
- E – The charge asymmetry in events with one electron or muon and ≥ 2 jets ($A_c^{(1)} = \frac{N(l^+) - N(l^-)}{N(l^+) + N(l^-)}$). The value of the observable dividing the signature into two classes is 0.065.
- F – The peak of the missing energy distribution. The value of the observable dividing the signature into two classes is 160 GeV.
- G – Y/X ; Y = Number of events with same sign different flavor (SSDF) dileptons and ≥ 2 jets, X = Number of events with 1 tau and ≥ 2 jets. The value of the observable dividing the signature into two classes is 0.5.

Although there exist other signatures which can distinguish among some of the above constructions, the above set of signatures turn out to be the most economic and useful in distinguishing all constructions considered⁹. We understand that some of these signatures are not

⁷The ratio (Y/X) is computed only when both signatures X and Y are above the observable limit.

⁸This signature is not very realistic in the first two years. Please read the discussion in this subsection as to why this signature is still used.

⁹It is important to understand that these signatures were useful in distinguishing constructions which have at least some models giving rise to observable signatures with the given luminosity ($5 fb^{-1}$). With more luminosity, many more models of these constructions would give rise to observable signatures, so one would in general have a *different* set of useful distinguishing signatures.

Signature	A	B	C	D	E	F	G
Condition	> 1200	> 25	> 1.6	> 0.54	> 0.05	> 160GeV	> 0.58
HM-A	OC	OC	OC	OC	OC	Both	OC
HM-B	Both	Both	Both	Both	Both	Both	Both
HM-C	Both	Both	OC	Both	Both	Both	Both
PH-A	ONC	N.O.	OC	Both	ONC	ONC	Both
PH-B	N.O.	N.O.	N.O.	N.O.	N.O.	Both	N.O.
II-A	ONC	N.O.	ONC	OC	ONC	ONC	ONC
IIB-K	ONC	ONC	OC	ONC	Both	OC	ONC
IIB-L	ONC	N.O.	OC	Both	ONC	ONC	Both

Table 5.3: **The String Pattern Table**

An “OC” for the i^{th} row and j^{th} column means that the signature is observable for many models of the i^{th} construction. The value of the j^{th} signature for the i^{th} construction is (almost) always consistent with the condition in the second row and j^{th} column of the Table. An “ONC” also means that the signature is observable for many models of i^{th} construction. However, the value of the signature (almost) always does *not* consistent with the condition as specified in the second row and j^{th} column of the Table. A “Both” means that some models of the i^{th} construction have values of the j^{th} signature which are consistent the condition in the second row and the j^{th} column while other models of the i^{th} construction have values of the j^{th} signature which are not consistent with the condition. An “N.O.” for the i^{th} row and j^{th} column implies that the j^{th} signature is *not* observable for the i^{th} construction, i.e. the values of the observable for all (most) models of the construction are always below the observable limit as defined by (5.1), for the given luminosity ($5 fb^{-1}$). So, the construction is not observable in the j^{th} signature channel with the given amount of “data”.

very realistic. For example, the signature which counts the number of events with 0 leptons, 1 or 2 b jets and ≥ 6 jets is not very realistic initially because of difficulties associated with calibrating the fake missing \cancel{E}_T from jet mismeasurement in events with six or more jets. However, we have used this signature in our analysis at this stage because it helps in explaining our results and the approach in an economic way. Also, the fact that there are other useful signatures¹⁰ which distinguish these constructions gives us additional confidence about the robustness of our approach. These signatures were hand-picked by experience and by trial-and-error. Once the set of useful signatures was collected, the next task was to understand *why* the above set of signatures were useful in distinguishing the constructions based on their spectrum, soft parameters and their underlying theoretical setup. This is the subject of sections 5.4.3, 5.4.4 and 5.4.5 respectively. We hope that carrying out the same exercise for other constructions can help build intuition about the kind of signatures which any given theory can produce. This can eventually help in building a dictionary between structure of underlying theoretical constructions and their collider signatures.

The above list of signatures consists of counting signatures and distribution signatures at the LHC. The counting signatures denote number of events in excess of the Standard Model. Naively, one would think that the number of signatures is very large if one includes lepton charge and flavor information, and b jet tagging. However, it turns out that not all signatures are independent. In fact, they can be highly correlated with each other, drastically decreasing the effective dimensionality of signature space. Thus, in order to effectively distinguish signatures, one needs to use signatures sufficiently orthogonal to each other. This has been emphasized recently in [128]. We will see that having an underlying theoretical construction allows us to

¹⁰although they may be less economical in the sense that one would need more signatures to distinguish the same set of constructions.

actually find those useful signatures. Even though we have only listed a few useful signatures in Table 5.3, there are typically more than one (sometimes many) signatures which distinguish any two particular constructions. This is made possible by a knowledge of the structure of the underlying theoretical constructions.

5.4.2 Why is it possible to distinguish different Constructions?

In view of the above comments, one would like to understand why it is possible to distinguish different constructions in general and why the signatures described in the previous section are useful in distinguishing the various constructions in particular.

To understand the origin of distinguishability of constructions, one should first understand why each construction gives rise to a specific pattern of soft supersymmetry breaking parameters and in turn to a specific pattern of signatures. This is mainly due to *correlations in parameter space as well as in signature space*. Let's explain this in detail. A construction is characterized by its spectrum and couplings in general. These depend on the underlying structure of the theoretical construction, such as the form of the four-dimensional effective action, the mechanism to generate the hierarchy, the details of moduli stabilization and supersymmetry breaking, mediation of supersymmetry breaking etc. At the end of the day, the theoretical construction is defined by a small set¹¹ of microscopic input parameters in terms of which *all* the soft supersymmetry breaking parameters are computed. Since *all* soft parameters are calculated from the *same* set of underlying input parameters, this gives rise to correlations in the space of soft parameters for any given construction. These correlations carry through all the way to low energy experimental observables, as will be explicitly seen later. The fact that there exist correlations between different sets of parameters which have their origin in the

¹¹if they are indeed “good” theoretical constructions.

underlying theoretical structure allows us to gain insights about the underlying theory, and is much more powerful than completely phenomenological parameterizations such as mSUGRA, minimal gauge mediation, etc.

Since any two *different* theoretical constructions will differ in their underlying structure in some way *by definition*, the correlations obtained in their parameter and signature spaces will also be different in general. All these will in general have *different* effects on issues which influence low energy phenomenology in an important manner, such as the scale of supersymmetry breaking, unification of gauge couplings (or not), flavor physics, origins of CP violation, etc. These factors combined with experimental constraints allow different string constructions to be distinguished from each other in general.

We now wish to understand why the particular signatures described in section 5.4.1 are useful in distinguishing the studied constructions. In order to successfully do so, one has to understand the relevant features of the various constructions and their implications to hadron collider phenomenology, and devise signatures which are sensitive to those features.

In the following subsections, we explain how to distinguish the above constructions. In principle, one could directly try to connect patterns of signatures to underlying string constructions. However, in practice it is helpful to divide the whole process of connecting patterns of signatures to theoretical constructions in a few parts – first, the results of the pattern table for each construction are explained based on the spectrum of particles at the low scale; second, important features of the spectrum of superpartners at the low scale for the different constructions (which give rise to their characteristic signature patterns) are explained in terms of the soft supersymmetry breaking parameters at the high scale; and third, the structure of the soft parameters is explained in terms of the underlying theoretical structure of the constructions.

For readers not interested in the details in the next subsection, the main points to take away are that any given theoretical construction only gives rise to a specific pattern of observable signatures, and that one can understand and trust the regions of signature space that are populated by a given theoretical construction and that such regions are quite different for different constructions, illustrating in detail that LHC signatures can distinguish different theoretical constructions.

5.4.3 Explanation of Signatures from the Spectrum

In this subsection, we take the spectrum pattern for different constructions as given and explain patterns of signatures based on them. Then it is possible to treat all the constructions equally as far as the explanation of the pattern of signatures from the spectrum is concerned.

The characteristic features of the spectrum for the constructions considered are as follows:

- HM-A - Universal soft terms. Bino LSP (“coannihilation region”¹²). Moderate gluinos (550-650 GeV), slightly lighter scalars.
- HM-B – Universal soft terms. Has two (disconnected) regions. Region I similar to HM-A. Region II either “focus point region”¹³ or “funnel region”¹⁴ Scalars much heavier (> 800 GeV) than gauginos in region II.
- HM-C – Non-universal soft terms. Occupies a big region in signature space encompassing the two regions mentioned for the HM-B construction. Heavy scalars. Can have bino, wino or higgsino LSP. Spectrum and signature pattern quite complicated.
- PH-A — Non-universal soft terms. Bino, higgsino or mixed bino-higgsino LSP. Bino LSP has light gluino (< 600 GeV). Higgsino or mixed bino-higgsino LSP have gluinos ranging from moderately heavy to heavy (600 – 1200 GeV). Heavy scalar masses (≥ 2 TeV).
- PH-B – Non-universal soft terms. Wino and bino LSP. Light gluinos (200-550 GeV) always have wino LSPs while heavier gluinos can have bino or wino LSPs. Comparatively heavy LSP (can be upto 1 TeV), heavy scalar masses (≥ 1 TeV) except stau which is relatively light (≥ 500 GeV).
- II-A – Non-universal soft terms. Can have bino, wino, higgsino or mixed bino-higgsino LSP. Light or moderately heavy gluino (300 – 600 GeV), scalar masses heavier than gluinos but not very heavy (< 1 TeV). Stops can be as light as 500 GeV. Spectrum and signature pattern quite complicated.

¹²Explained in 5.4.5.

¹³Explained in 5.4.5

¹⁴Explained in 5.4.5.

- IIB-K – Non-universal soft terms. Heavy spectrum (≥ 1 TeV) in general, but possible to have light spectrum (≤ 1 TeV). Bino LSP¹⁵. Gluinos are greater than about 450 GeV while the lightest squarks (\tilde{t}_1) are greater than about 200 GeV. For some models, $\tilde{\tau}_1$ can be light as well.
- IIB-L – Non-universal soft terms. Mixed bino-higgsino LSP. The gluinos have a lower bound of about 350 GeV, while the lightest squark (\tilde{t}_1) has a lower bound of about 700 GeV.

As mentioned in the list of characteristic features of the spectrum above, the HM-B and HM-C constructions roughly occupy two regions in signature space, as can be seen from Figure 5.2. One of these regions overlaps with the HM-A construction. This is because the HM-B and HM-C constructions contain the HM-A construction as a subset. Since the three constructions have the same theoretical structure in a region of their high scale parameter space, the models of the three constructions in that particular region cannot be distinguished from each other from their signature pattern as their signatures will always overlap. However, since the HM-B and HM-C constructions have a bigger parameter space, they also occupy a bigger region of signature space compared to the HM-A construction. Thus, it is possible to distinguish the HM-A, HM-B and HM-C constructions in regions in which they don't overlap, i.e. in regions in which their underlying theoretical structure is different. This is the origin of “Probably Yes (PY)” in Table 5.1.

Figures 5.2 and 5.3 shows two (very)¹⁶ inclusive signature plots¹⁷. One can try to explain the differences in these signatures among the HM-A construction and the overlapping HM-B and HM-C constructions on the one hand and the PH-A, PH-B, II-A, IIB-K and IIB-L constructions on the other, from their spectra.

¹⁵We have only analyzed $\alpha > 0$.

¹⁶since we do not take into account the charge and flavor information for leptons, and the flavor information for jets (whether the jets are of heavy flavor or not).

¹⁷The figures are best seen in color.

The HM-A construction and the overlapping HM-B, HM-C constructions have a comparatively light spectrum at the low scale. These give rise to a subset of the well known mSUGRA boundary conditions, so after imposing constraints from low energy physics as in section 5.3, one finds that the allowed spectrum consists of light and moderately heavy gluinos, slightly lighter squarks and light sleptons. Thus, $\tilde{g}\tilde{q}$ production and $\tilde{q}\tilde{q}$ pair production are dominant with direct $\tilde{N}_2 \tilde{C}_1$ production also quite important.

Both squarks and gluinos ultimately decay to \tilde{N}_2 and \tilde{C}_1 and since most sleptons (including selectrons, smuons) are accessible, both \tilde{N}_2 and \tilde{C}_1 decay to leptons and the LSP via sleptons. Since the mass difference between \tilde{N}_2 , \tilde{C}_1 and LSP (\tilde{N}_1) is big (because of universal boundary conditions, $\Delta M_{\tilde{N}_2-\tilde{N}_1}, \Delta M_{\tilde{C}_1-\tilde{N}_1} \sim M_{\tilde{N}_1}$), most of the leptons produced pass the cuts. The \tilde{N}_2 and \tilde{C}_1 by themselves are also comparatively light (< 200 GeV). On the other hand, the PH-A, PH-B, II-A and IIB-L constructions are required to have heavy scalars and gluinos varying in mass from light to heavy. So, the \tilde{N}_2 and \tilde{C}_1 produced from gluinos decay to the LSP mostly through a virtual Z and W respectively, which makes their branching ratio to leptons much smaller. Because of *non-universal* soft terms, $\Delta M_{\tilde{N}_2-\tilde{N}_1}$ and $\Delta M_{\tilde{C}_1-\tilde{N}_1}$ can be bigger or smaller than in the universal case. In the PH-A, PH-B, II-A and IIB-L constructions, they are required to be comparatively smaller, leading to leptons which are comparatively softer on average, many of which do not pass the cuts.

For clean dilepton events, direct production of \tilde{N}_2 and \tilde{C}_1 is required. The HM-A construction and overlapping HM-B and HM-C constructions have comparatively lighter \tilde{N}_2 and \tilde{C}_1 , so \tilde{N}_2 and \tilde{C}_1 are directly produced. On the other hand, most models of the PH-B and II-A constructions have heavier \tilde{N}_2 and \tilde{C}_1 compared to the HM-A construction, making it harder to produce them directly. The PH-A and IIB-L constructions have some models with light \tilde{N}_2

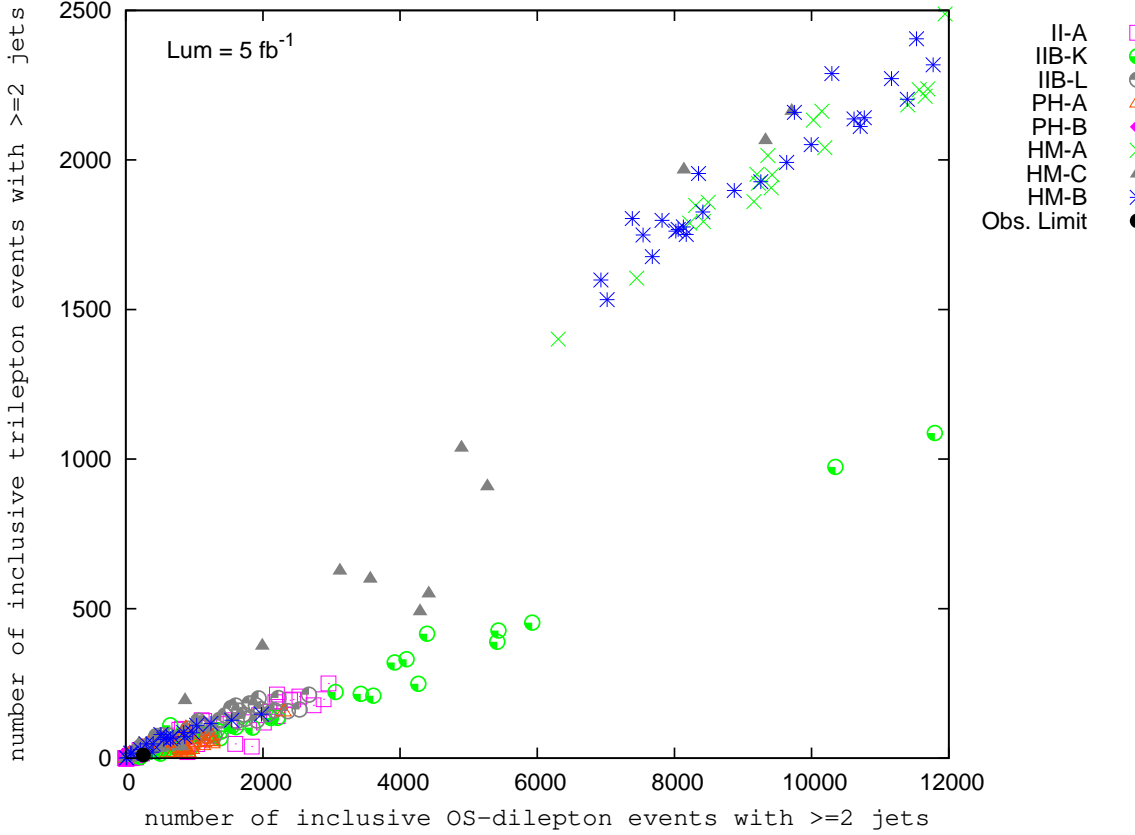


Figure 5.2: Plot of number of events with opposite-sign dileptons and ≥ 2 jets and number of events with three leptons and ≥ 2 jets. The black dot represents the lower limit of observability of the two signatures, according to conditions in equation (5.1). Note that the HM-A and overlapping HM-B and HM-C construction can be distinguished easily from the PH-A, PH-B, II-A, IIB-K and IIB-L constructions, as they occupy very different regions. The plots are best seen in color.

and \tilde{C}_1 , but the other factors (decay via virtual W and Z, and smaller mass separation between \tilde{N}_2 , \tilde{C}_1 and LSP) turn out to be more important, leading to no observable clean dilepton events. Therefore, the result is that *none* of the models of the PH-A, PH-B, II-A and IIB-L constructions have observable clean dilepton events. Thus, it is possible to distinguish the HM-A construction and overlapping HM-B and HM-C constructions from the PH-A, PH-B, II-A

and IIB-L constructions by signatures A and B in Table 5.3 (shown in Figures 5.2 and 5.3).

The case with the IIB-K construction is slightly different. These constructions have many models with a heavy spectrum which implies that those models do not have observable events with the given luminosity of $5 fb^{-1}$. However, these constructions can also have light gluinos and squarks with staus also being light in some cases. So $\tilde{g}\tilde{q}$ production is typically dominant for these models. The gluinos and squarks decay to \tilde{N}_2 and \tilde{C}_1 as for other constructions. Since for many IIB-K models, the lightest stau is heavier than \tilde{N}_2 and \tilde{C}_1 (even though it is relatively lighter than in the PH-A, PH-B, II-A and IIB-L constructions), the \tilde{N}_2 and \tilde{C}_1 decay to the LSP through a virtual Z and W respectively, making the branching fraction to leptons much smaller than for the HM-A and overlapping HM-B and HM-C constructions. In addition, the mass differences $\Delta M_{\tilde{N}_2-\tilde{N}_1}$ and $\Delta M_{\tilde{C}_1-\tilde{N}_1}$ are required to be smaller for the IIB-K construction in general compared to that for the HM-A and overlapping HM-B and HM-C constructions, making it harder for the leptons to pass the cuts. Some IIB-K models have comparable mass differences $\Delta M_{\tilde{N}_2-\tilde{N}_1}$ and $\Delta M_{\tilde{C}_1-\tilde{N}_1}$ as the HM-A construction, but they have much heavier gluinos compared to those for the HM-A construction, making their overall cross-section much smaller. Therefore, the IIB-K construction has fewer events for leptons in general (in particular for trileptons) compared to that for the HM-A and overlapping HM-B and HM-C constructions, as seen from Figure 5.2.

Region II of the HM-B construction and the non-overlapping region of the HM-C construction (with HM-A) cannot be cleanly distinguished from the PH-A, PH-B, II-A, IIB-K and IIB-L constructions from the above signatures. Region II of the HM-B construction (the “focus point” or “funnel region” of mSUGRA) however, can be distinguished from these constructions with

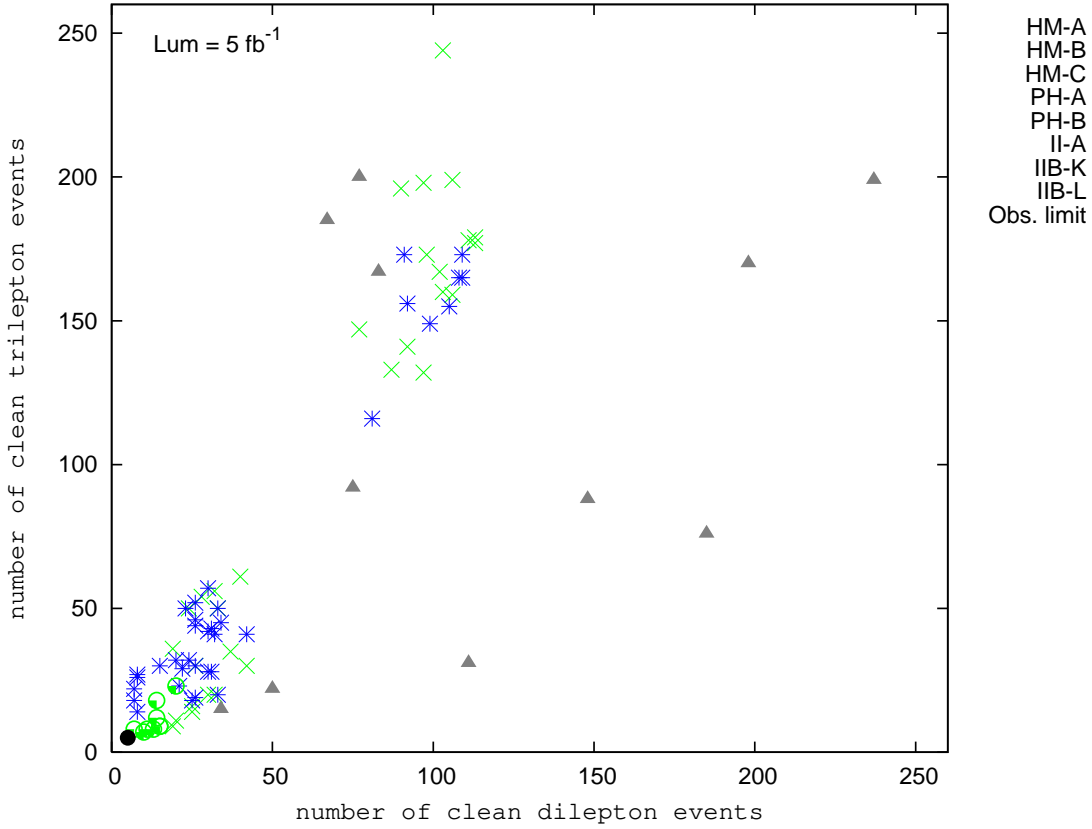


Figure 5.3: Plot of number of events with clean dileptons and number of events with clean trileptons. “clean” means not accompanied by jets. The black dot represents the lower limit of observability of the two signatures, according to conditions in equation (5.1). The models below the observable limit have not been shown. Note that the HM-A and overlapping HM-B and HM-C constructions can be distinguished from the PH-A, PH-B, II-A and IIB-L constructions, since the latter are not observable with the given luminosity. The plots are best seen in color.

the help of other signatures¹⁸. The non-overlapping region of the HM-C construction is a very

¹⁸For example, the signatures shown in Figure 5.4 can distinguish Region II of the HM-B construction (the HM-B models distinct from the PH-A, PH-B, IIB-K and IIB-L region all belong to Region II) with the PH-A, IIB-K and IIB-L constructions. As another example, the ratio of number of events with 0 b jets and ≥ 2 jets and number of events with ≥ 3 b jets and ≥ 2 jets can distinguish Region II of HM-B with PH-B, II-A and IIB-K constructions. These can be explained on the basis of their spectra, but has not been done here for simplicity. Also, the HM-B row in Table 5.3 has not been divided into two parts (to account for the two regions) to avoid clutter.

big region in signature space because of its big parameter space, making it relatively harder to distinguish it from some of the other constructions. Since we have not found signatures cleanly distinguishing the *whole* msoft-II region from some of the other constructions, we have put a “Probably Yes” in the corresponding rows and columns in Table 5.1.

Now we explain the distinguishability of the PH-A, PH-B, II-A, IIB-K and IIB-L constructions. Figure 5.4 shows that the PH-B and II-A constructions can be distinguished from the PH-A, IIB-K and IIB-L constructions (signature C in Table 5.3)¹⁹. Figure 5.5 shows that the PH-B and II-A constructions can be distinguished from each other and that the PH-A and IIB-L constructions can be *partially* distinguished from each other (signature D in Table 5.3). To understand why it is possible to do so, we look at these constructions in detail.

Let’s start with the IIB-K construction. As explained earlier, the IIB-K construction typically gives a heavy spectrum, although it is possible to have a light spectrum with light gluinos and squarks (stops) with the stau also being light in some cases. So, $\tilde{g}\tilde{q}$ production is typically dominant. First and second generation squarks are copiously produced. The first and second generation squarks decay to non b-jets and the gluino also decays more to non b jets than to b jets because the IIB-K construction always has a bino LSP. Therefore, as seen from Figure 5.5, the IIB-K construction has more events with 2 leptons, 0 b jets and ≥ 2 jets compared to those with 2 leptons, 1 or 2 b jets and ≥ 2 jets. Also, since the mass difference between \tilde{N}_2, \tilde{C}_1 and \tilde{N}_1 is only big enough for leptons to pass the cuts but not for jets to pass the cuts, the number of events with 0 leptons, 1 or 2 b jets and ≥ 6 jets is smaller than those with 2 leptons, 0 b jets and ≥ 2 jets, as seen from Figure 5.4.

¹⁹This signature may not be very realistic. However, as explained in section 5.4.1, it has been used here because it is very economical and illustrates the approach in a simple manner.

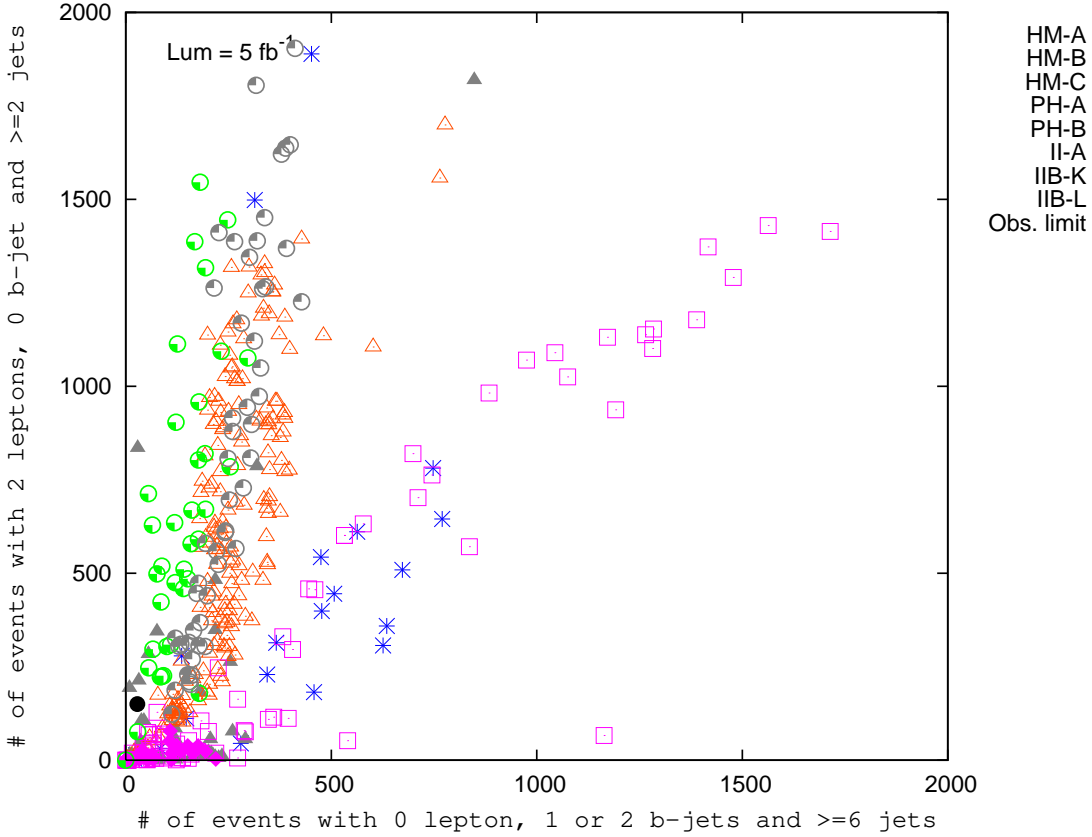


Figure 5.4: Plot of number of events with 0 leptons, 1 or 2 b jets and ≥ 6 jets and number of events with 2 leptons, 0 b jets and ≥ 2 jets. The black dot represents the lower limit of observability of the two signatures, according to conditions in equation (5.1). The models below the observable limit have also been shown to emphasize that the II-A construction has very different number of events for these signatures compared to other constructions even *without* imposing the observability constraint. Note that the PH-B and II-A constructions can be distinguished from the PH-A, IIB-K and IIB-L constructions because they have very different slopes. The plots are best seen in color.

The PH-B construction has scalars which are quite heavy (> 1 TeV). So, gluino pair production is dominant. The branching ratio of gluinos to $\tilde{C}_1 + \text{jets}$ is typically the largest for $\tan\beta \geq 20$, if it is kinematically allowed [129], followed by $\tilde{N}_i + \text{jets}$, $i = 1, 2, 3$, which are smaller. This is generally true for this construction.

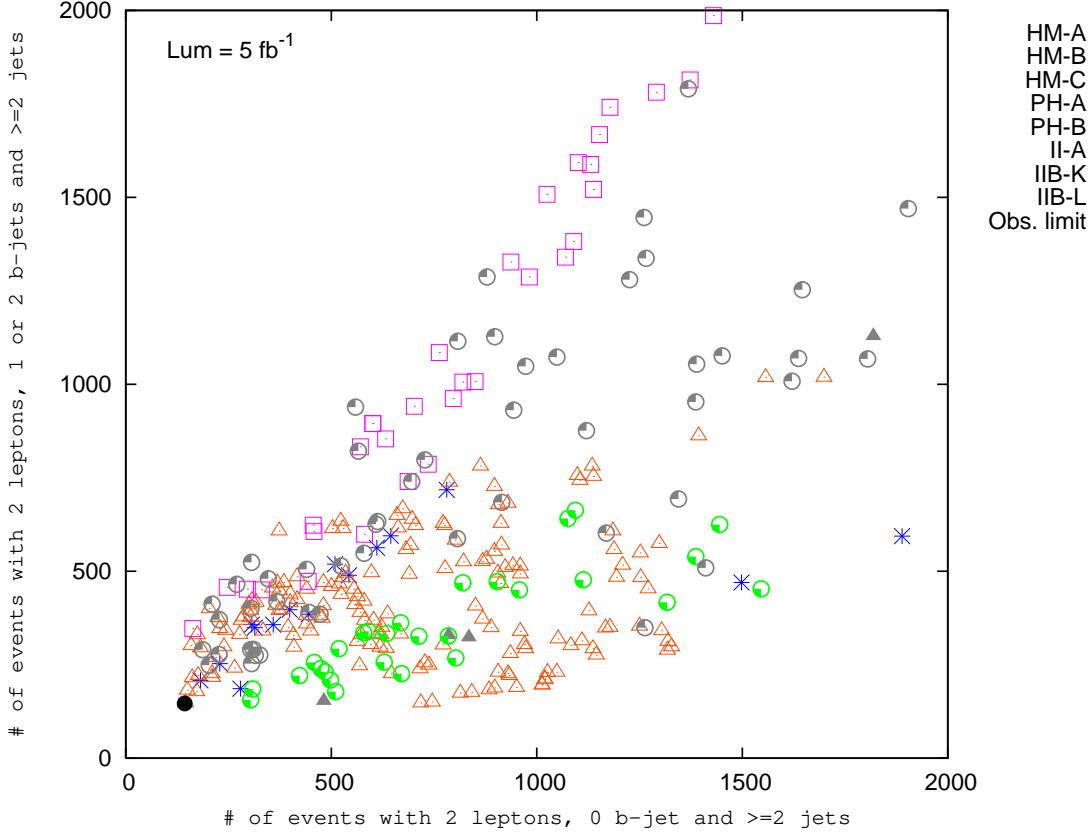


Figure 5.5: Plot of number of events with 2 leptons, 0 b jets and ≥ 2 jets and number of events with 2 leptons, 1 or 2 b jets and ≥ 2 jets. The black dot represents the lower limit of observability of the two signatures, according to conditions in equation (5.1). The models below the observable limit have not been shown. Note that the PH-B and II-A constructions can be distinguished from each other since the former is not observable while the latter is observable. One can also partially distinguish the PH-A and IIB-L constructions. The plots are best seen in color.

When the gluino is light (≤ 550 GeV), the PH-B construction has wino LSP. Since μ is large (> 1.3 TeV), $m_{\tilde{C}_1} \sim m_{\tilde{N}_1}$. Since \tilde{C}_1 and \tilde{N}_1 are wino and \tilde{N}_2 is bino, the gluino decays mostly to non b jets. Also, the leptons and jets coming from the decay of \tilde{C}_1 to \tilde{N}_1 are very soft and do not pass the cuts. When the gluino directly decays to \tilde{N}_1 , there are no leptons and only two jets. When the gluino is heavier (> 550 GeV), the PH-B construction can have wino as well

as bino LSPs. Because of a heavier gluino, the overall cross-section goes down. For the wino LSP case, the same argument as above applies in addition to the small cross-section implying even fewer lepton events. For the bino LSP case, the gluino again decays mostly to non b jets as \tilde{C}_1 and \tilde{N}_2 are wino and \tilde{N}_1 is bino. Also, $m_{\tilde{C}_1} \sim m_{\tilde{N}_2}$ but at the same time $\Delta M_{\tilde{N}_2-\tilde{N}_1}$ and $\Delta M_{\tilde{C}_1-\tilde{N}_1}$ are quite small (≤ 20 GeV), leading to soft leptons and jets many of which don't pass the cuts. So the result is that PH-B models have very few events with leptons and/or b jets. Therefore, as seen from Figures 5.4 and 5.5, the PH-B construction does not give rise to observable events for signatures *D* and *E* in Table 5.3.

The PH-A construction is required to have bino, higgsino or mixed bino-higgsino LSP with very heavy scalar masses (≥ 2 TeV). Light gluinos (≤ 600 GeV) have bino LSP, while higgsino or mixed bino-higgsino LSPs have heavier gluinos (600 – 1200 GeV). \tilde{N}_2 and \tilde{C}_1 are also quite light (< 250 GeV).

For the bino LSP case, gluinos typically decay to \tilde{N}_1 , \tilde{N}_2 and \tilde{C}_1 and non b jets most of the time compared to b jets, as \tilde{N}_1 is bino and \tilde{N}_2 and \tilde{C}_1 are wino. The decays of \tilde{N}_2 and \tilde{C}_1 can give rise to leptons passing the cuts. In addition, direct production of \tilde{N}_2 and \tilde{C}_1 is also important as they are light. They can also give rise to 2 leptons, 0 b jets and ≥ 2 jets. Therefore, in this case, one has more events with (two) leptons and non b jets compared to those with (two) leptons and b jets. This can be seen clearly from Figure 5.5. The decays of \tilde{N}_2 and \tilde{C}_1 also give jets (as they decay through virtual Z and W). Since the gluino is light, the cross-section is quite big implying that there are also a fair number of events with 0 leptons, 1 or 2 b jets and ≥ 6 jets. However, the number of events with 2 leptons, 0 b jets and ≥ 2 jets is more than with 0 leptons, 1 or 2 b jets and ≥ 6 jets due to the dominant branching ratio of gluinos to non b jets. This can be seen from Figure 5.4.

For the higgsino LSP case, the gluino is comparatively heavier (600 – 1200 GeV), leading to a significant decrease in cross-section. Now \tilde{N}_1 , \tilde{N}_2 and \tilde{C}_1 are mostly higgsino, leading to a lot of production of b jets as the relevant coupling is proportional to the mass of the associated quark. The fact that \tilde{N}_1 , \tilde{N}_2 and \tilde{C}_1 are mostly higgsino also makes their masses quite close to each other, implying that leptons and jets produced from the decays of \tilde{N}_2 and \tilde{C}_1 to \tilde{N}_1 are very soft and do not pass the cuts. Thus, these models have very few events with leptons. Since the jets coming from the decays of \tilde{N}_2 and \tilde{C}_1 to \tilde{N}_1 are also very soft, the PH-A higgsino LSP models also have very few events with 0 leptons, 1 or 2 b jets and ≥ 6 jets. Therefore, these do not give rise to observable events for the signatures in Figures 5.4 and 5.5.

For the mixed bino-higgsino LSP case, the gluino is again quite heavy (600 – 1200 GeV), making the cross section much smaller compared to the bino LSP case. Since \tilde{N}_1 , \tilde{N}_2 and \tilde{C}_1 have a significant higgsino fraction, the gluinos again decay more to b jets compared to non b jets. The mass separation between $\{\tilde{N}_2, \tilde{N}_3, \tilde{C}_1\}$ and \tilde{N}_1 is such that the decays of \tilde{N}_2 and \tilde{C}_1 to \tilde{N}_1 produce leptons which typically pass the cuts and jets which only sometimes pass the cuts. Therefore, these PH-A models have few events with 2 leptons, 0 b jets and ≥ 2 jets. They give rise to events with 2 leptons, 1 or 2 b jets and ≥ 2 jets but since the overall cross-section is much smaller than for the bino LSP case, the number of events for the above signature for these PH-A models is just a little above the observable limit, as can be seen from Figure 5.5. This is the origin of the “Both” entry for signature D in the row for the PH-A construction. Because of the small overall cross-section as well as the fact that jets produced from the decays of \tilde{N}_2 and \tilde{C}_1 only sometimes pass the cuts, the number of events for 0 leptons, 1 or 2 b jets and ≥ 6 jets is also small for these PH-A models, as seen from Figure 5.4.

The IIB-L construction always has a mixed bino-higgsino LSP, for both light and heavy gluino models. The light gluino IIB-L models have a large overall cross-section. The gluinos decay both to non b jets and b jets owing to the mixed bino-higgsino nature of the LSP. Also, the mass separation between \tilde{N}_2 , \tilde{C}_1 and \tilde{N}_1 is not large which means that the leptons produced from the decays of \tilde{N}_2 and \tilde{C}_1 pass the cuts but the jets produced seldom pass the cuts. So, the IIB-L construction has many events with 2 leptons, 0 b jets and ≥ 2 jets as well as with 2 leptons 1, or 2 b jets and ≥ 2 jets but not as many with 0 leptons, 1 or 2 b jets and ≥ 6 jets, as seen from Figures 5.4 and 5.5.

From Figure 5.5, one sees that the IIB-L construction can be distinguished *partially* from the PH-A construction, leading to a “Probably Yes (PY)” in the pattern table. One can understand it as follows - as mentioned above, the IIB-L construction always has a mixed bino-higgsino LSP while the PH-A construction has a mixed bino higgsino LSP only when the gluino is heavy (i.e. for a heavy spectrum). For light gluino models, as mentioned before, the PH-A construction has a bino LSP. Therefore, *for light gluino models*, the ratio of number of events with 2 leptons, 1 or 2 b jets and ≥ 2 jets and number of events with 2 leptons 0 b jets and ≥ 2 jets is much more for the IIB-L construction compared to the PH-A construction. These are the models which differentiate the IIB-L and PH-A constructions in Figure 5.5. It turns out that mixed bino-higgsino LSP models with heavy gluinos in both constructions have very similar spectra²⁰, leading to very similar signatures in all studied channels. Therefore, the IIB-L construction and the PH-A construction are not distinguishable in this special region of spectrum and signature space with the present set of signatures. Using more sophisticated signatures may help distinguish these signatures more cleanly. As already mentioned before,

²⁰This has been explicitly checked.

the PH-A construction also has models with a pure higgsino LSP. Those models have very heavy gluinos however, leading to no observable events in Figures 5.4 and 5.5.

Moving on to the II-A construction, we note that it can have a bino, wino, higgsino or mixed bino-higgsino LSP with light to moderately heavy gluino (300 – 600 GeV) and moderately heavier scalars (stops can be specially light). The spectrum and signature pattern are quite complicated. Let's analyze all possible cases.

In this construction, the branching ratio of gluinos to $\tilde{C}_1 + \text{jets}$ is the largest as mentioned before, since $\tan\beta \geq 20$. For the wino LSP case, since $M_{\tilde{C}_1} \sim M_{\tilde{N}_1}$ the leptons and jets from the decays of \tilde{C}_1 to \tilde{N}_1 are very soft and do not pass the cuts. The decay of the gluino to \tilde{C}_1 is accompanied by non b jets since \tilde{N}_1 and \tilde{C}_1 are wino and \tilde{N}_2 is bino. So, the II-A models with wino LSP do not give rise to observable events with leptons and/or b jets. This implies that the signatures in Figures 5.4 and 5.5 are not observable for these II-A models.

For the bino LSP case, \tilde{N}_2 and \tilde{C}_1 are quite heavy (> 350 GeV), sometimes being even heavier than the gluino, in which case only the decay of gluino to \tilde{N}_1 is allowed leading to no leptons. Even when the decays of gluino to \tilde{C}_1 and \tilde{N}_2 are allowed, they are mostly accompanied by comparatively soft non b jets (due to kinematic reasons). Since these II-A models are required to have \tilde{N}_2 and \tilde{C}_1 much heavier than the PH-A bino LSP models, the direct production of \tilde{N}_2 and \tilde{C}_1 which could be a source of events with 2 leptons, 0 b jets and ≥ 2 jets, is also relatively suppressed. Therefore these models do not give rise to observable events with 2 leptons 0 b jets and ≥ 2 jets as well as with 2 leptons, 1 or 2 b jets and ≥ 2 jets. However, there are some bino LSP II-A models which also have light squarks (stops mostly) and light gluinos in addition to having heavy \tilde{N}_2 and \tilde{C}_1 as above. For these bino LSP models, $\tilde{q}\tilde{q}$ pair production is quite important. These squarks mostly decay to a gluino and quarks, followed by

the decay of the gluino to mostly the LSP and jets (both b and non b jets). Thus, these bino LSP II-A models have many events with 0 leptons, 1 or 2 b jets and ≥ 6 jets but no observable events with 2 leptons, 1 or 2 b jets and ≥ 2 jets.

For the higgsino LSP case, since $\tan\beta \geq 20$, the gluino mostly decays to $\tilde{C}_1 + \text{b jets}$ as the associated coupling is proportional to the mass of the relevant quark. Also, in this case \tilde{N}_1 , \tilde{N}_2 and \tilde{C}_1 are all higgsino like and very close to each other. So, leptons from the decays of \tilde{N}_2 and \tilde{C}_1 to \tilde{N}_1 are very soft and do not pass the cuts. Therefore II-A models with higgsino LSP do not give rise to observable events with leptons and/or non b jets. For some of these higgsino LSP II-A models, there are still a fair number of events with 0 leptons 1 or 2 b jets and ≥ 6 jets. This is because even though $\tilde{q}\tilde{q}$ pair production is less important compared to those in bino LSP II-A models, the branching ratio of gluinos to b jets is much bigger (due to a higgsino LSP).

For the mixed bino-higgsino LSP case, the decay of gluino to $\tilde{C}_1 + \text{b jets}$ is dominant since \tilde{C}_1 is mostly higgsino. The next important decays are to \tilde{N}_1 , \tilde{N}_2 and $\tilde{N}_3 + \text{b jets}$ followed by a small fraction to non b jets. The mass separation between $\{\tilde{N}_2, \tilde{N}_3, \tilde{C}_1\}$ and \tilde{N}_1 is such that leptons produced can easily pass the cuts, while the jets produced sometimes pass the cuts. Some of these mixed bino-higgsino LSP II-A models also have comparatively light squarks, implying that $\tilde{q}\tilde{q}$ and $\tilde{q}\tilde{g}$ production are also important. The squark decays to a quark and a gluino, followed by the usual decays of the gluino. For these models, \tilde{N}_2 and \tilde{C}_1 are also light, implying that in such cases direct production of \tilde{N}_2 and \tilde{C}_1 is also possible. The decays of \tilde{N}_2 and \tilde{C}_1 can give rise to events with 2 leptons, 0 b jets and ≥ 2 jets.

Therefore, the conclusion is that for II-A models with mixed bino-higgsino LSP and light squarks, there are observable events with 2 leptons, 1 or 2 b jets and ≥ 2 jets; with 0 leptons,

1 or 2 b jets and ≥ 6 jets as well as with 2 leptons 0 b jets and ≥ 2 jets. The number of events with 2 leptons, 1 or 2 b jets and ≥ 2 jets is greater than those with 2 leptons, 0 b jets and ≥ 2 jets because of the dominant branching fraction of gluinos to b jets. Therefore, signature D (ratio of the above two type of events - Figure 5.5) can distinguish the II-A and PH-B constructions as the II-A construction has observable events while the PH-B construction does not give rise to observable events. The number of events for 0 leptons 1 or 2 b jets and ≥ 6 jets will be larger than those with 2 leptons, 0 b jets and ≥ 2 jets, again due to the dominant branching ratio of the gluino to b jets. So, signature C (ratio of the above two type of events - Figure 5.4) can distinguish the PH-A, IIB-K and IIB-L constructions from the II-A and PH-B constructions. The above results can be seen from Figures 5.4 and 5.5, where the qualitative difference between the constructions is clear. The II-A models shown above the observable limit have mixed bino-higgsino LSP with lighter squarks than in other II-A cases.

We are now left with explaining the distinguishability of the PH-A and IIB-L constructions on the one hand and the IIB-K construction on the other. Figures 5.6 and 5.7 show that the IIB-K construction can be distinguished from the PH-A and IIB-L constructions. The reason is as follows - As explained earlier, the IIB-K construction can have a light spectrum with light gluinos, light stop and sometimes a light stau. So, $\tilde{g}\tilde{q}$ production is typically dominant. Since up-type squarks are produced preferentially at the LHC (as it is a pp collider), they decay preferentially to a positive chargino \tilde{C}_1^+ , which in turn decays preferentially to a positively charged lepton l^+ (in its leptonic decays). Therefore, the asymmetry in number of events with a single electron or muon and ≥ 2 jets ($A_c^{(1)}$)²¹ is much greater than in the case of PH-A and

²¹ $A_c^{(1)} \equiv \frac{N(l^+) - N(l^-)}{N(l^+) + N(l^-)}$, where for example $N(l^+)$ is the number of events with a single positively charged electron or muon and ≥ 2 jets.

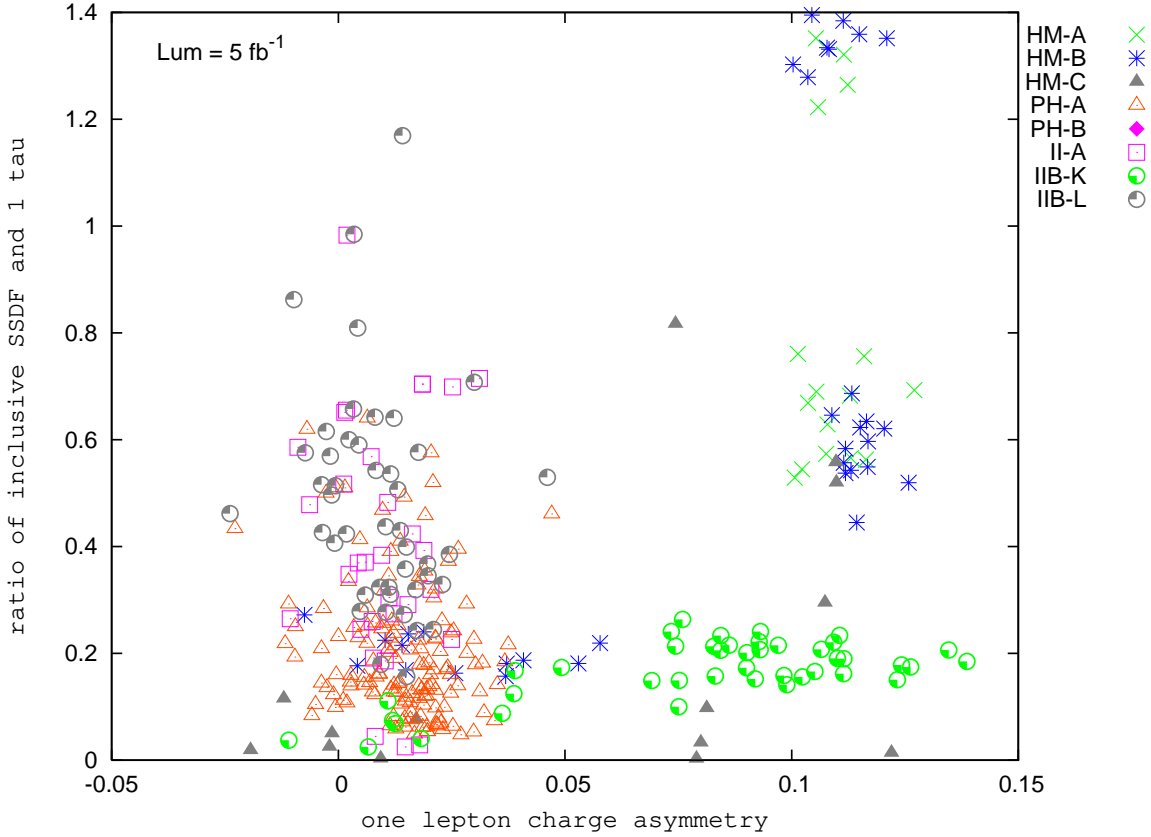


Figure 5.6: Plot of the charge asymmetry in events with a single electron or muon & ≥ 2 jets & the ratio of number of events with same sign different flavor (SSDF) dileptons and ≥ 2 jets and number of events with 1 tau and ≥ 2 jets. The models which are below the observable limit as defined by (5.1) are not shown. Note that the IIB-K construction can be distinguished from the PH-A and IIB-L constructions, as the former occupies a mostly horizontal region while the latter occupy a mostly vertical region. The overlapping IIB-K and PH-A models can be distinguished from Figure 5.7. The plots are best seen in color.

IIB-L constructions where $\tilde{g}\tilde{g}$ pair production is dominant. There are a few IIB-K models which have a small $A_e^{(1)}$ and which overlap with some PH-A models (seen in Figure 5.6) even though $\tilde{g}\tilde{g}$ production is dominant. This is due to some special features of their spectrum, such as the lightest stop and/or the lightest stau being very light. These features either suppress the

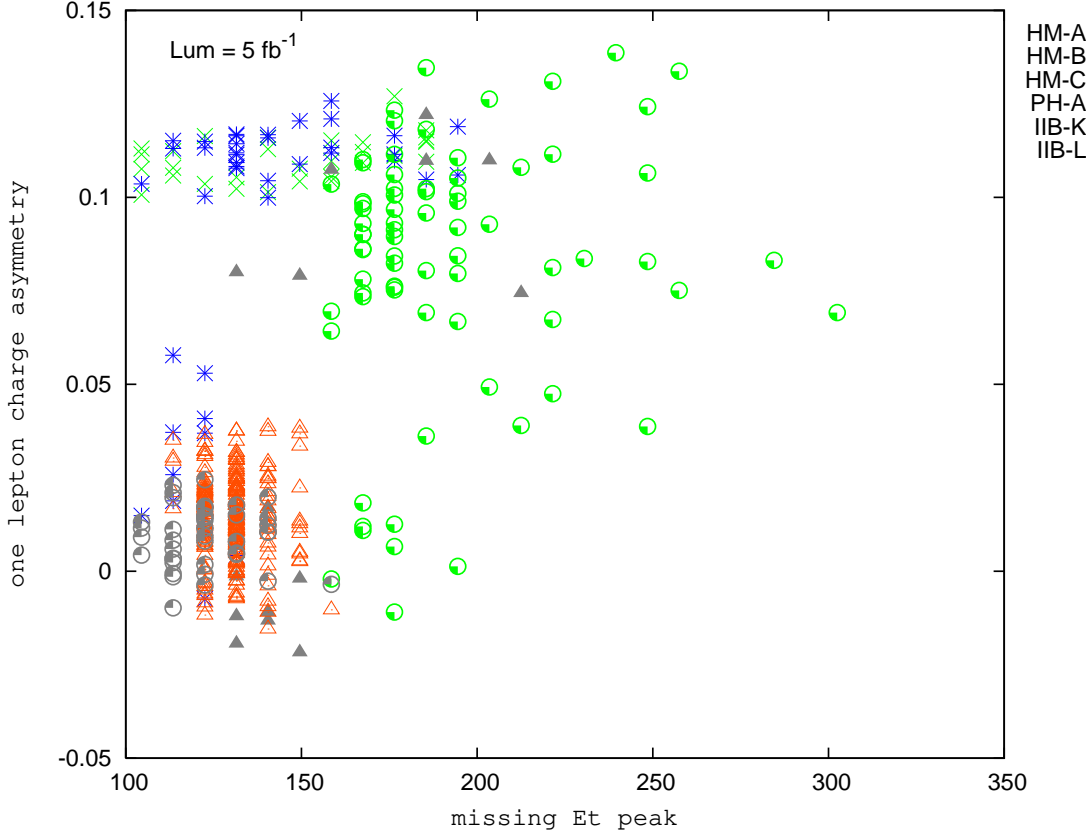


Figure 5.7: Plot of the peak of the \cancel{E}_T distribution and the charge asymmetry in events with a single electron or muon & ≥ 2 jets. The models which are below the observable limit as defined by (5.1) are not shown. Note that this plot distinguishes the overlapping PH-A and IIB-K models in Figure 5.6. The plots are best seen in color.

production of \tilde{C}_1^+ or suppress the decay of \tilde{C}_1^+ to electrons or muons. However, as seen from Figure 5.7, these overlapping IIB-K models can be distinguished from the PH-A and IIB-L constructions by the peak of the \cancel{E}_T distribution. This is related to the mass of the LSP. The IIB-K constructions (which are observable with $5 fb^{-1}$) have a comparatively heavier LSP than the IIB-L constructions in general, making the peak of the \cancel{E}_T distribution larger than those for

the IIB-L constructions²². The PH-A models which overlap with the small $A_c^{(1)}$ IIB-K models have bino LSPs which are lighter than that of the IIB-K models. So, the PH-A models have a smaller \not{E}_T peak than the overlapping IIB-K models in Figure 5.6, as can be seen from Figure 5.7.

We have thus explained the distinguishability of all constructions based on the spectrum at the low scale. Typically, there are more than one (sometimes many) signatures which can distinguish any two given constructions. This redundancy gives us confidence that our analysis is robust and that the conclusions will not be affected with more sophisticated analysis. For simplicity, we have only explained one signature distinguishing a pair of constructions but all such signatures can be understood similarly.

5.4.4 Explanation of Spectrum from the Soft Parameters

We now turn to understanding the origin of the spectrum of particles at the low scale (which are responsible for the signature pattern) for the constructions in terms of pattern of soft parameters. For illustrative purposes, we carry out this exercise for two constructions – the HM-A construction and the PH-B construction. If we take the soft parameters at the string (or unification) scale as given, then it does not matter that these are really only toy constructions. The kind of analysis carried out for these constructions below can also be carried out for more well motivated constructions such as the KKLT and Large Volume ones, as well. However, to go to the final step, i.e. from the soft parameters to the structure of the underlying theoretical construction, it makes sense to stick to the more well motivated constructions – the KKLT and Large Volume constructions, as we will in the following subsection.

²²This is because the IIB-K models with a light spectrum have the lightest stop correlated with the mass of the LSP ($m_{\tilde{t}_1} \geq m_{\tilde{N}_1}$) [118]; \tilde{t}_1 cannot be too light, else it would be directly seen at the Tevatron.

Starting with the HM-A construction, one would like to understand its characteristic spectrum, viz. $m_{\tilde{g}} \sim m_{\tilde{q}} > m_{\tilde{l}}$. Why does the gluino mass lie in the range 550 – 650 GeV? We note that the HM-A construction is a heterotic M theory construction compactified on a Calabi-Yau with only one Kähler modulus. This implies that the soft terms obtained at the unification scale are universal [130]. Thus, the soft terms obtained at the unification scale are a special case of the well studied mSUGRA boundary condition. Now, phenomenological studies of the mSUGRA boundary condition have shown that in order to get a small relic density (satisfying the WMAP upper bound ²³), there are three allowed regions in the $m - M$ plane [131] ²⁴. Here m stands for the universal scalar mass parameter while M stands for the universal gaugino mass parameter. These three regions are the following:

- The stau coannihilation region – In this region, the stau is almost degenerate with the LSP which is a bino. One gets an acceptable relic density because of coannihilation of the stau and the LSP to a tau. This requires $m < M$ with m roughly between 100 and 150 GeV and M roughly between 150 and 300 GeV (assuming $A_0 = 0$).
- The focus point region – This region requires a large scalar mass parameter ($m > M$) at the unification scale, and gives rise to a higgsino LSP with acceptable relic density.
- The funnel region – In this region, the LSP is annihilated by a s -channel pole, with $m_{LSP} \approx m_A/2$. This also requires $m > M$.

In the case of the HM-A construction, the soft mass parameters always have the hierarchy $M > m$ [130], which implies that only the stau coannihilation region is possible for the HM-A

²³Typically, a lower bound on the relic density is also imposed. However, we have only used the upper bound in our analysis, as explained in section 5.3. The area covered by the three regions can change depending on whether a lower bound is also imposed.

²⁴One usually assumes $A_0 = 0$ in these plots.

construction. Also, the allowed ranges for the m and M parameters roughly explains the mass scale of the gluino and squarks at the low scale from standard RG evolution. Therefore, one has to now understand the origin of the allowed values of the m and M parameters from the nature of the expressions for soft terms and the “theory” input parameters.

The expressions for the soft terms depend on three input parameters – the goldstino angle θ , the gravitino mass $m_{3/2}$ and the parameter $\alpha(t+\bar{t})$ with t as the Kähler modulus, in addition to $\tan\beta$. For further details, the reader is referred to [130]. The expressions for the soft parameters are given by :

$$\begin{aligned}
M &= \frac{\sqrt{3}Cm_{3/2}}{(s+\bar{s})+\alpha(t+\bar{t})} \left\{ (s+\bar{s})\sin(\theta)e^{-i\gamma_s} + \frac{\alpha(t+\bar{t})}{\sqrt{3}}\cos(\theta)e^{-i\gamma_t} \right\} \quad (5.2) \\
m^2 &= V_0 + m_{3/2}^2 - \frac{3m_{3/2}^2C^2}{3(s+\bar{s})+\alpha(t+\bar{t})} \left\{ \alpha(t+\bar{t}) \left(2 - \frac{\alpha(t+\bar{t})}{3(s+\bar{s})+\alpha(t+\bar{t})} \right) \sin^2(\theta) + \right. \\
&\quad \left. (s+\bar{s}) \left(2 - \frac{3(s+\bar{s})}{3(s+\bar{s})+\alpha(t+\bar{t})} \right) \cos^2(\theta) - \right. \\
&\quad \left. \frac{2\sqrt{3}\alpha(t+\bar{t})(s+\bar{s})}{3(s+\bar{s})+\alpha(t+\bar{t})} \sin(\theta)\cos(\theta)\cos(\gamma_s-\gamma_t) \right\} \\
A &= \sqrt{3}Cm_{3/2} \left\{ -1 + \frac{3\alpha(t+\bar{t})}{3(s+\bar{s})+\alpha(t+\bar{t})} \sin(\theta)e^{-i\gamma_s} + \right. \\
&\quad \left. \sqrt{3} \left(-1 + \frac{3(s+\bar{s})}{3(s+\bar{s})+\alpha(t+\bar{t})} \right) \cos(\theta)e^{-i\gamma_t} \right\}
\end{aligned}$$

where we are using the following parameterization, which define F terms for the moduli [66]:

$$\begin{aligned}
F^s &= \sqrt{3}m_{3/2}C(s+\bar{s})\sin(\theta)e^{-i\gamma_s} \quad (5.3) \\
F^t &= m_{3/2}C(t+\bar{t})\cos(\theta)e^{-i\gamma_t} \\
C^2 &= 1 + \frac{V_0}{3m_{3/2}^2}
\end{aligned}$$

The ratio of the scalar to the gaugino mass parameter $r \equiv m/|M|$ is shown in the first plot in Figure 5.8 as a function of the goldstino angle θ . For the stau coannihilation region, the ratio

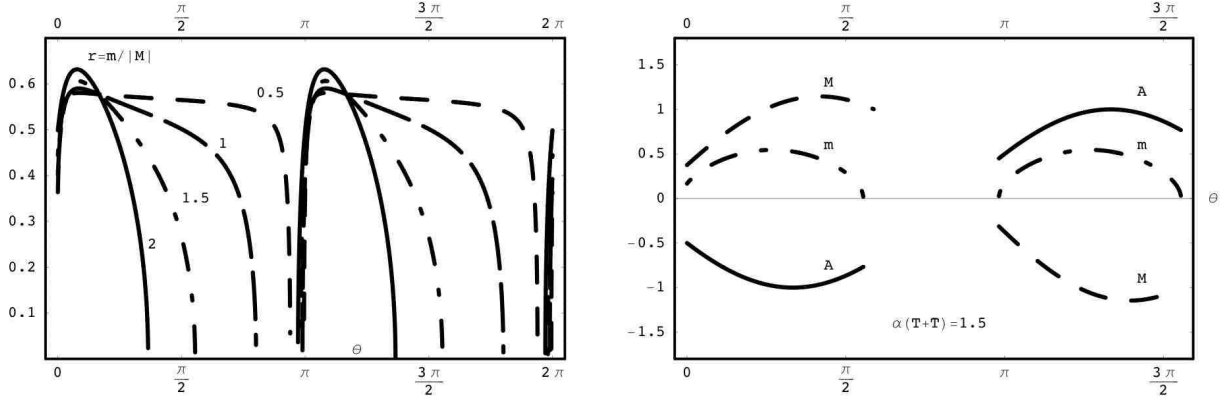


Figure 5.8: Left : The ratio $r \equiv m/|M|$ as a function of θ for four different values of $\alpha(T + \bar{T})$ represented by various curves. Right: The universal soft parameters as a function of θ for $\alpha(T + \bar{T}) = 1.5$. The solid curve stands for trilinears, dotted dashed curve for scalars and dashed curve for gauginos.

r has to be roughly $0.5 - 0.6$. We see that for this value of r , one set of allowed values of θ lie near $0, \pi, 2\pi$ for all allowed values of $\alpha(T + \bar{T})$. This means that the supersymmetry breaking is moduli dominated ($F_s \approx 0$). In addition, there also exist other values of θ which are closer to $(\frac{1}{2}\pi, \frac{3}{2}\pi)$ rather than to $(0, \pi, 2\pi)$. However, these values are ruled out by constraints on low energy phenomenology, as the trilinear parameter A_0 for these values is pretty large, as seen from the second plot in Figure 5.8. This is because a very large value of the trilinear parameter makes the scalar mass squared run negative at the low scale and also causes problems for EWSB. Once the correct ratio r of the gaugino mass parameter to the scalar mass parameter is obtained, one can get their correct absolute scales by tuning $m_{3/2}$ as all the soft parameters are proportional to them. One thus gets a gluino in the $550 - 650$ GeV range. The allowed values of $m_{3/2}$ lie in the TeV range.

Moving on to the PH-B construction, one would again like to understand the origin of

the characteristic features of its spectrum, viz. heavy squarks (≥ 1 TeV), moderately heavy sleptons except the stau which is considerably lighter, and gluinos which can vary from being light (250 – 450 GeV) to heavy (≥ 1000 GeV). Light gluinos (< 450 GeV) in this construction *always* give rise to a wino LSP while the heavier ones give rise to bino or wino LSPs, as we explain below.

The PH-B construction is a weakly coupled heterotic string construction with a tree level Kähler potential and two gaugino condensates. The soft terms for this construction depend on the “theory” input parameters – the gravitino mass $m_{3/2}$, the Green-Schwarz coefficient δ_{GS} and the *vev* of the Kähler modulus t , in addition to $\tan\beta$. In these kind of constructions, it was further noted that a minimum with $F_s = 0$ and $F_t \neq 0$ is preferred with t being stabilized at values slightly greater than 1. For details, refer to [132]. The result is that all soft terms are zero at tree level. The expressions for the soft parameters are approximately given by [133]:

$$\begin{aligned}
 M_a &\approx \frac{g_a^2}{2} \left[\left(2 \frac{\delta_{GS}}{16\pi^2} + b_a \right) G_2(t, \bar{t}) + 2b_a m_{3/2} \right]; & G_2(t, \bar{t}) &\equiv \left(2\zeta(t) + \frac{1}{t + \bar{t}} \right) & (5.4) \\
 m_i^2 &\approx \gamma_i m_{3/2}^2 \\
 A_{ijk} &\approx m_{3/2} (\gamma_i + \gamma_j + \gamma_k)
 \end{aligned}$$

where $\zeta(t)$ is the Riemann zeta function. The dominant contribution to the soft scalar mass parameters is proportional to the gravitino mass with the proportionality constant being the anomalous dimension of the respective fields (γ_i). Since the anomalous dimension of the quarks is bigger than that of the leptons, the squarks turn out to be heavier than the sleptons. Also, the anomalous dimension of the stau ($\tilde{\tau}$) is the smallest (smaller by a factor of about 3 compared to that for \tilde{Q}_3), leading to the stau as the lightest slepton. To get the absolute scale correct, one has to realize that soft terms in this case arise from one loop contributions. Thus, they are

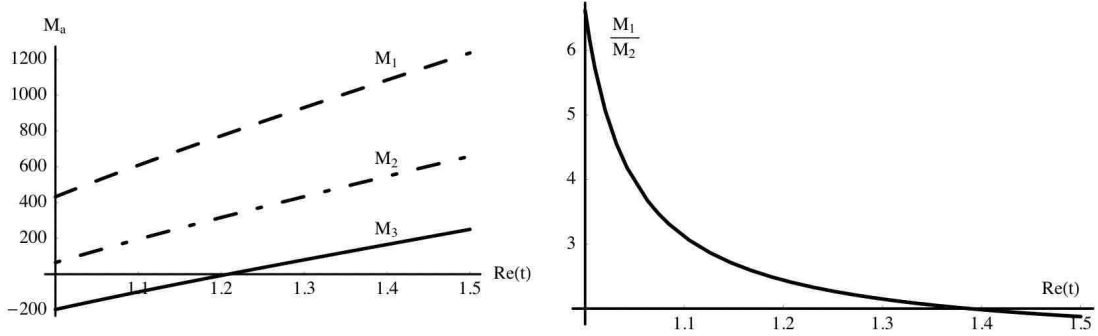


Figure 5.9: Left : Plots for gaugino mass parameters as a function of $Re(t)$: The solid curve stands for M_3 , dotted-dashed for M_2 and dashed for M_1 . Right : The ratio M_1/M_2 as a function of $Re(t)$. $Re(t)$ varies from 1 to 1.5. The plots are shown for a given value of δ_{GS} and $m_{3/2}$. δ_{GS} is -15 and $m_{3/2}$ is 20 TeV.

suppressed and therefore need a much heavier $m_{3/2}$ (~ 20 TeV) in order to evade the chargino, neutralino and higgs mass lower bounds. This is the reason for the heavy squarks, moderately heavy sleptons and a light stau at the low scale.

For the gaugino sector, it is instructive to look at the plots of the variation of gaugino mass parameters as a function of $Re(t)$ and the ratio of bino and wino mass parameter ($\frac{M_1}{M_2}$) as functions of $Re(t)$ for a given value of δ_{GS} and $m_{3/2}$. Choosing different values of δ_{GS} does not change the qualitative feature of the plots. Since all gaugino mass parameters are proportional to $m_{3/2}$, changing $m_{3/2}$ changes the overall scale of all gaugino mass parameters. We first explain why light gluinos give rise to a wino LSP while heavier ones to a bino LSP for a fixed $m_{3/2}$. We then consider the effects of changing $m_{3/2}$. The first plot in Figure 5.9 shows that the gluino mass parameter is the smallest of the three (taking the sign into account) at the unification scale. This arises from the fact that the combination $(G_2(t, \bar{t}) + 2m_{3/2})$ in (5.4) is negative and the one loop beta function coefficient b_3 is the largest for M_3 [133]. From the

second plot, we see that ratio $\frac{M_1}{M_2}$ is greater than 2 for $\text{Re}(t)$ smaller than a certain value, which is around 1.4 for the value of δ_{GS} chosen in the figure. Since we roughly have :

$$M_{1_{low}} \approx 0.45 M_{1_{unif}}; \quad M_{2_{low}} \approx 0.9 M_{2_{unif}}, \quad (5.5)$$

it implies that if the ratio $\frac{M_{1_{unif}}}{M_{2_{unif}}}$ is greater than 2, we have $M_{1_{low}} > M_{2_{low}}$, leading to a wino LSP. Therefore for $\text{Re}(t)$ smaller than a certain value (1.4 in the figure), one obtains a wino LSP while for greater values of $\text{Re}(t)$ one obtains a bino LSP. From the first plot, one now sees that for values of $\text{Re}(t)$ smaller than the critical value, the gluino mass is quite small at the unification scale. Thus for a given $m_{3/2}$, PH-B models with small gluino masses have wino LSPs while those with heavy gluinos have bino LSPs. If we now change the gravitino mass, we change the overall scale of the gaugino mass parameters. Since the scalars are also proportional to $m_{3/2}$, it is not possible to make $m_{3/2}$ very small as the higgs mass bound will be violated. But one can have a large gravitino mass giving rise to a large gluino mass, with both wino and bino LSPs. Bino LSP models however have heavier gluino masses than those with wino LSP as M_3 is bigger for the bino LSP models, as explained above. One also finds that for $\text{Re}(t)$ around a particular value (1.2 in the above figure), the gluino mass almost vanishes leading to a gluino LSP at the low scale, which is not considered in our analysis. Therefore that region in $\text{Re}(t)$ is not allowed. Another region which is not allowed by low energy constraints is the region near $\text{Re}(t)=1$, where M_2 becomes very small, leading to incompatibilities with the lightest chargino and LSP bounds.

5.4.5 Explanation of Soft Parameters from the Underlying Theoretical Construction

One finally needs to explain the structure of soft terms (which explains the spectrum pattern and hence the signature pattern) from the structure of the underlying theoretical construction. This would complete the sequence of steps to go from LHC signatures to string theory. As explained before, we carry out this exercise for the KKLT and Large Volume constructions, since they are well defined from a microscopic point of view, and have a reasonably well understood mechanism of supersymmetry breaking and moduli stabilization.

Both of the constructions have complex structure moduli and dilaton stabilized by turning on generic fluxes. The Kähler moduli are stabilized by including non-perturbative corrections to the superpotential. In Large Volume (IIB-L) vacua, a certain kind of α' correction is also taken into account in the scalar potential unlike that in the KKLT (IIB-K) vacua. In type IIB-K constructions, the flux superpotential has to be fine-tuned so as to give a small (\sim TeV) gravitino mass. For the IIB-L construction however, no fine-tuning of the flux superpotential is required. This gives rise to a relatively low (intermediate scale) string scale if one wants a small gravitino mass.

The common feature of these two constructions is that the Kähler moduli are stabilized mostly by non-perturbative corrections. This leads to a particular feature in the gaugino sector. It was shown in [90] that the gaugino masses are suppressed relative to the gravitino mass ($\sim m_{3/2}/\ln(m_{pl}/m_{3/2})$) in all type IIB vacua with matter residing on stacks of D7-branes and with all Kähler moduli stabilized mostly by non-perturbative corrections to the superpotential.

For the IIB-K constructions studied mostly in the literature, there is only one overall Kähler modulus, the F-term of which is suppressed. Since both the scalar masses and trilinear terms

are proportional to this F-term, they are both suppressed relative to the gravitino in the IIB-K construction [118]. Anomaly mediated contributions to soft terms have to be added as they are comparable with those at tree level, leading to mixed modulus-anomaly soft supersymmetry breaking terms. The above feature survives for cases with more Kähler moduli, if all of them are stabilized mostly by non-perturbative effects [134]. On the other hand, the IIB-L constructions require the presence of a large volume limit – this means that the Calabi-Yau manifold must have at least two Kähler moduli- one of which is small (T_s) and the other is big (T_b)[22]. The presence of the perturbative α' correction in the Kähler potential gives a contribution to the scalar potential of the same order as the non-perturbative corrections for the “big” Kähler modulus, in contrast to that in the IIB-K construction. The F-term of the small Kähler modulus (F_s) is suppressed by $\ln(m_{pl}/m_{3/2})$, while that of the big Kähler modulus (F_b) is not suppressed. Since only D7-branes wrapping the small 4-cycle (represented by the small modulus) give a reasonable gauge coupling, the visible sector gaugino masses are proportional to F_s and are suppressed relative to $m_{3/2}$. However both F_s and F_b enter into the expression for scalar masses and trilinear terms. Since F_b is not suppressed, therefore for the IIB-L construction, only the gaugino sector has mixed modulus-anomaly terms, with the scalars and trilinears generically of the same order as the gravitino mass. This characteristic feature is also true for Calabi-Yaus with more Kähler moduli provided they admit a large volume limit, though the explicit soft terms are hard to obtain. Another difference between the IIB-K and IIB-L constructions is that the soft terms for the IIB-K construction are first computed at the unification scale ($\sim 10^{16}$ GeV) while those for the IIB-L construction are computed at the intermediate string scale ($\sim 10^{11}$ GeV).

The above analysis thus explains the origin of the pattern of soft parameters in terms of

the structure of the underlying theoretical construction for the two constructions which leads to a distinguishable signature pattern at the LHC. The important thing to take home from this analysis is that different constructions lead to different effective actions and therefore to different expressions for the soft terms in terms of the underlying microscopic input parameters. In addition, the relations *among* the different soft parameters (M_a, m_i^2 & A_{ijk}) also change for different constructions. Therefore, a proper understanding of these relations and their implications for relevant features of the phenomenology is the key to relating high scale theory and data. In this sense, we think that the approach advocated here is likely to work even if one has much more realistic constructions from different parts of the M-theory amoeba which stabilize all the moduli, generate a stable hierarchy and also give a realistic spectrum and couplings.

5.5 Distinguishing Theories Qualitatively

In the previous section, we analyzed the eight constructions in great detail – in particular, we computed the LHC signatures of these constructions and understood the origin of these signatures from features of the theoretical constructions. It is worthwhile to ask whether one can abstract important lessons from this exercise so that one could use them to analyze other classes of constructions, and to draw qualitative reliable conclusions from data.

For example, one could try to first extract relevant phenomenological features of the effective beyond-the-Standard Model theory from data and then focus on classes of M theory vacua which give rise to those particular features. This alternative may also be more helpful to people who are interested primarily in understanding general features of beyond-the-Standard Model (BSM) physics from LHC data rather than connecting it to an underlying high scale theory like string

theory. From our studies, we find that a combination of features of any construction crucially determine the broad pattern of LHC signatures. For concreteness, we write our results in the framework of low-scale supersymmetry as BSM physics, similar results will hold true for other approaches as well. The important features we find²⁵ are:

- The universality (or not) of gaugino masses at the unification (or compactification) scale.
- If gauginos are non-universal - the origin of the non-universality, i.e. whether the non-universality is present at tree-level itself as opposed to arising mostly due to one-loop anomaly mediated contributions.
- If gauginos are non-universal - the hierarchy between M_1 , M_2 , M_3 and μ .
- The relative hierarchy between the scalars and gauginos at the string scale, i.e. whether the scalars are of the same order as the gauginos as opposed to being heavier or lighter than the gauginos.
- Nature and content of the LSP.
- Hierarchy among scalars at the string scale, particularly third family *vs* the first and second families.

Some comments are in order. These features are not always independent of each other. For example, the hierarchy between M_1 , M_2 and M_3 determines the nature of the LSP (combined with a knowledge of μ). Also, if tree-level gaugino masses are small so that non-universality arises only due to the anomaly mediated contributions, then the gauginos are typically suppressed relative to the scalars and the hierarchy between M_1 , M_2 and M_3 is fixed. Another

²⁵There could be more such features.

important fact which should be kept in mind is that a combination of all the features above gives rise to the observed *pattern* of LHC signatures, not just a particular one. Therefore, once one obtains data, the task boils down to figuring out the correct combination of “relevant features” which reproduces the data (at least roughly). Let’s explain this with two examples - the HM-A construction and the IIB-L construction. Since we are only concerned with relevant features of the effective BSM theory, all constructions considered can be treated equally.

The HM-A and overlapping HM-B and HM-C constructions have universal gaugino masses at the unification scale and have a bino LSP. They also have scalars of the same order as the gauginos at the unification scale, so RGE effects make the scalars (the third generation in particular) lighter than the gauginos at the low scale. This combination of “relevant features” determines the broad pattern of LHC signatures for these constructions. Since the gauginos are universal at the unification scale, the ratio of M_1 , M_2 and M_3 at the low scale is $1 : 2 : 7$, which controls the lower bound on the gluino mass and the LSP mass due to experimental constraints on the chargino mass. Also, since scalars are slightly lighter than gluinos at the low scale, both $\tilde{g}\tilde{q}$ and $\tilde{q}\tilde{q}$ pair production are comparable. The fact that the LSP is bino-like is also due to universal gaugino masses as well as the fact that the scalars are comparable to gauginos at the unification scale. A bino LSP can then reduce its relic density by stau coannihilation, which can only happen if the stau is light and almost degenerate with the LSP. All these factors give rise to a very specific set of signature pattern, as analyzed in section 5.4.3.

In contrast, the IIB-L construction has a different set of “relevant features” which determine its broad pattern of LHC signatures and also allow it to be distinguishable from the other constructions. The gaugino masses are non-universal at the string scale²⁶ and the scalars are

²⁶One does not have standard gauge unification at 2×10^{16} GeV in these models with $W_0 = O(1)$ [22].

heavier than the gauginos at the low scale²⁷. One also has a mixed bino-higgsino LSP in this case. Since the scalars are heavier than the gauginos, $\tilde{g}\tilde{g}$ pair production is the dominant production mechanism. Also, the only way to decrease the relic density of a bino-like LSP is to have a significant higgsino fraction as the stau (or stop) coannihilation channel is not open. Again, these features result in a very specific set of signature pattern, as analyzed in section 5.4.3.

We therefore see that the features mentioned above are crucial in determining the pattern of signatures at the LHC. Having said that, it is important to remember that these features only determine the broad pattern of LHC signatures and one needs more inputs to explain the entire signature pattern in detail.

5.6 Possible Limitations

One may raise questions about a few aspects of our analysis. The first concerns the sampling of the parameter space of each construction. One may worry that by only considering ~ 50 models (~ 100 for the PH-A construction)²⁸, the parameter space of each construction is sampled very sparsely and adding more models could qualitatively change the overall signature pattern of the constructions. We think however, that it is reasonable to expect that that is not true. This is because, as explained in the previous sections, we have outlined the origin of the pattern of signatures of the various constructions on the basis of their spectrum and in turn on the basis of their underlying theoretical setup. Since the dependence of the soft terms on the microscopic input parameters as well as relations between the soft terms are known and have been understood, we expect our results for the pattern table to be robust even when the parameter space is sampled more densely. This will be strictly true only if one understands

²⁷This implies that the scalars are also heavier than the gauginos at the string scale.

²⁸Not all 50(or 100) models simulated will be above the observable limit in general.

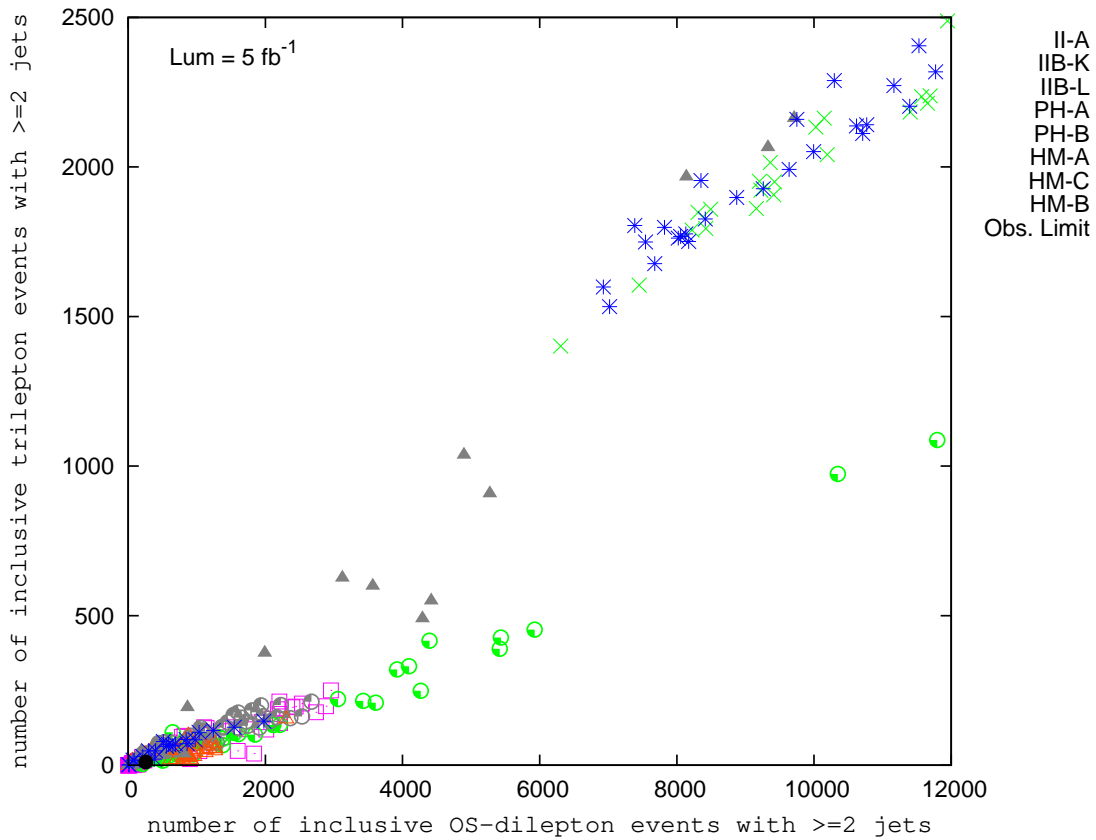


Figure 5.10: Plot of number of events with 1 lepton and ≥ 2 jets and number of events with opposite sign dileptons and ≥ 2 jets, each sampled with ~ 50 models, except PH-A (~ 100 models).

the theoretical construction well enough so that one has a “representative sample” of the entire parameter space of that construction. We expect this to be true for our constructions. In order to confirm our expectation, we simulated ~ 400 models for the PH-A construction and ~ 100 for the IIB-K construction and we found that the results obtained with ~ 100 (and ~ 50) models did not change when other models were added in our analysis. This can be seen from Figures 5.10 and 5.11 as well as Figures 5.12 and 5.13. The other signatures also do not change the final result. In the future, we plan to do a much more comprehensive analysis with a dense

sampling of the parameter space for all the other constructions.

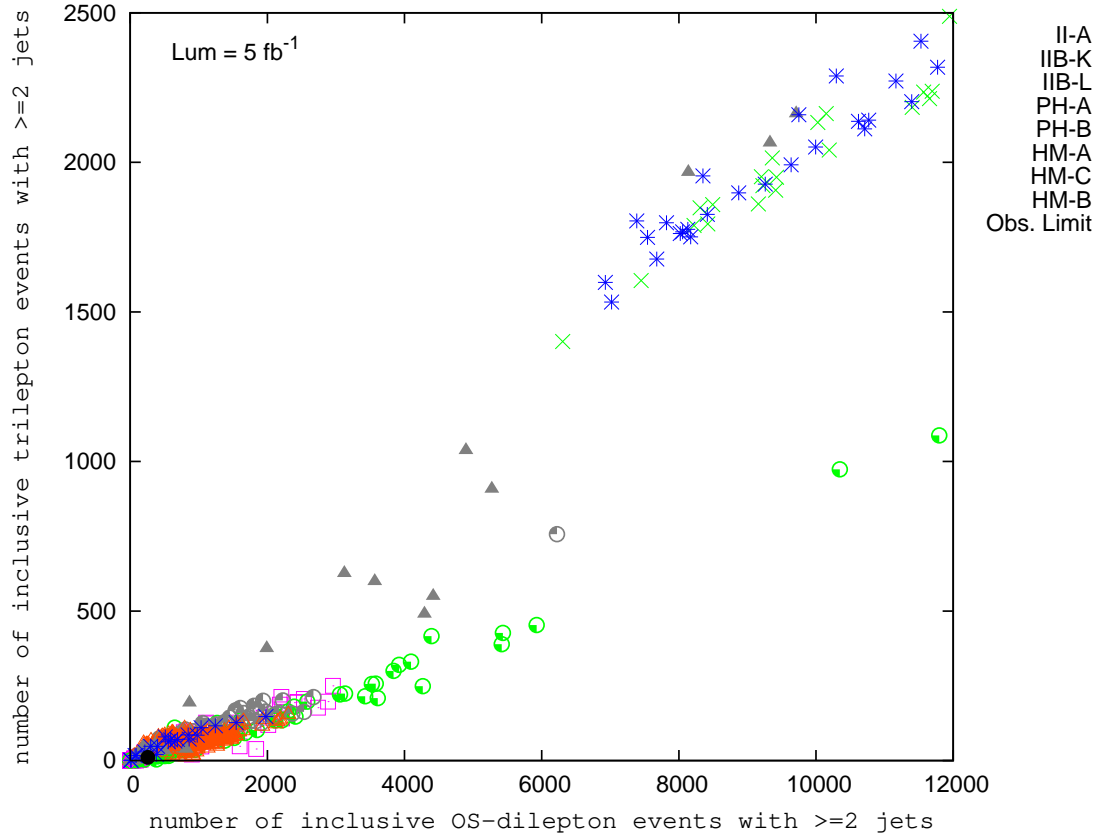


Figure 5.11: The same plot as in Figure 5.10, in which the IIB-K construction is sampled with ~ 100 models and the PH-A construction with ~ 400 models.

Another possible objection could be that the procedure of dividing a signature into two classes arbitrarily and distinguishing them on the basis of falling into one class or the other is too naive and may lead to misleading results arising from intrinsic statistical uncertainties and background uncertainties in the value of each signature and impreciseness of the boundary. While this is a valid concern in general, we think that this does not affect the main results of our analysis at this level. This can again be attributed to the fact that the pattern of signatures is understood on the basis of their underlying theoretical structure. We are also

encouraged as there are typically more than one (sometimes many) signatures distinguishing any two particular constructions.

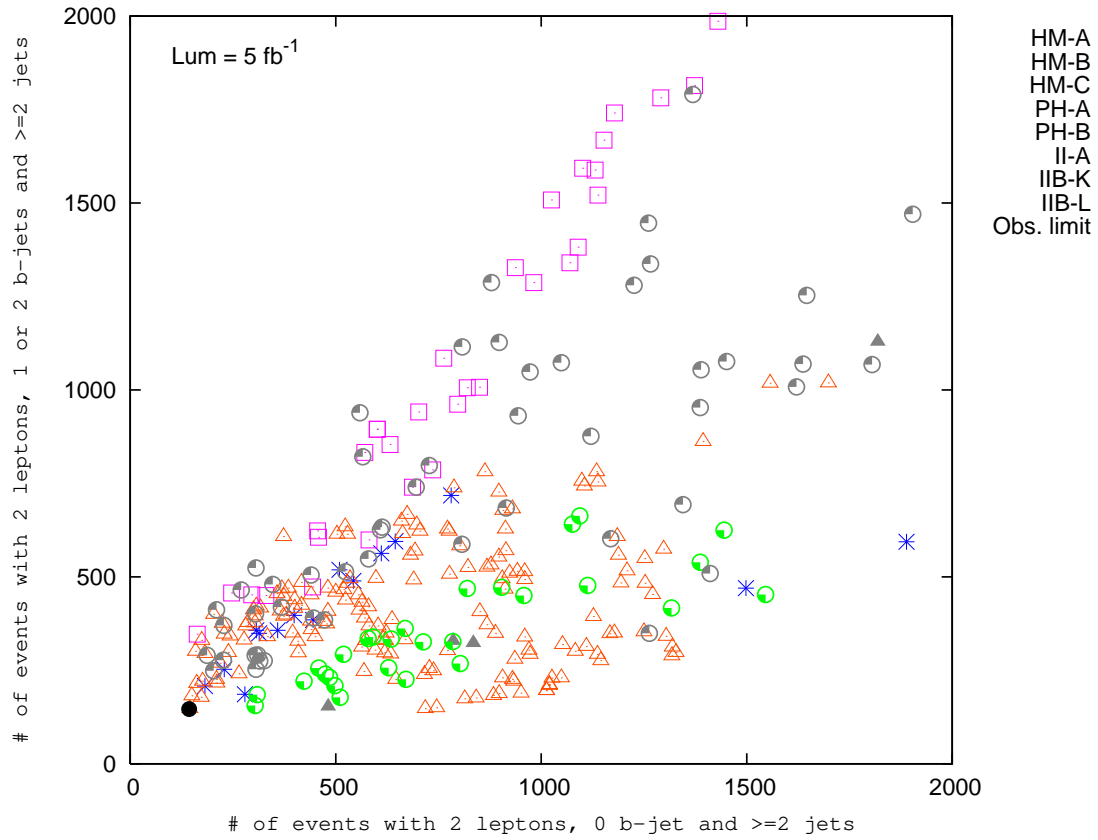


Figure 5.12: Plot with x axis showing number of events with 2 leptons, 0 b jets and ≥ 2 jets, and y axis showing the number of events with 2 leptons, 1 or 2 b jets and ≥ 2 jets each sampled with ~ 50 models, except PH-A (~ 100 models).

Another possible limitation which one could point out is that distinguishing theoretical constructions on the basis of two dimensional signature plots is not very powerful. Since we are only looking at various two-dimensional projections of a multi-dimensional signature space, it is possible that two different theoretical constructions occupy different regions in the multi-dimensional signature space even though they overlap in all the two-dimensional projections.

One would then not be able to cleanly distinguish two constructions by this approach even though they are intrinsically distinguishable. However, one can get around this limitation by tagging individual models of each theoretical construction. It would then be possible to figure out if two different constructions are distinguishable even if they overlap in all two dimensional signature plots. As already noted in section 5.2, our purpose was to outline the approach in a simple manner. It is clear that the approach has to be made more sophisticated for more complicated situations.

For a mathematically precise way of distinguishing pairs of constructions, one could use the following procedure. Imagine dividing the parameter space of the two constructions into a coarse grid with coordinates given by their parameter vectors \vec{x} . For example, for the PH-A construction, $\vec{x} = \{m_{3/2}, a_{np}, \tan(\beta)\}$ [133]. We can then construct a χ^2 -like variable defined as follows:

$$(\Delta S)_{AB} = \min_{\{\tilde{x}, \tilde{y}\}} \sum_{i=1}^{n_{\text{sig}}} \left(\frac{s_A^i(\tilde{x}) - s_B^i(\tilde{y})}{\sigma_{AB}^i} \right)^2 \quad (5.6)$$

where A and B stand for the two constructions, s_i stands for the i -th signature and σ_{AB}^i stands for the error bar assigned between the A and B constructions for the i -th signature. σ_{AB}^i can be determined from statistical errors of the i -th signature for constructions A and B as well as the standard model background error for the i -th signature.

Since we minimize with respect to the parameter vectors \vec{x} and \vec{y} of the two constructions, equation (5.6) can be geometrically visualized as the “minimum distance squared” in the full multi-dimensional signature space between the two constructions A and B with an appropriate “metric” ²⁹, and serves as a measure of the difference between the two constructions A and B . Carrying out the minimization procedure in practice is quite a non-trivial task, especially

²⁹The inverse square of the error σ_{AB}^i acts like the metric in signature space.

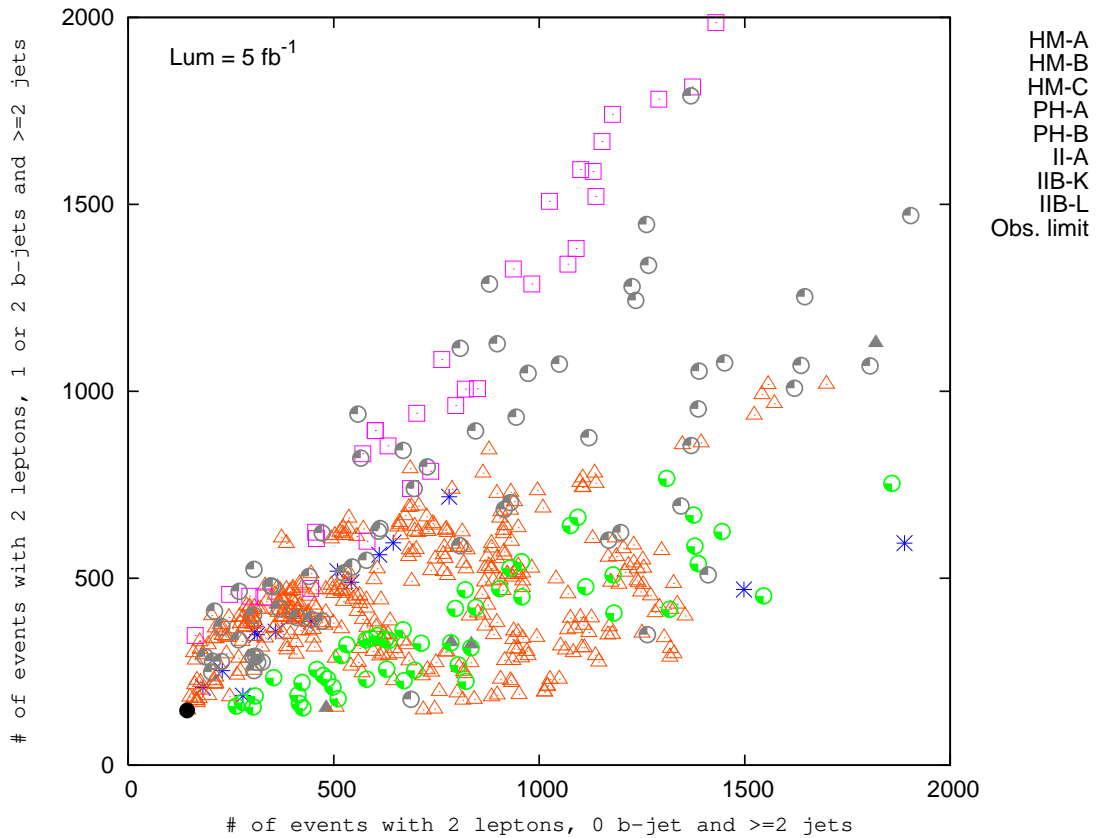


Figure 5.13: The same plot as in Figure 5.12, in which the IIB-K construction is sampled with ~ 100 models and the PH-A construction with ~ 400 models.

when the parameter vectors have many components, as the time required to complete the minimization procedure in a satisfactory way is too large. However techniques have been introduced to get around this problem, for example see [135]. In the future, we plan to do a comprehensive analysis with more statistics and a precise method to distinguish models, as explained above.

Finally, one might object to the approach of figuring out experimental predictions for various classes of underlying theoretical constructions and distinguishing different theoretical constructions from each other before actual data, instead of the more “standard” approach of comparing

each theoretical construction with actual data. Many reasons can be given in this regard. From a conceptual point of view, this approach fits well with the philosophy of addressing the Inverse Problem in a general framework. It is also crucial to addressing the question of predictivity of an underlying theory like string theory in general and the particular string vacuum we live in, in particular. From a more practical point of view, studying the various subtle aspects of connecting an underlying theoretical construction with collider signatures is quite a non-trivial and subtle exercise and requires considerable time and investment. It is therefore very helpful to build knowledge and intuition in this regard and be prepared for actual data. Carrying out this exercise could help discover important properties of the low-energy implications of various classes of theoretical constructions, in turn pointing to new classes of collider observables as well as helping design new analysis techniques.

5.7 Summary and Future Directions

In this work, we have tried to address the goal of learning about the underlying theory from LHC data - the deeper Inverse Problem. We have proposed an approach by which it can be shown that the two prerequisites to addressing the deeper Inverse Problem, namely, a) To reliably go from a microscopic theory to the space of experimental observables, and b) To distinguish among the various classes of microscopic theoretical constructions on the basis of their experimental signatures, can be satisfied for many semi-realistic string constructions which can be described within the supergravity approximation. In our opinion, the work is seminal in the sense that it proposes a new way of thinking about fundamental theory, model-building and collider phenomenology such that there is a better synergy between each of these subfields. Perhaps the most important result, which has never before been presented, is that different

classes of string constructions give *finite* footprints in signature space and that different string constructions give practically overlapping but different and distinguishable footprints.

The reason it is possible to distinguish theoretical constructions is that patterns of experimental observables (for eg. signatures at the LHC) are *sensitive* to the structure of the underlying theoretical constructions, because of correlations (see section 5.4.2). More precisely, this means that a given theoretical construction occupies a *finite* region of signature space which is in general different from another theoretical construction. Moreover, the origin of this difference can be understood from the underlying structure of the construction. Therefore, even though we have carried out a simplified analysis in terms of the imposition of cuts, detection efficiencies of particles, detector simulation and calculation of backgrounds, we still have confidence in the robustness of our results. We have analyzed two classes of string vacua and six other string-motivated constructions in detail. The point of this exercise was to illustrate our approach, the same procedure should be carried out for more classes of realistic vacua so that the procedure becomes more-and-more useful. If the approach fails, it will not be because of these and similar issues discussed above, but rather because many regions of the entire M theory amoeba cannot yet be analyzed by the approach we use. However, we think that rather than giving up ahead of time, the best attitude is to continue to expand both theoretical understanding as well as our approach, and confront them with data.

There are two directions in which the approach advocated in this work can be generalized and sharpened further. The first concerns theoretical issues – efforts should be made to go beyond toy models focussing on few aspects of theory and phenomenology to more holistic ones that address (if not solve) all of the issues an underlying string theoretic construction might be expected to explain. For instance, a better understanding of the theory can fix some (or

all) of the microscopic input parameters of a given construction, increasing the predictivity of the construction. The approach advocated by M. Douglas and W. Taylor, *viz.* to look for correlations in the space of observables by analyzing different classes of vacua is very similar to our approach in principle.

The second concerns the analysis and interpretation of data and its connection to the underlying theory. Creative thinking is needed in identifying collider observables which more directly probe the key features of the Beyond-the-Standard Model (BSM) lagrangian and its connection to the underlying theory. We were able to identify some useful observables by examining specific constructions. In addition, one should find ways in which observables from all fields – collider physics, flavor physics, cosmology, etc. could be used in conjunction to distinguish among, and favor or exclude, many classes of string constructions in a quick and robust manner. Our proposed technique is very useful in this regard as it is very easy to add non-collider observables – such as from flavor physics, cosmology, etc. to the collider observables such that they are all treated in a uniform manner.

It is important to understand that the proposed approach should be applied at various stages, with different tools and techniques useful for each stage. The first stage would consist of distinguishing many classes of constructions with limited amount of data by using simple signatures and simple analysis techniques. This has the advantage that one can rule out various classes of constructions with relative ease. However, in order to go further, it is important to develop more specialized analysis techniques and use more exclusive signatures. This is best done in subsequent stages, when one zooms in to a more limited set of constructions and also obtains more data. Since one has better statistics, one can use optimized and more exclusive signatures as well as use more sophisticated analysis techniques to get more detailed

information about the constructions. Many of these sophisticated analysis techniques already exist in the literature [136], although they have been applied to very special scenarios like minimal supergravity, minimal gauge mediation, etc. One would now need to apply similar techniques (suitably modified) to the set of constructions consistent with limited data. Also, in the past year, a lot of progress has been made towards uncovering the low energy spectrum and parameters from (simulated) LHC signatures in the form of “blackboxes” constructed by some groups. This has been the program of the *LHC Olympics* Workshops in the past year [137].

Combining these sophisticated techniques with (some) knowledge of the connection between theoretical constructions and data obtained in the first stage, we hope that one can further distinguish the remaining constructions, learn more about underlying theoretical issues, like supersymmetry breaking and mediation, moduli stabilization, inflation, etc.

CHAPTER VI

From Low Scale Data to High Scale Theory - Obstacles and Resolutions

In the previous chapter, we analyzed low energy predictions for physical observables - signatures at the LHC, for many theoretical models of supersymmetry breaking arising in string theory or strongly motivated from string theory. In this chapter, we would like to analyze a more bottom-up approach to the Inverse Problem, *viz.* to go from data to theory in a more model-independent way. Of course, addressing the problem in complete generality is extremely challenging. So, we will make some assumptions about the nature of new physics which are well motivated from a theoretical point of view and also make the problem more tractable.

Following our arguments for the solution of the hierarchy problem in chapter III and similar to chapter V, we will assume that the new physics fits in the framework of low energy supersymmetry. Since the apparent unification of gauge couplings in the MSSM suggests an underlying grand unified theoretical framework, we will consider new physics consistent with gauge unification. Finally, we will assume that “forthcoming” LHC data provides us with at least rough values of the superpartner spectrum. Even with these assumptions, the problem of unravelling the underlying high-scale theory is complicated if the low scale spectrum is not

measured completely or precisely, or if there is new physics at heavy scales (consistent with gauge unification) beyond the reach of collider experiments. In this chapter we will study some of these obstacles to running up, and we investigate how to get around them. Our main conclusion is that even though such obstacles can make it very difficult to accurately determine the values of all the soft parameters at the high scale, there exist a number of special combinations of the soft parameters that can avoid these difficulties. We also present a systematic application of our techniques in an explicit example.

Taking gauge unification as being more than accidental from above, we obtain significant constraints on the types of new physics that can arise between the electroweak and the grand unification (GUT) scales. Any new phenomenon that enters the effective theory in this energy range ought to maintain the unification of couplings, and should be consistent with a (possibly generalized) GUT interpretation. The simplest scenario is a *grand desert*, in which there is essentially no new physics at all below the unification scale M_{GUT} . In this case, if supersymmetry is discovered at the Tevatron or the LHC, it will be possible to extrapolate the measured soft supersymmetry breaking parameters to much higher scales using the renormalization group (RG). Doing so may help to reveal the details of supersymmetry breaking, and possibly also the fundamental theory underlying it.

If supersymmetry is observed in a collider experiment, it will be challenging to extract all the supersymmetry breaking parameters from the collider signals. While some work has been put into solving this problem [138], there is still a great deal more that needs to be done. The parameters extracted in this way will be subject to experimental uncertainties, especially if the supersymmetric spectrum is relatively heavy. There will also be theoretical uncertainties from higher loop corrections in relating the physical masses to their running

values [139]. These uncertainties in the supersymmetry breaking parameters, as well as those in the supersymmetric parameters, will complicate the extrapolation of the soft masses to high energies [140, 141]. Much of the previous work along these lines has focused on running the parameters of particular models from the high scale down. This is useful only if the new physics found resembles one of the examples studied. Our goal is to study the running from low to high [142].

Evolving the soft parameters from collider energies up to much higher scales can also be complicated by new physics at intermediate energies below M_{GUT} . The apparent unification of gauge couplings suggests that if this new physics is charged under the MSSM gauge group, it should come in the form of complete GUT multiplets or gauge singlets. Indeed, the observation of very small neutrino masses already suggests the existence of new physics in the form of very heavy gauge singlet neutrinos [143]. With new physics that is much heavier than the electroweak scale, it is often very difficult to study it experimentally, or to even deduce its existence. If we extrapolate the MSSM parameters without including the effects of heavy new physics, we will obtain misleading and incorrect values for the high scale values of these parameters [144].

In the present work we study some of these potential obstacles to the RG evolution of the MSSM soft parameters. In Section 6.1 we investigate how uncertainties in the low-scale parameter values can drastically modify the extrapolated high-scale values. We focus on the so-called S term (*a.k.a.* the hypercharge D term) within the MSSM, which depends on all the soft masses in the theory, and can have a particularly large effect on the running if some of these soft masses go unmeasured at the LHC. In Sections 6.2 and 6.3, we study two possible examples of heavy new physics. Section 6.2 investigates the effects of adding complete vector-like GUT multiplets on the running of the soft parameters. Section 6.3 describes how including heavy

Majorana neutrinos to generate small neutrino masses can alter the running of the MSSM soft parameters. In Section 6.4 we combine our findings and illustrate how they may be put to use with an explicit example. Finally, Section 6.5 is reserved for our conclusions. A summary of some useful combinations of scalar soft masses is given in an Appendix.

Our main result is that the high scale values of many Lagrangian parameters can be very sensitive to uncertainties in their low-scale values, or to the presence of heavy new physics. However, in the cases studied we also find that there are particular combinations of the Lagrangian parameters that are stable under the RG evolution, or that are unaffected by the new physics. These special parameter combinations are therefore especially useful for making a comparison with possible high-scale theories.

Throughout our analysis, we simplify the RG equations by setting all flavor non-diagonal soft terms to zero and keeping only the (diagonal) Yukawa couplings of the third generation. Under this approximation, we work to two loop order for the running of the MSSM parameters, and interface with Suspect 2.3.4 [120] to compute one-loop threshold corrections at the low scale. For concreteness, we take this scale to be 500 GeV. The additional running due to new physics introduced at scales much larger than the weak scale is only performed at one-loop. We also implicitly assume that the mass scale of the messengers that communicate supersymmetry breaking to the visible sector lies at or above the GUT scale, $M_{GUT} \simeq 2.5 \times 10^{16}$ GeV. Even so, our methods and general analysis will also be applicable to scenarios that have lighter messenger particles, such as gauge mediation [145, 146]. We also neglect the effects of hidden sector running, which can be significant if there are interacting states in the hidden sector significantly lighter than M_{GUT} [147, 148, 149]. While this manuscript was in preparation, methods similar to those considered in the present work were proposed in Ref. [149] to deal

with these additional uncertainties in the high scale values of the soft parameters.

In this work, we focus on low-energy supersymmetric models, and particular forms of intermediate scale new physics. Despite this restriction, we expect that our general techniques will be applicable to other solutions of the gauge hierarchy problem, or to more exotic forms of new intermediate scale physics.

6.1 Uncertainties Due to the S Term

The one-loop renormalization group (RG) equations of the MSSM soft scalar masses have the form [150]

$$(16\pi^2)\frac{dm_i^2}{dt} = \tilde{X}_i - \sum_{a=1,2,3} 8g_a^2 C_i^a |M_a|^2 + \frac{6}{5}g_1^2 Y_i S, \quad (6.1)$$

where $t = \ln(Q/M_Z)$, \tilde{X}_i is a function of the soft squared masses and the trilinear couplings, M_a denotes the a -th gaugino mass, and the S term is given by

$$\begin{aligned} S &= \text{Tr}(Y m^2) \\ &= m_{H_u}^2 - m_{H_d}^2 + \text{tr}(m_Q^2 - 2m_U^2 + m_E^2 + m_D^2 - m_L^2) \end{aligned} \quad (6.2)$$

where the first trace runs over all hypercharge representations, and the second runs only over flavors.

The S term is unusual in that it connects the running of any single soft mass to the soft masses of every other field with non-zero hypercharge. Taking linear combinations of the RG equations for the soft scalar masses, the one-loop running of S in the MSSM is given by

$$(16\pi^2)\frac{dS}{dt} = -2b_1 g_1^2 S, \quad (6.3)$$

where $b_1 = -33/5$ is the one-loop beta-function coefficient. Using Eq. (6.3) in Eq. (6.1) and neglecting the Yukawa-dependent terms \tilde{X}_i (which are expected to be small for the first and

second generations) the effect of $S \neq 0$ is to shift the high scale value the soft mass would have had were $S(t_0) = 0$ by an amount

$$\Delta m_i^2(t) = \frac{Y_i}{\text{Tr}(Y^2)} \left[\frac{g_1^2(t)}{g_1^2(t_0)} - 1 \right] S(t_0). \quad (6.4)$$

The one-loop RG equation for S is homogeneous. Thus, if S vanishes at any one scale, it will vanish at all scales (at one-loop). In both minimal supergravity (mSUGRA) and simple gauge-mediated models, S does indeed vanish at the (high) input scale, and for this reason the effects of this term are often ignored.

From the low-energy perspective, there is no reason for $S(t_0)$ to vanish, and in many cases its effects can be extremely important. Since g_1 grows with increasing energy, the mass shift due to the S term grows as well. For $t_0 \simeq t_{M_Z}$ and $t \rightarrow t_{GUT}$, the prefactor in Eq. (6.4) is about $(0.13) Y_i$. The value of $S(t_0)$ depends on all the scalar soft masses, and the experimental uncertainty in its value will therefore be set by the least well-measured scalar mass. In particular, if one or more of the soft masses aren't measured at all, $S(t_0)$ is unbounded other than by considerations of naturalness. Fortunately, this uncertainty only affects the soft scalar masses. The S term does not enter directly into the running of the other soft parameters until three-loop order [150, 151], and therefore its effects on these parameters is expected to be mild.

There is also a theoretical uncertainty induced by the S term. Such a term is effectively equivalent to a Fayet-Iliopoulos (FI) D term for hypercharge [151]. To see how this comes about, consider the hypercharge D -term potential including a FI term,

$$\mathcal{L} = \dots + \frac{1}{2} D_1^2 + \xi D_1 + \sqrt{\frac{3}{5}} g_1 D_1 \sum_i \bar{\phi}_i Y_i \phi^i - \sum_i \tilde{m}_i^2 |\phi^i|^2, \quad (6.5)$$

where we have also included the soft scalar masses. Eliminating the D_1 through its equation

of motion, we find

$$\mathcal{L} = \dots - \frac{1}{2}\xi^2 - \frac{g_1^2}{2} \left(\sum_i \bar{\phi}_i Q_i \phi^i \right)^2 - \sum_i \bar{\phi}_i \left(\tilde{m}_i^2 + \sqrt{\frac{3}{5}} g_1 Y_i \xi \right) \phi^i. \quad (6.6)$$

Thus, except for the constant addition to the vacuum energy, the effect of the FI term is to shift each of the soft squared masses by an amount

$$\tilde{m}_i^2 \rightarrow m_i^2 := \tilde{m}_i^2 + \sqrt{\frac{3}{5}} g_1 Y_i \xi. \quad (6.7)$$

The low-energy observable quantities are the $\{m_i^2\}$, not the $\{\tilde{m}_i^2\}$. Since we can't extract the shift in the vacuum energy, the low-energy effects of the FI term are therefore invisible to us, other than the shift in the soft masses. This shift is exactly the same as the shift due to the S term. Let us also mention that the S term, as we have defined it in Eq. (6.2), runs inhomogeneously at two-loops and above, so the exact correspondence between a hypercharge D term and the S term of Eq. (6.2) does not hold beyond one-loop order.

A simple way to avoid both the large RG uncertainties in the soft masses and the theoretical ambiguity due to the S term is apparent from Eq. (6.4). Instead of looking at individual soft masses, it is safer to consider the mass differences

$$Y_j m_i^2 - Y_i m_j^2, \quad (6.8)$$

for any pair of fields. These differences are not affected by the mass shifts of Eq. (6.4). They are also independent of the value of the FI term.

In the rest of this section, we show how the S term can complicate the running of the soft masses to high energies with a particular example. If one of the scalar soft masses is unmeasured, it is essential to use the linear mass combinations given in Eq. (6.8) instead of the individual masses themselves. We also discuss how the special RG properties of the S

term provide a useful probe of high scale physics if all the scalar soft masses are determined experimentally.

6.1.1 Example: SPS-5 with an Unmeasured Higgs Soft Mass

To illustrate the potential high-scale uncertainties in the RG-evolved soft parameters due to the S term, we study the sample mSUGRA point SPS-5 [152] under the assumption that one of the scalar soft masses goes unmeasured at the LHC. If this is the case, the S parameter is undetermined, and the precise values of the high-scale soft terms are no longer precisely calculable. Even if the value of the S term is bounded by considerations of naturalness, the uncertainties in the high-scale values of the soft scalar masses can be significant.

The SPS-5 point is defined by the mSUGRA input values $m_0 = 150$ GeV, $m_{1/2} = 300$ GeV, $A_0 = -1000$, $\tan\beta = 5$, and $\text{sgn}(\mu) > 0$, at M_{GUT} . The mass spectrum for this point has relatively light sleptons around 200 GeV, and somewhat heavier squarks with masses near 400-600 GeV. The LSP of the model is a mostly Bino neutralino, with mass close to 120 GeV. The perturbation we consider for this point is a shift in the down-Higgs soft mass, $m_{H_d}^2$.

Of the soft supersymmetry breaking parameters in the MSSM, the soft terms associated with the Higgs sector can be particularly difficult to deduce from LHC measurements. At tree-level, the independent Lagrangian parameters relevant to this sector are [1]

$$v, \quad \tan\beta, \quad \mu, \quad M_A, \quad (6.9)$$

where $v \simeq 174$ GeV is the electroweak breaking scale, $\tan\beta = v_u/v_d$ is the ratio of the H_u and H_d VEVs, μ is the supersymmetric μ -term, and M_A is the pseudoscalar Higgs boson mass. Other Higgs-sector Lagrangian parameters, such as $m_{H_d}^2$ and $m_{H_u}^2$, can be expressed in terms of these using the conditions for electroweak symmetry breaking in the MSSM.

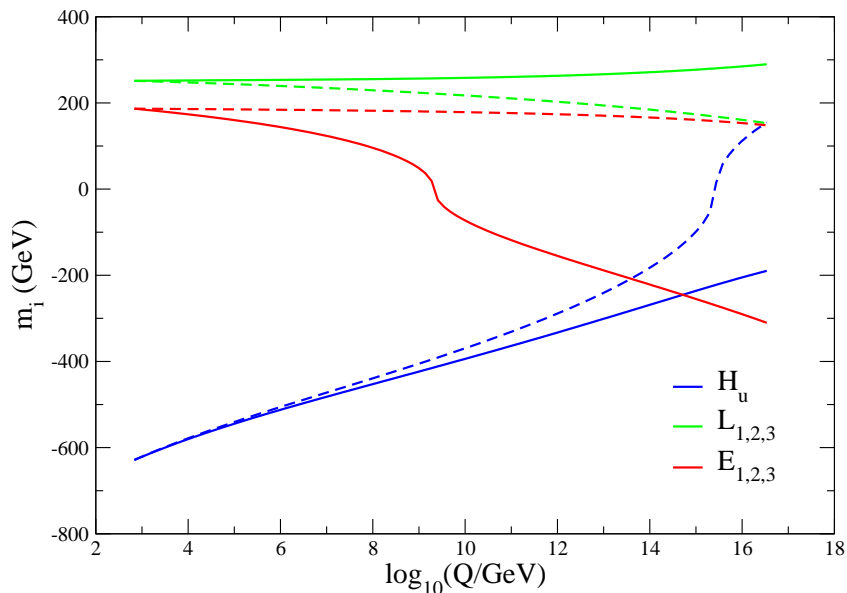


Figure 6.1: Deviations in the running of some of the SPS-5 soft masses due to setting $m_{H_d}^2 = (1000 \text{ GeV})^2$ at the low scale. The solid lines show the running of $m_{H_u}^2$, m_{E}^2 , and m_L^2 with this perturbation, while the dashed lines show the unperturbed running of these soft masses. The unperturbed low-scale value of the down-Higgs soft mass is $m_{H_d}^2 \simeq (235 \text{ GeV})^2$.

Among the Higgs sector parameters listed in Eq. (6.9), only the value of v is known. The value of μ can potentially be studied independently of the Higgs scalar sector by measuring neutralino and chargino masses and couplings [138, 152, 153], although it is likely to be poorly determined if only hadron colliders are available. A number of observables outside the Higgs sector may also be sensitive to $\tan \beta$, especially if it is large, $\tan \beta \geq 20$. For example, the dilepton invariant mass distributions in the inclusive $2\ell + jets + \cancel{E}_T$ channel can vary significantly depending on the value of $\tan \beta$, but this dependence is such that the value of $\tan \beta$ can at best only be confined to within a fairly broad ranges [154]. Determining M_A at the LHC typically requires the discovery of one of the heavier MSSM Higgs boson states. Finding these states can

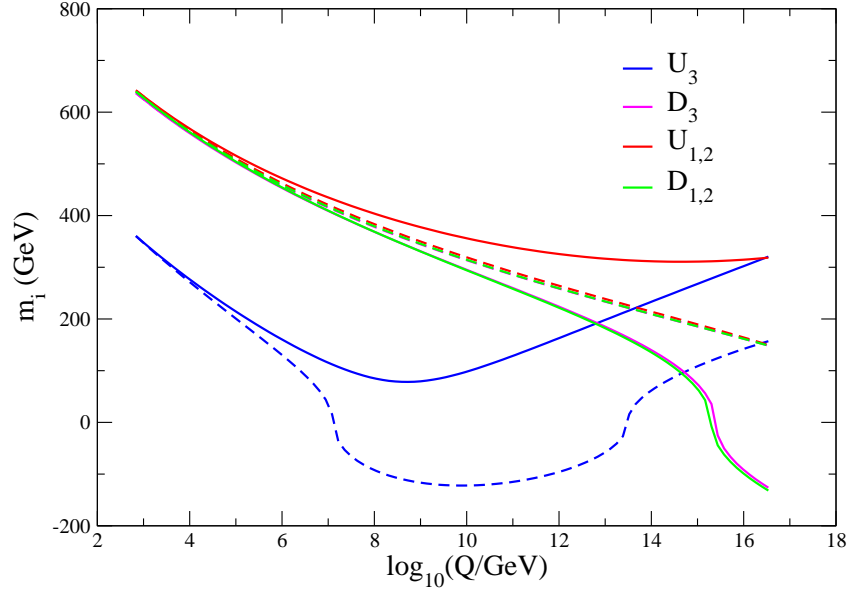


Figure 6.2: Deviations in the running of some of the SPS-5 soft masses due to setting $m_{H_d}^2 = (1000 \text{ GeV})^2$ at the low scale. The solid lines show the running of $m_{U_{1,2}}^2$, $m_{D_{1,2}}^2$, $m_{U_3}^2$, and $m_{D_3}^2$ with this perturbation, while the dashed lines show the unperturbed running of these soft masses.

also help to determine $\tan \beta$ [155]. Unfortunately, the LHC reach for the heavier Higgs states is limited, especially for larger values of M_A and intermediate or smaller values of $\tan \beta \leq 20$ [156]. If none of the heavier Higgs bosons are found at the LHC, it does not appear to be possible to determine both of the Higgs soft masses, $m_{H_u}^2$ and $m_{H_d}^2$.

For the low-scale parameters derived from SPS-5, the pseudoscalar Higgs mass M_A is about 700 GeV. With such a large value of M_A , and $\tan \beta = 5$, only the lightest SM-like Higgs boson is within the reach of the LHC [156]. Motivated by this observation, we examine the effect of changing the low-scale value of $m_{H_d}^2$ on the running of the other soft parameters. The actual low-scale value of $m_{H_d}^2$ is about $(235 \text{ GeV})^2$. The perturbation we consider is to set this value

to $(1000 \text{ GeV})^2$, while keeping $\tan\beta$ fixed. Such a perturbation does not ruin electroweak symmetry breaking, and tends to push the heavier higgs masses to even larger values. In the present case, the heavier Higgs masses increase from about 700 GeV to over 1200 GeV.¹

The effects of this perturbation in $m_{H_d}^2$ on some of the soft scalar masses are shown in Figs. 6.1 and 6.2. In these plots, we show $m_i = m_i^2 / \sqrt{|m_i^2|}$. The deviations in the soft masses are substantial, and the S parameter is the source of this uncertainty. In addition to the S term, varying $m_{H_d}^2$ can also modify the running of the Higgs mass parameters and the down-type squarks and sleptons through the Yukawa-dependent terms X_i in the RG equations, Eq. (6.1). In the present case these Yukawa-dependent effects are very mild since for $\tan\beta = 5$, the b and τ Yukawas are still quite small. This can be seen by noting the small difference between the perturbed running of $m_{U_{1,2}}^2$ and $m_{U_3}^2$ in Fig. 6.2. For larger values of $\tan\beta$, the down-type Yukawa couplings can be enhanced and this non- S effect from $m_{H_d}^2$ can be significant. However, we also note that as these Yukawa couplings grow larger, it becomes much easier for the LHC to detect one or more of the heavier Higgs states. To the extent that the Yukawa-dependent shifts can be neglected, the linear mass combinations of Eq. (6.8) remove most of the uncertainty due to an unknown $m_{H_d}^2$ in the running of the soft masses that are measured. The effect of not knowing $m_{H_d}^2$ has only a very small effect on the running of the gaugino masses and the trilinear terms.

In this example we have assumed that $m_{H_d}^2$ is the only unmeasured soft scalar mass. Several of the other soft scalar masses may be difficult to reconstruct from LHC data as well. For example, within many SUSY scenarios the third generation squarks and some of the heavier sleptons have very small LHC production rates. If there are other unmeasured soft scalar masses

¹The values of μ and $B\mu$ also change, although the variation in μ is very mild: $\mu \simeq 640 \text{ GeV} \rightarrow 670 \text{ GeV}$.

besides $m_{H_d}^2$, the uncertainties due to the S term in the extrapolation of the measured scalar soft masses will be even greater than what we have presented here. The mass combinations of Eq. (6.8) will be necessary to study the high scale supersymmetry breaking spectrum in this case.

6.1.2 Origins and Uses of the S Term

While the S term can complicate the extrapolation of the soft scalar masses if one of them goes unmeasured, the simple scale dependence of this term also makes it a useful probe of the high scale theory if all the masses are determined. The essential feature is the homogeneous RG evolution of the S term, given in Eq. (6.3), which is related to the non-renormalization of FI terms in the absence of supersymmetry breaking.

A non-vanishing S term can arise from a genuine FI term present in the high scale theory, or from non-universal scalar soft masses at the high input scale. The size of a fundamental hypercharge FI term, ξ , is naïvely on the order of the large input scale. Such a large value would either destabilize the gauge hierarchy or lead to $U(1)_Y$ breaking at high energies. However, the non-renormalization of FI terms implies that it is technically natural for ξ to take on much smaller values. In this regard, a small value for ξ is analogous to the μ problem in the MSSM. Adding such a FI term to mSUGRA provides a simple one-parameter extension of this model, and can have interesting effects [157, 158]. Note, however, that in a GUT where $U(1)_Y$ is embedded into a simple group, a fundamental hypercharge FI term in the full theory is forbidden by gauge invariance.

It is perhaps more natural to have the S term emerge from non-universal scalar soft masses [159, 160]. This is true even in a GUT where $U(1)_Y$ is embedded into a simple group.

Within such GUTs, the contribution to S from complete GUT multiplets vanishes. However, non-zero contributions to S can arise from multiplets that are split in the process of GUT breaking. For example, in $SU(5)$ with H_u and H_d states embedded in $\mathbf{5}$ and $\bar{\mathbf{5}}$ multiplets, a non-zero low-energy value of S can be generated when the heavy triplet states decouple provided the soft masses of the respective multiplets are unequal. Whether it is zero or not, the low-scale value of the S term provides a useful constraint on the details of a GUT interpretation of the theory.

So far we have only considered the S term corresponding to $U(1)_Y$. If there are other gauged $U(1)$ symmetries, there will be additional S term-like factors for these too. In fact, the homogeneity of the S term evolution also has a useful implication for any non-anomalous *global* $U(1)$ symmetry in the theory. The only candidate in the MSSM is $U(1)_{B-L}$, up to linear combinations with $U(1)_Y$ [161]. Let us define S_{B-L} by the combination

$$\begin{aligned} S_{B-L} &= \text{Tr}(Q_{B-L}m^2) \\ &= \text{tr}(2m_Q^2 - m_U^2 - m_D^2 - 2m_L^2 + m_E^2), \end{aligned} \tag{6.10}$$

where the second trace runs only over flavors.² We can think of S_{B-L} as the effective S term for a gauged $U(1)_{B-L}$ in the limit of vanishing coupling. At one loop order, the RG running of S_{B-L} is given by

$$\begin{aligned} (16\pi^2)\frac{dS_{B-L}}{dt} &= \frac{3}{5}\text{Tr}(Q_{B-L}Y)g_1^2 S \\ &= n_g \frac{16}{5} g_1^2 S, \end{aligned} \tag{6.11}$$

where $n_g = 3$ is the number of generations. If S is measured and vanishes, S_{B-L} provides

²Up to flavor mixing, we can also define an independent S_{B-L} for each generation.

a second useful combination of masses that is invariant under RG evolution,³ and yields an additional constraint on possible GUT embeddings of the theory.

6.2 New Physics: Complete GUT Multiplets

As a second line of investigation, we consider the effects of some possible types of new intermediate scale physics on the running of the MSSM soft terms. If this new physics is associated with supersymmetry breaking as in gauge mediation [145], then it is of particular interest in its own right. Indeed, in this case the low-energy spectrum of soft terms may point towards the identity of the new physics after RG evolution. On the other hand, there are many kinds of possible new intermediate scale physics that are not directly related to supersymmetry breaking. The existence of this type of new phenomena can make it much more difficult to deduce the details of supersymmetry breaking from the low-energy soft terms.

A useful constraint on new physics is gauge coupling unification. To preserve unification, the SM gauge charges of the new physics should typically be such that all three MSSM gauge beta functions are modified in the same way.⁴ This is automatic if the new matter fills out complete multiplets of a simple GUT group into which the MSSM can be embedded. Such multiplets can emerge as remnants of GUT symmetry breaking.

As an example of this sort of new physics, we consider vector-like pairs of complete $SU(5)$ multiplets. For such multiplets, it is possible to write a down a supersymmetric mass term of the form

$$\mathcal{W} \supset \tilde{\mu} \bar{\mathcal{X}} \mathcal{X}, \tag{6.12}$$

³This non-evolution of mass combinations corresponding to non-anomalous global symmetries persists at strong coupling. In models of conformal sequestering, this can be problematic [147].

⁴For an interesting exception, see Ref. [162].

where X and \bar{X} denote the chiral superfields of the exotic multiplets. We also assume that the exotic multiplets have no significant superpotential (Yukawa) couplings with the MSSM fields. Under these assumptions, the exotic $SU(5)$ multiplets can develop large masses independently of the details of the MSSM. They will interact with the MSSM fields only through their gauge interactions.

If the supersymmetric mass $\tilde{\mu}$ is much larger than the electroweak scale, it will be very difficult to deduce the presence of the additional GUT multiplets from low-energy data alone. Moreover, an extrapolation of the measured soft masses using the RG equations appropriate for the MSSM will lead to incorrect values of the high-scale parameters. In this section, we characterize the sizes and patterns of the deviations in the high scale soft spectrum induced by additional vector-like GUT multiplets. We also show that even though the new matter interferes with the running of the MSSM soft parameters, it is often still possible to obtain useful information about the input spectrum, such as the relative sizes of the gaugino masses and whether there is inter-generational splitting between the soft scalar masses.

6.2.1 Shifted Gauge Running

The main effect of the exotic GUT multiplets is to shift the running of the $SU(3)_c$, $SU(2)_L$, and $U(1)_Y$ gauge couplings. Recall that in the MSSM, the one-loop running of these couplings is determined by

$$\frac{dg_a^{-2}}{dt} = \frac{b_a}{8\pi^2}, \quad (6.13)$$

with $(b_1, b_2, b_3) = (-33/5, -1, 3)$. The presence of a massive GUT multiplet shifts each of the b_a up by an equal amount above the heavy threshold at $t = t_I = \ln(\tilde{\mu}/M_Z)$,

$$\Delta b = -N_{\mathbf{5} \oplus \bar{\mathbf{5}}} - 3 N_{\mathbf{10} \oplus \bar{\mathbf{10}}} + \dots \quad (6.14)$$

where $N_{\mathbf{5} \oplus \bar{\mathbf{5}}}$ is the number of additional $\mathbf{5} \oplus \bar{\mathbf{5}}$ representations and $N_{\mathbf{10} \oplus \bar{\mathbf{10}}}$ is the number of $\mathbf{10} \oplus \bar{\mathbf{10}}$'s. The modified one-loop solution to the RG equations is therefore,

$$g_a^{-2}(t) = \begin{cases} g_a^{-2}(t_0) + \frac{b_a}{8\pi^2}(t - t_0) & t < t_I, \\ g_a^{-2}(t_0) + \frac{b_a}{8\pi^2}(t - t_0) + \frac{\Delta b}{8\pi^2}(t - t_I) & t > t_I. \end{cases} \quad (6.15)$$

It follows that the unification scale is not changed, but the value of the unified gauge coupling is increased. Note that the number of new multiplets is bounded from above for a given value of $\tilde{\mu}$ if gauge unification is to be perturbative.⁵

The change in the gauge running shifts the running of all the soft parameters, but the greatest effect is seen in the gaugino masses. At one-loop, these evolve according to

$$\frac{dM_a}{dt} = -\frac{b_a}{8\pi^2} g_a^2 M_a. \quad (6.16)$$

It follows that M_a/g_a^2 is RG invariant above and below the heavy threshold. If the threshold is also supersymmetric, M_a will be continuous across it at tree-level. Since g_a is also continuous across the threshold at tree-level, the addition of heavy vector-like matter does not modify the one-loop scale invariance of the ratio M_a/g_a^2 . This holds true whether or not the new matter preserves gauge unification, but it is most useful when unification holds. When it does, the measurement of the low-energy gaugino masses immediately translates into a knowledge of their ratio at M_{GUT} [163].

From Eq. (6.15) and the one-loop scale invariance of M_a/g_a^2 , the shift in the gaugino masses due to the additional matter is

$$M_a(t) = \bar{M}_a(t) \left[1 + \frac{\Delta b \bar{g}_a^2}{8\pi^2} (t - t_I) \right]^{-1}, \quad (6.17)$$

⁵Note that the parts of $\tilde{\mu}$ corresponding to the doublet and triplet components of the $\mathbf{5}$ will run differently between M_{GUT} and the intermediate scale. This will induce additional threshold corrections that we do not include in our one-loop analysis.

where \bar{g}_a and \bar{M}_a denote the values these parameters would have for $\Delta b = 0$ (*i.e.* the values obtained using the MSSM RG equations). For $t = t_{GUT}$, the shift coefficient is identical for $a = 1, 2, 3$ provided gauge unification occurs. The shift in the running of the gauge couplings and the gaugino masses due to seven sets of $\mathbf{5} \oplus \bar{\mathbf{5}}$'s at 10^{11} GeV is illustrated in Fig. 6.3. An unperturbed universal gaugino mass of $M_{1/2} = 700$ GeV is assumed. Both the values of the unified gauge coupling and the universal gaugino mass at M_{GUT} are increased by the additional multiplets.

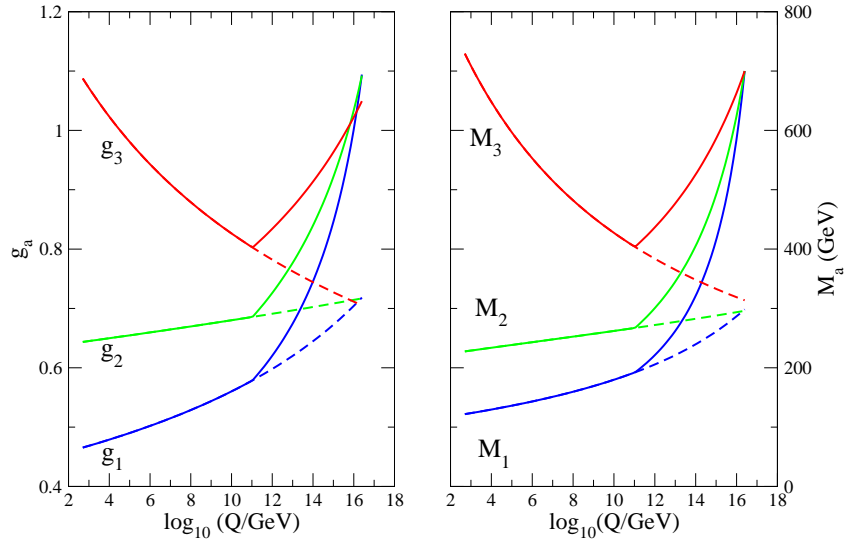


Figure 6.3: The shift in the running of the gauge couplings (left) and the gaugino masses (right) due to 7 sets of $\mathbf{5} \oplus \bar{\mathbf{5}}$'s with mass $\tilde{\mu} = 10^{11}$ GeV. The universal gaugino mass is taken to be 700 GeV.

The running of the soft masses also depends on the running of the gauge couplings and gaugino masses, and is modified by the appearance of new matter. At one-loop order, in the limit that we can neglect the Yukawa couplings, it is not hard to find the shifts in the soft

masses. We can divide these shifts into two contributions,

$$m_i^2(t) = \bar{m}_i^2 + \Delta m_{i_\lambda}^2 + \Delta m_{i_S}^2, \quad (6.18)$$

where \bar{m}_i^2 is the value of the soft mass obtained by running the measured value up in the absence of the new matter, $\Delta m_{i_\lambda}^2$ is the shift due to the modified gaugino masses, and $\Delta m_{i_S}^2$ is due to the change in the running of the S term.

The first shift, $\Delta m_{i_\lambda}^2$, can be obtained straightforwardly from Eqs. (6.1,6.13,6.16), and is given by

$$\Delta m_{i_\lambda}^2 = \sum_a 2 C_i^a \left| \frac{M_a}{g_a^2} \right|^2 \Delta I_a \quad (6.19)$$

where C_i^a the Casimir invariant of the a -th gauge group and

$$\Delta I_a = \frac{1}{(b_a + \Delta b)} (g_a^4 - g_{a_I}^4) - \frac{1}{b_a} (\bar{g}_a^4 - g_{a_I}^4), \quad (6.20)$$

with g_a the actual gauge coupling at scale $t > t_I$ (including the extra matter), g_{a_I} the gauge coupling at the heavy threshold t_I , and \bar{g}_a the gauge coupling at scale $t > t_I$ in the absence of new matter.

New chiral matter can also modify the running of the soft scalar masses through the S parameter. The new matter shifts the running of S by changing the running of g_1 , but it can also contribute to the S term directly at the heavy threshold. Combining these effects, the value of S above threshold is

$$\begin{aligned} S(t) &= \left(\frac{g_1}{g_{1_0}} \right)^2 S(t_0) + \left(\frac{g_1}{g_{1_I}} \right)^2 \Delta S \\ &= \bar{S}(t) + \left(\frac{g_1^2 - \bar{g}_1^2}{g_{1_0}^2} \right) S(t_0) + \left(\frac{g_1}{g_{1_I}} \right)^2 \Delta S, \end{aligned} \quad (6.21)$$

where ΔS is the shift in the value of S at the threshold, g_{1_0} is the low-scale value of the gauge coupling, and $\bar{S}(t)$ is the value the S term would have in the absence of the new matter.

Inserting this result into Eq. (6.1), the effect of the new matter on the running of the soft scalar masses through the S term is

$$\begin{aligned} \frac{5}{3Y_i} \Delta m_{i_s}^2 &= \frac{1}{b_1} \left[\left(\frac{\bar{g}_1}{g_{1_0}} \right)^2 - \left(\frac{g_{1_I}}{g_{1_0}} \right)^2 \right] S_0 - \frac{1}{(b_1 + \Delta b)} \left[\left(\frac{g_1}{g_{1_0}} \right)^2 - \left(\frac{g_{1_I}}{g_{1_0}} \right)^2 \right] S_0 \\ &\quad - \frac{1}{(b_1 + \Delta b)} \left[\left(\frac{g_1}{g_{1_I}} \right)^2 - 1 \right] \Delta S. \end{aligned} \tag{6.22}$$

As before, the effects of the S term on the soft masses are universal up to the hypercharge prefactor. Thus, they still cancel out of the linear combinations given in Eq. (6.8).

6.2.2 Yukawa Effects and Useful Combinations

We have so far neglected the effects of the MSSM Yukawa couplings on the modified running of the soft masses. As a result, the shifts in the running of the soft scalar masses written above are family universal. There are also non-universal shifts in the soft scalar masses. These arise from the Yukawa-dependent terms in the soft scalar mass beta functions, which themselves depend on the Higgs and third-generation soft scalar masses. As a result, the low-energy spectrum obtained from a theory with universal scalar masses at the high scale and additional GUT multiplets can appear to have non-universal soft masses at the high scale if the extra GUT multiplets are not included in the RG evolution. These non-universal shifts are usually a subleading effect, but as we illustrate below they can be significant when the supersymmetric mass of the new GUT multiplets is within a few orders of magnitude of the TeV scale.

Non-universal mass shifts obscure the relationship between the different MSSM generations and the source of supersymmetry breaking. This relationship is closely linked to the SUSY flavor problem [164], and possibly also to the origin of the Yukawa hierarchy. For example, third generation soft masses that are significantly different from the first and second generation

values is one of the predictions of the model of Ref. [165], in which strongly-coupled conformal dynamics generates the Yukawa hierarchy and suppresses flavor-mixing soft terms. The relative sizes of the high scale soft masses for different families is therefore of great theoretical interest.

Even when there are non-universal shifts from new physics, it is sometimes still possible to obtain useful information about the flavor structure of the soft scalar masses at the high scale. To a very good approximation, the flavor non-universal contributions to the RG evolution of the soft masses are proportional to the third generation Yukawa couplings or the trilinear couplings. There is also good motivation (and it is technically allowed) to keep only the trilinear couplings for the third generation. In this approximation, the Yukawa couplings and the A terms only appear in the one-loop RG equations for the soft masses through three independent linear combinations. Of the seven soft masses whose running depends on these combinations, we can therefore extract four mass combinations whose evolution is independent of Yukawa effects at one-loop order [166].⁶ They are:

$$\begin{aligned}
 m_{A_3}^2 &= 2 m_{L_3}^2 - m_{E_3}^2 & (6.23) \\
 m_{B_3}^2 &= 2 m_{Q_3}^2 - m_{U_3}^2 - m_{D_3}^2 \\
 m_{X_3}^2 &= 2 m_{H_u}^2 - 3 m_{U_3}^2 \\
 m_{Y_3}^2 &= 3 m_{D_3}^2 + 2 m_{L_3}^2 - 2 m_{H_d}^2
 \end{aligned}$$

The cancellation in the first two terms occurs because the linear combinations of masses correspond to L and B global symmetries. They run only because these would-be symmetries are anomalous under $SU(2)_L$ and $U(1)_Y$. The other mass combinations can also be related to anomalous global symmetries of the MSSM.

⁶We also assume implicitly that the soft masses are close to diagonal in the super CKM basis, as they are quite constrained to be [164].

These mass combinations have the same one-loop RG running as certain combinations of masses involving only the first and second generations. For example, the $m_{B_3}^2$ combination runs in exactly the same way at one-loop as

$$m_{B_i}^2 = 2 m_{Q_i}^2 - m_{U_i}^2 - m_{D_i}^2, \quad (6.24)$$

for $i = 1, 2$. If these linear combinations are unequal at the low scale, the corresponding soft masses will be non-universal at the high scale. This holds in the MSSM, as well as in the presence of any new physics that is flavor universal and respects baryon number. On the other hand, $m_{B_3}^2 = m_{B_1}^2$ does not imply family-universal high scale masses. For example, within a $SO(10)$ GUT, a splitting between the soft masses of the $\mathbf{16}$'s containing the first, second, and third generations will not lead to a difference between the mass combinations in Eq. (6.23) at the low-scale. A similar conclusion holds for the mass combinations $m_{A_i}^2$.

In the case of $m_{X_3}^2$ and $m_{Y_3}^2$, it is less obvious what to compare them to. The trick here is to notice that in the absence of Yukawa couplings, $m_{H_d}^2$ runs in the same way as $m_{L_1}^2$ since they share the same gauge quantum numbers. If the S term vanishes as well, $m_{H_u}^2$ also has the same RG evolution as $m_{L_1}^2$. This motivates us to define

$$\begin{aligned} m_{X_i}^2 &= 2 m_{L_i}^2 - 3 m_{U_i}^2, \\ m_{Y_i}^2 &= 3 m_{D_i}^2, \end{aligned} \quad (6.25)$$

for $i = 1, 2$. These mass combinations can be compared with $m_{X_3}^2$ and $m_{Y_3}^2$ in much the same way as for $m_{B_i}^2$ and $m_{A_i}^2$ (although comparing the $m_{X_i}^2$'s is only useful for $S = 0$). They also correspond to anomalous global symmetries in the limit that the first and second generation Yukawa couplings vanish.

The mass combinations listed above can be useful if there is heavy new physics that hides the relationships between the high scale masses. For instance, suppose the high scale soft spectrum obtained using the MSSM RG equations applied to the measured soft scalar masses shows a large splitting between $m_{Q_3}^2$ and $m_{Q_1}^2$. If the corresponding splitting between $m_{B_3}^2$ and $m_{B_1}^2$ (at any scale) is very much smaller, this feature suggests that there is new physics that should have been included in the RG running, or that there exists a special relationship between $m_{Q_i}^2$, $m_{U_i}^2$, and $m_{D_i}^2$ at the high scale. A similar conclusion can be made for the other mass combinations.

6.2.3 Some Numerical Results

In our numerical analysis, we follow a similar procedure to the one used in the previous section. The MSSM running is performed at two-loop order, and we interface with Suspect 2.3.4 [120] to compute the low-scale threshold corrections. New physics, in the form of vector-like GUT multiplets at an intermediate scale is included only at the one-loop level. Unlike the previous section, we define our high-energy spectrum using a simple mSUGRA model in the $\Delta b \neq 0$ theory, and include the new physics effects in generating the low-energy spectrum. We then evolve this spectrum back up to the unification scale using the MSSM RG evolution, with $\Delta b = 0$. Our goal is to emulate evolving the MSSM soft parameters in the presence of unmeasured and unknown high-scale new physics.

The running of the soft masses with $N_{\mathbf{5} \oplus \bar{\mathbf{5}}} = 7$ sets of $\mathbf{5} \oplus \bar{\mathbf{5}}$ multiplets with an intermediate scale mass of $\tilde{\mu} = 10^{11}$ GeV is shown in Fig. 6.4 for the mSUGRA parameters $m_0 = 300$ GeV, $m_{1/2} = 700$ GeV, $\tan \beta = 10$, and $A_0 = 0$. These parameters are used to find the low energy spectrum, which is then RG evolved back up to the high scale with $\Delta b = 0$. From this figure, we see that a naïve MSSM extrapolation of the soft parameters (*i.e.* with $\Delta b = 0$) yields predictions

for the high-scale soft scalar masses that are significantly larger than the actual values. In the same way, the MSSM predicted values of the high-scale gaugino masses are smaller than the correct values, as can be seen in Fig. 6.3. Note that for $\tilde{\mu} = 10^{11}$ GeV, $N_{\mathbf{5} \oplus \bar{\mathbf{5}}} = 7$ is about as large as possible while still keeping the gauge couplings perturbatively small all the way up to M_{GUT} .

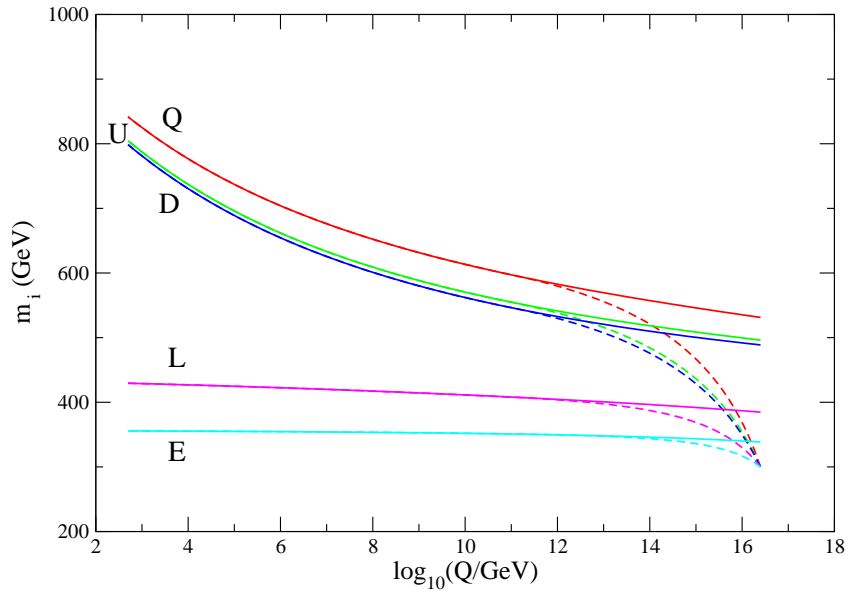


Figure 6.4: Running of the first generation soft scalar masses with $N_{\mathbf{5} \oplus \bar{\mathbf{5}}} = 7$ and $\tilde{\mu} = 10^{11}$ GeV for the mSUGRA input parameters $m_0 = 300$ GeV, $m_{1/2} = 700$ GeV, $\tan \beta = 10$, and $A_0 = 0$. The dashed lines show the actual running of these parameters, while the solid lines show the running from low to high using the RG equations of the MSSM, ignoring the additional heavy multiplets.

Besides confusing the relationship between the high scale gaugino and scalar soft masses, heavy GUT multiplets can also obscure the comparison of the high scale scalar masses from different generations. As discussed above, this arises from the backreaction in the Yukawa-

dependent terms in the RG equations for the third generation soft scalar masses. Numerically, we find that the splitting is quite small compared to the absolute scale of the masses for $\tilde{\mu} \geq 10^{11}$ GeV. This is illustrated in Fig. 6.5. We also find that an approximate preservation of universality persists for other values of m_0 , A_0 , and $\tan \beta$ as well. The reason for this appears to be that for $\tilde{\mu} \geq 10^{11}$ GeV, the Yukawa couplings are smaller than the gauge couplings by the time the new physics becomes relevant.

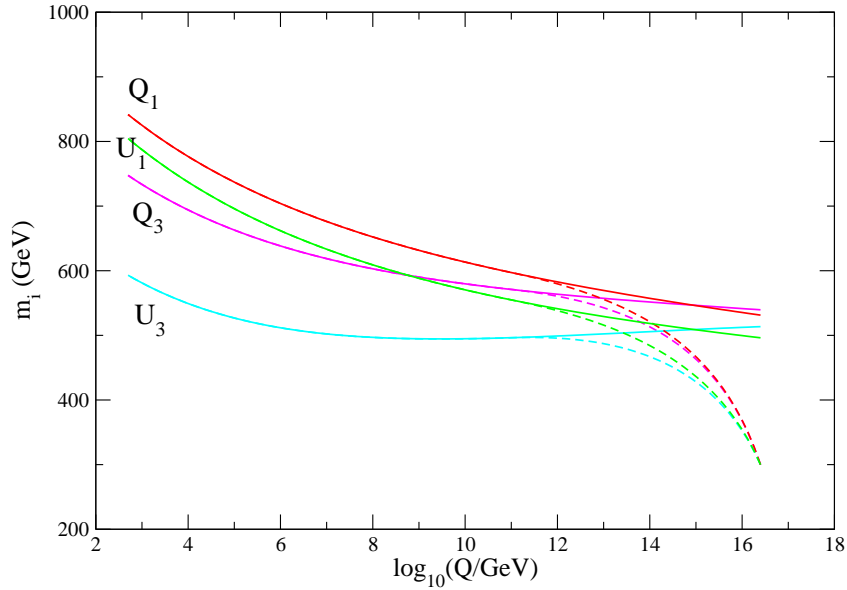


Figure 6.5: Running of the soft scalar masses of $Q_{1,3}$ and $U_{1,3}$ with $N_{\mathbf{5} \oplus \bar{\mathbf{5}}} = 7$ and $\tilde{\mu} = 10^{11}$ GeV for the mSUGRA input parameters $m_0 = 300$ GeV, $m_{1/2} = 700$ GeV, $\tan \beta = 10$, and $A_0 = 0$. The dashed lines show the actual running of these parameters, while the solid lines show the running from low to high using the RG equations of the MSSM, ignoring the additional heavy multiplets.

A much greater splitting between the high scale values of $m_{Q_1}^2$ and $m_{Q_3}^2$, and $m_{U_1}^2$ and $m_{U_3}^2$, is obtained for lower values of $\tilde{\mu}$. This effect is shown in Fig. 6.6 for $N_{\mathbf{5} \oplus \bar{\mathbf{5}}} = 3$ sets of $\mathbf{5} \oplus \bar{\mathbf{5}}$

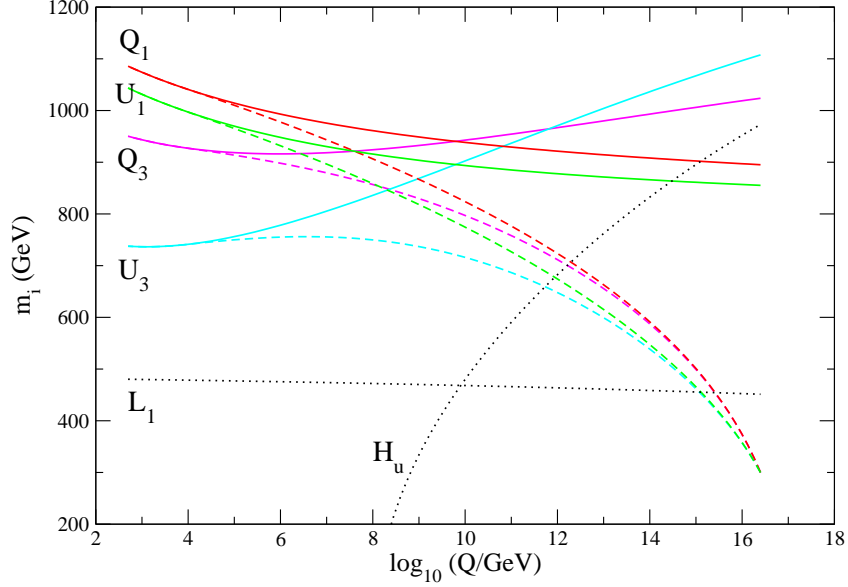


Figure 6.6: Running of the soft scalar masses of $Q_{1,3}$ and $U_{1,3}$ with $N_{\mathbf{5} \oplus \bar{\mathbf{5}}} = 3$ and $\tilde{\mu} = 10^4$ GeV for the mSUGRA input parameters $m_0 = 300$ GeV, $m_{1/2} = 700$ GeV, $\tan \beta = 10$, and $A_0 = 0$. The dashed lines show the actual running of these parameters, while the solid lines show the running from low to high using the RG equations of the MSSM, ignoring the additional heavy multiplets.

multiplets with an intermediate scale mass of $\tilde{\mu} = 10^4$ GeV, and the mSUGRA parameters $m_0 = 300$ GeV, $m_{1/2} = 700$ GeV, $\tan \beta = 10$, and $A_0 = 0$. The value of the gauge couplings at unification here is very similar to the $\tilde{\mu} = 10^{11}$ GeV and $N_{\mathbf{5} \oplus \bar{\mathbf{5}}} = 7$ case. As might be expected, the Yukawa-dependent terms in the soft scalar mass RG running become important at lower scales where the top Yukawa approaches unity.

It is also interesting to note that in both Figs. 6.5 and 6.6, the soft masses appear to take on family universal values, $m_{Q_1}^2 = m_{Q_3}^2$ and $m_{U_1}^2 = m_{U_3}^2$, at the same scale, near 10^{15} GeV in Fig. 6.5, and close to 10^{10} GeV in Fig. 6.6. It is not hard to show, using the mass combinations

in Eqs. (6.23,6.24,6.25), that this feature holds exactly at one-loop order provided $S = 0$, the high scale masses are family-universal, and the only relevant Yukawa coupling is that of the top quark. In this approximation, all the family-dependent mass splittings are proportional to $(m_{H_u}^2 - m_{L_1}^2)$, and hence vanish when $m_{H_u}^2 = m_{L_1}^2$. This relationship can be seen to hold approximately in Fig. 6.6, which also includes two-loop and bottom Yukawa effects.

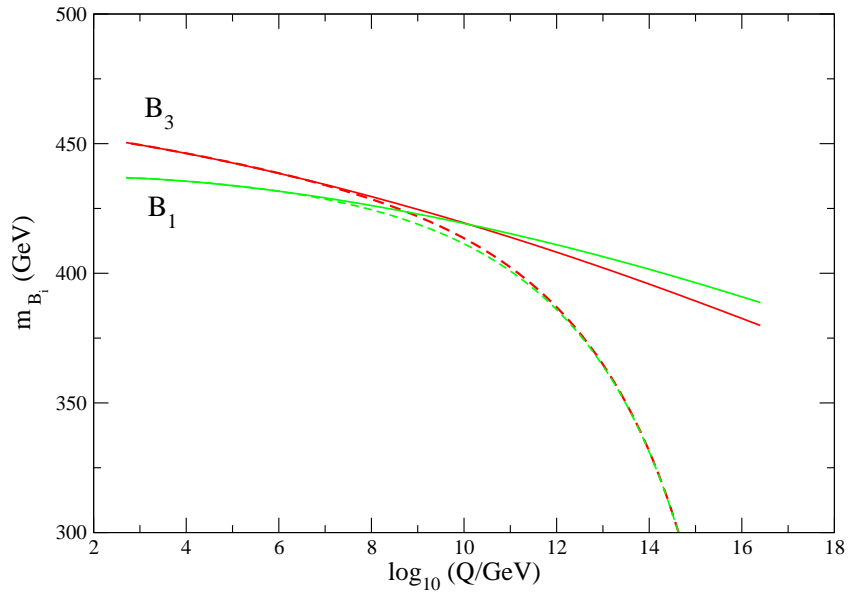


Figure 6.7: Running of the soft scalar mass combinations m_{B_3} and m_{B_1} with $N_{\mathbf{5} \oplus \bar{\mathbf{5}}} = 3$ and $\tilde{\mu} = 10^4$ GeV for the mSUGRA input parameters $m_0 = 300$ GeV, $m_{1/2} = 700$ GeV, $\tan \beta = 10$, and $A_0 = 0$. The dashed lines show the actual running of these parameters, while the solid lines show the running from low to high using the RG equations of the MSSM, ignoring the additional heavy multiplets. The small deviations in these figures arise from higher loop effects.

In Figs. 6.7 and 6.8 we show the running of the mass combinations $m_{B_{1,3}}$ and $m_{X_{1,3}}$ (where $m_i = m_i^2 / \sqrt{|m_i^2|}$) for $N_{\mathbf{5} \oplus \bar{\mathbf{5}}} = 3$ and $\tilde{\mu} = 10^4$ GeV with the high scale mSUGRA input values

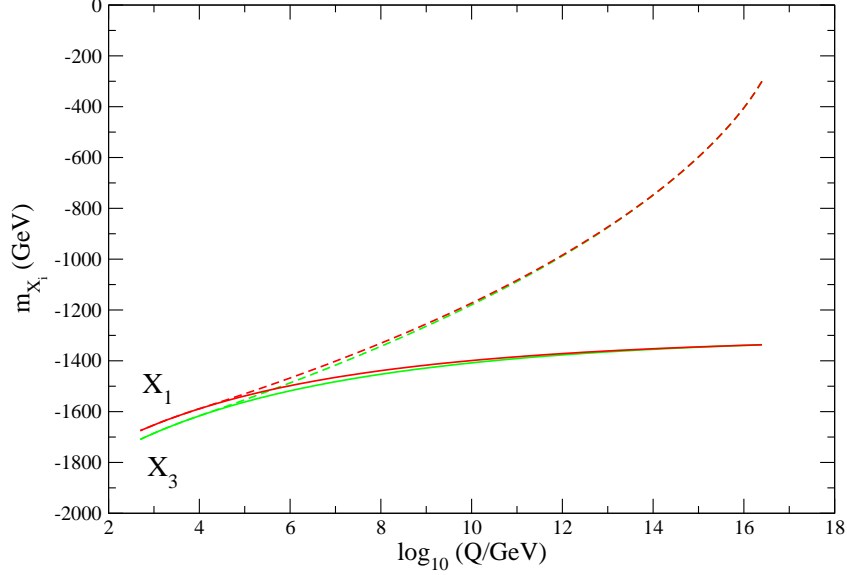


Figure 6.8: Running of the soft scalar mass combinations m_{X_3} and m_{X_1} with $N_{\mathbf{5} \oplus \bar{\mathbf{5}}} = 3$ and $\tilde{\mu} = 10^4$ GeV for the mSUGRA input parameters $m_0 = 300$ GeV, $m_{1/2} = 700$ GeV, $\tan \beta = 10$, and $A_0 = 0$. The dashed lines show the actual running of these parameters, while the solid lines show the running from low to high using the RG equations of the MSSM, ignoring the additional heavy multiplets. The small deviations in these figures arise from higher loop effects.

$m_0 = 300$ GeV, $M_{1/2} = 700$ GeV, $\tan \beta = 10$, and $A_0 = 0$. These figures also show the values of $m_{B_{1,3}}$ and $m_{X_{1,3}}$ that would be obtained by running up without including the effects of the heavy new physics. Comparing these figures to Figs. 6.5 and 6.6, it is apparent that the splittings between $m_{B_1}^2$ and $m_{B_3}^2$, and $m_{X_1}^2$ and $m_{X_3}^2$, are very much less than the high scale splittings between the Q and U soft masses.

These relationship between the B and X soft mass combinations from different families is a footprint left by the full theory (including the heavy GUT multiplets) on the low-energy spectrum. Since the scalar masses in the full theory are universal at the high scale, the low

scale splittings between the B and X soft mass combinations are very small. On the other hand, running the low scale Q and U scalar soft masses up within the MSSM does not suggest any form of family universality among these masses. Therefore, as we proposed above, the low-energy values of these particular combinations of soft scalar masses can provide evidence for heavy new physics.⁷

The analysis in this section shows that even though new physics in the form of additional heavy GUT multiplets can significantly disrupt the predictions for the high scale soft spectrum obtained by running in the MSSM, certain key properties about the input spectrum can still be deduced using collider scale measurements. Most significantly, the low-scale values of the gaugino masses and gauge couplings can be used to predict the approximate ratios of the high-scale values, provided gauge unification is preserved.

The effect of additional GUT multiplets on the scalar soft masses is more severe. Extrapolating the soft masses without including the contributions from the heavy GUT multiplets leads to a prediction for the input soft masses that are generally too low. The splittings between the soft masses from different generations can be shifted as well. Despite this, some of the flavor properties of the input soft mass spectrum can be deduced by comparing the evolution of the mass combinations in Eqs. (6.23), (6.24), and (6.25). For example, $m_{B_3}^2 = m_{B_1}^2$ and $m_{L_1}^2 = m_{L_3}^2$ suggests some form of flavor universality (or an embedding in $SO(10)$), even if the scalar masses extrapolated within the MSSM do not converge at M_{GUT} . We expect that these special mass combinations could prove useful for studying other types of heavy new physics as well.

⁷We have checked that the small splittings between m_{B_1} and m_{B_3} , as well as between m_{X_1} and m_{X_3} , arise from higher loop effects.

6.3 The (S)Neutrino Connection

We have seen in the previous sections that taking the unification of the gauge couplings as a serious theoretical input still leaves considerable room for experimental uncertainties and new physics to modify the extrapolated values of the soft supersymmetry breaking parameters at very high energies. For example, a Fayet-Iliopoulos D -term for hypercharge or additional complete GUT multiplets with intermediate scale masses will not disrupt gauge coupling unification, but will in general change the running of the parameters of the model. In this section we wish to study the effect of additional intermediate scale singlet matter with significantly large Yukawa couplings to the MSSM matter fields. A particularly well-motivated example of this, and the one we consider, are heavy singlet neutrino multiplets.

The observed neutrino phenomenology can be accommodated by extending the matter content of the MSSM to include at least two right handed (RH) neutrino supermultiplets that are singlets under the SM gauge group [143]. Throughout the present work, we will assume there are three RH neutrino flavors. The superpotential in the lepton sector is then given by

$$\mathcal{W}_l = \mathbf{y}_e L H_d E + \mathbf{y}_\nu L H_u N_R - \frac{1}{2} \mathbf{M}_R N_R N_R, \quad (6.26)$$

where L , E , and N_R are respectively the $SU(2)_L$ doublet, $SU(2)_L$ singlet, and neutrino chiral supermultiplets, each coming in three families. The quantities \mathbf{y}_e , \mathbf{y}_ν , and \mathbf{M}_R are 3×3 matrices in lepton family space. The H_d and H_u fields represent the usual Higgs multiplets. The gauge-invariant interactions among leptons and Higgs superfields are controlled by the family-space Yukawa matrices \mathbf{y}_e and \mathbf{y}_ν . As is conventional, we shall implicitly work in a basis where \mathbf{y}_e is diagonal. Since the N_R are singlets, we can also add to the superpotential a Majorana mass \mathbf{M}_R for these fields.

Assuming the eigenvalues of \mathbf{M}_R lie at a large intermediate mass scale, $10^9 - 10^{14}$ GeV, we can integrate out the RH neutrino superfields and obtain a term in the effective superpotential that leads to small neutrino masses through the see-saw mechanism,

$$\mathcal{W}_{m_\nu} = -\frac{1}{2}\mathbf{y}_\nu^T \mathbf{M}_R^{-1} \mathbf{y}_\nu LH_u LH_u. \quad (6.27)$$

After electroweak symmetry breaking, the neutrino mass matrix becomes

$$(\mathbf{m}_\nu) = \mathbf{y}_\nu^T \mathbf{M}_R^{-1} \mathbf{y}_\nu v_u^2, \quad (6.28)$$

where $v_u = \langle H_u \rangle$. The mass matrix can be conveniently diagonalized by the transformation

$$(\mathbf{m}_\nu^{\text{diag}}) = \mathbf{U}^T (\mathbf{m}_\nu) \mathbf{U}, \quad (6.29)$$

with \mathbf{U} a unitary matrix. This matrix \mathbf{U} is the usual PMNS matrix that describes lepton mixing relative to the flavor basis where the charged lepton Yukawa matrix \mathbf{y}_e is diagonal.

One can also write the neutrino Yukawa matrix as [167]

$$\mathbf{y}_\nu = \frac{1}{v_u} \sqrt{\mathbf{M}_R^{\text{diag}}} \mathbf{R} \sqrt{\mathbf{m}_\nu^{\text{diag}}} \mathbf{U}^\dagger \quad (6.30)$$

where $v_u = \langle H_u \rangle$ and R is a complex orthogonal matrix that parametrizes our ignorance of the neutrino Yukawas. As an estimate, Eq. (6.30) shows that the size of the neutrino Yukawa couplings will be on the order of

$$y_\nu \simeq \frac{0.57}{\sin \beta} \left(\frac{M_R}{10^{14} \text{GeV}} \right)^{\frac{1}{2}} \left(\frac{m_\nu}{0.1 \text{eV}} \right)^{\frac{1}{2}}. \quad (6.31)$$

Thus, the neutrino Yukawa couplings can take large $\mathcal{O}(1)$ values comparable to the top Yukawa coupling for $M_R \sim 10^{14}$ GeV. If this is the case, then above the see-saw mass threshold the effects on the RG running of the MSSM soft parameters due to the neutrino Yukawas can be substantial.

The addition of RH neutrinos to the MSSM can lead to lepton flavor violation (LFV) through the RG running of the off-diagonal slepton mass terms [168, 169]. In this work we will only consider simple scenarios of neutrino phenomenology in which the amount of lepton flavor violation induced by the heavy neutrino sector is small. However, the observation of LFV signals could potentially provide information about a heavy neutrino sector [168, 169, 170, 171]. Precision measurements of the slepton mass matrices can also be used to constrain possible heavy neutrino sectors [172, 173]. Heavy singlet neutrinos may also be related to the source of the baryon asymmetry through the mechanism of leptogenesis [174].

6.3.1 Running Up

The strategy we use in this section is similar to the one followed in the previous sections. We assume a universal high scale mass spectrum at M_{GUT} , and RG evolve the model parameters down to the low scale $M_{low} = 500 \text{ GeV}$ including the additional effects of the neutrino sector parameters. The resulting low scale spectrum is then run back up to M_{GUT} using the RG equations for the MSSM without including the neutrino sector contributions. As before, we use this procedure to illustrate the discrepancy between the extrapolated parameter values and their true values if the new physics effects are not included in the running.

To simplify the analysis, we make a few assumptions about the parameters in the neutrino sector. We choose the orthogonal matrix R to be purely real, and we take the heavy neutrino mass matrix \mathbf{M}_R to be proportional to the unit matrix, $\mathbf{M}_R = M_R \mathbf{I}$. We also take the physical neutrino masses to be degenerate. This allows us to write

$$\mathbf{y}_\nu = \frac{0.57}{\sin \beta} \left(\frac{M_R}{10^{14} \text{ GeV}} \right)^{\frac{1}{2}} \left(\frac{m_\nu}{0.1 \text{ eV}} \right)^{\frac{1}{2}} \mathbf{R} \mathbf{U}^\dagger := y_\nu \mathbf{R} \mathbf{U}^\dagger, \quad (6.32)$$

so that the neutrino Yukawa couplings have the form of a universal constant multiplying a

unitary matrix. To fix the value of y_ν , we will set $m_\nu = 0.1 \text{ eV}$.⁸ This choice is close to being as large as possible while remaining consistent with the cosmological bounds on the sum of the neutrino masses, $\sum_\nu < 0.68 \text{ eV}$ [175]. Note that larger values of the neutrino masses tend to maximize the size of the resulting neutrino Yukawa couplings.

We also need to impose boundary conditions on the RH sneutrino masses and trilinear couplings. We take these new soft parameters to have universal and diagonal boundary conditions at the unification scale,

$$m_{N_{ij}}^2 = m_0^2 \delta_{ij}, \quad \text{and} \quad a_{\nu_{ij}} = A_0 y_{\nu_{ij}}, \quad (6.33)$$

where m_0 and A_0 are the same universal soft scalar mass and trilinear coupling that we will apply to the MSSM fields in the analysis to follow. With these choices for the neutrino parameters, the effects of the neutrino sector on the (one-loop) RG running of the MSSM soft terms take an especially simple form. In particular, the amount of leptonic flavor mixing induced is expected to be very small, and the diagonal and universal form of the neutrino sector soft terms, Eq. (6.33), is approximately maintained at lower scales.

To illustrate the effects of the neutrino sector, we set the high scale spectrum to coincide with the SPS-5 benchmark point, and we extend the corresponding soft terms to the neutrino sector. The input values at M_{GUT} for this point are $m_0 = 150 \text{ GeV}$, $m_{1/2} = 300 \text{ GeV}$, $A_0 = -1000 \text{ GeV}$, and $\tan \beta = 5$ with μ positive. These input values tend to magnify the effects of the neutrino sector because the large value of A_0 feeds into the running of the soft masses. Large neutrino Yukawa couplings alter the running of the top Yukawa coupling as well.

⁸The diagonal neutrino mass matrix $\mathbf{m}_\nu^{\text{diag}}$ and the lepton mixing matrix \mathbf{U} are measured at low scales, and one should really evaluate them at the intermediate scale M_R by running the Yukawa couplings up [171]. Since we are most interested in the effect of the neutrino Yukawas after reaching the intermediate scale, we will neglect this additional running below M_R .

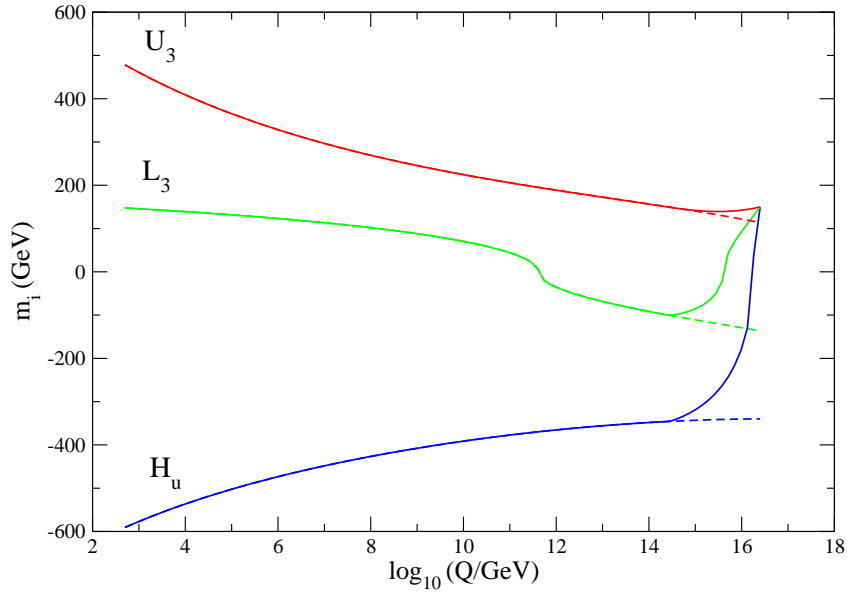


Figure 6.9: Running of the soft scalar masses of H_u , L_3 , and U_3 for SPS-5 input parameters at M_{GUT} with three additional heavy RH neutrinos of mass $M_R = 10^{14}$ GeV. The solid lines show the full running, including the neutrino sector effects, while the dashed lines show the low-to-high running of the soft masses in the MSSM, with the neutrino sector effects omitted.

Of the MSSM soft parameters, the greatest effects of the heavy neutrino sector are seen in the soft scalar masses and the trilinear A terms. The gaugino masses are only slightly modified. The evolution of the soft masses for the H_u , L_3 , and U_3 fields from low to high are shown in Fig. 6.9, both with and without including the effects of the neutrino sector for $M_R = 3 \times 10^{14}$ GeV. For this value of M_R and with $\tan \beta = 5$, the Yukawa coupling is close to being as perturbatively large as possible. The extrapolated values of $m_{H_u}^2$ and $m_{L_3}^3$ deviate significantly from the actual input values if the effects of the neutrino sector are not taken into account in the RG evolution. These fields are particularly affected because they couple directly

to the heavy neutrino states through the neutrino Yukawa coupling. The shift in the running of $m_{U_3}^2$ arises indirectly from the effect of the neutrino Yukawas on $m_{H_u}^2$ and the top Yukawa coupling y_t .

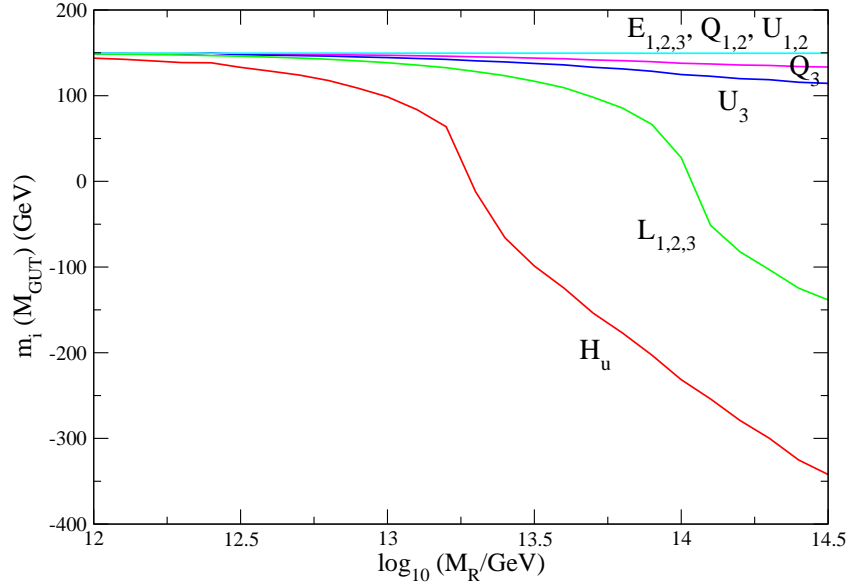


Figure 6.10: The high scale (M_{GUT}) values of the soft scalar masses extrapolated using the MSSM RG equations, without including neutrino sector effects. The low-scale (500 GeV) values of the soft masses used in the extrapolation were obtained from SPS-5 input parameters at M_{GUT} with three additional heavy RH neutrinos of mass M_R . The deviations from $m_i(M_{GUT}) = 150$ GeV represent the discrepancy between the MSSM extrapolated values and the correct value in the full theory with heavy RH neutrinos. These discrepancies are shown as a function of the heavy neutrino scale M_R .

In Fig. 6.10 we show the size of the discrepancies in the extrapolated high scale values of a few of the soft scalar masses if the neutrino sector effects are not included in the running. These discrepancies are plotted as a function of the heavy neutrino mass scale M_R . As above,

the high scale input spectrum consists of the SPS-5 values. Again, the soft masses $m_{H_u}^2$ and $m_{L_i}^2$ are altered the most, although the third generation squark soft masses also get shifted somewhat as a backreaction to the changes in $m_{H_u}^2$ and the top Yukawa coupling. This plot also shows that the sizes of the discrepancies remain quite small for M_R less than 10^{13} GeV. Values of M_R considerably less than this are favored if leptogenesis is to be the source of the baryon asymmetry [174]. Neutrino masses well below 0.1 eV would also lead to less pronounced deviations in the extrapolated soft masses.

The deviations induced by not including the new neutrino sector physics in the running take a similar form to those obtained by not taking account of heavy GUT multiplets. For both cases, the gaugino mass running is only modified in a very controlled way, while the soft scalar masses and trilinear couplings deviate more unpredictably. In particular, the high scale flavor structure of the soft masses can be obscured. With large neutrino Yukawa couplings, the third generation squark masses receive additional contributions to their running relative to the first and second generations due to the potentially large effect of the neutrino Yukawa couplings on $m_{H_u}^2$. The sizes of these additional family-dependent shifts tend to be fairly small, as can be seen in Fig. 6.10. Furthermore, these effects cancel out in the mass combinations $m_{B_i}^2$ defined in Eqs. (6.23) and (6.24), and we find $m_{B_1}^2 \simeq m_{B_3}^2$ at all scales, regardless of whether or not the neutrino effects are included. On the other hand, the running of $m_{A_3}^2$ relative to $m_{A_1}^2$, $m_{X_3}^2$ relative to $m_{X_1}^2$, and $m_{Y_3}^2$ relative to $m_{Y_1}^2$ need no longer coincide if there is a heavy neutrino sector.

Finally, let us also mention that for more general neutrino sector parameters than those we have considered, there can arise significant lepton flavor mixing couplings in the MSSM slepton soft terms from the RG running [168]. Measurements of this mixing in lepton flavor violating

processes can therefore provide an experimental probe of the heavy neutrino multiplets [168, 169, 170, 171]. A measured splitting among the three slepton masses $m_{L_i}^2$ would also constitute another indication of the existence of a neutrino sector with sizeable Yukawa couplings and nontrivial flavor structure. Both high and intermediate energy data may be complementary and very useful in extrapolating the MSSM soft terms to high energies.

6.4 Putting it All Together: an Example

In this section we summarize some of our previous results with an explicit example. We begin with a low energy spectrum of MSSM soft supersymmetry breaking parameters that we assume to have been measured at the LHC to an arbitrarily high precision. We then attempt to deduce the essential features of the underlying high scale structure by running the low energy parameters up and applying some of the techniques discussed in the previous sections.

In our example we will make the following assumptions:

- The possible types of new physics beyond the MSSM are:
 - Complete $\mathbf{5} \oplus \bar{\mathbf{5}}$ GUT multiplets with a common (SUSY) mass scale $\tilde{\mu}$.
 - Three families of heavy singlet (RH) neutrinos at the mass scale M_R .
 - A fundamental hypercharge D term.

In the case of complete GUT multiplets, we will assume further that there are no superpotential interactions with the MSSM states as in Section 6.2. For heavy RH neutrinos, we will make the same set of assumptions about the form of the mixing and mass matrices as in Section 6.3.

- The high scale spectrum has the form of a minimal SUGRA model (up to the scalar mass shifts due to a hypercharge D -term) at the high scale $M_{GUT} \simeq 2.5 \times 10^{16}$ GeV.
- This mSUGRA spectrum also applies to the soft parameters corresponding to any new physics sectors. For example, a trilinear A term in the RH neutrino sector has the form $\mathbf{a}_\nu = A_0 \mathbf{y}_\nu$ at M_{GUT} , where A_0 is the universal trilinear parameter.

These assumptions are not entirely realistic, but they make the analysis tractable. Moreover, even though this exercise is highly simplified compared to what will be necessary should the LHC discover supersymmetry, we feel that it illustrates a number of useful techniques that could be applied in more general situations. With this set of assumptions, the underlying free parameters of the theory are:

$$m_0, \quad m_{1/2}, \quad A_0, \quad \xi, \quad N_{\mathbf{5} \oplus \bar{\mathbf{5}}}, \quad \tilde{\mu}, \quad M_R. \quad (6.34)$$

where m_0 , $m_{1/2}$ and A_0 are common mSUGRA inputs at M_{GUT} , ξ is the fundamental hypercharge D term, $N_{\mathbf{5} \oplus \bar{\mathbf{5}}}$ is the number of additional $\mathbf{5} \oplus \bar{\mathbf{5}}$ multiplets in the theory with a supersymmetric mass $\tilde{\mu}$, and M_R is the heavy neutrino scale.

6.4.1 Step 1: Running Up in the MSSM

As a first step, we run the low energy spectrum up to the high scale M_{GUT} using the RG equations for the MSSM, without including any potential new physics effects. The low energy MSSM soft spectrum we consider, defined at the low scale $M_{low} = 500$ GeV, is given in Table 6.1. In addition to these soft terms, we also assume that $\tan \beta = 7$ has been determined, and that the first and second generation soft scalar masses are equal. With this set of soft terms, we have verified that the low energy superpartner mass spectrum is phenomenologically

acceptable using SuSpect 2.3.4 [120]. The lightest Higgs boson mass is 114 GeV for a top quark mass of $m_t = 171.4$ GeV.

Even before extrapolating the soft parameters, it is possible to see a number of interesting features in the spectrum. The most obvious is that the low scale gaugino masses have ratios close to $M_1 : M_2 : M_3 \simeq 1 : 2 : 6$. This suggests that the high scale gaugino masses have a universal value $m_{1/2}$, and provides further evidence for gauge unification. The low-energy value of the S term, as defined in Eq. (6.2), is also non-zero and is in fact quite large, $S(M_{low}) \simeq (620 \text{ GeV})^2$. This indicates that there are significant contributions to the effective hypercharge D term in the high scale theory. Since the S term is non-zero, it is also not surprising that $S_{B-L} \simeq (446 \text{ GeV})^2$, as defined in Eq. (6.10), is non-zero as well.

The values of the soft parameters extrapolated to M_{GUT} within the MSSM are listed in Table 6.1. The MSSM running of the soft scalar masses is also shown in Fig. 6.11. As anticipated, the gaugino masses unify approximately to a value $M_1 \simeq M_2 \simeq M_3 \simeq m_{1/2} = 350$ GeV at M_{GUT} . The high scale pattern of the soft scalar masses (and the trilinear A terms) shows less structure, and is clearly inconsistent with mSUGRA high scale input values.

Since $S(M_{low})$ is large and non-zero, we are motivated to look for a hypercharge D term contribution to the soft scalar masses. Such a contribution would cancel in the mass combinations

$$\Delta m_{ij}^2 = (Y_j m_i^2 - Y_i m_j^2)/(Y_j - Y_i). \quad (6.35)$$

If the high scale soft masses have the form $m_i^2 = m_0^2 + \sqrt{\frac{3}{5}} g_1 Y_i \xi$, as in mSUGRA with a hypercharge D term, these combinations will all be equal to m_0^2 at this scale. The high scale soft masses here, extrapolated within the MSSM, exhibit no such relationship. Even so, these mass combinations will prove useful in the analysis to follow.

It is also interesting to compare the pairs of mass combinations $m_{A_i}^2$, $m_{B_i}^2$, $m_{X_i}^2$, and $m_{Y_i}^2$ for $i = 1, 3$, as defined in Section 6.2. Of these, the most useful pair is $m_{B_1}^2$ and $m_{B_3}^2$. At the low and high scales (extrapolating in the MSSM) this pair obtains the values

$$\begin{aligned} m_{B_1}^2(M_{low}) &\simeq (441 \text{ GeV})^2, & m_{B_3}^2(M_{low}) &\simeq (452 \text{ GeV})^2, \\ m_{B_1}^2(M_{GUT}) &\simeq (392 \text{ GeV})^2, & m_{B_3}^2(M_{GUT}) &\simeq (392 \text{ GeV})^2. \end{aligned} \quad (6.36)$$

The near equalit

comparison,

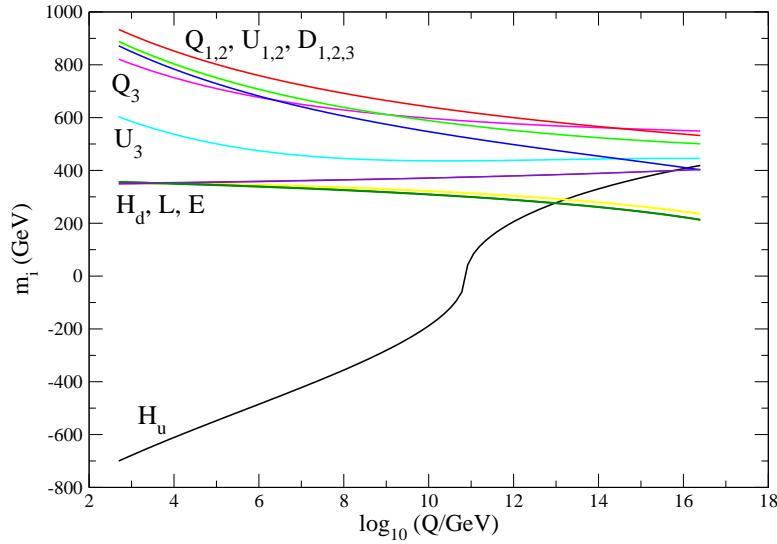


Figure 6.11: Scale dependence of the soft scalar masses for the input soft parameters given in Table 6.1. No new physics effects beyond the MSSM were included in the running.

there is a significant inter-family splitting that occurs between the high scale soft masses of U_1 and U_3 ,

$$m_{U_1}^2(M_{GUT}) = (402 \text{ GeV})^2, \quad m_{U_3}^2(M_{GUT}) = (445 \text{ GeV})^2. \quad (6.37)$$

This apparent fine-tuning among the soft masses that make up the B -type combinations is suggestive of an underlying structure in the theory. However, based on the values of the

individual soft masses extrapolated within the MSSM, such a structure is not obvious. Instead, we can interpret this as a hint for new intermediate scale physics.

Without our guiding assumptions, the high scale spectrum listed in Table 6.1 obtained by running up in the MSSM does not exhibit any particularly remarkable features aside from the universality of the gaugino masses. Even so, the curious relationship between the $m_{B_1}^2$ and $m_{B_3}^2$ mass combinations provides a strong hint that we are missing something. It is not clear how strong this hint would have been had we also included reasonable uncertainties in the low scale parameter values.

6.4.2 Step 2: Adding GUT Multiplets

As a first attempt to fit the low energy soft spectrum to the class of models outlined above, let us consider adding additional vector-like GUT multiplets to the theory at the scale $\tilde{\mu}$. We try this first because, as we found in Sections 6.2 and 6.3, the contributions from such multiplets are potentially much larger than those due to heavy singlet neutrinos.

In adding the new GUT multiplets, we will make use of our starting assumptions about the possible forms of new physics. Given the large value of $S(M_{low})$, there appears to be significant hypercharge D term. Also from our assumptions, this D term will contribute to the soft scalar masses of the heavy GUT multiplets, which will in turn feed into the running of the MSSM scalar masses through the S term above the scale $\tilde{\mu}$. For this reason, it is safer to work with the mass differences defined in eq. (6.35) whose running (to one-loop) does not depend on the S -term.

Among the low scale soft masses listed in Table 6.1, we expect the slepton soft mass $m_{E_1}^2$ to be among the easiest to measure, and the least susceptible to new physics effects. Thus, we

will use it as a reference mass in all but two of the differences we choose. The mass differences we consider are

$$\begin{aligned}
&\Delta m_{Q_1 E_1}^2, \quad \Delta m_{U_1 E_1}^2, \quad \Delta m_{D_1 E_1}^2, \quad \Delta m_{L_1 E_1}^2 \\
&\Delta m_{H_d E_1}^2, \quad \Delta m_{H_u E_1}^2, \quad \Delta m_{Q_1 D_1}^2, \quad \Delta m_{Q_3 D_1}^2, \\
&\Delta m_{Q_3 E_1}^2, \quad \Delta m_{U_3 E_1}^2, \quad \Delta m_{D_3 E_1}^2, \quad \Delta m_{L_3 E_1}^2.
\end{aligned} \tag{6.38}$$

These depend on several independent mass measurements.

In Fig. 6.12 we show the high scale values of these mass differences obtained by running up the low scale soft masses while including a given number of $N_{\mathbf{5} \oplus \bar{\mathbf{5}}}$ additional $\mathbf{5} \oplus \bar{\mathbf{5}}$ GUT multiplets at the scale $\tilde{\mu}$. For each of the plots, nearly all the mass differences unify approximately, as they would be expected to do if the underlying theory has a mSUGRA spectrum. The best agreement with a mSUGRA model is obtained for $N_{\mathbf{5} \oplus \bar{\mathbf{5}}} = 5$ with $\tilde{\mu} = 10^{10}$ GeV. (More precisely, the agreement is obtained when a shift $\Delta b = -5$ is applied to the gauge beta function coefficients b_i at the scale $\tilde{\mu} = 10^{10}$ GeV).

Taking $N_{\mathbf{5} \oplus \bar{\mathbf{5}}} = 5$ and $\tilde{\mu} = 10^{10}$ GeV, the high scale values of the mass differences are

$$\begin{aligned}
\Delta m_{Q_1 E_1}^2 &= (200 \text{ GeV})^2 = \Delta m_{U_1 E_1}^2 = \Delta m_{D_1 E_1}^2 = \Delta m_{H_d E_1}^2 \\
\Delta m_{Q_3 E_1}^2 &= (197 \text{ GeV})^2, \quad \Delta m_{D_3 E_1}^2 = (200 \text{ GeV})^2 \\
\Delta m_{H_u E_1}^2 &= -(157 \text{ GeV})^2, \quad \Delta m_{L_{1,3} E_1}^2 = (183 \text{ GeV})^2
\end{aligned} \tag{6.39}$$

Most of these high scale values coincide, suggesting a mSUGRA value for the universal soft scalar mass of about $m_0 = 200$ GeV. On the other hand, the soft mass differences involving the H_u and L fields show a significant deviation from this near-universal value. Based on the results of Section 6.3, these are precisely the scalar masses that are most sensitive to a heavy singlet neutrino sector.

Using this same choice of new physics parameters, we can also estimate the values of the

other mSUGRA parameters. Heavy singlet neutrinos are not expected to significantly alter the running of the gaugino soft mass parameters. If we run these up to M_{GUT} including $N_{\mathbf{5} \oplus \bar{\mathbf{5}}} = 5$ additional GUT multiplets at $\tilde{\mu} = 10^{10}$ GeV, we find $m_{1/2} \simeq 700$ GeV. Doing the same for the trilinear couplings, we do not find a unified high scale value for them. Instead, we obtain $A_t(M_{GUT}) = -401$ GeV, $A_\tau = -407$ GeV, and $A_b = -500$ GeV. This is not surprising since a heavy RH neutrino sector would be expected to primarily modify A_t and A_τ , while having very little effect on A_b . Thus, we also expect $A_0 \simeq -500$ GeV.

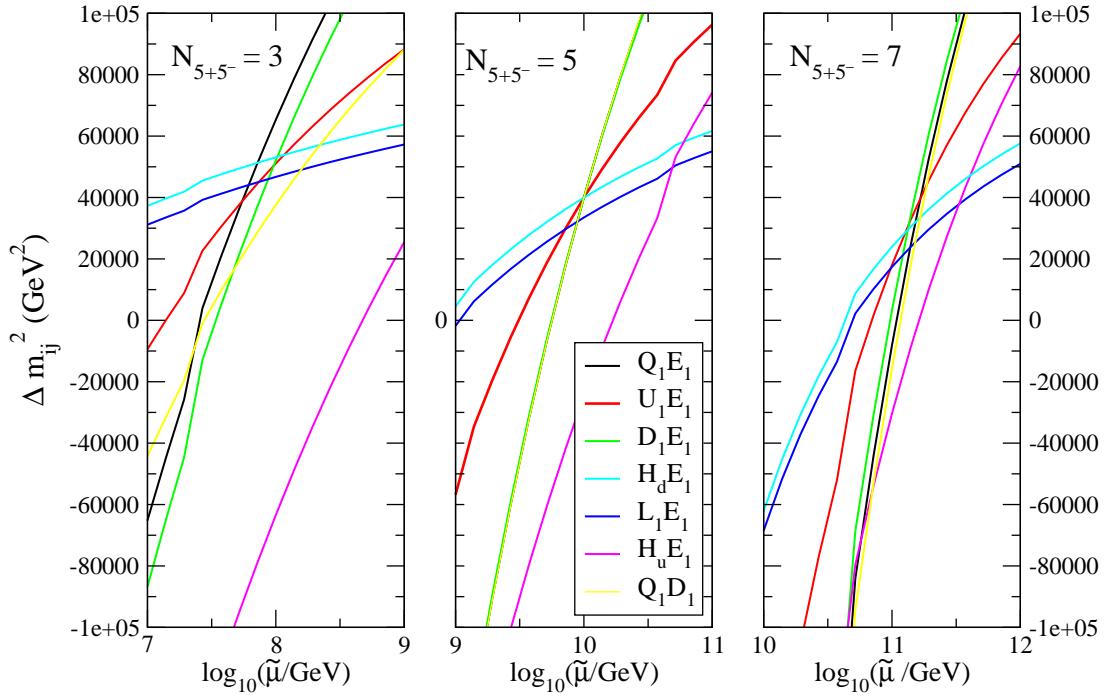


Figure 6.12: High scale values for the soft scalar mass differences Δm_{ij}^2 defined in Eq. (6.38) as a function of the mass scale $\tilde{\mu}$ of the $N_{\mathbf{5} \oplus \bar{\mathbf{5}}}$ heavy GUT multiplets for $N_{\mathbf{5} \oplus \bar{\mathbf{5}}} = 3, 5, 7$.

It is possible to estimate the value of the hypercharge D term as well. Using the hypothesis

$m_i^2 = m_0^2 + \sqrt{\frac{3}{5}} g_1 Y_i \xi$ at the high scale, we find

$$\xi(M_{GUT}) = \sqrt{\frac{5}{3}} \frac{1}{g_1} (m_{E_1}^2 - m_{H_d}^2) / (Y_E - Y_{H_d}) \simeq (494 \text{ GeV})^2. \quad (6.40)$$

We obtain similar values from the corresponding combinations of other mass pairs with the exception of L and H_u . Based on our previous findings, we suspect that the L and H_u soft masses are modified by a heavy RH neutrino sector.

Note that had we included experimental and theoretical uncertainties it would have been considerably more difficult to distinguish different values of $N_{\mathbf{5} \oplus \bar{\mathbf{5}}}$ and $\tilde{\mu}$. Instead of finding a single value for $\mathbf{5} \oplus \bar{\mathbf{5}}$ and a precise value for $\tilde{\mu}$, it is likely that we would have only been able to confine $N_{\mathbf{5} \oplus \bar{\mathbf{5}}}$ and $\tilde{\mu}$ to within finite ranges.

6.4.3 Step 3: Adding a Heavy Neutrino Sector

By adding $N_{\mathbf{5} \oplus \bar{\mathbf{5}}} = 5$ complete $\mathbf{5} \oplus \bar{\mathbf{5}}$ multiplets at the scale $\tilde{\mu} = 10^{10}$ GeV and a hypercharge D term, we are nearly able to fit the low scale spectrum given in Table 6.1 to a mSUGRA model with $m_0 = 200$ GeV, $m_{1/2} = 700$ GeV, and $A_0 = -500$ GeV. However, there are several small deviations from this picture, most notably in the soft masses for H_u and L as well as the trilinear couplings A_t and A_τ . We attempt to fix these remaining discrepancies by including heavy RH neutrinos at the scale M_R .

Given our initial assumptions about the form of a possible RH neutrino sector, the only independent parameter in this sector is the heavy mass scale M_R . To investigate the effects of RH neutrinos, we examine the high scale values of the mass differences given in Eq. (6.35) for the third generation scalars and H_u , using $m_{E_1}^2$ as a reference mass. We add a RH neutrino sector with heavy mass M_R and run the low scale parameters listed in Table 6.1 subject to the additional neutrino effects, as well as those from $N_{\mathbf{5} \oplus \bar{\mathbf{5}}} = 5$ heavy GUT multiplets with

$\tilde{\mu} = 10^{10}$ GeV. The result is shown in Fig. 6.13, in which we scan over M_R . This plot shows that if we include heavy RH neutrinos at the mass scale near $M_R = 10^{14}$ GeV, all the mass differences will flow to a universal value of about $m_0 = 200$ GeV at the high scale.

We can further confirm this result by examining the high scale trilinear couplings obtained by this procedure. These also attain a universal value, $A_0 = -500$ GeV, at the high scale for $M_R = 10^{14}$ GeV as shown in Figure 6.14. These universal values are consistent with those we hypothesized before the inclusion of heavy neutrino sector effects. Similarly, we can also study the value of ξ obtained using Eq. (6.40), but using the high scale L and H_u soft masses computed by including heavy RH neutrinos in their RG evolution. As before, we obtain a value $\xi \simeq (494 \text{ GeV})^2$.

6.4.4 Results

We have succeeded in deducing a high scale mSUGRA model augmented by heavy new physics effects that reproduces the soft spectrum in Table 6.1. The relevant parameter values are:

$$\begin{aligned}
 m_0 &= 200 \text{ GeV}, & m_{1/2} &= 700 \text{ GeV}, & A_0 &= -500 \text{ GeV}, \\
 N_{\mathbf{5} \oplus \bar{\mathbf{5}}} &= 5, & \tilde{\mu} &= 10^{10} \text{ GeV}, \\
 M_R &= 10^{14} \text{ GeV}, & \xi &= (494 \text{ GeV})^2.
 \end{aligned} \tag{6.41}$$

Our example did not include potential uncertainties in the input soft parameter values. It is likely that such uncertainties would make the analysis more challenging.

Running the low scale soft parameters up to M_{GUT} within the MSSM, and without including any new physics, we obtained a reasonable but mostly unremarkable high scale soft spectrum. The most obvious feature of this spectrum is the unification of the gaugino masses. A more subtle aspect of the high scale spectrum is the small splitting between $m_{B_1}^2$ and $m_{B_3}^2$ relative to

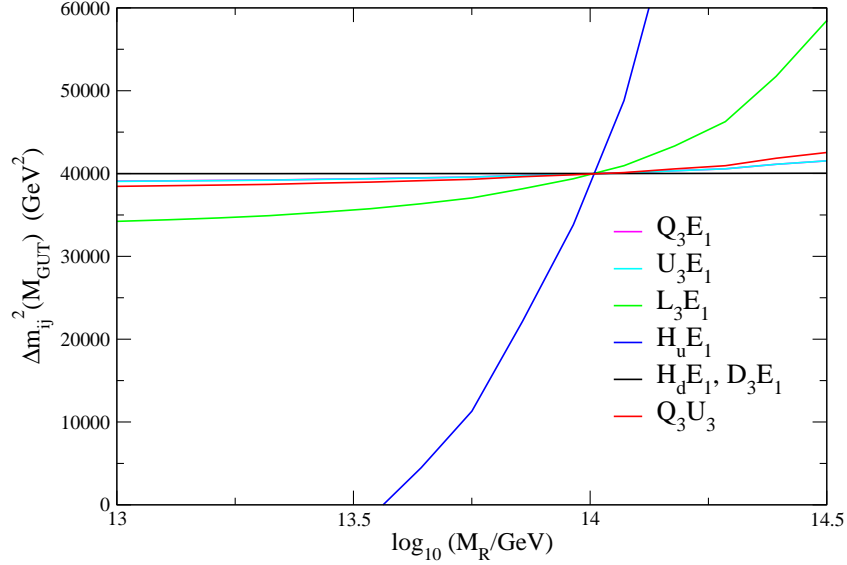


Figure 6.13: High scale values for third family and Higgs boson soft scalar mass differences Δm_{ij}^2 (as defined in Eq. (6.35)) as a function of the mass scale M_R of the heavy RH neutrinos. $N_{\mathbf{5} \oplus \bar{\mathbf{5}}} = 5$ GUT multiplets were included in the running above the scale $\tilde{\mu} = 10^{10}$ GeV.

that between the $m_{Q_1}^2$ and m_{Q_3} , and $m_{U_1}^2$ and $m_{U_3}^2$. This feature hinted at an underlying family-universal flavor spectrum obscured by new physics effects. It is not clear whether this hint would survive in a more complete treatment that included uncertainties in the input parameter values. By adding new physics, in the form of heavy GUT multiplets and RH neutrinos, a simple mSUGRA structure emerged.

6.5 Summary

If supersymmetry is discovered at the LHC, the primary challenge in theoretical particle physics will be to deduce the source of supersymmetry breaking. By doing so, we may perhaps

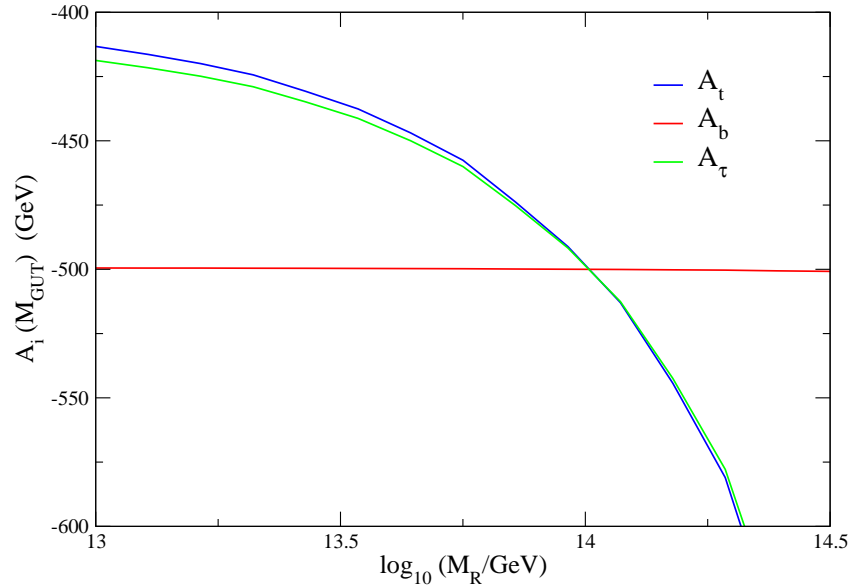


Figure 6.14: High scale values for the soft trilinear A terms as a function of the mass scale of the heavy RH neutrinos. $N_{\mathbf{5} \oplus \bar{\mathbf{5}}} = 5$ GUT multiplets were included in the running above the scale $\tilde{\mu} = 10^{10}$ GeV.

learn about the more fundamental theory underlying this source. In most models of supersymmetry breaking, the relevant dynamics take place at energies much larger than those that will be directly probed by the LHC. It is therefore likely that the soft supersymmetry breaking parameters measured by experiment will have to be extrapolated to higher scales using the renormalization group. Given the apparent unification of gauge couplings in the MSSM only slightly below M_{Pl} , we may hope that there is little to no new physics between the LHC scale and the supersymmetry breaking scale so that such an extrapolation can be performed in a straightforward way.

Gauge unification still allows for some types of new physics at intermediate scales such

as complete GUT multiplets and gauge singlets. If this new physics is present, RG evolving the MSSM soft parameters without including the new physics effects can lead to an incorrect spectrum of soft parameters at the high scale. Even without new intermediate physics, if some of the MSSM soft parameters are only poorly determined at the LHC, or not measured at all, there can arise significant uncertainties in the RG running of the soft masses that have been discovered.

In the present work we have investigated both of these potential obstacles to running up in the MSSM. The soft scalar masses are particularly sensitive to these effects, but we find that the gaugino soft masses, and their ratios in particular, are considerably more robust. If any one of the scalar soft masses goes unmeasured at the LHC, the running of the remaining these soft terms can be significantly modified by the effects of the hypercharge S term. These effects are especially severe for the slepton soft masses, which otherwise do not tend to run very strongly at all. We find that the uncertainties due to the S term can be avoided if we consider the soft mass differences $(Y_j m_i^2 - Y_i m_j^2)$, where Y_i denotes the hypercharge of the corresponding field. If all the soft mass are measured, the soft scalar mass combinations S and S_{B-L} , defined in Eqs. (6.2) and (6.10), provide useful information about potential GUT embeddings of the theory.

We have also investigated the effects of two plausible types of new physics beyond the MSSM that preserve consistency with gauge unification; namely complete vector-like GUT multiplets and heavy singlet neutrinos. In the case of complete GUT multiplets, extrapolating the measured low-energy soft parameter values without including the additional charged matter in the RG running leads to high scale predictions for the gaugino masses that are too small, and soft scalar masses that are too large. Even so, the ratios of the gaugino masses at the high scale

are not modified at leading order, and can be predicted from the low-energy measured values provided gauge unification occurs. The extrapolated values of the scalar masses are shifted in more complicated ways, and relationships such as family universality at the high-scale can be obscured. Despite this, certain hints about the underlying flavor structure of the soft masses can still be deduced from the properties of special linear combinations of the soft masses, such as $(2m_{Q_3}^2 - m_{U_3}^2 - m_{D_3}^2)$ relative to $(2m_{Q_1}^2 - m_{U_1}^2 - m_{D_1}^2)$.

The running of the MSSM soft masses can also be modified if there are heavy singlet neutrino chiral multiplets in the theory. These can induce small masses for the standard model neutrinos through the see-saw mechanism. If the singlet neutrino scale is very heavy, greater than about 10^{13} GeV, the corresponding neutrino Yukawa couplings can be large enough to have a significant effect on the running of the soft masses of H_u and L . We have studied the size of these effects, as well as the shifts in the other soft masses. The extrapolated values of the gaugino masses and the squark soft masses are only weakly modified by heavy neutrino sector effects.

In Section 6.4 we applied the methods described above to a specific example. In this example, the scalar masses have a common high scale value, up to a hypercharge D term. However, because of the presence of heavy new physics, this simple structure does not emerge when the low scale soft scalar masses are extrapolated up to M_{GUT} using the RG equations of the MSSM. Based on the low-energy spectrum alone, we were able to deduce the presence of the hypercharge D term. The presence of additional new physics was suggested by the fact that the splitting between $m_{U_3}^2$ and $m_{U_1}^2$ was considerably larger than the related splitting between $m_{B_3}^2$ and $m_{B_1}^2$. By studying the scalar mass combinations of Eq. (6.35) and including heavy GUT multiplets and a right-handed neutrino sector, we were able to reproduce the low-energy

soft spectrum with an underlying mSUGRA model.

One can also invert this perspective of overcoming new physics obstacles, and instead view these obstacles as providing information and opportunities. As the example of Section 6.4 illustrates, analyses of the kind we consider here probe new physics in indirect ways that can lead to convincing arguments for its existence or absence. Such analyses may be the main way to learn about new physics that cannot be studied directly.

If the LHC discovers new physics beyond the standard model, it will be a challenge to extract the Lagrangian parameters from the data. It may also be difficult to correctly extrapolate these parameters to higher scales in order to deduce the underlying theory that gives rise to the low energy Lagrangian. In the present work we have begun to study this second aspect of the so-called LHC inverse problem, and we have found a few techniques to address some of the potential obstacles. However, our study is only a beginning. We expect that a number of additional techniques for running up could be discovered with more work. A similar set of techniques could also be applied to understanding the high scale origin of other types of new physics beyond the standard model. These techniques deserve further study.

Soft Parameter	Low Scale Value (GeV)	High Scale Value (GeV)
M_1	146	356
M_2	274	355
M_3	859	370
A_t	-956	-766
A_b	-1755	-818
A_τ	-737	-524
m_{H_u}	-700	419
m_{H_d}	350	236
m_{Q_3}	821	549
m_{U_3}	603	445
m_{D_3}	884	501
m_{L_3}	356	213
m_{E_3}	349	404
m_{Q_1}	934	532
m_{U_1}	872	402
m_{D_1}	888	501
m_{L_1}	357	213
m_{E_1}	352	404

Table 6.1: The low-energy scale ($M_{low} = 500$ GeV) soft supersymmetry breaking spectrum used in our analysis. The soft scalar masses listed in the table correspond to the signed square roots of the actual masses squared. In this table we also the high scale values of these soft parameters obtained by running them up to $M_{GUT} \simeq 2.5 \times 10^{16}$ GeV using the RG evolution appropriate for the MSSM.

CHAPTER VII

Conclusions

The focus of this thesis has been the Deeper Inverse Problem. It has proposed a pragmatic approach to attacking this important problem and has studied the various steps which have to be completed in order to address the deeper inverse problem in a meaningful way. In this regard, two classes of string/ M theory constructions – Type IIA intersecting D-brane constructions on toroidal orientifolds and M theory constructions on singular G_2 holonomy manifolds, were studied with particular emphasis on their implications for low-energy physics. The effective four-dimensional theory resulting from both these constructions fits within the framework of low-energy supersymmetry. Then, predictions for LHC signatures for many classes of string-motivated constructions in the literature were studied. The effective theory of all the studied constructions lies within the framework of low-energy supersymmetry; this was done because low-energy supersymmetry seems to provide the most natural and appealing solution to the hierarchy problem. It was shown that it is possible to distinguish microscopic constructions on the basis of their patterns of experimental observables (here LHC signatures) and that, more importantly, the origin of distinguishability can be understood in terms of their underlying theoretical structure. Finally, a more bottom-up approach of going to theory from data was

studied within the framework of low-energy supersymmetry and gauge coupling unification and it was shown that even though many obstacles can make it very difficult to accurately determine the nature of the high scale theory, it is still possible to get some insight about it.

The techniques developed and results obtained in this thesis will be very important in making further progress on the deeper inverse problem. Moreover, these can be systematically improved to make the approach more sophisticated. String/ M theory constructions should be made more holistic in the sense that they address all relevant issues in particle physics and cosmology. Creative thinking is required to identify more experimental observables which probe features of the underlying theory. A few such observables were indeed found in the studies above, many more should be identified. More techniques for correctly identifying the high-scale structure of the theory from low scale data should be developed.

The results obtained in this thesis give us hope and confidence that string phenomenology is a useful and illuminating exercise. In the presence of a vast landscape of four dimensional string vacua and the absence of a dynamical vacuum selection principle, the most pragmatic approach one can take (and which is proposed by the thesis) is to compute predictions for low energy experimental observables for as many classes of realistic string vacua as possible and try to learn how information from experimental data may favor some regions of the M-theory amoeba over others. Doing so will lead to a deeper understanding of string/ M theory, and could be crucial to learning how or if string/ M theory can be related to the real world.

APPENDICES

APPENDIX A

Some Soft Supersymmetry Breaking Parameters for Intersecting D-brane Models

Here, we list the formulas for the soft scalar mass parameters and the trilinear parameters. It turns out that for the matter content in Table 2, we have the following independent soft parameters :

- Trilinear parameters (A):

$$\begin{aligned}
 A_{Q_L H_u U_R} &= \frac{-\sqrt{3}m_{3/2}}{4\pi} [2\pi(\Theta_2 + \Theta_3) + [(\Theta_3 - \Theta_2) (\Psi(\theta_{ab}^2) + \Psi(\theta_{ab}^3) - \Psi(\theta_{ca}^2) - \Psi(\theta_{ca}^3)) \\
 &\quad + \Theta_1 (\Psi(\theta_{ab}^2) - \Psi(\theta_{ab}^3) - \Psi(\theta_{ca}^2) + \Psi(\theta_{ca}^3))] \sin(2\pi\alpha)] \quad (\text{A.1})
 \end{aligned}$$

$$\begin{aligned}
 A_{Q_L H_d D_R} &= -\frac{\sqrt{3}m_{3/2}}{4\pi} [2\pi(\Theta_2 + \Theta_3) + [(\Theta_3 - \Theta_2) (\Psi(\theta_{ab}^2) + \Psi(\theta_{ab}^3) - \Psi(\theta_{c^*a}^2) - \Psi(\theta_{c^*a}^3)) \\
 &\quad + \Theta_1 (\Psi(\theta_{ab}^2) - \Psi(\theta_{ab}^3) - \Psi(\theta_{c^*a}^2) + \Psi(\theta_{c^*a}^3))] \sin(2\pi\alpha)] \quad (\text{A.2})
 \end{aligned}$$

$$A_{Q_L H_d D_R} = A_{LH_d E_R}; \quad A_{Q_L H_u U_R} = A_{LH_u N_R}$$

- Scalar Mass parameters (\tilde{m}^2):

$$\begin{aligned}
\tilde{m}_{QL}^2 &= \frac{-m_{3/2}^2}{16\pi^2} [-12\pi \{ \Theta_1^2 (\Psi(\theta_{ab}^2) - \Psi(\theta_{ab}^3)) - (\Theta_2^2 - \Theta_3^2) (\Psi(\theta_{ab}^2) + \Psi(\theta_{ab}^3)) \} \times \\
&\quad \sin(2\pi\alpha) + 3 \{ -2\Theta_1(\Theta_2 - \Theta_3) (\Psi'(\theta_{ab}^2) - \Psi'(\theta_{ab}^3)) + \Theta_1^2 (\Psi'(\theta_{ab}^2) + \Psi'(\theta_{ab}^3)) + \\
&\quad (\Theta_2 - \Theta_3)^2 (\Psi'(\theta_{ab}^2) + \Psi'(\theta_{ab}^3)) \} \sin^2(2\pi\alpha) + \pi [(-4\pi) + \\
&\quad 3 \{ \Theta_1^2 (\Psi(\theta_{ab}^2) - \Psi(\theta_{ab}^3)) + (\Theta_2 - \Theta_3)^2 (\Psi(\theta_{ab}^2) - \Psi(\theta_{ab}^3)) - \\
&\quad 2\Theta_1(\Theta_2 - \Theta_3) (\Psi(\theta_{ab}^2) + \Psi(\theta_{ab}^3)) \} \sin(4\pi\alpha)]] \tag{A.3}
\end{aligned}$$

$$\begin{aligned}
\tilde{m}_{UR}^2 &= \frac{-m_{3/2}^2}{16\pi^2} [-12\pi \{ \Theta_1^2 (\Psi(\theta_{ac}^2) - \Psi(\theta_{ac}^3)) - (\Theta_2^2 - \Theta_3^2) (\Psi(\theta_{ac}^2) + \Psi(\theta_{ac}^3)) \} \times \\
&\quad \sin(2\pi\alpha) + 3 \{ -2\Theta_1(\Theta_2 - \Theta_3) (\Psi'(\theta_{ac}^2) - \Psi'(\theta_{ac}^3)) + \Theta_1^2 (\Psi'(\theta_{ac}^2) + \Psi'(\theta_{ac}^3)) + \\
&\quad (\Theta_2 - \Theta_3)^2 (\Psi'(\theta_{ac}^2) + \Psi'(\theta_{ac}^3)) \} \sin^2(2\pi\alpha) + \pi [(-4\pi) + \\
&\quad 3 \{ \Theta_1^2 (\Psi(\theta_{ac}^2) - \Psi(\theta_{ac}^3)) + (\Theta_2 - \Theta_3)^2 (\Psi(\theta_{ac}^2) - \Psi(\theta_{ac}^3)) - \\
&\quad 2\Theta_1(\Theta_2 - \Theta_3) (\Psi(\theta_{ac}^2) + \Psi(\theta_{ac}^3)) \} \sin(4\pi\alpha)]] \tag{A.4}
\end{aligned}$$

$$\begin{aligned}
\tilde{m}_{DR}^2 &= \frac{-m_{3/2}^2}{16\pi^2} [-12\pi \{ \Theta_1^2 (\Psi(\theta_{ac^*}^2) - \Psi(\theta_{ac^*}^3)) - (\Theta_2^2 - \Theta_3^2) (\Psi(\theta_{ac^*}^2) + \Psi(\theta_{ac^*}^3)) \} \times \\
&\quad \sin(2\pi\alpha) + 3 \{ -2\Theta_1(\Theta_2 - \Theta_3) (\Psi'(\theta_{ac^*}^2) - \Psi'(\theta_{ac^*}^3)) + \Theta_1^2 (\Psi'(\theta_{ac^*}^2) + \Psi'(\theta_{ac^*}^3)) + \\
&\quad (\Theta_2 - \Theta_3)^2 (\Psi'(\theta_{ac^*}^2) + \Psi'(\theta_{ac^*}^3)) \} \sin^2(2\pi\alpha) + \pi [(-4\pi) + \\
&\quad 3 \{ \Theta_1^2 (\Psi(\theta_{ac^*}^2) - \Psi(\theta_{ac^*}^3)) + (\Theta_2 - \Theta_3)^2 (\Psi(\theta_{ac^*}^2) - \Psi(\theta_{ac^*}^3)) - \\
&\quad 2\Theta_1(\Theta_2 - \Theta_3) (\Psi(\theta_{ac^*}^2) + \Psi(\theta_{ac^*}^3)) \} \sin(4\pi\alpha)]] \tag{A.5}
\end{aligned}$$

$$\tilde{m}_{QL}^2 = \tilde{m}_L^2; \quad \tilde{m}_{UR}^2 = \tilde{m}_{NR}^2; \quad \tilde{m}_{DR}^2 = \tilde{m}_{ER}^2$$

The above formulas are subject to the constraint $|\Theta_1|^2 + |\Theta_2|^2 + |\Theta_3|^2 = 1$, as can be seen clearly below equation (4.24).

APPENDIX B

Kähler metric for visible chiral matter in M theory

As stated in section 4.2.7.4, we will generalize the result obtained for the Kähler metric for visible sector chiral matter fields in toroidal orientifold constructions in IIA [49] to that in M theory. The result obtained for the Kähler metric for the (twisted) chiral matter fields (ϕ_α) in the supergravity limit ($\alpha' \rightarrow 0$) in [49] is:

$$\begin{aligned} \tilde{K}_{\bar{\alpha}\beta}^0 &= \prod_{i=1}^3 \left(\frac{\Gamma(1 - \theta_i^\alpha)}{\Gamma(\theta_i^\alpha)} \right)^{1/2} \delta_{\bar{\alpha}\beta} \\ \tan(\pi\theta_i^\alpha) &= \frac{U_2^i}{U_1^i + q_i^\alpha/p_i^\alpha}; \quad U^i \equiv U_1^i + iU_2^i \end{aligned} \quad (\text{B.1})$$

where $i = 1, 2, 3$ denote the number of moduli in the specific IIA example, $\{p, q\}$ are integers and U^i are the complex structure moduli in type IIA in the geometrical basis. As mentioned before, we will restrict to factorized rectangular tori with commuting magnetic fluxes, for which $U_1^i = 0$. Then

$$\tan(\pi\theta_i^\alpha) = \frac{p_i^\alpha}{q_i^\alpha} U_2^i \quad (\text{B.2})$$

The first step towards the generalization is to identify the G_2 moduli in terms of IIA toroidal moduli by imposing consistency between results of IIA and M theory. The consistency check is

the formula for κ^2 - the physically measured four dimensional gravitational coupling. We have:

$$\begin{aligned}\kappa^2 &= \frac{\kappa_{11}^2}{\text{Vol}(X_7)}, & M \text{ Theory} . \\ \kappa^2 &= \frac{\kappa_{10}^2 g_s^2}{\text{Vol}(X_6)}, & IIA \text{ String Theory} .\end{aligned}\tag{B.3}$$

where X_7 and X_6 are the volumes of the internal 7-manifold and 6-manifold (in IIA) respectively. The M theory gravitational coupling κ_{11}^2 and the string theory gravitational coupling κ_{10}^2 can be written in terms of the string coupling in IIA ($g_s \equiv e^{\phi_{10}^A}$) and α' :

$$\begin{aligned}\kappa_{11}^2 &= \frac{1}{2}(2\pi)^8 g_s^3 (\alpha')^{9/2} [173] \\ \kappa_{10}^2 &= \frac{1}{2}(2\pi)^7 \alpha'^4 \text{ (eqn. 13.3.24 of [174])}\end{aligned}\tag{B.4}$$

Also, the volumes of X_7 and X_6 (for a IIA toroidal orientifold) can be written as:

$$\begin{aligned}\text{Vol}(X_7) &= V_X l_M^7 \quad \text{where } V_X = \prod_{i=1}^N (s_i)^{a_i}; \quad \frac{l_M^9}{4\pi} = \kappa_{11}^2 \\ \text{Vol}(X_6) &= (2\pi R_1^{(1)})(2\pi R_2^{(1)})(2\pi R_1^{(2)})(2\pi R_2^{(2)})(2\pi R_1^{(3)})(2\pi R_2^{(3)})\end{aligned}\tag{B.5}$$

Using (B.4), we get

$$l_M = 2\pi\alpha'^{1/2} g_s^{1/3}\tag{B.6}$$

which gives rise to the following expression for κ in M theory:

$$\kappa^2 = \frac{\pi\alpha' g_s^{2/3}}{V_X}\tag{B.7}$$

In IIA String theory, the definition of the IIA moduli T_i and U_i in terms of the geometry of the torus is given below. We will stick to the case of a factorized T^6 , rectangular tori, and commuting magnetic fluxes (in the type IIB dual) for simplicity, in which case only the

imaginary parts of the moduli are important:

$$\begin{aligned} \text{Im}(T)^i &\equiv T_2^{(i)} = \frac{R_2^{(i)}}{R_1^{(i)}} \\ \text{Im}(U)^i &\equiv U_2^{(i)} = \frac{R_1^{(i)} R_2^{(i)}}{\alpha'}; \quad i = 1, 2, 3. \end{aligned} \quad (\text{B.8})$$

where $R_1^{(i)}, R_2^{(i)}$ are the radii of the i^{th} IIA torus along the x and y axes respectively.

Now, from (B.3), (B.4), (B.5) and (B.8) we get:

$$\kappa^2 = \frac{\pi \alpha' g_s^2}{U_2^{(1)} U_2^{(2)} U_2^{(3)}} \quad (\text{B.9})$$

Combining (B.7) and (B.9) gives:

$$\boxed{V_X = \frac{U_2^{(1)} U_2^{(2)} U_2^{(3)}}{g_s^{4/3}}} \quad (\text{B.10})$$

The above formula (eqn.(B.10)) is quite general and should always hold¹, since it has been derived by requiring consistency between formulas for the physically measured gravitational coupling constant. To identify the individual G_2 moduli however, is harder and model-dependent. In the next subsection, we will do the mapping for the case of a simple toroidal G_2 orbifold (T^7/Z_3) considered in [178], where it can be shown that eqn (B.10) is satisfied.

B.0.1 Particular Case

In [178], the definitions of the G_2 moduli (eqn 2.4) and the Kähler potential (eqn 2.10) are not given in a dimensionless form. Therefore, we will make them dimensionless as is done in [93]. So, we have:

$$s^i \equiv \frac{a^i}{l_M^3} = \frac{\int_{C^i} \tilde{\phi}}{l_M^3}; \quad K = -3 \ln \left(\frac{\text{Vol}(X_7)}{l_M^7} \right) + \text{constant} \quad (\text{B.11})$$

¹within the limits of the IIA setup considered.

The volume of the manifold and the moduli in this compactification are explicitly given as [178]:

$$\begin{aligned} \text{Vol}(X_7) &= \prod_{i=1}^7 R_i; \quad a^1 = R_1 R_2 R_7; \quad a^2 = R_1 R_3 R_6; \quad a^3 = R_1 R_4 R_5; \\ a^4 &= R_2 R_3 R_5; \quad a^5 = R_2 R_4 R_6; \quad a^6 = R_3 R_4 R_7; \quad a^7 = R_5 R_6 R_7. \end{aligned} \quad (\text{B.12})$$

From (B.12), we can write $\text{Vol}(X_7) = (a^1 a^2 a^3 a^4 a^5 a^6 a^7)^{1/3}$, which implies that $V_X = \prod_{i=1}^7 (s_i)^{1/3}$. Therefore, in the notation of [93], $a_i = 1/3$; $i = 1, 2, \dots, 7$. We will identify the M theory circle radius as R_7 , the remaining six radii can just be identified as the x and y radii of the three tori in IIA:

$$\begin{aligned} R_1 &= (2\pi)R_1^{(1)}; \quad R_2 = (2\pi)R_2^{(1)}; \quad R_3 = (2\pi)R_1^{(2)}; \quad R_4 = (2\pi)R_2^{(2)} \\ R_5 &= (2\pi)R_1^{(3)}; \quad R_6 = (2\pi)R_2^{(3)}; \quad R_7 = (2\pi)g_s \alpha'^{1/2}. \end{aligned} \quad (\text{B.13})$$

With these identifications, and using (B.6), we can write the individual G_2 moduli in terms of the IIA moduli:

$$\begin{aligned} s^1 &= U_2^{(1)}; \quad s^6 = U_2^{(2)}; \quad s^7 = U_2^{(3)}; \\ s_2 &= \frac{1}{g_s} \left(\frac{T_2^{(3)} U_2^{(1)} U_2^{(2)} U_2^{(3)}}{T_2^{(1)} T_2^{(2)}} \right)^{1/2}; \quad s_3 = \frac{1}{g_s} \left(\frac{T_2^{(2)} U_2^{(1)} U_2^{(2)} U_2^{(3)}}{T_2^{(1)} T_2^{(3)}} \right)^{1/2}; \\ s_4 &= \frac{1}{g_s} \left(\frac{T_2^{(1)} U_2^{(1)} U_2^{(2)} U_2^{(3)}}{T_2^{(2)} T_2^{(3)}} \right)^{1/2}; \quad s_5 = \frac{1}{g_s} \left(T_2^{(1)} T_2^{(2)} T_2^{(3)} U_2^{(1)} U_2^{(2)} U_2^{(3)} \right)^{1/2}. \end{aligned}$$

Therefore, we get:

$$V_X = \prod_{i=1}^7 (s^i)^{1/3} = \frac{U_2^{(1)} U_2^{(2)} U_2^{(3)}}{g_s^{4/3}} \quad (\text{B.14})$$

which is the same as (B.10). So, for the particular case, this suggests the following generalization:

$$\begin{aligned}\tilde{K}_\alpha &= \prod_{i=1,6,7} \left(\frac{\Gamma(1-\theta_i^\alpha)}{\Gamma(\theta_i^\alpha)} \right)^{1/2} \\ \tan(\pi\theta_i^\alpha) &= \frac{p_i^\alpha}{q_i^\alpha} s_i; \quad i = 1, 6, 7\end{aligned}\tag{B.15}$$

B.0.2 General Case

For more general G_2 manifolds with many moduli, the precise map of the individual moduli is not completely clear. However, it seems plausible that the complex structure moduli appearing in the Kähler metric in IIA map to a subset of the G_2 moduli in a similar way, as in the particular case.

Therefore, we use the following expression for the Kähler metric for visible chiral matter fields in M theory:

$$\begin{aligned}\tilde{K}_\alpha &= \prod_{i=1}^p \left(\frac{\Gamma(1-\theta_i^\alpha)}{\Gamma(\theta_i^\alpha)} \right)^{1/2}; \quad i = 1, 2, \dots, p \leq N(\equiv N) \\ \tan(\pi\theta_i^\alpha) &= c_i^\alpha (s_i)^l; \quad c_i^\alpha = \text{constant}; \quad l = \text{rational number of } \mathcal{O}(1).\end{aligned}\tag{B.16}$$

The derivatives of the Kähler metric w.r.t the moduli are very important as they appear in the soft scalar masses, the trilinears as well as the anomaly mediated gaugino masses, as seen from section 4.2.7.4. The first derivatives appear in the trilinears and anomaly mediated gaugino masses while the second derivatives appear in the scalar masses. For the metric in (B.16), these can be written as follows:

$$\begin{aligned}\partial_n \ln(\tilde{K}_\alpha) &= \psi_n^\alpha \left(\frac{\partial \theta_n^\alpha}{\partial z^n} \right); \quad \psi_n^\alpha(\theta_n^\alpha) \equiv \frac{1}{2} \frac{d}{d\theta_n^\alpha} \ln \left(\frac{\Gamma(1-\theta_n^\alpha)}{\Gamma(\theta_n^\alpha)} \right) \\ \partial_{\bar{m}} \partial_n \ln(\tilde{K}_\alpha) &= \delta_{\bar{m}n} \left[\psi_{\bar{m}n}^\alpha \left(\frac{\partial \theta_n^\alpha}{\partial \bar{z}^n} \right) \left(\frac{\partial \theta_n^\alpha}{\partial z^n} \right) + \psi_n^\alpha \left(\frac{\partial^2 \theta_n^\alpha}{\partial \bar{z}^n \partial z^n} \right) \right]; \quad \psi_{\bar{m}n}^\alpha(\theta_n^\alpha) \equiv \frac{d}{d\theta_m^\alpha} \psi_n^\alpha\end{aligned}\tag{B.17}$$

The functions ψ_n^α and ψ_{nn}^α depend on the angular variable θ_n^α , which in turn depend on the moduli. The first and second derivatives of θ_n^α with respect to z_n are given by:

$$\begin{aligned}\frac{\partial \theta_n^\alpha}{\partial z^n} &= \frac{1}{2i} \frac{\partial \theta_n^\alpha}{\partial s^n} = \frac{l}{4\pi i s^n} \sin(2\pi\theta_n^\alpha) \\ \frac{\partial^2 \theta_n^\alpha}{\partial \bar{z}^n \partial z^n} &= \frac{1}{4} \frac{\partial^2 \theta_n^\alpha}{\partial (s^n)^2} = \frac{l}{16\pi (s^n)^2} [l \sin(4\pi\theta_n^\alpha) - 2 \sin(2\pi\theta_n^\alpha)]\end{aligned}\tag{B.18}$$

The dependence of the soft parameters in section 4.2.7.4 on θ_n^α is extremely simple. Instead of reexpressing the dependence on θ_n^α in terms of the moduli, it is much more convenient to retain the dependence on θ_n^α , as $\theta_n^\alpha \in [0, 1)$ [49] and the variation of relevant functions with θ_n^α in the allowed range can be plotted easily. In particular, the function $F(\theta_n^\alpha) \equiv \frac{1}{2\pi} \{\psi_n^\alpha \sin(2\pi\theta_n^\alpha)\}$ appears in the expression for the anomaly mediated gaugino masses (eqn. (4.303)) and the trilinears (eqn. (4.311)), the function $G(\theta_n^\alpha) \equiv \ln\left(\frac{\Gamma(1-\theta_n^\alpha)}{\Gamma(\theta_n^\alpha)}\right)$ appears in the expression for the trilinears (eqn. (4.311)) and the function $H(\theta_n^\alpha) \equiv \frac{1}{4\pi} \{l^2 \psi_{nn}^\alpha \sin^2(2\pi\theta_n^\alpha) + l^2 \psi_n^\alpha \sin(4\pi\theta_n^\alpha) - 2l \psi_n^\alpha \sin(2\pi\theta_n^\alpha)\}$ appears in the expression for the scalars (eqn. (4.315)). The variation of these functions with θ_n^α is quite mild as seen from Figure B.0.2: Since the functions F , G and H

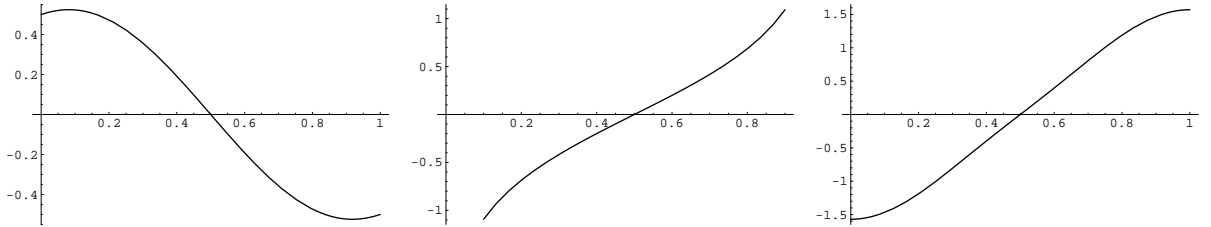


Figure B.1: Left: F as a function of θ_n^α . Middle: G as a function of θ_n^α . Right: H as a function of θ_n^α (for $l=1$). From [49], $\theta_n \in [0, 1)$.

vary very mildly with θ_n^α and are $\mathcal{O}(1)$ in the whole range, it is reasonable to replace the above functions by $\mathcal{O}(1)$ numbers, as is done in section 4.2.7.4. This is justified since we are only interested in estimating the rough overall scales of various soft parameters.

APPENDIX C

Useful Combinations of Scalar Masses

Here, we collect some combinations of soft scalar masses that are particularly useful for running up.

C.0.3 S Term Effects

The mass differences

$$\Delta m_{ij}^2 = (Y_j m_i^2 - Y_i m_j^2)/(Y_j - Y_i) \quad (\text{C.1})$$

are useful when there is a non-vanishing hypercharge D term. A hypercharge D term can shift the low energy values of the soft scalar masses, and can also modify their RG running through the S term, as discussed in Section 6.1, and in Refs. [159, 160, 179]. The effects of a hypercharge D term cancel out these mass differences, as well as in the RG equations for them.

This feature is helpful for running up because the effect of the D term on the running is determined by the low scale value of the S -term, which depends on all the soft scalar masses (of hypercharged fields) in the theory. If one of these soft masses goes unmeasured, there will be a large uncertainty in the value of the S term, and this in turn will induce a significant uncertainty in the high scale values of the soft scalar masses after RG evolution. By focusing on the mass differences of Eq. (C.1), these ambiguities cancel each other out.

On the other hand, if all the MSSM soft scalar masses are measured, the low scale values of the soft scalar mass combinations

$$\begin{aligned} S &= \text{Tr}(Y m^2), \\ S_{B-L} &= \text{Tr}[(B-L)m^2], \end{aligned} \tag{C.2}$$

provide useful information about the high scale theory, and can be used to test possible GUT embeddings of the MSSM [160].

Flavor Splitting Effects

New physics can obscure the underlying flavor structure of the soft scalar masses. Family-universal soft masses derived from a theory containing new physics can generate a low-energy spectrum that does not appear to be family-universal after it is evolved back up to the high scale without including this new physics. This is true even if the new physics couples in a flavor universal way to the MSSM. We presented a particular example of this in Section 6.2, where the new physics took the form of complete GUT multiplets having no superpotential couplings with the MSSM sector.

There are four pairs of soft mass combinations that are helpful in this regard [166]. By comparing these pairs (at any given scale), it is sometimes possible to obtain clues about the underlying flavor structure of the MSSM soft masses. These combinations are:

$$\begin{aligned} m_{A_3}^2 &= 2 m_{L_3}^2 - m_{E_3}^2 & \leftrightarrow & m_{A_1}^2 = 2 m_{L_1}^2 - m_{E_1}^2 \\ m_{B_3}^2 &= 2 m_{Q_3}^2 - m_{U_3}^2 - m_{D_3}^2 & \leftrightarrow & m_{B_1}^2 = 2 m_{Q_1}^2 - m_{U_1}^2 - m_{D_1}^2 \\ m_{X_3}^2 &= 2 m_{H_u}^2 - 3 m_{U_3}^2 & \leftrightarrow & m_{X_1}^2 = 2 m_{L_1}^2 - 3 m_{U_1}^2 \\ m_{Y_3}^2 &= 3 m_{D_3}^2 + 2 m_{L_3}^2 - 2 m_{H_d}^2 & \leftrightarrow & m_{Y_1}^2 = 3 m_{D_1}^2 \end{aligned} \tag{C.3}$$

If the high scale soft scalar masses are family-universal, we expect that each of these pairs, with the possible exception of the $m_{X_i}^2$, to be roughly equal at the low scale in the MSSM. The $m_{X_i}^2$ combinations are expected to match only if $S = 0$ as well.

To apply the soft mass combinations in Eq. (C.3), one should compare them to the splitting between individual soft masses after running all soft masses up to the high scale within the MSSM (without new physics). For instance, an inequality of the form

$$|m_{B_3}^2 - m_{B_1}^2| \ll \max \{ |m_{Q_3}^2 - m_{Q_1}^2|, |m_{U_3}^2 - m_{U_1}^2|, |m_{D_3}^2 - m_{D_1}^2| \}, \quad (\text{C.4})$$

is suggestive of high scale family-universality or a particular relationship between the Q , U , and D soft masses that has been obscured by new physics. This can arise from GUT multiplets as in Section 6.2, or from a heavy RH neutrino sector as in Section 6.3. Note that heavy neutrinos can disrupt the relationships between the A , X , and Y pairs.

BIBLIOGRAPHY

BIBLIOGRAPHY

- [1] For reviews, see: H. E. Haber and G. L. Kane, Phys. Rept. **117**, 75 (1985), S. P. Martin, *A supersymmetry primer*, hep-ph/9709356; D. J. H. Chung, L. L. Everett, G. L. Kane, S. F. King, J. D. Lykken and L. T. Wang, Phys. Rept. **407**, 1 (2005) [hep-ph/0312378]; M. A. Luty, [hep-th/0509029].
- [2] S. R. Coleman and J. Mandula, Phys. Rev. **159**, 1251 (1967).
- [3] R. Haag, J. T. Lopuszanski and M. Sohnius, Nucl. Phys. B **88**, 257 (1975).
- [4] L. E. Ibanez and G. G. Ross, Phys. Lett. B **110**, 215 (1982).
- [5] L. Alvarez-Gaume, M. Claudson and M. B. Wise, Nucl. Phys. B **207**, 96 (1982).
- [6] K. Inoue, A. Kakuto, H. Komatsu and S. Takeshita, Prog. Theor. Phys. **67**, 1889 (1982). K. Inoue, A. Kakuto, H. Komatsu and S. Takeshita, Prog. Theor. Phys. **68**, 927 (1982) [Erratum-ibid. **70**, 330 (1983)]. K. Inoue, A. Kakuto, H. Komatsu and S. Takeshita, Prog. Theor. Phys. **71**, 413 (1984).
- [7] S. Dimopoulos, S. Raby and F. Wilczek, Phys. Rev. D **24**, 1681 (1981).
- [8] S. Dimopoulos and H. Georgi, Nucl. Phys. B **193**, 150 (1981).
- [9] N. Sakai, Z. Phys. C **11**, 153 (1981).
- [10] C. Giunti, C. W. Kim and U. W. Lee, Mod. Phys. Lett. A **6** (1991) 1745.
- [11] U. Amaldi, W. de Boer and H. Furstenau, Phys. Lett. B **260**, 447 (1991).
- [12] P. Langacker and M. x. Luo, Phys. Rev. D **44**, 817 (1991).
- [13] J. R. Ellis, S. Kelley and D. V. Nanopoulos, Phys. Lett. B **260**, 131 (1991).
- [14] H. Pagels and J. R. Primack, Phys. Rev. Lett. **48**, 223 (1982).
- [15] H. Goldberg, Phys. Rev. Lett. **50**, 1419 (1983).
- [16] M. Dine, R. Rohm, N. Seiberg and E. Witten, Phys. Lett. B **156**, 55 (1985).

- [17] P. Horava, Phys. Rev. D **54**, 7561 (1996) [arXiv:hep-th/9608019].
- [18] R. Blumenhagen, M. Cvetič, P. Langacker and G. Shiu, Ann. Rev. Nucl. Part. Sci. **55**, 71 (2005) [arXiv:hep-th/0502005].
T. R. Taylor, G. Veneziano and S. Yankielowicz, Nucl. Phys. B **218**, 493 (1983).
- [19] B. Acharya, K. Bobkov, G. Kane, P. Kumar and D. Vaman, Phys. Rev. Lett. **97**, 191601 (2006) [arXiv:hep-th/0606262].
B. S. Acharya, K. Bobkov, G. L. Kane, P. Kumar and J. Shao, arXiv:hep-th/0701034.
- [20] S. B. Giddings, S. Kachru and J. Polchinski, Phys. Rev. D **66**, 106006 (2002) [arXiv:hep-th/0105097].
- [21] S. Kachru, R. Kallosh, A. Linde and S. P. Trivedi, Phys. Rev. D **68**, 046005 (2003) [arXiv:hep-th/0301240].
- [22] V. Balasubramanian, P. Berglund, J. P. Conlon and F. Quevedo, “Systematics of moduli stabilisation in Calabi-Yau flux JHEP **0503**, 007 (2005) [arXiv:hep-th/0502058]. J. P. Conlon, F. Quevedo and K. Suruliz, “Large-volume flux compactifications: Moduli spectrum and D3/D7 soft JHEP **0508**, 007 (2005) [arXiv:hep-th/0505076]. B. C. Allanach, F. Quevedo and K. Suruliz, arXiv:hep-ph/0512081.
- [23] M. Berg, M. Haack and E. Pajer, arXiv:0704.0737 [hep-th].
- [24] H. L. Verlinde, Nucl. Phys. B **580**, 264 (2000) [arXiv:hep-th/9906182].
C. S. Chan, P. L. Paul and H. L. Verlinde, Nucl. Phys. B **581**, 156 (2000) [arXiv:hep-th/0003236].
- [25] E. Witten, Nucl. Phys. B **443**, 85 (1995) [arXiv:hep-th/9503124].
- [26] L. J. Dixon, D. Friedan, E. J. Martinec and S. H. Shenker, Nucl. Phys. B **282**, 13 (1987);
S. Hamidi and C. Vafa, Nucl. Phys. B **279**, 465 (1987);
I. Antoniadis, J. R. Ellis, J. S. Hagelin and D. V. Nanopoulos, Phys. Lett. B **231**, 65 (1989);
G. Cleaver, M. Cvetič, J. R. Espinosa, L. L. Everett, P. Langacker and J. Wang, Phys. Rev. D **59**, 115003 (1999) [arXiv:hep-ph/9811355];
G. B. Cleaver, A. E. Faraggi, D. V. Nanopoulos and J. W. Walker, Mod. Phys. Lett. A **15**, 1191 (2000) [arXiv:hep-ph/0002060];
L. J. Dixon, V. Kaplunovsky and J. Louis, Nucl. Phys. B **329**, 27 (1990);
L. J. Dixon, V. Kaplunovsky and J. Louis, Nucl. Phys. B **355**, 649 (1991);
L. E. Ibanez and D. Lust, Nucl. Phys. B **382**, 305 (1992) [arXiv:hep-th/9202046];
H. P. Nilles and S. Stieberger, Nucl. Phys. B **499**, 3 (1997) [arXiv:hep-th/9702110].
P. Binetruy, M. K. Gaillard and B. D. Nelson, Nucl. Phys. B **604**, 32 (2001)

- [arXiv:hep-ph/0011081].
 A. Font, L. E. Ibanez, F. Quevedo and A. Sierra, Nucl. Phys. B **331**, 421 (1990).
- [27] E. Witten, Nucl. Phys. B **471**(1996) 135.
 A. Lukas, B. A. Ovrut and D. Waldram, Nucl. Phys. B **532**, 43 (1998) [arXiv:hep-th/9710208].
 A. Lukas, B. A. Ovrut, D. Waldram, JHEP **9904** (1999) 009.
- [28] T. Banks and M. Dine, Nucl. Phys. B **479** (1996) 137.
 T. Banks and M. Dine, arXiv:hep-th/9609046.
- [29] B.S. Acharya and E. Witten, arXiv:hep-th/0109152.
- [30] B. S. Acharya, Adv. Theor. Math. Phys. **3** (1999) 227 [arXiv:hep-th/9812205]
 B. S. Acharya, arXiv:hep-th/0011089.
- [31] M. Atiyah and E. Witten, Adv. Theor. Math. Phys. **6**, 1 (2003) [arXiv:hep-th/0107177].
- [32] B. S. Acharya and S. Gukov, Phys. Rept. **392** (2004) 121 [arXiv:hep-th/0409191].
 T. Friedmann and E. Witten, Adv. Theor. Math. Phys. **7** (2003) 577 [arXiv:hep-th/0211269].
- [33] C. Angelantonj and A. Sagnotti, Phys. Rept. **371** (2002) 1 [Erratum-ibid. **376** (2003) 339] [hep-th/0204089].
 R. Blumenhagen, L. Görlich and B. Körs, Nucl. Phys. B **569** (2000) 209 [hep-th/9908130].
 R. Blumenhagen, L. Görlich and B. Körs, JHEP **0001** (2000) 040 [hep-th/9912204].
 G. Pradisi, Nucl. Phys. B **575** (2000) 134 [hep-th/9912218].
 R. Blumenhagen, L. Görlich and B. Körs, hep-th/0002146.
 C. Angelantonj, I. Antoniadis, E. Dudas and A. Sagnotti, Phys. Lett. B **489** (2000) 223 [hep-th/0007090].
 S. Förste, G. Honecker and R. Schreyer, Nucl. Phys. B **593** (2001) 127 [hep-th/0008250].
 C. Angelantonj and A. Sagnotti, hep-th/0010279.
 S. Förste, G. Honecker and R. Schreyer, JHEP **0106** (2001) 004 [hep-th/0105208].
- [34] R. Blumenhagen, B. Kors, D. Lust and T. Ott, Nucl. Phys. B **616**, 3 (2001) [arXiv:hep-th/0107138].
- [35] G. Shiu and S. H. H. Tye, Phys. Rev. D **58**, 106007 (1998) [arXiv:hep-th/9805157].
- [36] M. Cvetič, P. Langacker and G. Shiu, Phys. Rev. D **66**, 066004 (2002) [arXiv:hep-ph/0205252].

- [37] D. Lust and S. Stieberger, arXiv:hep-th/0302221.
- [38] I. Antoniadis, E. Kiritsis and T. N. Tomaras, Phys. Lett. B **486**, 186 (2000) [arXiv:hep-ph/0004214].
- [39] D. Cremades, L. E. Ibanez and F. Marchesano, JHEP **0207**, 009 (2002) [arXiv:hep-th/0201205].
- [40] R. Blumenhagen, D. Lust and S. Stieberger, JHEP **0307**, 036 (2003) [arXiv:hep-th/0305146].
- [41] M. Berg, M. Haack and B. Kors, Phys. Rev. D **71**, 026005 (2005) [arXiv:hep-th/0404087].
- [42] D. Cremades, L. E. Ibanez and F. Marchesano, JHEP **0307**, 038 (2003) [arXiv:hep-th/0302105].
- [43] D. Cremades, L. E. Ibanez and F. Marchesano, JHEP **0405**, 079 (2004) [arXiv:hep-th/0404229].
- [44] M. Cvetič and I. Papadimitriou, Phys. Rev. D **68**, 046001 (2003) [Erratum-ibid. D **70**, 029903 (2004)] [arXiv:hep-th/0303083].
- [45] S. A. Abel and A. W. Owen, Nucl. Phys. B **682**, 183 (2004) [arXiv:hep-th/0310257], Nucl. Phys. B **664**, 3 (2003) [arXiv:hep-th/0303124].
- [46] B. Kors and P. Nath, Nucl. Phys. B **681**, 77 (2004) [arXiv:hep-th/0309167].
- [47] D. Lust, P. Mayr, R. Richter and S. Stieberger, Nucl. Phys. B **696**, 205 (2004) [arXiv:hep-th/0404134].
- [48] M. Berg, M. Haack and B. Kors, JHEP **0511**, 030 (2005) [arXiv:hep-th/0508043].
- [49] M. Bertolini, M. Billo, A. Lerda, J. F. Morales and R. Russo, [arXiv:hep-th/0512067].
- [50] G. Aldazabal, S. Franco, L. E. Ibanez, R. Rabadan and A. M. Uranga, JHEP **0102**, 047 (2001) [arXiv:hep-ph/0011132].
- [51] G. Aldazabal, S. Franco, L. E. Ibanez, R. Rabadan and A. M. Uranga, J. Math. Phys. **42**, 3103 (2001) [arXiv:hep-th/0011073].
- [52] R. Blumenhagen, L. Gorlich, B. Kors and D. Lust, JHEP **0010**, 006 (2000) [arXiv:hep-th/0007024].
- [53] R. Blumenhagen, B. Kors and D. Lust, JHEP **0102**, 030 (2001) [arXiv:hep-th/0012156].

- [54] T. Ott, Fortsch. Phys. **52**, 28 (2004) [arXiv:hep-th/0309107].
- [55] M. Berkooz, M. R. Douglas and R. G. Leigh, Nucl. Phys. B **480**, 265 (1996) [arXiv:hep-th/9606139]
- [56] A. Uranga Nucl. Phys. B **598**, 225 (2001) [arXiv:hep-th/0011048]
- [57] M. Cvetič, G. Shiu and A. M. Uranga, Phys. Rev. Lett. **87**, 201801 (2001) [arXiv:hep-th/0107143]. M. Cvetič, G. Shiu and A. M. Uranga, Nucl. Phys. B **615**, 003 (2001) [arXiv:hep-th/0107166]. M. Cvetič, T. Li and T. Liu, Nucl. Phys. B **698**, 163 (2004) [arXiv:hep-th/0403061]. M. Cvetič, P. Langacker, T. j. Li and T. Liu, arXiv:hep-th/0407178.
- [58] G. Honecker, Nucl. Phys. B **666**, 175 (2003) [arXiv:hep-th/0303015]
- [59] R. Blumenhagen, L. Gorlich and T. Ott, JHEP **0301**, 021 (2003) [arXiv:hep-th/0211059]
- [60] G. Honecker and T. Ott, arXiv:hep-th/0404055.
- [61] C. Kokorelis, arXiv:hep-th/0309070.
- [62] D. Cremades, L. E. Ibanez and F. Marchesano, JHEP **0207**, 022 (2002) [arXiv:hep-th/0203160].
C. Kokorelis, Nucl. Phys. B **677**, 115 (2004) [arXiv:hep-th/0207234].
- [63] M. Cvetič, P. Langacker and J. Wang, Phys. Rev. D **68**, 046002 (2003) [arXiv:hep-th/0303208].
- [64] H. P. Nilles, Phys. Rept. **110** (1984) 1.
- [65] V. S. Kaplunovsky and J. Louis, Phys. Lett. B **306**, 269 (1993) [arXiv:hep-th/9303040].
- [66] A. Brignole, L. E. Ibanez and C. Muñoz, Nucl. Phys. B **422**, 125 (1994) [Erratum-ibid. B **436**, 747 (1995)] [arXiv:hep-ph/9308271]. A. Brignole, L. E. Ibanez and C. Muñoz, arXiv:hep-ph/9707209.
- [67] F. Marchesano and G. Shiu, Phys. Rev. D **71**, 011701 (2005) [arXiv:hep-th/0408059].
- [68] L. Gorlich, S. Kachru, P. K. Tripathy and S. P. Trivedi, arXiv:hep-th/0407130.
- [69] F. Ardalan, H. Arfaei and M. M. Sheikh-Jabbari, JHEP **9902**, 016 (1999) [arXiv:hep-th/9810072].
- [70] T. W. Grimm and J. Louis, arXiv:hep-th/0403067.

- [71] H. Jockers and J. Louis, arXiv:hep-th/0409098.
- [72] E. Cremmer, S. Ferrara, L. Girardello and A. Van Proeyen, Nucl. Phys. B **212**, 413 (1983).
- [73] I. R. Klebanov and E. Witten, Nucl. Phys. B **664**, 3 (2003) [arXiv:hep-th/0304079].
- [74] D. Lust, S. Reffert and S. Stieberger, Nucl. Phys. B **706**, 3 (2005) [arXiv:hep-th/0406092].
- [75] D. Lust, S. Reffert and S. Stieberger, Nucl. Phys. B **727**, 264 (2005) [arXiv:hep-th/0410074].
- [76] A. Font and L. E. Ibanez, JHEP **0503**, 040 (2005) [arXiv:hep-th/0412150].
- [77] Y. Kawamura, T. Kobayashi and T. Komatsu, Phys. Lett. B **400**, 284 (1997) [arXiv:hep-ph/9609462].
- [78] A. Djouadi, J. L. Kneur and G. Moultaka, arXiv:hep-ph/0211331.
- [79] K. Eguchi *et al.* [KamLAND Collaboration], Phys. Rev. Lett. **90**, 021802 (2003) [arXiv:hep-ex/0212021].
- [80] M. Kawasaki and T. Moroi, Prog. Theor. Phys. **93**, 879 (1995) [arXiv:hep-ph/9403364].
- [81] M. Fujii and K. Hamaguchi, Phys. Lett. B **525**, 143 (2002) [arXiv:hep-ph/0110072].
- [82] S. Kasuya and M. Kawasaki, Phys. Rev. D **61**, 041301 (2000) [arXiv:hep-ph/9909509]. J. R. Ellis, J. E. Kim and D. V. Nanopoulos, Phys. Lett. B **145**, 181 (1984).
- [83] S. R. Coleman, Nucl. Phys. B **262**, 263 (1985) [Erratum-ibid. B **269**, 744 (1986)].
T. Gherghetta, G. F. Giudice and J. D. Wells, Nucl. Phys. B **559**, 27 (1999) [arXiv:hep-ph/9904378].
- [84] I. Affleck and M. Dine, Nucl. Phys. B **249**, 361 (1985). M. Dine, L. Randall and S. Thomas, Nucl. Phys. B **458**, 291 (1996) [arXiv:hep-ph/9507453].
- [85] S. W. Barwick *et al.* [HEAT Collaboration], Phys. Rev. Lett. **75**, 390 (1995) [arXiv:astro-ph/9505141]. S. W. Barwick *et al.* [HEAT Collaboration], Astrophys. J. **482**, L191 (1997) [arXiv:astro-ph/9703192].
- [86] C. Lechanoine-Leluc, Nucl. Instrum. Meth. B **214**, 103 (2004). V. Bonvicini *et al.* [PAMELA Collaboration], Nucl. Instrum. Meth. A **461** (2001) 262.

- [87] P. Gondolo, J. Edsjo, L. Bergstrom, P. Ullio and E. A. Baltz, arXiv:astro-ph/0012234.
- [88] G. L. Kane, L. T. Wang and J. D. Wells, Phys. Rev. D **65**, 057701 (2002) [arXiv:hep-ph/0108138]. G. L. Kane, L. T. Wang and T. T. Wang, Phys. Lett. B **536**, 263 (2002) [arXiv:hep-ph/0202156]. D. Hooper and J. Silk, arXiv:hep-ph/0409104.
- [89] L. Randall and R. Sundrum, Phys. Rev. Lett. **83**, 3370 (1999) [arXiv:hep-ph/9905221].
L. Randall and R. Sundrum, Phys. Rev. Lett. **83**, 4690 (1999) [arXiv:hep-th/9906064].
- [90] J. P. Conlon and F. Quevedo, arXiv:hep-th/0605141.
- [91] P. Binetruiy, M. K. Gaillard and B. D. Nelson, Nucl. Phys. B **604**, 32 (2001) [arXiv:hep-ph/0011081].
- [92] B. S. Acharya, K. Bobkov, G. L. Kane, P. Kumar and J. Shao, To Appear.
- [93] B. S. Acharya, F. Denef and R. Valandro, JHEP **0506**, 056 (2005) [arXiv:hep-th/0502060].
- [94] T. Friedmann and E. Witten, Adv. Theor. Math. Phys. **7** (2003) 577 [arXiv:hep-th/0211269].
- [95] D. Krefl and D. Lust, JHEP **0606**, 023 (2006) [arXiv:hep-th/0603166].
R. Kallosh and A. Linde, JHEP **0412**, 004 (2004) [arXiv:hep-th/0411011].
J. J. Blanco-Pillado, R. Kallosh and A. Linde, JHEP **0605**, 053 (2006) [arXiv:hep-th/0511042].
- [96] D.D. Joyce, ‘Compact Manifolds with Special Holonomy,’ Oxford University Press, 2000; A. Kovalev, arXiv:math.dg/0012189.
- [97] V. Braun, Y. H. He, B. A. Ovrut and T. Pantev, JHEP **0605**, 043 (2006) [arXiv:hep-th/0512177].
B. A. Ovrut, Fortsch. Phys. **54**, 160 (2006).
V. Bouchard and R. Donagi, Phys. Lett. B **633**, 783 (2006) [arXiv:hep-th/0512149].
- [98] O. Lebedev, H. P. Nilles and M. Ratz, Phys. Lett. B **636**, 126 (2006) [arXiv:hep-th/0603047].
- [99] N. Seiberg, Phys. Rev. D **49**, 6857 (1994) [arXiv:hep-th/9402044].
N. Seiberg, Phys. Lett. B **318**, 469 (1993) [arXiv:hep-ph/9309335].
- [100] D. Finnell and P. Pouliot, Nucl. Phys. B **453**, 225 (1995) [arXiv:hep-th/9503115].

- [101] E. Witten, arXiv:hep-ph/0201018.
- [102] M. Cvetič, G. Shiu and A. M. Uranga, arXiv:hep-th/0111179.
- [103] S. F. King, I. N. R. Peddie, G. G. Ross, L. Velasco-Sevilla and O. Vives, JHEP **0507**, 049 (2005) [arXiv:hep-ph/0407012].
- [104] M. K. Gaillard, B. D. Nelson and Y. Y. Wu, Phys. Lett. B **459**, 549 (1999) [arXiv:hep-th/9905122].
J. A. Bagger, T. Moroi and E. Poppitz, JHEP **0004**, 009 (2000) [arXiv:hep-th/9911029].
- [105] G. L. Kane, P. Kumar and J. Shao, arXiv:hep-ph/0610038.
- [106] J. P. Conlon, S. S. Abdussalam, F. Quevedo and K. Suruliz, arXiv:hep-th/0610129.
- [107] K. Choi, A. Falkowski, H. P. Nilles and M. Olechowski, Nucl. Phys. B **718**, 113 (2005) [arXiv:hep-th/0503216].
R. Kitano and Y. Nomura, Phys. Lett. B **631**, 58 (2005) [arXiv:hep-ph/0509039].
A. Pierce and J. Thaler, arXiv:hep-ph/0604192.
H. Baer, E. K. Park, X. Tata and T. T. Wang, arXiv:hep-ph/0604253.
- [108] P. Binetruiy, G. L. Kane, B. D. Nelson, L. T. Wang and T. T. Wang, Phys. Rev. D **70**, 095006 (2004) [arXiv:hep-ph/0312248].
- [109] S. Weinberg, Phys. Rev. D **13**, 974 (1976).
T. W. Appelquist, D. Karabali and L. C. R. Wijewardhana, Phys. Rev. Lett. **57**, 957 (1986).
B. Holdom and J. Terning, Phys. Lett. B **247**, 88 (1990).
C. T. Hill, Phys. Lett. B **345**, 483 (1995) [arXiv:hep-ph/9411426]. M. A. Luty and T. Okui, arXiv:hep-ph/0409274.
T. Appelquist, N. Christensen, M. Piai and R. Shrock, Phys. Rev. D **70**, 093010 (2004) [arXiv:hep-ph/0409035].
M. Perelstein, JHEP **0410**, 010 (2004) [arXiv:hep-ph/0408072].
- [110] N. Arkani-Hamed, S. Dimopoulos and G. R. Dvali, Phys. Lett. B **429**, 263 (1998) [arXiv:hep-ph/9803315].
N. Arkani-Hamed, S. Dimopoulos and G. R. Dvali, Phys. Rev. D **59**, 086004 (1999) [arXiv:hep-ph/9807344].
N. Arkani-Hamed, S. Dimopoulos, G. R. Dvali and J. March-Russell, Phys. Rev. D **65**, 024032 (2002) [arXiv:hep-ph/9811448].
N. Arkani-Hamed, S. Dimopoulos, G. R. Dvali and N. Kaloper, Phys. Rev. Lett. **84**, 586 (2000) [arXiv:hep-th/9907209].
Phys. Lett. B **436**, 257 (1998) [arXiv:hep-ph/9804398].
I. Antoniadis, Phys. Lett. B **246**, 377 (1990).

- [111] L. Randall and R. Sundrum, Nucl. Phys. B **557**, 79 (1999) [arXiv:hep-th/9810155].
 L. Randall and R. Sundrum, Phys. Rev. Lett. **83**, 3370 (1999) [arXiv:hep-ph/9905221].
 L. Randall and R. Sundrum, Phys. Rev. Lett. **83**, 4690 (1999) [arXiv:hep-th/9906064].
- [112] Y. Nomura, JHEP **0311**, 050 (2003) [arXiv:hep-ph/0309189].
 C. Csaki, C. Grojean, J. Hubisz, Y. Shirman and J. Terning, Phys. Rev. D **70**, 015012 (2004) [arXiv:hep-ph/0310355].
 C. Csaki, C. Grojean, H. Murayama, L. Pilo and J. Terning, Phys. Rev. D **69**, 055006 (2004) [arXiv:hep-ph/0305237].
 C. Csaki, C. Grojean, L. Pilo and J. Terning, Phys. Rev. Lett. **92**, 101802 (2004) [arXiv:hep-ph/0308038].
 R. S. Chivukula, E. H. Simmons, H. J. He, M. Kurachi and M. Tanabashi, Phys. Lett. B **603**, 210 (2004) [arXiv:hep-ph/0408262].
- [113] D. B. Kaplan, H. Georgi and S. Dimopoulos, Phys. Lett. B **136**, 187 (1984).
 H. Georgi and D. B. Kaplan, Phys. Lett. B **145**, 216 (1984).
 R. S. Chivukula, C. Hoelbling and N. J. Evans, Phys. Rev. Lett. **85**, 511 (2000) [arXiv:hep-ph/0002022].
 K. Agashe, R. Contino and A. Pomarol, Nucl. Phys. B **719**, 165 (2005) [arXiv:hep-ph/0412089].
- [114] N. Arkani-Hamed, A. G. Cohen, E. Katz, A. E. Nelson, T. Gregoire and J. G. Wacker, JHEP **0208**, 021 (2002) [arXiv:hep-ph/0206020].
 N. Arkani-Hamed, A. G. Cohen, E. Katz and A. E. Nelson, JHEP **0207**, 034 (2002) [arXiv:hep-ph/0206021].
 S. Chang and J. G. Wacker, Phys. Rev. D **69**, 035002 (2004) [arXiv:hep-ph/0303001].
 M. Schmaltz, JHEP **0408**, 056 (2004) [arXiv:hep-ph/0407143].
 M. Schmaltz and D. Tucker-Smith, arXiv:hep-ph/0502182.
- [115] N. Arkani-Hamed and S. Dimopoulos, JHEP **0506**, 073 (2005) [arXiv:hep-th/0405159].
 G. F. Giudice and A. Romanino, Nucl. Phys. B **699**, 65 (2004) [Erratum-ibid. B **706**, 65 (2005)] [arXiv:hep-ph/0406088].
 N. Arkani-Hamed, S. Dimopoulos, G. F. Giudice and A. Romanino, Nucl. Phys. B **709**, 3 (2005) [arXiv:hep-ph/0409232].
- [116] S. Kachru, R. Kallosh, A. Linde, and S. P. Trivedi, “De Sitter vacua in string theory.” *Phys. Rev.* **D68** (2003) 046005,
- [117] C. P. Burgess, R. Kallosh and F. Quevedo, JHEP **0310**, 056 (2003) [arXiv:hep-th/0309187].

- [118] K. Choi, A. Falkowski, H. P. Nilles, M. Olechowski and S. Pokorski, *JHEP* **0411**, 076 (2004) [arXiv:hep-th/0411066].
 K. Choi, A. Falkowski, H. P. Nilles and M. Olechowski, *Nucl. Phys. B* **718**, 113 (2005) [arXiv:hep-th/0503216].
 A. Falkowski, O. Lebedev and Y. Mambrini, *JHEP* **0511**, 034 (2005) [arXiv:hep-ph/0507110].
 K. Choi, K. S. Jeong, T. Kobayashi and K. i. Okumura, *Phys. Lett. B* **633**, 355 (2006) [arXiv:hep-ph/0508029].
 H. Baer, E. K. Park, X. Tata and T. T. Wang, “Collider and dark matter searches in models with mixed modulus-anomaly arXiv:hep-ph/0604253.
 M. Endo, M. Yamaguchi and K. Yoshioka, *Phys. Rev. D* **72**, 015004 (2005) [arXiv:hep-ph/0504036].
- [119] M.K. Gaillard, B.D. Nelson and Y.-Y. Wu, *Phys. Lett. B* **459** (1999) 549.
 J. Bagger, T. Moroi and E. Poppitz, *JHEP* **0004** (2000) 009.
- [120] A. Djouadi, J. L. Kneur and G. Moultaka, [arXiv:hep-ph/0211331].
- [121] B. C. Allanach, *Comput. Phys. Commun.* **143**, 305 (2002) [arXiv:hep-ph/0104145].
- [122] K. Abe *et al.* [Belle Collaboration], *Phys. Lett. B* **511**, 151 (2001) [arXiv:hep-ex/0103042].
 D. Cronin-Hennessy *et al.* [CLEO Collaboration], *Phys. Rev. Lett.* **87**, 251808 (2001) [arXiv:hep-ex/0108033].
 R. Barate *et al.* [ALEPH Collaboration], *Phys. Lett. B* **429**, 169 (1998).
- [123] G. W. Bennett *et al.* [Muon g-2 Collaboration], *Phys. Rev. Lett.* **89**, 101804 (2002) [Erratum-*ibid.* **89**, 129903 (2002)] [arXiv:hep-ex/0208001].
 G. W. Bennett *et al.* [Muon g-2 Collaboration], *Phys. Rev. Lett.* **92**, 161802 (2004) [arXiv:hep-ex/0401008].
- [124] T. Sjostrand, L. Lonnblad, S. Mrenna and P. Skands, LU TP 06-13, FERMILAB-PUB-06-052-CD-T [hep-ph/0603175].
- [125] <http://www.physics.ucdavis.edu/~conway/research/software/pgs/pgs4-general.htm>.
- [126] <http://physics.princeton.edu/~verlinde/research/lhco/>
<http://www.phys.washington.edu/users/strasslr/LHCO.BBpage.html>.
- [127] H. Baer, C. h. Chen, F. Paige and X. Tata, *Phys. Rev. D* **53**, 6241 (1996) [arXiv:hep-ph/9512383].
 H. Baer, C. h. Chen, F. Paige and X. Tata, *Phys. Rev. D* **52**, 2746 (1995) [arXiv:hep-ph/9503271].

- [128] N. Arkani-Hamed, G. L. Kane, J. Thaler and L. T. Wang, JHEP **0608**, 070 (2006) [arXiv:hep-ph/0512190].
- [129] A. Bartl, W. Majerotto and W. Porod, Z. Phys. C **64**, 499 (1994) [Erratum-ibid. C **68**, 518 (1995)].
- [130] K. Choi, H. B. Kim and C. Munoz, Phys. Rev. D **57**, 7521 (1998) [arXiv:hep-th/9711158].
- [131] J. R. Ellis, K. A. Olive, Y. Santoso and V. C. Spanos, Phys. Lett. B **565**, 176 (2003) [arXiv:hep-ph/0303043].
J. L. Feng, eConf **C0307282**, L11 (2003) [arXiv:hep-ph/0405215].
- [132] J. A. Casas, Z. Lalak, C. Munoz and G. G. Ross, Nucl. Phys. B **347**, 243 (1990).
B. de Carlos, J. A. Casas and C. Munoz, Nucl. Phys. B **399**, 623 (1993) [arXiv:hep-th/9204012].
B. de Carlos, J. A. Casas and C. Munoz, Phys. Lett. B **299**, 234 (1993) [arXiv:hep-ph/9211266].
A. de la Macorra and G. G. Ross, Nucl. Phys. B **404**, 321 (1993) [arXiv:hep-ph/9210219].
- [133] G. L. Kane, J. D. Lykken, S. Mrenna, B. D. Nelson, L. T. Wang and T. T. Wang, Phys. Rev. D **67**, 045008 (2003) [arXiv:hep-ph/0209061].
- [134] F. Denef, M. R. Douglas, B. Florea, A. Grassi and S. Kachru, Adv. Theor. Math. Phys. **9**, 861 (2005) [arXiv:hep-th/0503124].
- [135] B. C. Allanach, D. Grellscheid and F. Quevedo, JHEP **0407**, 069 (2004) [arXiv:hep-ph/0406277].
- [136] J. L. Kneur and G. Moultaka, Phys. Rev. D **59**, 015005 (1999) [arXiv:hep-ph/9807336].
A. Djouadi *et al.* [MSSM Working Group], arXiv:hep-ph/9901246.
J. L. Kneur and G. Moultaka, Phys. Rev. D **61**, 095003 (2000) [arXiv:hep-ph/9907360].
C. G. Lester, M. A. Parker and M. J. White, JHEP **0601**, 080 (2006) [arXiv:hep-ph/0508143].
J. A. Aguilar-Saavedra *et al.*, arXiv:hep-ph/0511344.
B. C. Allanach *et al.*, arXiv:hep-ph/0602198.
- [137] <http://physics.princeton.edu/~verlinde/research/lhco/>
<http://ph-dep-th.web.cern.ch/ph-dep-th/lhcOlympics/2ndWin06/program.html>

- [138] For recent work on this subject, see: P. M. Zerwas *et al.*, hep-ph/0211076; B. C. Allanach, G. A. Blair, S. Kraml, H. U. Martyn, G. Polesello, W. Porod and P. M. Zerwas, hep-ph/0403133; G. Weiglein *et al.* [LHC/LC Study Group], Phys. Rept. **426**, 47 (2006) [hep-ph/0410364]; R. Lafaye, T. Plehn and D. Zerwas, hep-ph/0404282. P. Bechtle, K. Desch and P. Wienemann, Comput. Phys. Commun. **174**, 47 (2006) [hep-ph/0412012]; N. Arkani-Hamed, G. L. Kane, J. Thaler and L. T. Wang, JHEP **0608**, 070 (2006) [hep-ph/0512190].
- [139] Y. Yamada, Phys. Rev. D **54**, 1150 (1996) [hep-ph/9602279]; D. M. Pierce, J. A. Bagger, K. T. Matchev and R. j. Zhang, Nucl. Phys. B **491**, 3 (1997) [hep-ph/9606211]. Y. Yamada, Phys. Lett. B **623**, 104 (2005) [hep-ph/0506262]; S. P. Martin, Phys. Rev. D **74**, 075009 (2006) [hep-ph/0608026].
- [140] G. A. Blair, W. Porod and P. M. Zerwas, Phys. Rev. D **63**, 017703 (2001) [hep-ph/0007107]. G. A. Blair, W. Porod and P. M. Zerwas, Eur. Phys. J. C **27**, 263 (2003) [hep-ph/0210058]. G. A. Blair, A. Freitas, H. U. Martyn, G. Polesello, W. Porod and P. M. Zerwas, Acta Phys. Polon. B **36**, 3445 (2005) [hep-ph/0512084];
- [141] S. P. Martin, in *Proc. of the APS/DPF/DPB Summer Study on the Future of Particle Physics (Snowmass 2001)* ed. N. Graf, *In the Proceedings of APS / DPF / DPB Summer Study on the Future of Particle Physics (Snowmass 2001), Snowmass, Colorado, 30 Jun - 21 Jul 2001, pp P327.*
- [142] M. Carena, P. H. Chankowski, M. Olechowski, S. Pokorski and C. E. M. Wagner, Nucl. Phys. B **491**, 103 (1997) [hep-ph/9612261].
- [143] For a review, see: R. N. Mohapatra *et al.*, [hep-ph/0510213].
- [144] H. Baer, M. A. Diaz, P. Quintana and X. Tata, JHEP **0004**, 016 (2000) [hep-ph/0002245].
- [145] M. Dine and A. E. Nelson, Phys. Rev. D **48**, 1277 (1993) [hep-ph/9303230]; M. Dine, A. E. Nelson and Y. Shirman, Phys. Rev. D **51**, 1362 (1995) [hep-ph/9408384]; M. Dine, A. E. Nelson, Y. Nir and Y. Shirman, Phys. Rev. D **53**, 2658 (1996) [hep-ph/9507378].
- [146] For a review, see G. F. Giudice and R. Rattazzi, Phys. Rept. **322**, 419 (1999) [hep-ph/9801271].
- [147] M. A. Luty and R. Sundrum, Phys. Rev. D **65**, 066004 (2002) [hep-th/0105137]; M. Luty and R. Sundrum, Phys. Rev. D **67**, 045007 (2003) [hep-th/0111231]; R. Harnik, H. Murayama and A. Pierce, JHEP **0208**, 034 (2002) [hep-ph/0204122]; R. Sundrum, Phys. Rev. D **71**, 085003 (2005) [hep-th/0406012]; M. Ibe, K. I. Izawa,

- Y. Nakayama, Y. Shinbara and T. Yanagida, Phys. Rev. D **73**, 015004 (2006) [hep-ph/0506023]; M. Ibe, K. I. Izawa, Y. Nakayama, Y. Shinbara and T. Yanagida, Phys. Rev. D **73**, 035012 (2006) [hep-ph/0509229]; M. Schmaltz and R. Sundrum, JHEP **0611**, 011 (2006) [hep-th/0608051].
- [148] M. Dine, P. J. Fox, E. Gorbatov, Y. Shadmi, Y. Shirman and S. D. Thomas, Phys. Rev. D **70**, 045023 (2004) [hep-ph/0405159].
- [149] A. G. Cohen, T. S. Roy and M. Schmaltz, hep-ph/0612100.
- [150] S. P. Martin and M. T. Vaughn, Phys. Rev. D **50**, 2282 (1994) [hep-ph/9311340].
- [151] I. Jack and D. R. T. Jones, Phys. Lett. B **473**, 102 (2000) [hep-ph/9911491]; I. Jack, D. R. T. Jones and S. Parsons, Phys. Rev. D **62**, 125022 (2000) [hep-ph/0007291]; I. Jack and D. R. T. Jones, Phys. Rev. D **63**, 075010 (2001) [hep-ph/0010301].
- [152] B. C. Allanach *et al.*, in *Proc. of the APS/DPF/DPB Summer Study on the Future of Particle Physics (Snowmass 2001)* ed. N. Graf, Eur. Phys. J. C **25**, 113 (2002) [eConf **C010630**, P125 (2001)] [hep-ph/0202233].
- [153] H. Baer, C. h. Chen, F. Paige and X. Tata, Phys. Rev. D **53**, 6241 (1996) [hep-ph/9512383]; H. Baer, C. h. Chen, M. Drees, F. Paige and X. Tata, Phys. Rev. D **59**, 055014 (1999) [hep-ph/9809223]; H. Bachacou, I. Hinchliffe and F. E. Paige, Phys. Rev. D **62**, 015009 (2000) [hep-ph/9907518]; I. Hinchliffe and F. E. Paige, Phys. Rev. D **61**, 095011 (2000) [hep-ph/9907519].
- [154] D. Denegri, W. Majerotto and L. Rurua, Phys. Rev. D **60**, 035008 (1999) [hep-ph/9901231].
- [155] K. A. Assamagan, J. Guasch, S. Moretti and S. Penaranda, Czech. J. Phys. **55**, B787 (2005) [hep-ph/0409189]; R. Kinnunen, S. Lehti, F. Moortgat, A. Nikitenko and M. Spira, Eur. Phys. J. C **40N5**, 23 (2005) [hep-ph/0503075].
- [156] For reviews, see: J. F. Gunion, L. Poggioli, R. Van Kooten, C. Kao and P. Rowson, eConf **C960625**, LTH092 (1996) [hep-ph/9703330]; K. A. Assamagan, Y. Coadou and A. Deandrea, Eur. Phys. J. directC **4**, 9 (2002) [hep-ph/0203121]; M. Carena and H. E. Haber, Prog. Part. Nucl. Phys. **50**, 63 (2003) [hep-ph/0208209]; V. Buscher and K. Jakobs, Int. J. Mod. Phys. A **20**, 2523 (2005) [hep-ph/0504099].
- [157] A. de Gouvêa, A. Friedland and H. Murayama, Phys. Rev. D **59**, 095008 (1999) [hep-ph/9803481].
- [158] T. Falk, Phys. Lett. B **456**, 171 (1999) [hep-ph/9902352].

- [159] M. Drees, Phys. Lett. B **181**, 279 (1986); J. S. Hagelin and S. Kelley, Nucl. Phys. B **342**, 95 (1990); Y. Kawamura, H. Murayama and M. Yamaguchi, Phys. Lett. B **324**, 52 (1994) [hep-ph/9402254]. Y. Kawamura, H. Murayama and M. Yamaguchi, Phys. Rev. D **51**, 1337 (1995) [hep-ph/9406245]; H. C. Cheng and L. J. Hall, Phys. Rev. D **51**, 5289 (1995) [hep-ph/9411276]; C. F. Kolda and S. P. Martin, Phys. Rev. D **53**, 3871 (1996) [hep-ph/9503445]; S. P. Martin, Phys. Rev. D **61**, 035004 (2000) [hep-ph/9907550].
- [160] A. E. Faraggi, J. S. Hagelin, S. Kelley and D. V. Nanopoulos, Phys. Rev. D **45**, 3272 (1992); A. Lleyda and C. Munoz, Phys. Lett. B **317**, 82 (1993) [hep-ph/9308208]; Y. Kawamura, T. Kobayashi and H. Shimabukuro, Phys. Lett. B **436**, 108 (1998) [hep-ph/9805336]; H. Baer, M. A. Diaz, J. Ferrandis and X. Tata, Phys. Rev. D **61**, 111701 (2000) [hep-ph/9907211]; M. R. Ramage, Nucl. Phys. B **720**, 137 (2005) [hep-ph/0412153].
- [161] A. H. Chamseddine and H. K. Dreiner, Nucl. Phys. B **447**, 195 (1995) [hep-ph/9503454].
- [162] S. P. Martin and P. Ramond, Phys. Rev. D **51**, 6515 (1995) [hep-ph/9501244].
- [163] G. L. Kane, J. D. Lykken, B. D. Nelson and L. T. Wang, Phys. Lett. B **551**, 146 (2003) [hep-ph/0207168].
- [164] See, for example, F. Gabbiani, E. Gabrielli, A. Masiero and L. Silvestrini, Nucl. Phys. B **477**, 321 (1996) [hep-ph/9604387]; M. Misiak, S. Pokorski and J. Rosiek, Adv. Ser. Direct. High Energy Phys. **15**, 795 (1998) [hep-ph/9703442].
- [165] A. E. Nelson and M. J. Strassler, JHEP **0009**, 030 (2000) [hep-ph/0006251]; T. Kobayashi and H. Terao, Phys. Rev. D **64**, 075003 (2001) [hep-ph/0103028]; A. E. Nelson and M. J. Strassler, JHEP **0207**, 021 (2002) [hep-ph/0104051].
- [166] L. E. Ibanez and C. Lopez, Nucl. Phys. B **233**, 511 (1984); L. E. Ibanez, C. Lopez and C. Munoz, Nucl. Phys. B **256**, 218 (1985); M. Carena, M. Olechowski, S. Pokorski and C. E. M. Wagner, Nucl. Phys. B **419**, 213 (1994) [hep-ph/9311222]. M. Carena, M. Olechowski, S. Pokorski and C. E. M. Wagner, Nucl. Phys. B **426**, 269 (1994) [hep-ph/9402253].
- [167] J. A. Casas and A. Ibarra, Nucl. Phys. B **618**, 171 (2001) [hep-ph/0103065].
- [168] F. Borzumati and A. Masiero, Phys. Rev. Lett. **57**, 961 (1986). J. Hisano, T. Moroi, K. Tobe, M. Yamaguchi and T. Yanagida, Phys. Lett. B **357**, 579 (1995) [hep-ph/9501407]; J. Hisano, T. Moroi, K. Tobe and M. Yamaguchi, Phys. Rev. D **53**, 2442 (1996) [hep-ph/9510309].

- [169] J. A. Casas, J. R. Espinosa, A. Ibarra and I. Navarro, Nucl. Phys. B **573**, 652 (2000) [hep-ph/9910420].
- [170] F. Deppisch, H. Pas, A. Redelbach, R. Ruckl and Y. Shimizu, Eur. Phys. J. C **28**, 365 (2003) [hep-ph/0206122]; T. Blazek and S. F. King, Nucl. Phys. B **662**, 359 (2003) [hep-ph/0211368]; A. Masiero, S. K. Vempati and O. Vives, Nucl. Phys. Proc. Suppl. **137**, 156 (2004) [hep-ph/0405017]; E. Arganda and M. J. Herrero, Phys. Rev. D **73**, 055003 (2006) [hep-ph/0510405].
- [171] S. T. Petcov, T. Shindou and Y. Takanishi, Nucl. Phys. B **738**, 219 (2006) [hep-ph/0508243].
- [172] H. Baer, C. Balazs, J. K. Mizukoshi and X. Tata, Phys. Rev. D **63**, 055011 (2001) [hep-ph/0010068].
- [173] S. Davidson and A. Ibarra, JHEP **0109**, 013 (2001) [hep-ph/0104076].
- [174] A recent review of this topic can be found in: W. Buchmuller, R. D. Peccei and T. Yanagida, Ann. Rev. Nucl. Part. Sci. **55**, 311 (2005) [hep-ph/0502169].
- [175] D. N. Spergel *et al.*, [astro-ph/0603449].
- [176] T. Friedmann and E. Witten, Adv. Theor. Math. Phys. **7**, 577 (2003) [arXiv:hep-th/0211269].
- [177] J. Polchinski, *String Theory, Volume II*, Cambridge University Press.
- [178] A. Lukas and S. Morris, Phys. Rev. D **69**, 066003 (2004) [arXiv:hep-th/0305078].
- [179] This effect can play an important role in models of gaugino mediation of supersymmetry breaking. See, for example, D. E. Kaplan, G. D. Kribs and M. Schmaltz, Phys. Rev. D **62**, 035010 (2000) [hep-ph/9911293]; Z. Chacko, M. A. Luty, A. E. Nelson and E. Ponton, JHEP **0001**, 003 (2000) [hep-ph/9911323]; D. E. Kaplan and T. M. P. Tait, JHEP **0006**, 020 (2000) [hep-ph/0004200]; M. Schmaltz and W. Skiba, Phys. Rev. D **62**, 095005 (2000) [hep-ph/0001172]; M. Schmaltz and W. Skiba, Phys. Rev. D **62**, 095004 (2000) [hep-ph/0004210]; H. Baer, C. Balazs, A. Belyaev, R. Dermisek, A. Mafi and A. Mustafayev, JHEP **0205**, 061 (2002) [hep-ph/0204108]; C. Balazs and R. Dermisek, JHEP **0306**, 024 (2003) [hep-ph/0303161]; W. Buchmuller, J. Kersten and K. Schmidt-Hoberg, JHEP **0602**, 069 (2006) [hep-ph/0512152]; W. Buchmuller, L. Covi, J. Kersten and K. Schmidt-Hoberg, JCAP **0611**, 007 (2006) [hep-ph/0609142]; J. L. Evans, D. E. Morrissey and J. D. Wells, [hep-ph/0611185].

ABSTRACT

Connecting String/ M Theory to the Electroweak Scale and to LHC Data

by

Piyush Kumar

Chairperson: Gordon L. Kane

The Standard Model of particle physics explains (almost) all observed non-gravitational microscopic phenomena but has many open theoretical questions. We are on the threshold of unravelling the mysteries of the Standard Model and discovering its extension. This could be achieved in the near future with the help of many experiments in particle physics and cosmology, the LHC in particular. Assuming that data confirming the existence of new physics beyond the Standard Model is obtained, one is left with the very important and challenging task of solving the “Inverse Problem”, *viz.* “How can one deduce the nature of the underlying (perhaps microscopic) theory from data?” This thesis explores this question in detail, and also proposes an approach to address the problem in a meaningful way which could prove crucial to the possible solution to this problem in the future. The proposed approach has three aspects - a) To systematically study classes of microscopic (string/ M theory) constructions to the extent that they could be connected to low energy physics (electroweak scale), b) To find patterns

of experimental observables which are sensitive to the properties of the underlying theoretical constructions thereby allowing us to distinguish among different constructions, and c) To try to get insights about the qualitative features of the theoretical model from data in a bottom-up approach which complements the top-down approach and strengthens it as well. This thesis studies all the above aspects in detail. The methods used and results obtained in this thesis will hopefully be of great importance in solving the Inverse Problem.